6

Theoretical Basis of Catalytic Cracking

6.1 PROCESS THERMODYNAMICS

The thermodynamic analysis of catalytic cracking, as in any process, involves:

The determination of the heat of reaction in the process

The calculation of the chemical equilibrium of the main and secondary reactions as a means of understanding the chemical transformations taking place

The first issue was dealt with in Section 1.1 for all processes involving the conversion of hydrocarbons.

The method suitable for catalytic cracking determines the heat of reaction as the difference between the heats of combustion of the products and of the feed, using for this purpose the graphs of Figures 1.1 and 1.2.

Experimental studies [232] using a reactor simulating the conditions in a practical isothermal riser reactor found at 500–550°C a reaction heat of 800–1070 kJ/kg. The feed was a gas oil: $d = 0.9292$, S = 0.72 wt %, IBP = 259°C, temperature at 50 wt % = 377°C, EP = 527°C, 10.62% paraffins, and 39.76% cycloparaffins. The two catalysts used were Octanat and GX30.

The lower values for the heat of reaction—677 kJ/kg—obtained earlier [233] are attributed to nonisothermal reaction conditions: a 20–40°C temperature drop is caused by the endothermic reaction.

The heat of combustion of the coke deposited on the catalyst depends on its hydrogen content and on the ratio CO/CO_2 in the flue gases. Its calculation is presented in Section 6.6.

The same method used for computing equilibrium concentrations for thermal cracking is valid also for catalytic cracking (see Figures 1.3 and 2.1–2.7), since the presence of the solid catalyst does not influence the equilibrium of the reactions that occur in vapor phase. Note however that knowledge of the equilibria of the reactions of the C_2–C_4 hydrocarbons is not sufficient.

The thermodynamic analysis of catalytic cracking requires information on the behavior of the heavier hydrocarbons contained in the gas oils, vacuum distillates, and even residual fractions. A major difficulty in performing this analysis resides in the limited knowledge of the thermodynamic constants for the hydrocarbons, which are typical for such fractions.

Despite the fact that for the above reason such an analysis is of limited value, it still gives useful information for understanding the thermodynamics of this process.

A problem of special interest is the adsorption equilibrium of the reaction products between the surface of the catalyst and the vapor phase. The adsorbed substances lead finally, following polymerization and condensations, to the formation of coke. The importance of this problem was emphasized in an earlier study by Raseev [1].

It is obvious that the main coke generators present in the feed are the resins and some of the condensed aromatic and hydro-aromatic hydrocarbons, and in the case of residue cracking, the asphaltenes. All these components are usually directly adsorbed on the catalyst and are gradually converted to coke.

But they are not the only coke generators. Coke deposits on the catalyst are produced even during the catalytic cracking of white oils or of paraffins. This proves that coke deposits are formed also as result of the decomposition of saturated hydrocarbons.

In order to clarify these processes, the thermodynamic calculations must be carried out for conditions in which the reaction products remain adsorbed on the catalyst. Since it is difficult to know the concentrations in the adsorbed layer, it was found useful to assume them to be equal to those in liquid phase. Indeed, at $500°C$, a given volume of liquid contains approximately the same number of molecules as an equal volume of gas under 100–200 bar. One plots in the same graph the equilibria for the liquid and gaseous phases. At high pressures (100–200 bar) the equilibrium curves for the two phases must intersect. Such plots are used in this book for thermodynamic analysis of catalytic cracking and also for other catalytic processes.

The computation of the equilibrium concentrations for the case presented below was performed by using the method given in the Chapter 1.2 [2], and taking into account that for reactions in the liquid phase the constant b in Table 1.5 is equal to zero.

Published thermodynamic constants were used [3]. For reactions in gaseous phase, the constants for 800 K, which is close to the catalytic cracking, were used. For reactions in liquid phase, the only available constants are for 298 K, and they were used as such.

In order to characterize the behavior of various cuts or of certain classes of compounds, some typical average values were used for the thermodynamic constants $\Delta H°_{800}$ and $\Delta S°_{800}$.

The results of equilibrium calculations were plotted for the following types of reactions:

Alkanes and alkenes cracking
Alkenes polymerization
Cycloalkanes ring opening and cyclization of alkenes
Dealkylation of alkyl-cyclanes
Dehydrogenation of cyclohexanes

Dealkylation of alkyl-aromatics
Dealkylation of polycyclic hydrocarbons
Cracking of sulfur-containing compounds
Cracking of nitrogen-containing compounds

In the final part of this section, conclusions are formulated about the vapor phase reactions that may take place during catalytic cracking, and about the reactions that may lead to the formation of products that remain adsorbed on the surface of the catalyst and are converted to coke.

6.1.1 Alkanes Cracking

The decomposition of butane, which was analyzed in Section 2.1, shows a conversion at equilibrium of about 90% at atmospheric pressure and at a temperature of 500°C, conversion which, at a pressure of 100 bar, decreased to about 20%.

The thermodynamic equilibrium taking into account for reactions of the form:

$$C_{(m+n)}H_{2(m+n)+2} \rightleftharpoons C_mH_{2m+2} + C_nH_{2n}$$
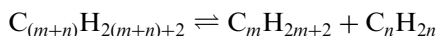
is analyzed in the following, for higher hydrocarbons, such as the normal and iso C_6–C_{20} paraffins. The calculations were performed for the extreme terms of the considered series of hydrocarbons, since their behavior allows one to draw the correct conclusions for the intermediary terms of the series.

The selection of specific iso-alkanes was guided by the structure of the hydrocarbons contained in the straight run gas oil: the monomethyl-derivatives are preponderant, the dimethyl- and ethyl-derivatives are present only in small amounts and compounds with quaternary carbon atoms are absent.

Concerning the products, those resulting from catalytic cracking were the only ones considered: the formation of hydrocarbons with less than 3 carbon atoms was neglected; among alkenes, only those with double bond in position 1 were considered.

The heats of reaction and the variation of the entropies for the selected reactions are:
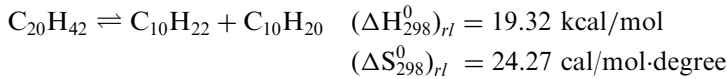
	$(\Delta H^0_{800})_r$ kcal/mol	$(\Delta S^0_{800})_r$ cal/mol·degree
$C_{20}H_{42} \rightleftharpoons C_3H_8 + C_{17}H_{34}$	18.93	33.62
$C_{10}H_{22} + C_{10}H_{20}$	18.60	34.23
$C_{17}H_{36} + C_3H_6$	18.61	33.91
$C_6H_{14} \rightleftharpoons C_3H_8 + C_3H_6$	18.92	33.42
2-methyl-nonane $\rightleftharpoons C_6H_{14} + $ i-C_4H_8	16.03	32.66
3-methyl-nonane $\rightleftharpoons C_5H_{12} + $ 2-methyl-butene-1	15.81	33.13
4-methyl-nonane $\rightleftharpoons C_4H_{10} + $ 2-methyl-pentene-1	17.07	34.51
2,3-dimethyl-octane $\rightleftharpoons C_5H_{12} + $ 2-methyl-butene-2	15.59	35.25
$\rightleftharpoons C_4H_{10} + $ 2,3-dimethyl-butene-1	15.30	35.51

These data show the almost identical behavior of the C_6–C_{20} *n*-alkanes, with very small differences that depend on the products of the reactions (the first 4 reactions in the table).

Concerning the iso-alkanes, somewhat larger differences are observed between the mono- and dimethyl-derivatives.

By using the simplified method developed in Section 1.2 and the thermo-dynamic constants given in the table above, the graph of Figure 6.1 for the equili-briums of these reactions was plotted. In the graph, the straight lines of constant conversion are shown for the values of 99% and 60%, which is enough for the analysis of the results. As in the graphs within Section 1.2, the scale of the tempera-ture in the ordinate is ascending.

Similar calculations were performed for the reactions in liquid phase, for which thermodynamic constants were available, and which can be assimilated with reac-tions in the adsorbed layer, namely:

$$C_{20}H_{42} \rightleftharpoons C_{10}H_{22} + C_{10}H_{20} \quad (\Delta H^0_{298})_{rl} = 19.32 \text{ kcal/mol}$$
$$(\Delta S^0_{298})_{rl} = 24.27 \text{ cal/mol·degree}$$

These data made it possible to plot the equilibrium (see Figure 6.1), correlated with the equilibrium for the same reactions in gas phase.

The data plotted in this graph confirm the well-known fact [1] that in the conditions for the catalytic cracking of distillates (temperatures of about 500°C and pressure a little above atmospheric), the decomposition of alkanes is not limited thermodynamically. The conversions at equilibrium are approximately 99% for *n*-alkanes and over 99% for *i*-alkanes.

The equilibrium conversions in liquid phase are identical with those in vapor phase at pressures of about 200–500 bar. They could be considered representative for
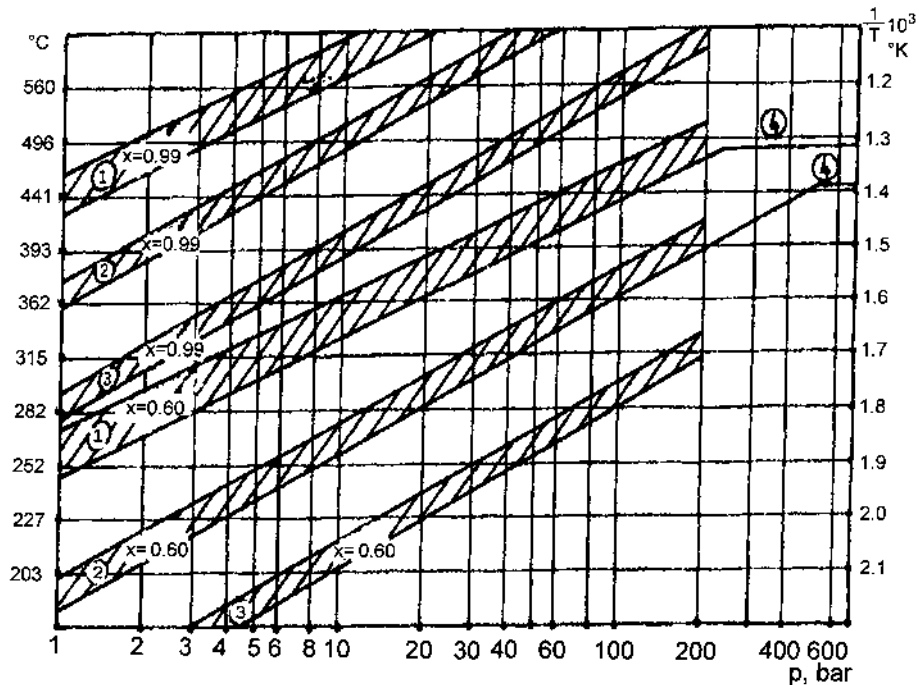

Figure 6.1 Alkanes and alkenes decomposition equilibrium. 1 – *n*-alkanes and *n*-alkenes, 2 – methyl-nonane, 3 – dimethyl-octanes, 4 – equilibrium in adsorbed layer equivalent to liquid state, *x* – conversion in molar fraction.

those in the adsorbed film on the surface of the catalyst. Different from those in the vapor phase, the conversions at equilibrium are in this case about 60% for *n*-alkanes and a little higher for *i*-alkanes at temperatures of catalytic cracking.
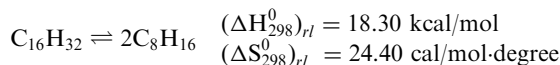
6.1.2 Alkenes Cracking

As in the previous case, the following table contains the reactions considered and the values of the heats and entropies of the reactions.

	$(\Delta H^0{}_{800})_r$ kcal/mol	$(\Delta S^0{}_{800})_r$ cal/mol·degree
$C_{20}H_{40} \rightleftharpoons 2C_{10}H_{20}$	18.60	34.24
$\rightleftharpoons C_5H_{10} + C_{15}H_{30}$	18.63	34.26
$C_6H_{12} \rightleftharpoons 2C_3H_6$	18.61	33.61

The values are practically identical to those of alkanes having the same structure.

The reaction of 1-dodecyl-hexene to 1-octene is taken as typical for reactions in liquid phase.

$$C_{16}H_{32} \rightleftharpoons 2C_8H_{16} \quad \begin{array}{l} (\Delta H^0_{298})_{rl} = 18.30 \text{ kcal/mol} \\ (\Delta S^0_{298})_{rl} = 24.40 \text{ cal/mol·degree} \end{array}$$

Since the thermodynamic values are practically identical with those corresponding to *n*-alkanes, the graph of Figure 6.1 is valid also for the equilibrium of the decomposition reactions of alkenes.

### 6.1.3 Alkenes Polymerization

The reactions of polymerization of alkenes are of great importance especially since the produced polymers adsorb on the catalyst and following further condensation and dehydrogenation reactions, leading to the formation of coke.

The available heats of reaction and the variation of the entropies for some representative dimerization reactions are listed in the following table:

	$(\Delta H^0{}_{800})_r$ kcal/mol	$(\Delta S^0{}_{800})_r$ cal/mol·degree
$2C_{10}H_{20} \rightleftharpoons n\text{-}C_{20}H_{40}$	−18.60	−34.24
$2C_8H_{16} \rightleftharpoons n\text{-}C_{16}H_{32}$	−18.59	−34.23
$2C_5H_{10} \rightleftharpoons n\text{-}C_{10}H_{20}$	−18.69	−34.29
$2C_4H_8 \rightleftharpoons n\text{-}C_8H_{16}$	−18.69	−33.49
$2C_3H_6 \rightleftharpoons n\text{-}C_6H_{12}$	−18.61	−33.61
$\rightleftharpoons$ 2-methylpentene-1	−20.84	−33.58
$\rightleftharpoons$ 3-methylpentene-1	−18.45	−33.48
$\rightleftharpoons$ 4-methylpentene-1	−19.71	−38.71
$\rightleftharpoons$ 2-methylpentene-2	−23.36	−35.99
$\rightleftharpoons$ 3-methylpentene-2 *cis*	−22.88	−35.99
$\rightleftharpoons$ 3-methylpentene-2 *trans*	−23.10	−35.18
$\rightleftharpoons$ 4-methylpentene-2 *cis*	−20.60	−36.15
$\rightleftharpoons$ 4-methylpentene-2 *trans*	−21.03	−36.16
$\rightleftharpoons$ 2,3-dimethylbutene-1	−21.05	−36.18
$\rightleftharpoons$ 2,3-dimethylbutene-2	−23.85	−40.54

The first four reactions refer to the dimerization of *n*-alkenes with double bonds in position 1 to dimers with the same structure. The rest of the reactions refer to the dimerization of propene to all the possible hexane isomers, except those that contain a quaternary carbon atom.

For reactions in the adsorbed layer, one takes into account the thermodynamic data for the liquid phase. The following reaction was selected as representative:

$$2C_8H_{16} \rightleftharpoons C_{16}H_{32}$$
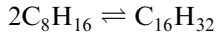
for which the heat of reaction and the variation of the entropy are:

$$(\Delta H^0_{298})_{rl} = -18.30 \text{ kcal/mol}$$
$$(\Delta S^0_{298})_{rl} = -24.40 \text{ cal/mol·degree}$$

All these data were used for plotting the dimerization equilibrium in Figure 6.2.

It must be remarked that the equilibrium conversions of the propene dimerization reactions show important differences depending on the isomer produced. Similar differences or possibly even more pronounced ones should exist for alkenes having a larger number of carbon atoms. This statement cannot be verified directly due to the lack of corresponding thermodynamic constants.

The graph of Figure 6.2 proves that in catalytic cracking (temperatures of about 500°C and pressures lower than 3 bar), the polymerization reactions in vapor phase are practically absent (conversions of about 1%). Concomitantly it is shown that these reactions could achieve conversions of about 50% if they were
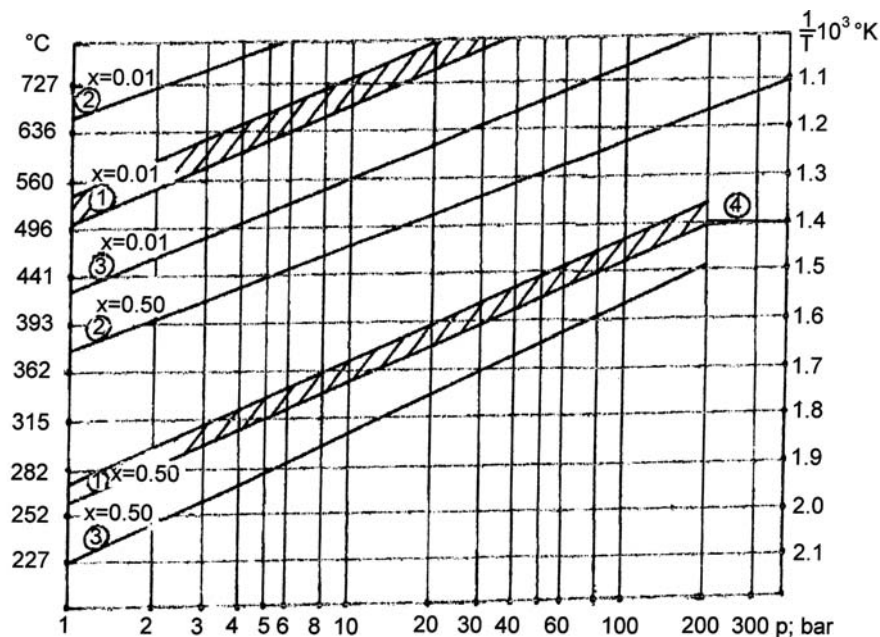

Figure 6.2 Equilibrium of alkenes dimerization. 1 – *n*-alkene 1C$_4$-1C$_{10}$, 2 – 2C$_3$H$_6$→3-methylpentene 2-trans, 3 – 2C$_3$H$_6$→4-methylpentene 1. Between 2 and 3 2C$_3$H$_6$-other isomers, 4 – equilibrium in adsorbed layer or in liquid state, x – conversion in molar fraction.
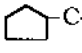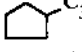
carried out in liquid phase or at pressures of the order 100 bar. This means that they may take place in the adsorbed layer on the surface of the catalyst.

The polymerization of alkenes is also possible during the catalytic cracking of heavy feedstocks in liquid or partial liquid phase.

6.1.4 Cycloalkanes Decyclization–Alkenes Cyclization

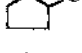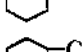This analysis is limited to the breaking of rings with 5- and 6-carbon atoms, the only present in significant amounts in crude oil fractions.

The reactions that are taken into account and the values of the respective thermodynamic constants are presented in the following table:

Reaction	$(\Delta H^0_{800})_r$ kcal/mol	$(\Delta S^0_{800})_r$ cal/mol·degree
⬠ ⇌ $C_5H_{10}(1)$	14.89	15.96
⬠–C ⇌ 2-methyl-pentene-1	14.43	13.38
4-methyl-pentene-1	15.56	14.88
⬡ ⇌ $C_6H_{12}(1)$	20.12	22.68
⬠–C–C ⇌ C_7H_{14}	16.53	13.30
⬠–C_3H_7 ⇌ C_8H_{16}	16.80	13.30
⬠–$C_{15}H_{31}$ ⇌ $C_{20}H_{40}$	16.54	13.35
⬡–C ⇌ C_7H_{14}	22.08	19.85
⬡–C–C ⇌ C_8H_{16}	21.23	19.49
⬡–$C_{14}H_{29}$ ⇌ $C_{20}H_{40}$	20.91	19.52

Taking into account that on acid catalysts tertiary ions are preferably formed, only the breaking of the bond in the β-position to the tertiary carbon was taken into account when examining the cracking of methyl-cyclopentane.

The lack of thermodynamic data for the higher methyl- and dimethyl-alkenes prevented the use of the same reasoning for the hydrocarbons in the two final groups of the table. In their case the data for n-alkene-1 were used, which constitutes of course an approximation.

The following reaction was selected as being illustrative for reactions in liquid phase:

⬡–$C_{10}H_{21}$ ⇌ $C_{16}H_{32}$ $(\Delta H^0_{298})_{rl} = 22.69$ kcal/mol

$(\Delta S^0_{298})_{rl} = 18.80$ cal/mol·degree
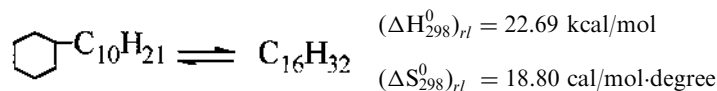
Since the breaking of the ring takes place without a change in the number of moles, the pressure does not influence the equilibrium. For this reason, x-t coordinates were selected for these equilibria.

Figure 6.3 depicts this equilibrium for some vapor-phase reactions.

Calculations show that in liquid phase reactions, temperatures of 505 and 539°C are required in order to obtain a 1% equilibrium concentration of alkenes, in the conversion of alkyl-cyclopentanes and alkyl-cyclohexanes, respectively. These conversions correspond to those obtained in vapor phase at almost the same temperatures. The graph of Figure 6.3 is actually valid for reactions in both vapor and liquid phases.

From this graph it follows that the naphthenic rings are much more stable than the alkanes and the alkenes chains, the extent of ring breaking having thermodynamic limitations.

The lack of thermodynamic data hinders the extension of this analysis to bi- and polycyclic cyclanes. Cyclization of the alkenes constitutes the reverse reaction to
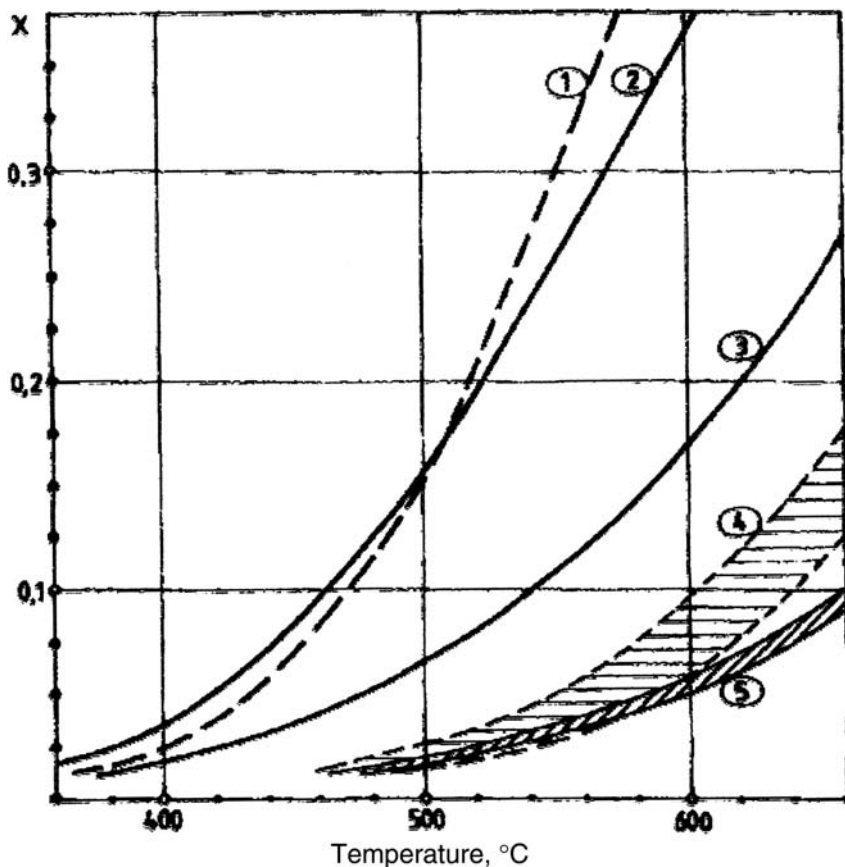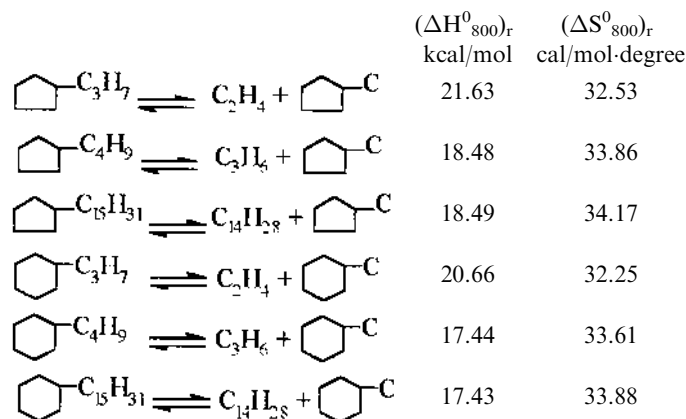

Figure 6.3 Cyclanes decyclization equilibrium. 1 – cyclohexane → hexene 1, 2 – cyclopentane → pentene 1, 3 – methylcyclopentane → 2 or 4 methylpentene 1, 4 – higher-alkylcyclohexanes → alkenes 1, 5 – higher-alkylcyclopentanes → alkenes 1.
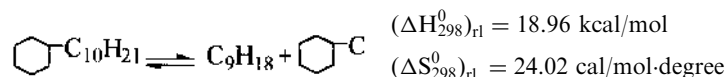
the breaking of the rings. Examination of Figure 6.3 allows the formulation of the following conclusions: 1. Thermodynamic calculations indicate that at temperatures of catalytic cracking the cyclization of the alkenes can take place with high conversion, about 80% for cyclization in methylcyclopentane or cyclohexane and up to 94–98% for cyclization in their homologues; 2. The probability of formation for rings with five and six carbon atoms is basically the same.

6.1.5 Dealkylation of Cycloalkanes

Taking into account the reaction mechanism and the available thermodynamic data, heats and the entropies of reaction were calculated for the following reactions:

	$(\Delta H^0_{800})_r$ kcal/mol	$(\Delta S^0_{800})_r$ cal/mol·degree
⬠—C_3H_7 ⇌ C_2H_4 + ⬠—C	21.63	32.53
⬠—C_4H_9 ⇌ C_3H_6 + ⬠—C	18.48	33.86
⬠—$C_{15}H_{31}$ ⇌ $C_{14}H_{28}$ + ⬠—C	18.49	34.17
⬡—C_3H_7 ⇌ C_2H_4 + ⬡—C	20.66	32.25
⬡—C_4H_9 ⇌ C_3H_6 + ⬡—C	17.44	33.61
⬡—$C_{15}H_{31}$ ⇌ $C_{14}H_{28}$ + ⬡—C	17.43	33.88

For reactions in liquid phase, the heaviest hydrocarbon was taken into account for which thermodynamic data were available:

⬡—$C_{10}H_{21}$ ⇌ C_9H_{18} + ⬡—C $\quad$ $(\Delta H^0_{298})_{rl} = 18.96$ kcal/mol

$(\Delta S^0_{298})_{rl} = 24.02$ cal/mol·degree

The graph of Figure 6.4 is based on these data.

In order to correctly compare the equilibrium conversions in the two phases, the equilibrium conversion in gaseous phase for the same hydrocarbon and reference temperature was also calculated:

⬡—$C_{10}H_{21}$ ⇌ C_9H_{18} + ⬡—C $\quad$ $(\Delta H^0_{298})_r = 18.78$ kcal/mol

$(\Delta S^0_{298})_r = 36.49$ cal/mol·degree
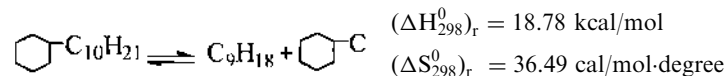
The insignificant differences between these values and the thermodynamic constants for 800 K, which were calculated before, prove that no errors were introduced when, due to the lack of thermodynamic data for the liquid state at 800 K different reference temperatures for the equilibrium in the liquid phase (298 K) and in the vapor phase (800 K) were used.

Examination of Figure 6.4 allows the conclusion that according to thermodynamic calculations the dealkylation of cycloalkanes can be carried out to completion in vapor phase at the temperatures and pressures of catalytic cracking but it is limited to a conversion of about 70% for the hydrocarbons adsorbed on the catalyst or for reactions in liquid phase.
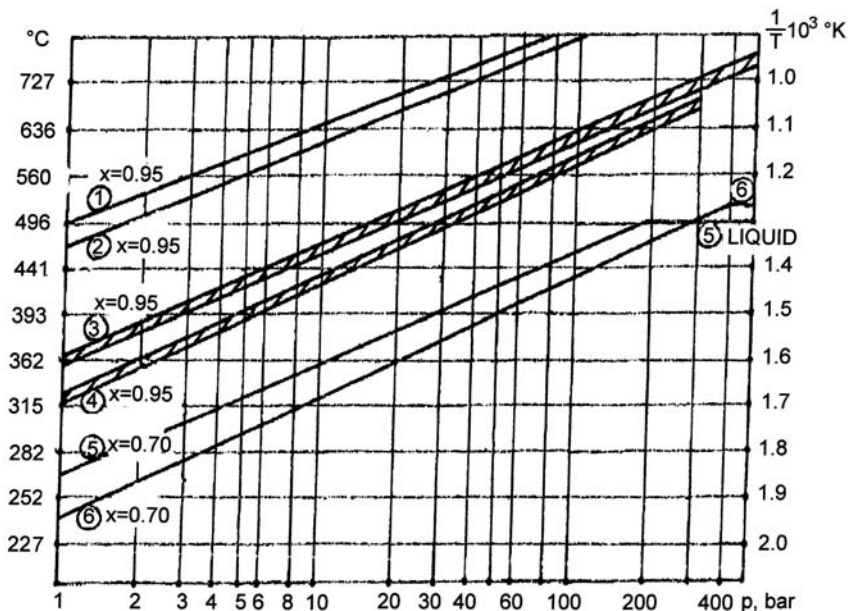
Figure 6.4 Alkylcyclanes dealkylation equilibrium.

1. cyclopentane–$C_3H_7 \rightleftharpoons C_2H_4 +$ cyclopentane–CH_3; 2. cyclohexane–$C_3H_7 \rightleftharpoons C_2H_4 +$ cyclohexane–CH_3;

3. cyclopentane–$C_nH_{2n+1} \rightleftharpoons C_{n-1}H_{2(n-1)} +$ cyclopentane–C for $n = 4$–15; 4. cyclohexane–$C_nH_{2n+1} \rightleftharpoons$

$C_{n-1}H_{2(n-1)} +$ cyclohexane–C for $n = 4 \div 15$; 5. cyclopentane–$C_{10}H_{21} \rightleftharpoons C_9H_{18} +$ cyclopentane–CH_3;

6. cyclohexane–$C_{10}H_{21} \rightleftharpoons C_9H_{18} +$ cyclohexane–CH_3. x – conversion in molar fraction.
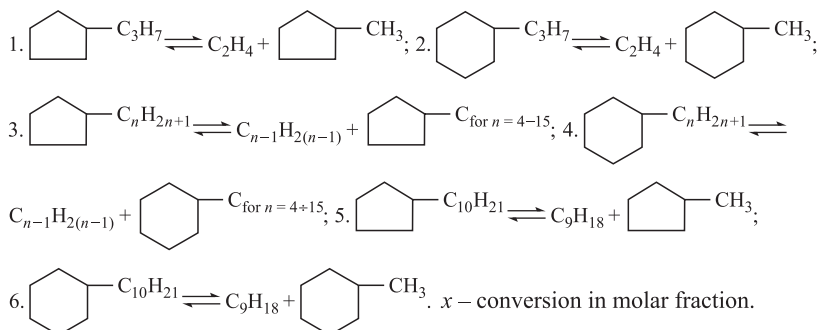
6.1.6 Dehydrogenation of Cyclohexanes

The following reactions were taken into account:

	$(\Delta H^0{}_{800})_r$ kcal/mol	$(\Delta S^0{}_{800})_r$ cal/mol·degree
cyclohexane $\rightleftharpoons$ benzene $+ 3H_2$	52.70	96.31
cyclohexane–C $\rightleftharpoons$ benzene–C $+ 3H_2$	51.75	94.89
cyclohexane–C–C $\rightleftharpoons$ benzene–C–C $+ 3H_2$	50.82	94.82
cyclohexane–$C_3 \rightleftharpoons$ benzene–$C_3 + 3H_2$	50.57	95.25

$\bigcirc\!-C_5 \rightleftharpoons \bigodot\!-C_5 + 3H_2$ 50.14   95.32

$\bigcirc\!-C_{14} \rightleftharpoons \bigodot\!-C_{14} + 3H_2$ 50.15   95.34
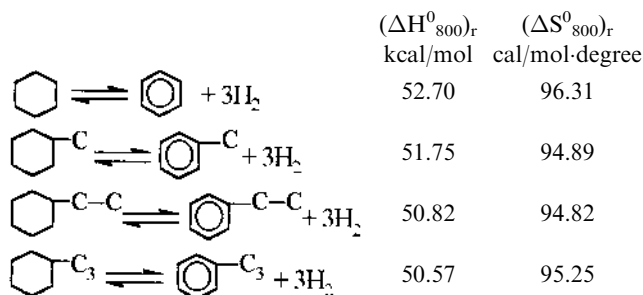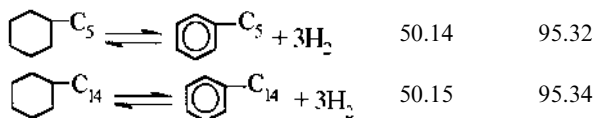
There are only minimum differences between the thermodynamic constants of these reactions. Therefore the graph for the dehydrogenation equilibrium of methyl-cyclohexane given in Figure 2.7 can be considered as representating all these reactions also. Thus, in the conditions of catalytic cracking the equilibrium is completely shifted towards dehydrogenation.
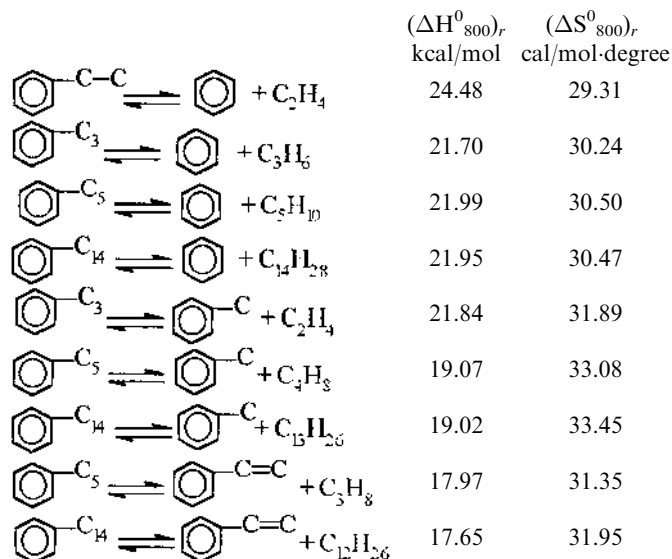
For the dehydrogenation of butyl-cyclohexane in liquid phase, one obtains:

$\bigcirc\!-C_4H_9 \rightleftharpoons \bigodot\!-C_4H_9 + 3H_2$
$$(\Delta H^0_{298})_{rl} = 47.63 \text{ kcal/mol}$$
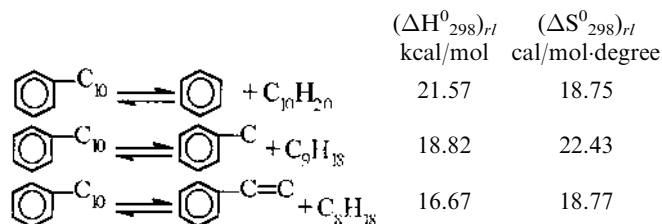$$(\Delta S^0_{298})_{rl} = 87.95 \text{ cal/mol·degree}$$
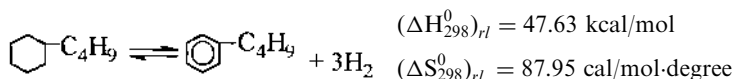
These values are similar to those for the vapor phase reactions and, accordingly also here, the equilibrium is completely displaced towards dehydrogenation. In fact, the escaping into the vapor phase of the hydrogen formed in the liquid phase reaction displaces this equilibrium further to the right.

6.1.7 Dealkylation of Alkylaromatics

The following reactions were taken into consideration:

	$(\Delta H^0_{800})_r$ kcal/mol	$(\Delta S^0_{800})_r$ cal/mol·degree
$\bigodot\!-C-C \rightleftharpoons \bigodot + C_2H_4$	24.48	29.31
$\bigodot\!-C_3 \rightleftharpoons \bigodot + C_3H_6$	21.70	30.24
$\bigodot\!-C_5 \rightleftharpoons \bigodot + C_5H_{10}$	21.99	30.50
$\bigodot\!-C_{14} \rightleftharpoons \bigodot + C_{14}H_{28}$	21.95	30.47
$\bigodot\!-C_3 \rightleftharpoons \bigodot\!-C + C_2H_4$	21.84	31.89
$\bigodot\!-C_5 \rightleftharpoons \bigodot\!-C + C_4H_8$	19.07	33.08
$\bigodot\!-C_{14} \rightleftharpoons \bigodot\!-C + C_{13}H_{26}$	19.02	33.45
$\bigodot\!-C_5 \rightleftharpoons \bigodot\!-C=C + C_3H_8$	17.97	31.35
$\bigodot\!-C_{14} \rightleftharpoons \bigodot\!-C=C + C_{12}H_{26}$	17.65	31.95

The following reactions were selected as representative of the chemical transformations in liquid phase:

	$(\Delta H^0_{298})_{rl}$ kcal/mol	$(\Delta S^0_{298})_{rl}$ cal/mol·degree
$\bigodot\!-C_{10} \rightleftharpoons \bigodot + C_{10}H_{20}$	21.57	18.75
$\bigodot\!-C_{10} \rightleftharpoons \bigodot\!-C + C_9H_{18}$	18.82	22.43
$\bigodot\!-C_{10} \rightleftharpoons \bigodot\!-C=C + C_8H_{18}$	16.67	18.77

For the liquid phase the values are less accurate than for the gas phase. The entropy value $S°_{298}$ = 124.24 cal/mol·degree for decyl benzene was obtained by extrapolation. Since this value is the same in calculations for all the examined reactions, the comparative results are not affected.

All these values were used for plotting the equilibrium parameters for the considered reactions in Figure 6.5.

The examination of this graph leads to the conclusion that the dealkylation reactions with the formation of benzene and alkene are thermodynamically less probable that those that lead to the formation of toluene and alkene or styrene and alkane.

If the last two reactions were carried out in vapor phase, at the conditions of temperature and pressure for catalytic cracking, the equilibrium conversion would reach between 95% and 99%.
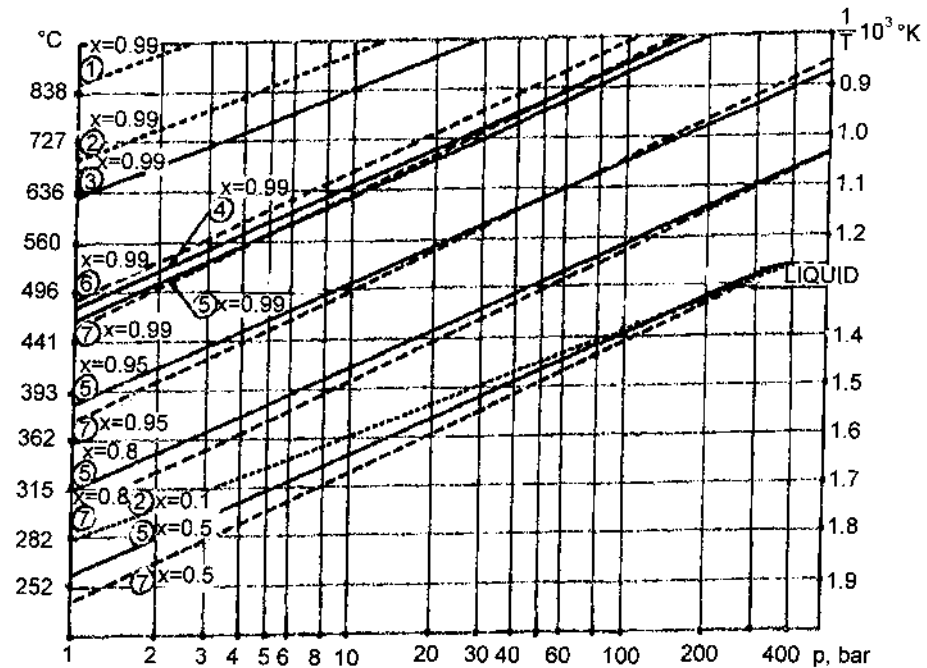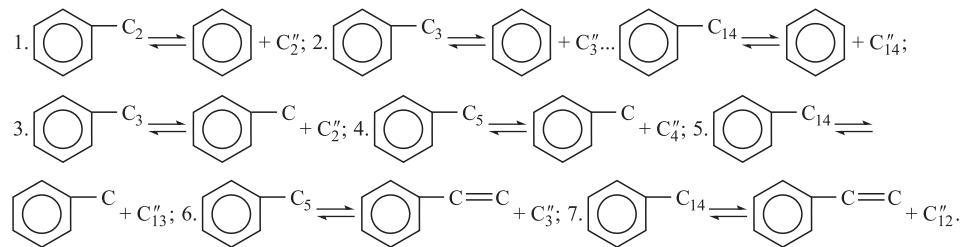

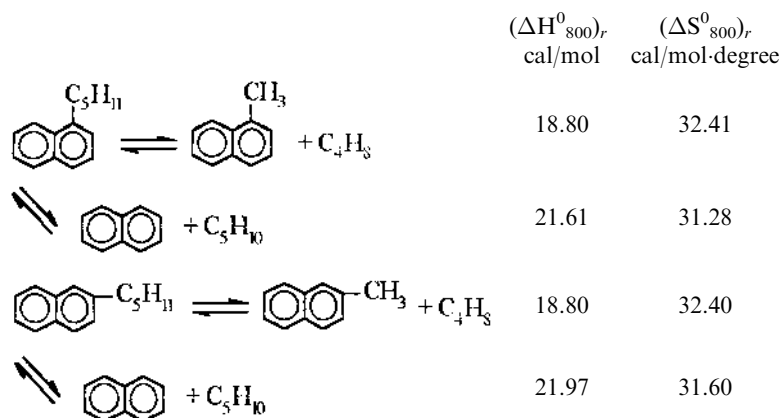**Figure 6.5** Alkyl-aromatics dealkylation equilibrium.

x – conversion in molar fraction.

In liquid phase, which is equivalent to pressures of the order of 200–300 bar when operating in vapor phase, the conversions at equilibrium are 50% for dealkylation with formation of toluene or styrene and only 10% if benzene is formed.

From here, an important conclusion is that dealkylation produces styrene and derivatives adsorbed on the catalyst, which may be important coke precursors.

6.1.8   Dealkylation of Polycyclic Hydrocarbons

The only available thermodynamic data are for alkyl-naphthalenes. On their basis, the following reactions may be analyzed:

	$(\Delta H^0_{800})_r$ cal/mol	$(\Delta S^0_{800})_r$ cal/mol·degree

	$(\Delta H^0_{800})_r$	$(\Delta S^0_{800})_r$
	18.80	32.41
	21.61	31.28
	18.80	32.40
	21.97	31.60

The data show that the position of the alkyl group exercises little influence upon thermodynamic properties.

The calculations show that at 490°C and atmospheric pressure the conversions reach 99% if methyl-naphthalenes are formed and of 90% if dealkylation results in the formation of naphthalene.

As in the case of alkyl-benzenes, thermodynamics favor the formation of methyl-naphthalene derivatives. Also, as in the case of alkyl-benzenes, the formation of hydrocarbons with unsaturated side chains similar to styrene is expected. No data is available for confirming this.
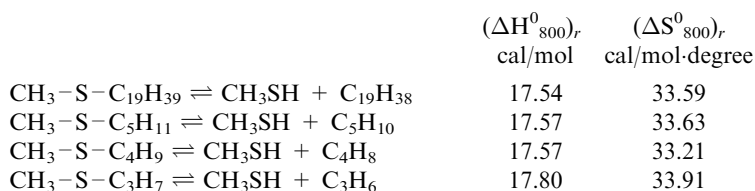
6.1.9   Cracking of S-Containing Compounds

6.1.9.1   Decomposition of Sulfides

The sulfides are decomposed according to the reaction:

Sulfide $\rightleftharpoons$ Mercaptan + alkene

The following reactions were considered and the parameters needed for thermodynamic analysis were calculated:

	$(\Delta H^0_{800})_r$ cal/mol	$(\Delta S^0_{800})_r$ cal/mol·degree
$CH_3-S-C_{19}H_{39} \rightleftharpoons CH_3SH + C_{19}H_{38}$	17.54	33.59
$CH_3-S-C_5H_{11} \rightleftharpoons CH_3SH + C_5H_{10}$	17.57	33.63
$CH_3-S-C_4H_9 \rightleftharpoons CH_3SH + C_4H_8$	17.57	33.21
$CH_3-S-C_3H_7 \rightleftharpoons CH_3SH + C_3H_6$	17.80	33.91

	(ΔH^0_{800})$_r$	(ΔS^0_{800})$_r$
$CH_3-S-C_2H_5 \rightleftharpoons CH_3SH + C_2H_4$	20.53	32.51
$C_2H_5-S-C_2H_5 \rightleftharpoons C_2H_5SH + C_2H_4$	20.67	33.99
$C_3H_7-S-C_3H_7 \rightleftharpoons C_3H_7SH + C_3H_6$	17.44	35.01
$C_4H_9-S-C_4H_9 \rightleftharpoons C_4H_9SH + C_4H_8$	17.97	35.22
$C_5H_{11}-S-C_5H_{11} \rightleftharpoons C_5H_{11}SH + C_5H_{10}$	18.06	35.96
$C_{10}H_{21}-S-C_{10}H_{21} \rightleftharpoons C_{10}H_{21}SH + C_{10}H_{20}$	18.03	35.92

The plots of Figure 6.6 are based on these values. The thermodynamic results indicate that the conditions of catalytic cracking favor the complete decomposition of sulphides to mercaptans and alkenes.

6.1.9.2 Decomposition of Mercaptans

The following reactions were selected for analyzing the behavior of mercaptans:

	(ΔH^0_{800})$_r$	(ΔS^0_{800})$_r$
	cal/mol	cal/mol·degree
$C_2H_5SH \rightleftharpoons H_2S + C_2H_4$	15.50	30.67
$C_3H_7SH \rightleftharpoons H_2S + C_3H_6$	12.66	31.63
$C_5H_{11}SH \rightleftharpoons H_2S + C_5H_{10}$	12.30	31.32
$C_{20}H_{41}SH \rightleftharpoons H_2S + C_{20}H_{40}$	12.25	31.29

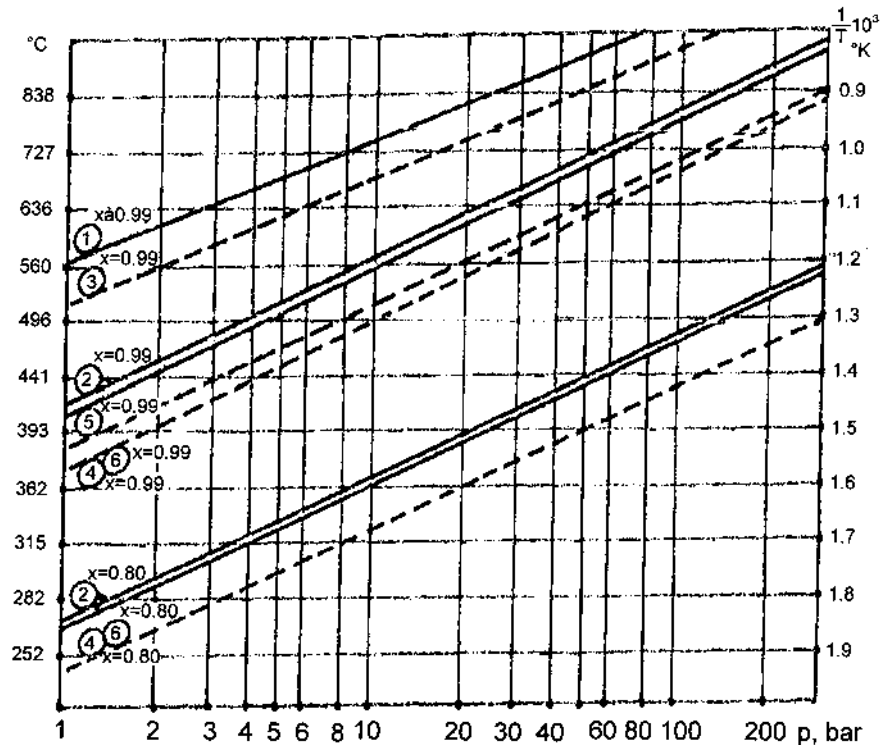**Figure 6.6** Equilibriums of sulfites decomposition to mercaptans and alkenes. The sulfites: 1. $CH_3-S-C_2H_5$; 2. $CH_3-S-C_3H_7 - - -CH_3-S-C_{19}H_{39}$; 3. $(C_2H_5)_2S$; 4. $(C_3H_7)_2S$; 5. $(C_4H_9)_2S$; 6. $(C_5H_{11})_2S - - -(C_{10}H_{21})_2S$. x – conversion in molar fraction.

Following the same procedure as in the previous cases, the parameters for thermodynamic equilibrium were plotted in Figure 6.7.

From the plotted data it results that during the catalytic cracking, the thermodynamics favor the complete conversion of mercaptans to alkenes and hydrogen sulfide.

6.1.9.3 Decomposition of the Cyclic Compounds With Sulfur

The available thermodynamic data allow the examination of the thermodynamic equilibrium of the following reactions:
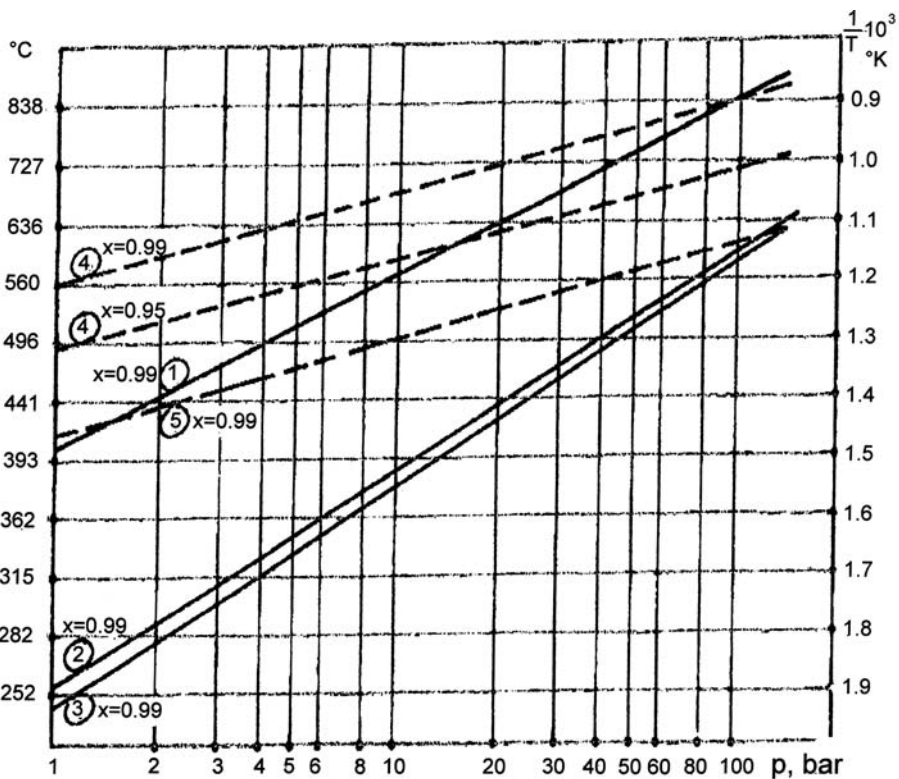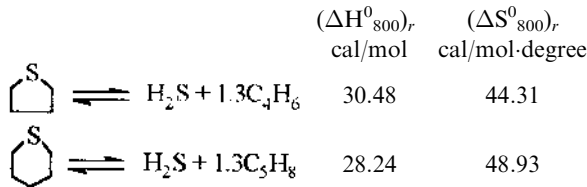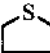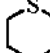
	$(\Delta H^0{}_{800})_r$ cal/mol	$(\Delta S^0{}_{800})_r$ cal/mol·degree
$\text{(thiophene)} \rightleftharpoons H_2S + 1.3 C_4H_6$	30.48	44.31
$\text{(thiane)} \rightleftharpoons H_2S + 1.3 C_5H_8$	28.24	48.93

Figure 6.7 Mercaptans and cyclic sulfur compounds decomposition equilibrium. 1. $C_2H_5SH \rightleftharpoons C_2H_4 + H_2S$; 2. $C_3H_7SH \rightleftharpoons C_3H_6 + H_2S$; 3. $C_nH_{2n+1}\ SH \rightleftharpoons C_nH_{2n} + H_2S$ for $n = 5$–20; 4. $\text{(thiophene)} \rightleftharpoons 1.3\ C_4H_6 + H_2S$; 5. $\text{(thiane)} \rightleftharpoons 1.3\ C_5H_8 + H_2S$; x – conversion in molar fraction.

The results of the calculations made on the basis of these data are presented in the graph of Figure 6.7.

It results that the cyclic compounds with sulfur are much more stable than the aliphatic compounds. Thiophen and its derivatives are even more stable.

6.1.10 Cracking of Nitrogen-Containing Compounds

6.1.10.1 Decomposition of Primary Amines

The following reactions were considered:

	$(\Delta H^0{}_{800})_r$ cal/mol	$(\Delta S^0{}_{800})_r$ cal/mol·degree
$C_2H_5NH_2 \rightleftharpoons NH_3 + C_2H_4$	12.42	30.31
$C_3H_7NH_2 \rightleftharpoons NH_3 + C_3H_6$	10.76	31.61
$C_4H_9NH_2 \rightleftharpoons NH_3 + C_4H_8$ (1)	10.58	31.59
$sec\text{-}C_4H_9NH_2 \rightleftharpoons NH_3 + C_4H_8$ (1)	13.40	34.36
$\rightleftharpoons NH_3 + C_4H_8$ (2)	11.05	31.77
$tert\text{-}C_4H_9NH_2 \rightleftharpoons NH_3 + \text{i-}C_4H_8$	12.71	33.88

These data and the plots of Figure 6.8, indicate that from a thermodynamic point of view, the primary amines are very reactive and may decompose completely at temperatures as low as 200–300°C.

6.1.10.2 The Decomposition of Diethyl- and Triethyl-amine

The following reactions were considered:

	$(\Delta H^0{}_{800})_r$ cal/mol	$(\Delta S^0{}_{800})_r$ cal/mol·degree
$\begin{matrix} C_2H_5 \\ \\ C_2H_5 \end{matrix} NH \rightleftharpoons C_2H_5NH_2 + C_2H_4$	18.26	35.49
$\begin{matrix} C_2H_5 \\ C_2H_5-N \\ C_2H_5 \end{matrix} \rightleftharpoons (C_2H_5)_2NH + C_2H_4$	18.25	38.40

These compounds are slightly more stable than the primary amines. However, their complete decomposition (99%) is thermodynamically possible at temperatures of 385°C to 322°C (Figure 6.8).

6.1.10.3 The Decomposition of Pyridine

Pyridine is decomposed according to the reaction:

	$(\Delta H^0{}_{800})_r$ cal/mol	$(\Delta S^0{}_{800})_r$ cal/mol·degree
(pyridine) $\rightleftharpoons NH_3 + 1.3 C_2H_6$	18.03	42.85

According to these data, the decomposition of pyridine is thermodynamically possible with essentially complete conversion at temperatures of above 240°C (Figure 6.8).
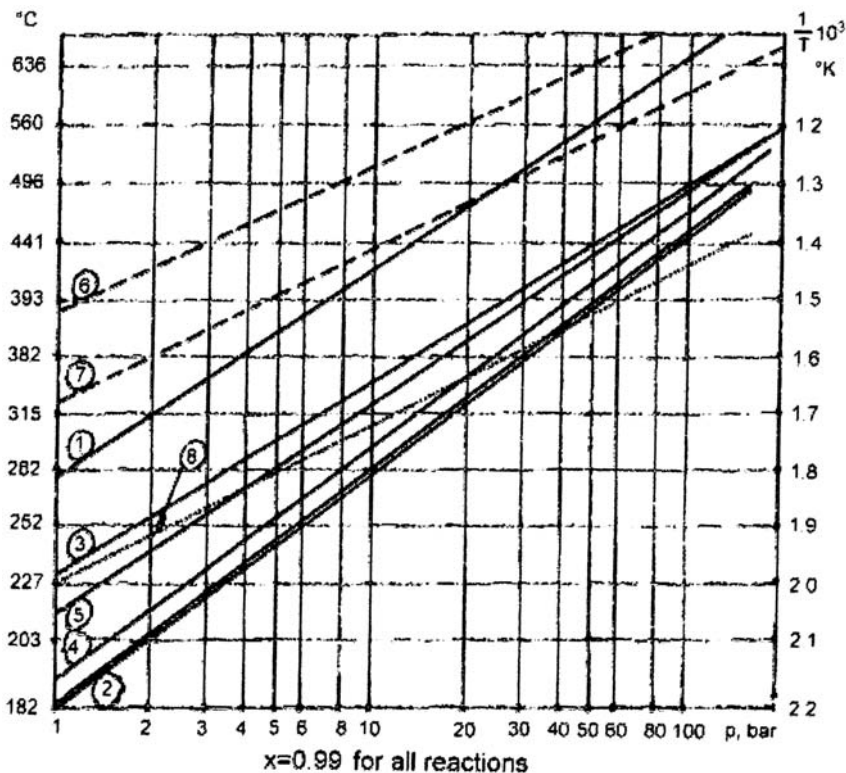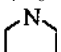
x=0.99 for all reactions

Figure 6.8 Nitrogen compounds decomposition equilibria. 1. $C_2H_5NH \rightleftharpoons C_2H_4 + NH_3$; 2. $C_3H_7NH_2 \rightleftharpoons C_3H_6 + NH_3$; or $C_4H_9NH_2 \rightleftharpoons C_4H_8(1) + NH_3$; 3. sec-$C_4H_9NH_2 \rightleftharpoons C_4H_8(1) + NH_3$; 4. sec-$C_4H_9NH_3 \rightleftharpoons C_4H_8(2) + NH_3$; 5. tert-$C_4H_9NH_2 \rightleftharpoons$ i-$C_4H_8 + NH_3$; 6. $(C_2H_5)_2NH \rightleftharpoons C_2H_5NH_2 + C_2H_4$; 7. $(C_2H_5)_3N \rightleftharpoons (C_2H_5)_2NH + C_2H_5$; 8. [pyrroline ring structure] $\rightleftharpoons$ 1,3 $C_4H_6 + NH_3$. x – conversion in molar fraction.

6.1.11 Conclusions

The above analysis of the reactions taking place in catalytic cracking allow the formulation of several conclusions on the directions of the thermodynamically possible transformations of substances in vapor phase, and of those which are adsorbed on the catalyst and lead to the gradual formation of coke.

Concerning the reaction in vapor phase, simple conclusions can be made on basis of the graphs of Figures 6.1–6.8, which take into account the process conditions in catalytic cracking reactors: temperatures ranging from 470–520°C, and pressure slightly above atmospheric.

In these conditions, thermodynamics do not limit the decomposition of alkanes and alkenes. The thermodynamic probability of decomposition is actually the same for both classes of hydrocarbons.

Also, neither the breaking off of alkylic chains attached to aromatic rings, nor the dehydrogenation of the cyclo-alkane rings of six carbon atoms to aromatic rings are limited from the thermodynamic point of view.

The cracking of the cyclo-alkane rings has a low thermodynamically probability and occurs with equilibrium conversions of only 3–15%. On the other hand, reaction conditions favor the dehydrogenation of cyclo-alkanes with 6 carbon atoms. The cyclo-alkane rings of 5 atoms will be either isomerized and dehydrogenated, or cracked. Therefore the cracking occurs with preference for the 5 carbon atoms rings.

The decomposition of alkane-thiols, dialkyl-sulphides, and alkyl-amines is not limited by thermodynamics. The sulfur-containing heterocyclic compounds and the dialkyldisulfides seem to be more resistant, but the available thermodynamic data are not sufficient for a satisfactory analysis.

The polymerization of the alkenes is essentially impossible in vapor phase, in catalytic cracking conditions. It can take place only in liquid phase or in the adsorbed layer on the surface of the catalyst.

In all the cases where the reactions are not limited by thermodynamics, the conversions of various compounds will be determined by the relative reaction rates, that is, by the kinetics of the process.

All these conclusions are in agreement with those expressed previously in other works [1,4,5] and have as their purpose only to complete and emphasize some quantitative aspects.

More complex and so far less explained is the thermodynamics of the reactions within the layer adsorbed on the catalyst. They lead to substances which are not desorbed but generate coke.

Thermodynamics show that the cracking of alkanes and alkenes, that are adsorbed on the catalyst can not exceed a conversion of 60% while the polymerization of alkenes can proceed with conversions of up to 50%. The breaking off of the side chains to the cyclo-alkanes with formation of alkenes can reach conversions of 70%. The de-alkylation of alkyl-aromatic hydrocarbons in the adsorbed layer can reach conversions of 50%. The breaking-off of side chains with formation of benzene has low thermodynamic probability. The dealkylation in the case of aromatics with unbranched side-chains leads, with thermodynamically equal chances, to the formation of toluene or of styrene. The dehydrogenation of cyclo-alkanes can exceed conversions of 99%.

These reactions that are fundamental different than those occurring in vapor phase explain fully the thermodynamically favored formation (by polymerization, dehydrogenation, and condensation reactions) of hydrocarbons with high molecular mass that do not desorb from the surface of the catalyst and lead eventually to the formation of coke.

The assumption made in the above deductions and calculations that the conditions within the adsorbed layer and those within the liquid phase are similar to those for vapors at pressures of the order of 100–200 bar seem realistic. In fact, the graphs show that the equilibrium conversions in the liquid phase are identical with those in vapor phase at pressures of the order 200–400 bar. The exact value depends on the reaction taken into consideration.

The thermodynamic analysis of the phenomena occurring in the adsorbed layer could be more detailed if thermodynamic data were available for bi- and polycyclic aromatic and naphthen-aromatic hydrocarbons and other more complex structures.

Thermodynamic analysis of the catalytic cracking of residues is much more difficult, first of all because no the thermodynamic constants are available for specific compounds contained in such fractions.

The fact that in this case the reactions take place in liquid phase allows one to extend to catalytic cracking of the residues the conclusions previously established concerning the direction of the reactions and the thermodynamic limitations that are specific to the reactions in liquid phase and in the adsorbed layer.

Thus, different from the processes in vapor phase, the decomposition reactions of the aliphatic hydrocarbons and the dealkylation of the cyclic ones will encounter thermodynamic limitations corresponding to conversions of 50–70%. The polymerization of alkenes can take place with conversions up to 50%. The dehydrogenation and possibly condensation reactions will be probably favored.

6.2 CRACKING CATALYSTS

The catalytic activity of aluminum chloride in the cracking of crude oil fractions was established in 1915–1918 by A.M. McAfee in the U.S. [16] and simultaneously by N.D. Zelinskyi in Russia [7]. Following the construction of a pilot plant at Kuzovsk [8] in the years 1919–1920, the process was abandoned owing to the excessive consumption of aluminum chloride [9].

The catalytic action of clays was discovered in 1911 by Ubbelhode and Voronin [10] and was followed by the implementation in 1928 by A.J. Houdry of their acid activation [6]. The difficulties related to the large deposits of coke on the catalyst delayed commercialization until 1936, by A.J. Houdry for Socony-Vacuum Oil. The coking problem was solved by the cyclic regeneration of the catalyst by means of burning the coke deposited thereon.

From that date on, cracking catalysts knew a rapid evolution, marked by the development and by the application at commercial scale of steadily improved types of catalysts:

1936   The use of activated natural clays
1940   The first catalyst of synthetic silica alumina (Houdry Process Corporation)
1946   First time use of microspherical catalysts
1950   Development and general use (1956) of catalysts with more than 25% Al_2O_3
1958   Development and commercialization (1960) of catalysts with 25–35% kaolin incorporated in the silica-alumina
1959   The synthesis and commercialization of Y zeolites
1962   First time use of zeolitic catalyst in catalytic cracking
1964   Inclusion of zeolite in a matrix
1964   Development of ultrastable catalysts (USY) and of those promoted with rare earths (REY)
1974   Additives of promoters for the combustion of CO to CO_2 in regenerator
1974   Additives for the fixation of SO_2 in the regenerator and its elimination as H_2S, in the reactor
1975   Catalyst passivation against nickel poisoning
1978   Catalyst passivation against vanadium poisoning
1983   Performance improvement by treating the catalyst with $(NH_3)_2SiF_6$
1986   Use of ZSM-5 – type additives for octane number enhancing
1988   Silicon enrichment by means of silicones (catalysts of the type LZ 210)[11]
1992   The experimentation in the U.S. and in Europe of the ALPHA and BETA catalysts.

Simultaneously, starting in 1980, in the U.S., residues were incorporated in catalytic cracking feed. Thus, in 1989–1990 the feed to FCC units could have 5% Conradson carbon and 10 ppm Ni + V [12]. These limits were almost doubled during the following years.

The catalytic cracking of residues poses special problems for the catalysts, mainly with reference to pore structure, passivation against poisonings, etc. The specific issues of these catalysts will be treated separately towards the final part of this chapter.

6.2.1 Activated Natural Clays

Despite the fact that activated natural clays have not been used as cracking catalysts for a long time, awareness of their characteristics is important since natural clays continue to be included in the composition of synthetic catalysts in order to reduce their cost. This technique, initially used in the production of silica alumina catalysts, is used today on a large scale in the production of zeolitic catalysts.

Montmorillonites, were the first natural clays used as cracking catalysts. They were activated by treating with diluted sulfuric acid or hydrochloric acid in order to increase the specific surface and the porosity. In the same time, the alkaline metals were eliminated together with a portion of the iron, which by reacting with sulfur compounds present in the feedstock, would decrease the activity of the catalyst [13].

Despite all the improvements brought to the activation including the use of special treatments [1], the stability of montmorillonite catalysts is insufficient and they were replaced by kaolin-based catalysts.

The kaolins, with a content of max. 2.5% Fe_2O_3, are activated by calcination in reducing medium, often in a fluidized bed in an ascendant current of flue gases, generator gas, or a mixture of methane and steam [1].

Catalysts obtained in this way have satisfactory stability and mechanical resistance.

6.2.2 Synthetic Silica-Aluminas

Silica is completely deprived of catalytic activity. The activity appears and increases after aluminum atoms are incorporated in its structure [11]. The Si–O–Al bonds that are formed confer acidity and therefore activity to the catalyst.

The first synthetic catalysts produced contained about 13% Al_2O_3.

The desire to increase the activity and the stability of the catalysts led to the production, at the end of the year 1950 of catalysts with about 25% Al_2O_3 content.

In the same time, catalysts of magnesia-silica were developed that produced higher gasoline yields with a lower octane number.

A comparison between the performances of natural catalysts and of classic synthetic ones containing aluminum or magnesium is given in Table 6.1 [14].

In order to reduce the price of the catalyst, kaolin was incorporated in its structure by dispersing 25–35% kaolin in the gel of silica-alumina. Such catalysts, called semisynthetic, were cheaper but were less active and had lesser mechanical resistance. Besides, a significant amount of unreacted products remained adsorbed on the catalyst after stripping and had to be burnt in the regenerator, which

Table 6.1 Pilot Plant Fluid Catalytic Cracking at Some Conversion on Natural and Synthetic Catalysts

Yields and gasoline quality	Synthetic catalysts		Natural catalysts	
	13% Al_2O_3	Mg-Si	Filtrol 58	Filtrol SR
C_1C_3, wt %	6.4	5.0	7.0	6.8
C_4H_{10}, vol %	9.0	5.1	6.9	7.8
C_4H_8, vol %	7.0	4.9	7.1	6.3
Gasoline, vapor tension, 517 mm, vol %	46.9	57.2	49.3	49.0
Gas oil, vol %	40.0	40.0	40.0	40.0
Coke, wt %	3.4	3.4	3.6	3.4
Gasoline ON research	93.7	90.3	89.9	92.8
Gasoline ON motor	81.0	78.6	79.2	80.5

Feed: gas oil, $d = 0.882$.

decreased the process performance. A catalyst of such a type (Sm-3-S/S) was commercialized by the firm Davidson in 1958 [14].

Socony-Mobil Co. used additions of chrome oxide for activating coke burning, a process used on large scale in the following years for the activation of zeolitic catalysts.

Several methods for the production of the synthetic silica-alumina catalysts were used [15,17]. One of the methods performs the coprecipitation of sodium silicate by soluble aluminum salts, usually aluminum sulfate. The two solutions mix by converging into a Y-junction, then discharged into a heated oil bath, obtaining a catalyst shaped as balls, or the mixture is pulverized in an oil solution to produce a microspherical catalyst.

The following steps are washing, elimination of the Na^+ ion, drying, and calcination. Details concerning this method were described earlier by the author [1].

In a variation to this method, the silica-alumina gel formed from mixing the two solutions is aged, followed by filtration, washing, and ion exchange for removing the Na^+ ion. A predrying step follows, during which various promoters are added: metal promoter for regeneration and hydrofluoric acid, or fluorides for increasing the activity [4]. Finally, the microspheric shape is obtained by the atomization of the catalyst slurry in a rising flow of warm air.

Still, another method impregnates the silica hydrogel with a solution of aluminum sulfate followed by hydrolysis and the precipitation of aluminum with an aqueous ammonia solution. The resulted silica-alumina hydrogel is washed, dried, and calcined [18].

The catalysts obtained by all the above methods have a content of about 13% Al_2O_3. An increase of the Al_2O_3 up to 25–30% is obtained by impregnation with soluble aluminum salts, precipitation with ammonia, washing, drying, and calcination.

6.2.3 Nature of Acid Sites

From the facts presented in the previous paragraph one may deduce that the catalytic activity of synthetic silica-alumina is due to the simultaneous presence of aluminum oxide and silicon oxide in a structure obtained by concomitant precipitation or by the formation in other ways of a mixed gel that contains both oxides.

The silicon dioxide has a tetrahedral structure with the oxygen atoms occupying the vertices of the tetrahedron, while those of silicon, the centers. The inclusion in the network of aluminum atoms, by the substitution of some of the tetravalent silicon atoms by trivalent aluminum atoms results in negative charges at the aluminum atoms. These are compensated by sodium cations, which were contained in the salts used for preparing the hydrogel (Figure 6.9).

The sodium cations are exchanged by ammonium cations. During the calcination step, the latter are decomposed, releasing ammonia, while the protons remain in the oxide lattice and constitute the acid centers, which are catalytically active.

The acid properties of the silica-alumina catalysts were first noticed by Gayer in 1933, while the explanation of the inclusion of the aluminum atoms in the tetrahedral network of silicon dioxide was given by Ch. Thomas in 1949 [19]. The acid character of natural clays was demonstrated as early as in 1891 by V.I. Vernadski [20].

Despite the agreement that prevails concerning the acid character of the silica-alumina catalysts, the structures that confer this character are still debated.

Several of the proposed representations for the acid sites of silica-aluminas are depicted in Figure 6.10. The representation of Figure 6.10a corresponds to the structure imagined by Ch. Thomas, described previously but which was not confirmed by spectroscopic studies.
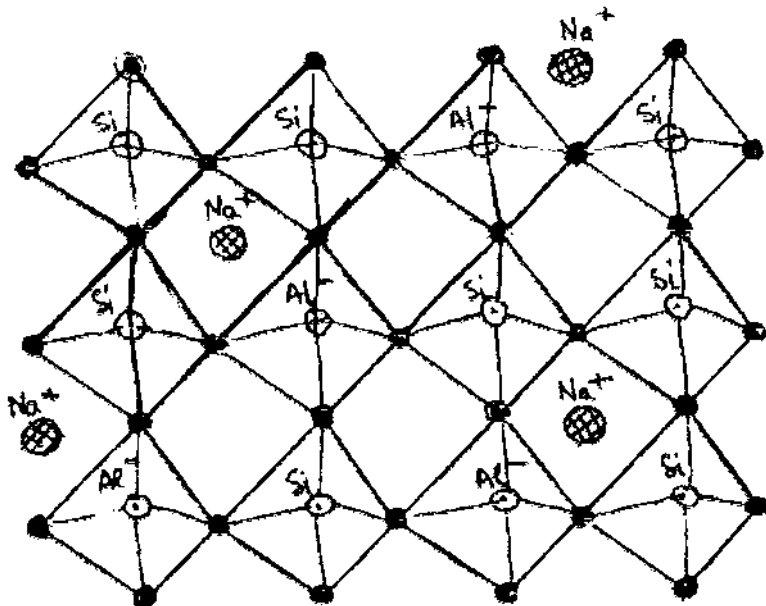

Figure 6.9 Alumo-silica gel structure. ● = Oxygen atoms.

Much more probable are considered the crypto-ionic forms, isomers of structure **a** of Figure 6.10, in which the aluminum and the silicon atoms or only the silicon atom are bound to acid hydroxyl groups (Figures 6–10b and c), susceptible to behave as hydrogen donors, thus as acids of the Brönsted type. The electronic deficiencies of the trivalent aluminum atoms contained in structures of the type of Figure 6.10c can generate acid centers of the Lewis type, Figure 6.10d. There are other representations, related to defects in the network of tetrahedrons, which explain the presence of the acid centers on the surface of silica-alumina [4], and still other representations concerning the possible structures of the acid centers [8].

The existence of both types of centers was experimentally proven by using the chemisorption of 2,6-dimethyl-pyridine and of the Hammett indicators, with the determination of the corresponding adsorption isotherms [21]. The fact that the 2,6-dimethyl-pyridine is adsorbed preferably on Brönsted centers and after heating to 380°C remains adsorbed exclusively on these centers, whereas the Hammett indi-
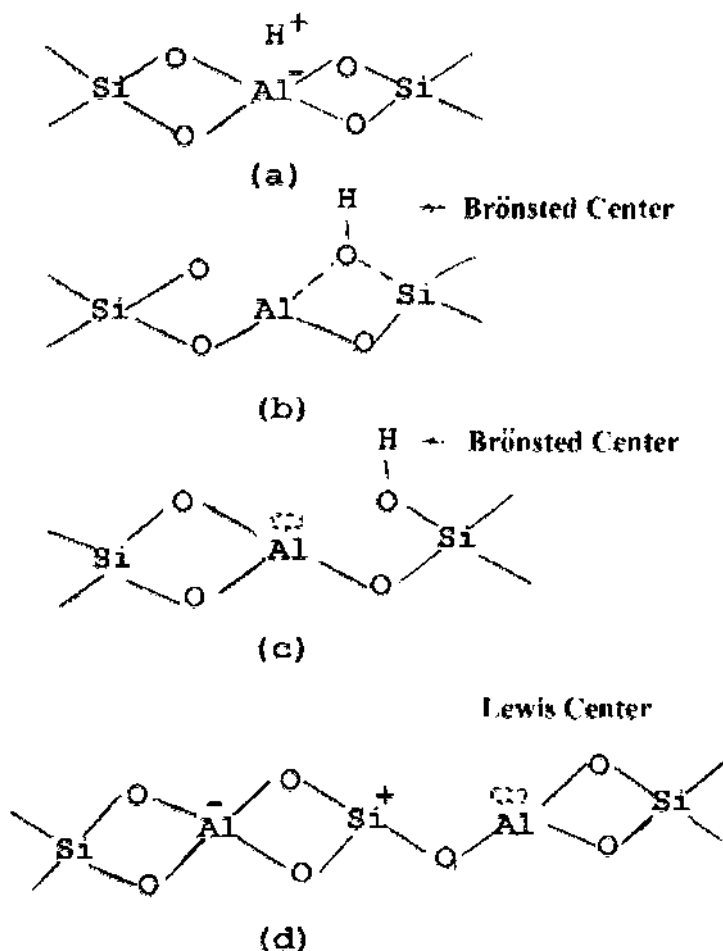

Figure 6.10 Opinions about alumo-silica acid centers. (From Ref. 4.)

cator is adsorbed on both (Lewis and Brönsted) types of acid centers, made possible their separate identification. From the adsorption isotherms the distribution of the acidity of the centers was determined. The conclusion was reached that both types of acid centers, are present: the Brönsted proton centers show a broader distribution of the acidity, while the aprotic centers of the type Lewis have a narrower one.

6.2.4 Zeolite Catalysts

Catalysts containing Y zeolites were first introduced in 1962 by Mobil Oil Co. and found widespread utilization. They displaced completely the natural and synthetic catalysts used previously*.

The properties and the performance of zeolitic catalysts has undergone continuous improvements with respect to the synthesis of zeolites, to the matrices used, to the additives, and to improvements by means of treatment of the produced catalyst. This activity goes on at a fast pace and is the object of a considerable number of publications and patents.

The characteristics of the zeolitic catalysts, the methods used for their improvement, and the additives used are closely tied to the nature of the process and the operation conditions of the fluid catalytic cracking. For a more ample documentation in the domain of the zeolites, the monographs published by J. Scherzer [6] and B.C. Gates [22] are recommended.

The catalysts for catalytic cracking on the basis of zeolites contain several components:

The zeolite Y, usually together with rare earths oxides

The matrix which may be inert or catalytically active

The promoters and additives that improve the performance of the catalyst and that may be introduced during the actual synthesis of the zeolite or of the matrix.

6.2.4.1 The Zeolite

The zeolite is mainly responsible for the activity, selectivity, and stability of the catalyst.

Among the synthetic zeolites the faujasites X and Y, the ophertites, the mordenites, and the erionites showed catalytic activity in the cracking process. Among these only the first two, but especially the faujasites Y which has a superior stability, have been used for the production of cracking catalysts. Thus, a catalyst of the classic type such as faujasite Y, which was submitted to ionic exchange with rare earths, preserves its crystalline structure after treatment during 12 hours with 20% steam at a temperature of 825°C, whereas a faujasite X prepared in the same way loses its crystalline structure after this treatment [11].

The basic structure of the zeolites X and Y is, as in classic synthetic catalysts, formed by groups of tetrahedrons with the aluminum and silicon atoms occupying their centers and the oxygen atoms the vertexes. In the case of zeolites, the groups of tetrahedrons form in fact regular structures of stumped octahedrons, known under

---

* In 1968, 85% of the catalytic cracking plants in the U.S. and Western Europe used catalysts on the basis of zeolites. Today, zeolites are used exclusively.

the name of *sodalite cage*. Each sodalite cage has 8 hexagonal sides, constructed of 6 tetrahedrons and 6 square sides constructed of 4 tetrahedrons, 24 vertexes and 36 edges (see Figure 6.11a).

The A-type molecular sieves have the basic element formed of four sodalite structures, the square faces of which are joined by prisms (see Figure 6.11b). In the type X- and Y-zeolites, the basic element is formed of six sodalite structures, the hexagonal faces of which are joined by prisms (see Figure 6.11c).

As a result of this difference in their structures, the cavities inside the X and Y zeolites have a mean diameter of 13 Å that communicate with the outside through 7.4 Å openings, whereas the type A molecular sieves have the inlet openings of 3 Å for the potassium form and 4 Å for the sodium form.
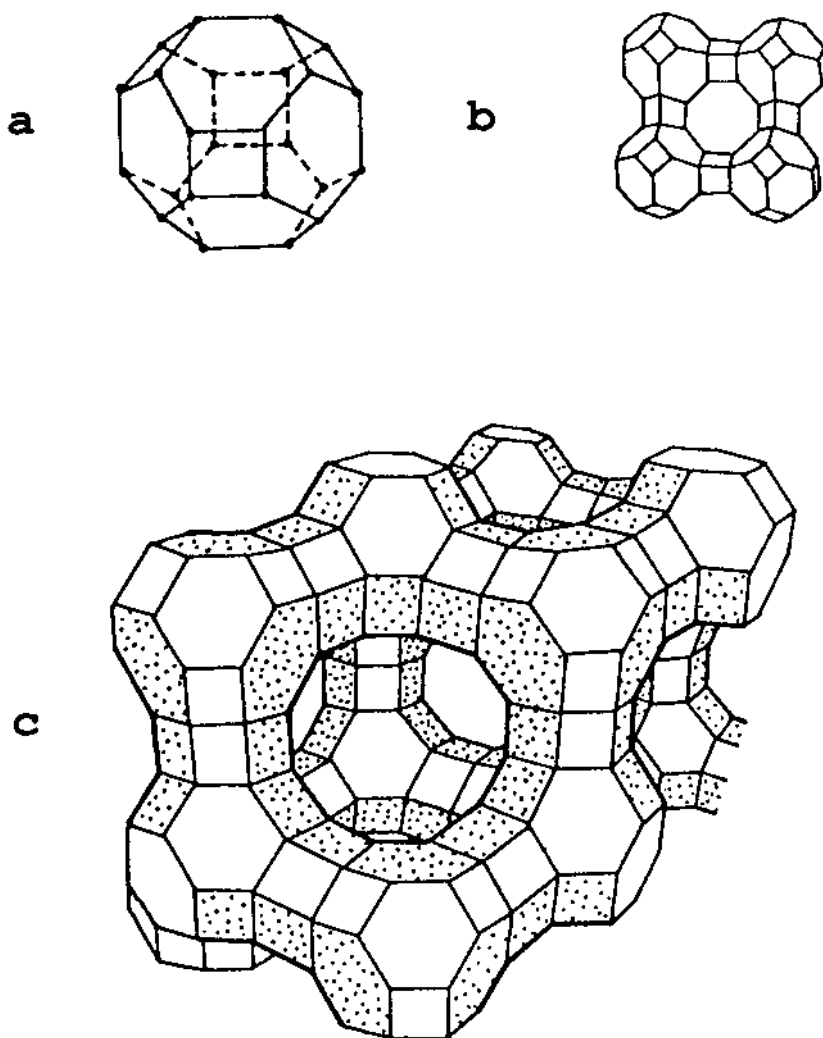

Figure 6.11 Structure of zeolites. a – sodalite, b – molecular sieve A, c – faujasite.

The inlet orifices in the X- and Y-zeolites allow the access of naphthalene molecules, whereas the type A molecular sieves allow exclusively the access of *n*-alkanes. Thus, basically the hydrocarbons contained in the atmospheric gas oil and the vacuum gas oil have access to the acid centers situated inside the cages of the X- and Y-zeolites.

Figure 6.12 [23] shows the sizes of the cavities and of the access openings of various types of zeolites, together with the necessary size for access through the pores of different types of hydrocarbons. This allows a more detailed examination of the size restrictions that can occur.

The raw formula of an elementary cell of a X- or Y-zeolite can be written as:

$$Na_n\left[(Al_2O_3)_n(SiO_2)_{192-n}\right] \cdot mH_2O$$

wherein *m* is approx. 250–260, and *n* has values ranging from 48–76 for Y-zeolites and between 77–96 for X-zeolites.

The study of zeolites by X-ray diffraction and by nuclear magnetic resonance, allowed the determination of the location of the cations that compensate the negative charges of the AlO_4-tetrahedrons. These locations are shown in Figure 6.13 [13]. Four types of acid sites exist, depending on the location they occupy within the crystalline structure of the faujasite: Sites I are situated inside the hexagonal prisms and I′ are situated inside the sodalite cages; sites II are situated inside the internal cavity of the zeolite in the proximity of the free hexagonal opening, while II′ is located farther from these orifices.

It is easy to ascertain that sites II and II′ being easy accessible, are strongly involved in the catalytic reactions, whereas sites I and I′, being accessible with difficulty, have a more reduced catalytic role.
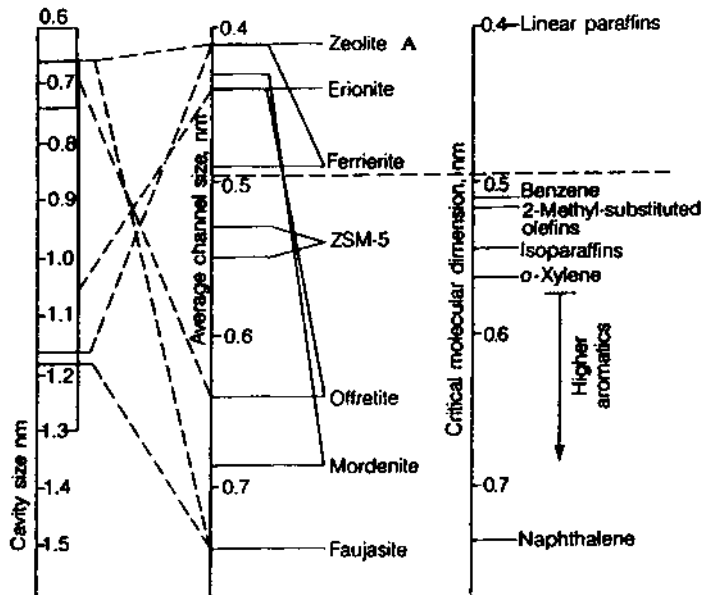

Figure 6.12 Cavities and orifices size, compared to molecules size (From Ref. 23.)
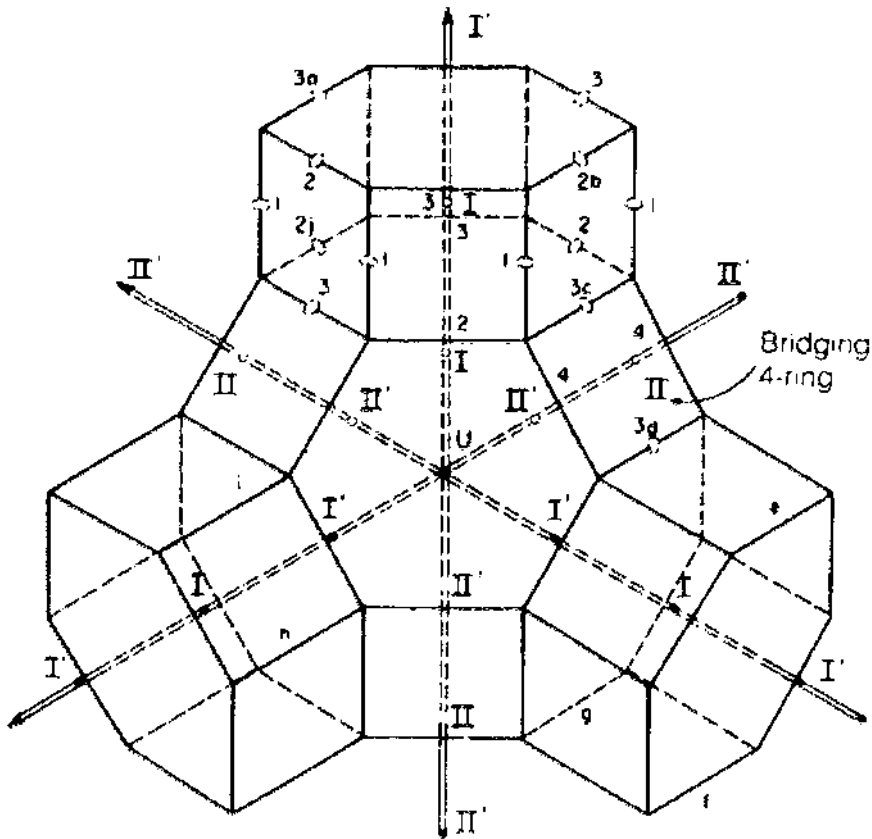
Figure 6.13 Positions of acid centers within elementary faujasite cell.

The synthesis of the X- and Y-zeolites is the object of a large number of publications and patents [24–35]; the examination of these methods of production exceeds the frame of the present book.

In principle, the zeolites of type Y are obtained by coprecipitation, starting from solutions of sodium silicate and aluminate in a strong basic medium (pH = 12–13) of the aluminosilicate gel. Maturation takes place during 5–10 hours at temperatures of 100–125°C, followed by filtration, washing, and drying at a temperature of about 150°C. The characteristics of the obtained zeolite depend to a large extent on the initial concentration of the solution of sodium silicate, on the amount of acid added to cause the gelation, on the manner and the conditions in which the aluminum salts are added, as well as on the conditions, the duration, and the maturation temperature.

Finally, the zeolite is obtained as sodium salts, which, contrary to the amorphous synthetic alumo-silica catalysts, possess an intrinsic catalytic activity. Ion exchange is necessary in order to increase activity.

Ion exchange for replacing sodium by ammonium, followed by its decomposition with elimination of ammonia, as practiced in the case of amorphous synthetic

catalysts, cannot be applied for many zeolites. During such a treatment, the zeolites tend to decompose and to lose their crystalline structure.

As a result of this situation, the zeolite catalysts of high activity are obtained by substituting bivalent cations (Ca, Mg, Mn), but especially trivalent cations such as the rare earths for the sodium ions. The polyvalent ions contribute to the stabilization of the crystalline network, which becomes resistant to the prolonged exposure to temperatures of 850–900°C. Concomitantly, they contribute to the formation of strongly acidic sites that catalyze intense cracking reactions. The mechanism proposed for explaining these phenomena is given in Figure 6.14 [4]. As result of the ion exchange between the trivalent cation and the negative charges of the aluminum atoms important bipolar moments are formed, together with the generation of intense electric fields. The electrical induction, produced by these fields modifies the electronic distribution, emphasizing the acidic character of the active catalytic sites.

As result of the treatment with rare earths, the catalysts on the basis of Y-zeolites will acquire a much higher number of acid sites of stronger acidity than the amorphous synthetic alumo-silicate catalysts. Nevertheless, these differences cannot explain fully the much higher activity of the zeolite catalysts. But what is actually important is that by using the proper synthesis method and by making use of the ion exchange with rare earths, the resulting catalysts are up to 10,000 times more active than the amorphous, synthetic alumo-silicates.*

6.2.4.2 Matrices and Binders

There are two main reasons that determine the use of matrices in which zeolite is incorporated. First, the excessive catalytic activity of the zeolites makes them unsuitable for use in units designed for conventional catalysts. The enormous difference
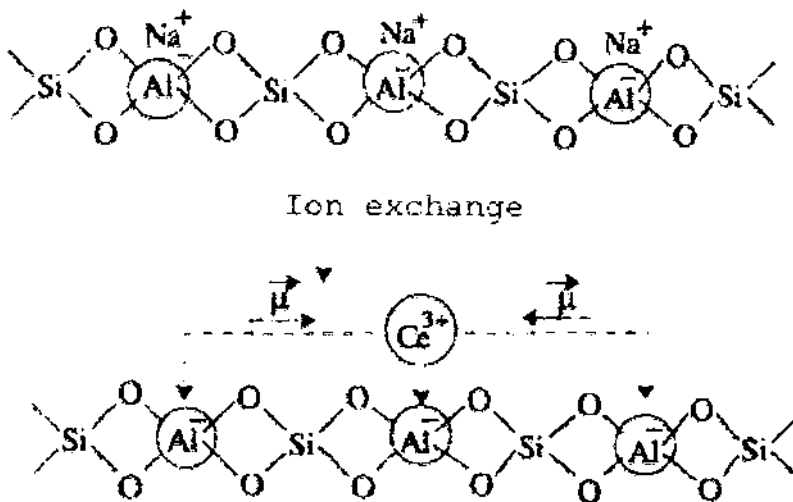

Figure 6.14 Catalyst active centers following sodium substitution by cerium. (From Ref. 4.)

---

* For comparison of activity the test of cracking of *n*-hexane was used.

between the activities of the two types of catalysts would require profound modifications to the working conditions and an expensive retrofitting of the units. The second reason is the relative high cost of the zeolite, which, owing to the losses by erosion would increase operation expenses. By incorporating the zeolite in a matrix, the cost of the catalyst is reduced by approximately a factor of 15 relative to the price of the zeolite while also obtaining a catalyst resistant to attrition.

The zeolite is incorporated into the matrix at a rate of 5–16%, as particles having a mean diameter between 2 and 20 μ. The matrix consists of solid particles, which may be natural components such as kaolin, or synthetic components. It represents 25–45% of the total weight of the catalyst. The balance is the binder, which ensures the uniform dispersion of the components within the catalyst particle, the final shape of the particles, and to a large extent, its resistance to attrition.

Recent studies [237] recommend to reduce the size of the zeolite crystals to 0.1 μ. A reduction in size from 1 μ to 0.1 μ increased the reaction rate and produced a gasoline with more alkenes and less aromatics [237].

The matrix may or may not have its own catalytic activity.

The molecules of gas oils with distillation end points below 480°C can pass through the 7.4 Å openings of the pores of the zeolite and therefore they will crack at the active sites within them. In this, the matrix does not have to possess its own catalytic activity and inert matrices are used.

Quite different is the situation of feeds with distillation end points in excess of 490°C, the heavy components of which have kinetic diameters of 10–100Å. Since these cannot enter the pores of the zeolite, and since the accessible active sites on its outer surface represents only about 3% of the total, it is necessary that the matrix is catalytically active on its own.

The catalytic activity of the matrix should not exceed the level required by the initial decomposition of the heavy molecules. The products generated in this first decomposition will diffuse into the pores of the zeolite where the reaction will continue on the catalytic sites. This will ensure improved selectivity (see Chapter 6.3).

The catalytic activity of the matrix may be due to the solid particles used for its production or to the binder.

The clays, which are usually the solid particles used, may be catalytically active or not, as discussed in Section 6.2.1, describing the natural catalysts. They may become catalytically active after the treatment to which the produced catalyst is submitted.

An example of a catalyst with a catalytically active matrix is that containing pseudo-boehmite [36]. This, at temperatures in excess of 320°C, is transformed into a form γ, very active, which possess both acid sites and hydroxy groups.

If the solid material used as a matrix is the only one having catalytic activity, the desired level of catalytic activity may be ensured by using adequate proportions of catalytic active material and inert material.

The binder may also be catalytically active. Thus, in the time period 1960–1972 the zeolite was incorporated in alumo-silica gels that had the composition of amorphous catalysts. Later on, the used mixtures of such gels with clay were similar to those used for the production of the amorphous semisynthetic catalysts.

At present, matrices containing a catalytically active binder are no longer in use [37]. Instead, catalytically inactive silica hydrosol is used, which ensures an improved

resistance to attrition and a better selectivity for the produced catalysts. The better selectivity is the result of the fact that the cracking reactions will take place exclusively on the zeolite when the matrix is made of inert materials, or mostly on the zeolite when the presence of heavy fractions in the feed requires that the matrix also possess a catalytic activity.

The compositions and properties for several typical matrices are given in Table 6.2 [37].

Detailed information concerning the preparation and characteristics of matrices produced by various methods and using various binders are given in J. Scherzer's monograph [6].

In all cases, the matrices must possess sufficient porosity and pore size distributions to allow the access of the reactants to the zeolite particles and, if necessary, also the transport of the molecules with large kinetic diameters, including liquid components.

Moreover, the matrices often ensure completion of the ionic exchange within the catalyst by supplying the di- or trivalent ions that will substitute the sodium ions that are still contained in the catalyst. The matrix may also fulfill functions related to the presence in the feed of some elements or complexes that are poisons for the zeolite. Thus it may react with the nitrogen contained in the feed [41] or it may increase the resistance of the catalyst to metals, especially vanadium [42], by fixing it. In this way, the zeolite is protected from the damaging effects upon its structure caused by such elements present in the feed. Matrices that contain active alumina may reduce SO_2 and SO_3 emissions from the regeneration gases [43]. Also, the matrix may contribute to the increase of the cetane number of the gas oil. It does this by increasing the aliphatic character of the feed by the decomposition in an adequate manner of the heavy molecules contained in the feed, by performing their cracking on its the active centers.

Table 6.2 Properties of FCC Matrices

Description	Microactivity of steamed matrix*	Attrition Davison index (DJ)	Apparent bulk density (g/cm^3)	Year of matrix technology commercialization
Alumo-silica gel (14% Al_2O_3)	35	40	0.50	1963
Alumo-silica gel (25% Al_2O_3) and clay	35	35	0.52	1965
Silica hydrosol and clay	10	6	0.77	1972
Silica hydrosol with increased matrix activity	25	6	0.76	1978
Alumina sol and clay	25	5	0.80	1980
Clay based XP	58	4	0.72	1986
Silica hydrosol with novel matrix chemistry	25	6	0.76	1990

* Steamed 6 hours at 1400°F (760°C) 100% steam 5 psig (1.35 bar).
Source: Ref. 37.

6.2.4.3 Additives

The additives are used for promoting some of the reactions, such as the burning of the coke deposited on catalyst or for the passivation of the damaging action of some compounds contained in the feed.

Additives may be added to the system in a number of ways:

As solid particles that have the same characteristics of fluidization as the used catalyst.

A liquid additive may be added directly to the system or in mixture with the feed.

Additives may be introduced during the preparation of the catalyst.

All these methods are used in practice. The selection depends on the type of additive required and on the method developed for its use.

Improvement of the combustion within the regenerator. The improvement (promotion) targets a more complete burning of carbon monoxide to carbon dioxide. In this way, a larger amount of heat is produced in the regenerator and the amount of coke necessary for maintaining the thermal balance of the reactor is reduced. A detailed analysis of the effect of the promoter on the thermal balance of the system reactor/regenerator and on the performance of the process was published [44].

To promote the oxidation of carbon monoxide, small amounts of noble metals, especially platinum, have been added [45–47]. Chromium oxide was introduced for use as a promoter in an amount of 0.15% by weight in the zeolite catalyst [48], a process which was abandoned owing to the toxicity of the chromium salts.

Studies [48] on the amount of platinum and on the way it is introduced in a zeolite catalyst lead to the conclusion that 1 mg platinum per kg of catalyst is sufficient. The results of tests carried out in two industrial catalytic cracking units, nonpromoted and promoted catalyst, showed an increase of the CO_2/CO ratio from 0.9 – 1.0 for the nonpromoted catalyst, to 5.0 – 7.0 for the promoted one [48].

Similar results were obtained by the promotion of the catalyst spheres used in a moving bed catalytic cracking unit [49].

Reduction of the content of SO_2 and SO_3 in the regenerator flue gases. Such a reduction, very important for the protection of the environment is performed by means of reacting the SO_2 and SO_3 to produce sulfite, respectively sulfate, by interaction with a metallic oxide or hydroxide, within the regenerator. The sulfite and the sulfate are carried by the regenerated catalyst to the reactor and stripper, where they are reduced to H_2S. This is captured without difficulty from the reaction gases.

The additives used for this purpose are compounds of aluminum and magnesium [50] and they are generally protected by patents [51].

Considering aluminum hydroxide as the active component, the reaction of sulfur dioxide in the regenerator can be written as:

$$2Al(OH)_3 + 3SO_2 \rightarrow (SO_3)_3Al_2 + 3H_2O$$
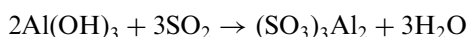
and the reduction of the aluminum sulfite in the reactor and in the stripper as:

$$(SO_3)_3Al_2 + 9H_2 \rightarrow 3H_2S + 2Al(OH)_3 + 3H_2O$$
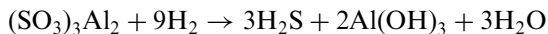
The reactions involving sulfur trioxide may be written in a similar manner.

The reduction of the content of nitrogen oxides from the flue gases. The elimination of nitrogen oxides from the combustion gases is more difficult than that of the sulfur oxides and until the present could not be solved by incorporating additives in catalyst formulation [6].

The adopted solution is to reduce the nitrogen oxides with ammonia, in the presence of a catalyst, to nitrogen and water [12] at 300–400°C. By using 0.6–0.9 moles NH_3 per mole of NO_x, 60–80% of the nitrogen oxides were eliminated; the resulting gases contained 1–5 ppm by volume of NH_3.

A very active catalyst (S-995) was developed recently by Shell; it allows the reduction of nitrogen oxides at a much lower temperature (150°C).

The passivation against nickel poisoning. The organo-nickel compounds contained in the feed lead to deposits of nickel, especially on the external surface of the catalyst particles. Owing to the dehydrogenating activity of the nickel, such deposits will increase the amount of coke and of gases on account of gasoline.

In the past, to fight against this effect the units with moving bed were operated in conditions in which the surface of the granules was eroded in the process; in this way a great proportion of nickel was eliminated [1]. Later on, zeolite catalysts with a high content of zeolite were used, which are less sensitive to poisoning [52].

The passivation of the dehydrogenating activity of nickel was shown to be more efficient. To this purpose, organometallic complexes of antimony and bismuth were added to the feed [52], beginning in 1977 and 1988 [50], respectively. Bismuth is generally preferred because it has a lesser toxicity. Also, the use of zirconium as a passivator was suggested, by adding to the catalyst of $ZrO(NO_3)_2$ [53].

The mechanism for the action of these promoters is not clear yet.

The passivation against poisoning with vanadium. The damaging action of the organo-vanadium compounds contained in the feed is manifested by the destabilization of the crystalline structure of the zeolite. It is supposed [54] that this destabilization is due to the formation of some compounds of zeolite-VO_4 that weaken the crystal structure, especially during the stripping of the catalyst.

Initially, calcium and magnesium were used [55]. Starting in 1980, tin [50] was used as a passivator. The passivation with tin must be made carefully, since if the amounts of tin necessary for passivation are exceeded, the opposite effect is produced.

The treatment of the catalyst with lanthanum chloride ($LaCl_3$) [53] was suggested as protection against poisoning by vanadium. This proposition does not seem to be applied commercially.

Compounds of bismuth and phosphor [6] were also suggested as passivation agents. It seems that iron also has a poisoning effect, which is however much less pronounced in comparison with nickel and vanadium.

6.2.5 Ultrastable Catalysts

Ultrastable zeolite catalysts are obtained by increasing the Si/Al ratio in the classic synthesis of zeolite catalysts Y. By increasing this ratio, the number of acidic centers is decreased while their acidity is increased. The decrease of the number of sites is the consequence of eliminating the trivalent aluminum atoms included in the network of tetrahedrons, which explains the increase of the stability of the crystalline network and therefore of the stability of the catalyst. The increase of the acidity of the remaining centers leads to the decrease of the role of the hydrogen transfer reactions and from here to the increase of the octane number of the gasoline [11].

It is to be remarked that the zeolites with a Si/Al ratio above 6 (the conventional Y-zeolites have a ratio of 5.0–5.5) obtained by direct synthesis are unstable products. The only way to obtain a Y-zeolite with a higher Si/Al ratio is by enriching in silicon a conventional catalyst [6].

A number of methods were developed for increasing the Si/Al ratio of a conventional Y-zeolite and obtaining ultrastable Y-zeolite, called USY-zeolites, which keep their structure intact up to temperatures of 1000°C.

The first method used [56] involves the stripping of the NH_4Y zeolite at temperatures of the order 760°C, which leads to the hydrolysis of the $Si-O-Al$ bonds with the corresponding decrease of the number of tetrahedrons wherein the aluminum occupies a central position. The alumina rests that are left behind act as non-selective catalytic agents.

A number of methods involving chemical treatment followed, that were used in combination or not with the hydrothermal treatment described above. These methods eliminate a portion of aluminum, with or without an introduction of silicon. To the first category belong treatments with F_2, $COCl_2$, BCl_3, or with a solution of NH_4BF_4, to the second category the treatment with a solution of $(NH_4)_2SiF_6$, or with vapors of $SiCl_4$ [6].

The treatments that involve the introduction of silicon achieve the substitution of aluminum atoms in the network with silicon atoms and are superior.

More extensively used is the treatment with a solution of ammonium fluorosilicate [57,58]; the aluminum is eliminated as soluble ammonium fluoro-aluminate:
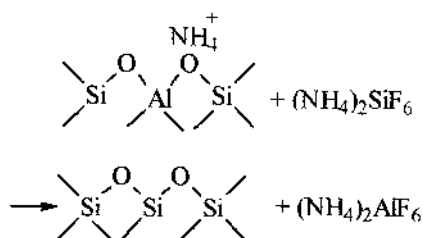
However, not all the aluminum eliminated from the network is replaced by silicon. Thus, vacant places remain within the network. Eventually, zeolites are obtained with a ratio Si/Al = 12, marked usually in the literature as zeolites AFSY. The increase of the ratio Si/Al over the value of 12 leads to zeolites that are unstable, owing to the excessively high proportion of vacant sites remaining in the network.

The improvement of the treatment method with ammonium fluorosilicate leads to the production by Union Carbide Co. and Catalystics Co., of the zeolite LZ210

(perfected subsequently as LZ210K [59]) and of the series of HSZ (High Stability Zone) catalysts. The Si/Al ratio can reach values of 10, 20 or 30 creating a broad flexibility in the performances of catalyst. It seems that the refinements that were implemented consist in the treatment of the zeolite in which the ammonium ion exchange was only partially completed with a solution of ammonium fluorosilicate at a rigorously controlled pH-value. The main problem encountered is that aluminum is eliminated from the crystalline structure faster than the silicon can replace it. This leads to cavities and to the weakening of the network. It seems that this deficiency was avoided by acting on the following factors [6]: a) the pH-value was increased to the range 3–7 and the concentration of ammonium fluorosilicate, which reduces the rate of aluminium elimination, was reduced somewhat; b) the increase of the reaction temperature, which increases the inclusion rate of silicon in the network. The regulation accordingly of these factors allows therefore improvement of the stability of the produced zeolite and the increase of the Si/Al ratio. Following these refinements, several series of catalysts were produced that show high octane improving performance, especially for the series ALPHA and BETA, which are amply described [11].

6.2.6 Octane-Enhancing Catalysts and the C_4 Cut

The superior octane performances of the ultrastable catalysts are usually enhanced by the use of ZSM-5 additions.

In fact this is a zeolite having a completely different structure than the Y-zeolites and possessing its own catalytic activity. Thus, ZSM-5 is used as a catalyst in the processes of xylenes isomerization, disproportionation of toluene, in the production of ethyl-benzene [60], and in the processes for dewaxing of distillates [61].

In catalytic cracking ZSM-5 is used as H-ZSM-5, but also as Zn-ZSM-5 and Cd-ZSM-5. It could be used under the form of separate zeolite particles, in which case it is included in a proportion of 25% in an inert matrix or could be included in the catalyst particles.

Detailed results concerning the effects of the addition of ZSM-5 are available from several published papers [6, 62, 234, 235, 236]. Overall, the increase of the octane number as a result of using ZSM-5 is accompanied by a decrease of the gasoline yield. In alkylation, this decrease is compensated by the increased production of alkylate as a result of the larger amounts of *iso*-butane produced. It seems that the size of the ZSM-5 particle has an important influence on the distribution of products [236].

There has been great interest in recent years in increasing the amount of *iso*-butylene produced in catalytic cracking. New catalysts, such as IsoPlus 1000 of Engelhard were developed for the special purpose of producing increased amounts of *iso*-butene [35]. Initially, *iso*-butene served for the production of methyl-*tert*-butylether (MTBE), the addition of which to gasolines was considered indispensable, for satisfying the clean air regulations in many countries. (see Chapter 9).

The comparative performance of a typical USY catalyst, IsoPlus 1000 and IsoPlus 1000 containing 3% ZSM-5, was determined in a high performance UOP cat cracker of the riser type. Compared to the standard USY catalyst the increase in *i*-butylene was of 0.57% and of 0.84% for the IsoPlus 1000, respectively without and

with ZSM-5. These effects correspond to an increase of about 50% of the MTBE potential [35].

Extensive research work currently underway will result in cracking catalysts of improved performance tuned to the selective synthesis of the products of high market demand. The interest in producing *iso*-butylene outlived the interest in MTBE and is kept alive by the increasing needs for alkylate gasoline.

6.2.7   Catalysts for Residue Cracking

The incorporation in the distillates fed to the cat crackers of up to 20% residual fractions does not require any change in the units; it was practiced in the U.S. since 1988 in 40% of catalytic cracking units. Catalytic cracking of the residues is covered in Chapter 7.

The inclusion of residues in the feed to cat crackers makes necessary the use of catalysts that are capable of handling the increased metal content and the larger sizes of the molecules within the feed. Thus, fractions with boiling temperatures of above 540°C contain molecules with more than 35 carbon atoms and sizes ranging from 10–25 Å. The vacuum residues contain molecules with molecular masses between 1,000–100,000, the sizes of which vary between 25–150 Å [63].

These dimensions require that the matrix used for the preparation of the catalysts for residue cracking has a certain structure and distribution of the pores, as well as an adequate ratio between the catalytic activity of the matrix and that of the zeolite. In order to correctly understand the issues at play here, it must be taken into account that molecules with kinetic diameters larger than those of the pore orifices (7.4Å) cannot penetrate the pores of the zeolite. The compounds contained in the vacuum gas oils or in residues, with the exception of *n*-alkanes, or of slightly branched *i*-alkanes, cannot be cracked on the active sites within the zeolite, but only on the active sites of the matrix. The products resulting from first-step cracking on the active centers of the matrix can penetrate in the pores of the zeolite, where the cracking is continued and gasoline is formed. Cracking on the active sites of the matrix should not exceed the conversion required for the formation of products having dimensions that allow them to penetrate inside the pores of the zeolite. Here, the cracking will continue in conditions of shape selectivity, ensured by the pores of the Y-zeolite.

The catalysts used in the cracking of residual fractions should show a certain optimal ratio between the catalytic activity of the zeolite and that of the matrix. In a first approximation, this can be expressed by the ratio of the respective specific surfaces. A decrease of this ratio, which means a too high activity of the matrix, leads to the increase of the conversion to dry gases (H_2, C_1, C_2) and to coke (see Figure 6.15) [64].

Another problem, of equal importance is the distribution of the pore sizes of the matrix. The matrix must possess [62]:

1.   Large pores with diameters over 100Å. They allow traffic of components with large molecular mass, that remain liquid at the reaction temperatures. The acid sites on the walls of these pores should possess a low catalytic activity for the limitation of the conversion until gases and coke.

2.   Pores of average size, with diameters ranging between 30–100Å. These pores have a more pronounced catalytic activity. Their role is to produce first-
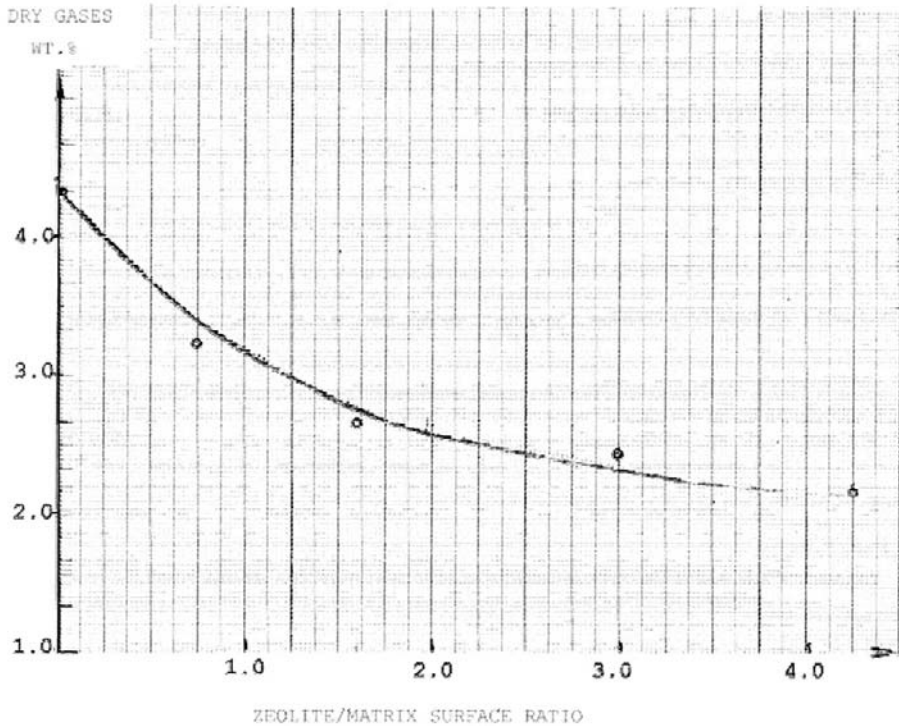
Figure 6.15 Conversion to dry gases function of zeolite/matrix surface ratio. Catalytic cracking at 500°C of a vacuum distillate $d = 0.9188$, $F_{\mathrm{UOP}} = 11.5$. (From Ref. 64.)

pass cracking of the heavy components, especially of naphthenes and of aromatic rings.

3.   Pores of small sizes below 20Å, have the most pronounced catalytic activity. Their role is to crack the light components possessing prevalent alkane structures but cannot penetrate through the orifices of the zeolite particles.

The ratios in which the three types of pores should be present depend on the ratio between the various cuts incorporated in the feed and chemical composition of the feedstock.

Of special concern is the high content of vanadium and nickel in feeds of residual origin. These metals are retained by the matrix in order to prevent their penetration inside the zeolite.

The vanadium is captured by tin compounds, by barium and strontium titanates, and by magnesium oxide, substances that in most cases are supported on inert particles.

The passivation of vanadium is done by means of antimony or bismuth compounds supported on the catalysts or introduced in the feed.

The reduction of sulfur oxides is performed by means of cerium or rare earths that may be incorporated in the catalyst, may form distinct particles, or may be supported on alumina by the spinel $(\mathrm{Mg \cdot Fe})\mathrm{O}(\mathrm{Al_2Fe})_2\mathrm{O}_3$ or by cerium supported on the spinel.

The catalysts used for the conversion of carbon monoxide to carbon dioxide during the regeneration use platinum or palladium supported on alumina or alumo-

silica [65–67], which may be added directly to the catalyst, in amounts of 5 ppm [45]. It must be mentioned that the use of antimony as a passivation agent for vanadium decreases the efficiency of the platinum and requires an increase of its concentration.

These protection measures are similar to those described previously for the cracking of distillates.

6.3 REACTION MECHANISMS

Different from the processes involving thermal cracking, where the active species that control the reactions are radicals, in catalytic cracking the active species are carbocations formed on the active sites of the catalyst. The difference between the results of the two processes is the consequence of the differences between the properties of the two types of active species.

It is to be mentioned that according to the IUPAC nomenclature, ions such as CH_3^+, which earlier were called carbonium ions, should be called *carbenium ions*, while those of the type CH_5^+ should be called *carbonium ions*. The term *carbocations* comprises both species and generally all the organic species that carry a positive charge. This nomenclature will be used in the present work.

6.3.1 Carbocation Formation

In general, there exist four possible ways to form carbocations:

1. The addition of a cation to an unsaturated molecule with the formation of a carbenium ion. Such a reaction occurs during the adsorption of an alkene at a Brönsted site of the catalyst; the formed ion remains adsorbed on the acid site.

$$R_1 - HC = CH - R_2 + HB \rightleftharpoons R_1 - H_2C - C^+H - R_2 + B^-$$
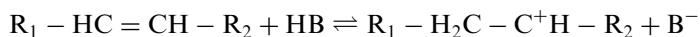
Such an interaction can take place also with an aromatic molecule, as was proved by use of calorimetric methods [68]:
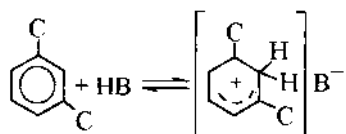
In this case the electric charge is delocalized, i.e. it is distributed over the entire aromatic molecule.

The formation of carbenium ions by the addition of a cation to an alkene is unanimously accepted and, when compared with the other ways of formation of carbocations, appears to take place at the highest rate on catalytic cracking catalysts. If alkenes are not present in the feed, they are formed as a result of reactions of thermal decomposition that takes place at sufficiently high rates at the temperature of catalytic cracking (500°C).

2. The generation of carbenium ions by means of the extraction of a hydride ion by a Lewis site. The reaction can be illustrated by:

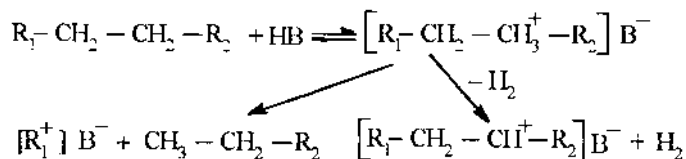$$RH + L \rightarrow [R]^+LH^-$$
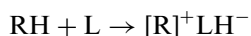
In this case also, the carbenium ion formed remains adsorbed on the active site.

Since, as discussed in Section 6.2.3, both types of sites exist on catalytic cracking catalysts, it is accepted that the carbenium ions are formed both by the interaction of the alkenes with Brönsted-type sites and by the interaction of the alkenes with Lewis sites.

3. The intermediate formation of the carbonium ions. This mechanism was proposed in 1984 by Haag and Dessau [69]. The reaction is supposed to take place by the intermediate formation of carbonium ions, which split, to produce lower alkenes and carbenium ions. As an alternate path, the carbonium ions may convert into a carbenium ions by the loss of a hydrogen molecule.

The mechanism can be depicted by the reactions:

$$R_1- CH_2 - CH_2 - R_2 + HB \rightleftharpoons \left[R_1 - CH_2 - CH_3^+ - R_2 \right] B^-$$

$$-H_2$$

$$[R_1^+] B^- + CH_3 - CH_2 - R_2 \qquad \left[R_1 - CH_2 - CH^+ - R_2 \right] B^- + H_2$$

4. Heterolytic decomposition. The reaction is analogous to the initiation of thermal cracking reactions by the splitting of a molecule into two radicals. The difference is that neither fragment keeps two electrons; therefore, the two fragments carry electric charges of opposite signs:

$$R_1 R_2 \rightarrow R_1^+ + R_2^-$$
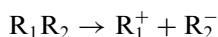
Heterolytic decomposition can take place in liquid phase processes; it does not seem to take place in catalytic cracking where the carbocations are formed as a result of the adsorption on the acid site of the catalyst.

6.3.2 Carbocation Reactions

The carbenium ions adsorbed on the active sites of the catalyst may initiate several types of reactions. A qualitative understanding of the direction of these reactions may be gained from the heats of the formation of the various ions involved.

It must be remarked that the these heats were not obtained from direct measurements, but by indirect calculations and evaluations performed in different ways by various authors. Thus, Evans and Polanyi [70] calculated the heat for the addition of a proton at an alkene. Pritchard [71] used the ionization energies and the affinities of the electrons at the carbon atom of the broken $C-H$ bond. Magaril [73] calculated the ionization potential of the radicals and the affinity for protons etc. The results are given in Table 6.3 and show that some of the values are quite different from one author to the next.

The second remark is that all the above values were calculated for gas phase and moderate temperatures, whereas the energies of the carbenium ions, which intervene in catalytic cracking, refer to ions adsorbed on the active sites of the catalyst and at temperatures of the order of $500°C$. Also, the values of the heats of adsorption are significant and depend on the type of adsorbed ions and on their molecular mass [73,81].

Despite all these caveats, the values of heats of formation calculated for the carbenium ion supply useful and sometimes important information, concerning the directions taken by the chemical transformations. Thus, the comparison of the heats

Table 6.3 Heats of the Reactions $RH \rightarrow R^+ + H^-$

Carbenium ion	Reaction heat $(\Delta H)_5$, kJ/mol				
	EG Evans, M Polanyi [70]	HO Pritchard [71]	BS Greensfelder [72]	JR Franklin [74]	RZ Magaril [73]
CH_3^+	0	0	0	0	0
$C_2H_5^+$	132	130	146	138	142
$C-C-C^+$	214	126	209	167	180
$C-C^+-C$	243	226	276	268	264
$C-C-C-C^+$	–	126	199	196	214
$C-C-C^+-C$	184	–	310	284	285
$C-\overset{+}{\underset{\mid}{C}}-C$ C	301	293	351	351	360

Differences assuming CH_3^+ formation as null.

of formation for the primary, secondary and tertiary ions of the same hydrocarbon—the heats of adsorption being in this case identical—supply quantitative information concerning the relative stability and the direction of the isomerization reactions.
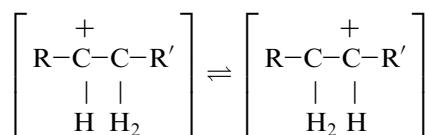
The heats of formation of the carbenium ions calculated by R.Z. Magaril [73] are given in By providing information for more ions than other sources, this author makes it possible to use data having the same degree of accuracy (since it was obtained by application of the same method) for calculating the heats of reaction of a large number of transformations.

The formation of carbocations constitutes the initial step of a sequence of reactions, which gives to the process the character of a decomposition in an unbranched chain, similar to the thermal decomposition.

The reactions that follow the formation of the adsorbed carbocations are skeleton or charge isomerization, interactions with unadsorbed molecules, the transfer of a hydride ion, as well as breaking of carbon–carbon bonds. The combination of the last two reactions confers on the process the character of a chain decomposition. The carbocations generate also secondary reactions, such as polymerization, cyclization etc., and which lead eventually to the formation of coke deposited on the catalyst.

6.3.2.1 Charge Isomerization

The charge isomerization can be exemplified by the reaction:

$$\left[\begin{array}{c} \overset{+}{R-C-C-R'} \\ \mid \quad \mid \\ H \quad H_2 \end{array}\right] \rightleftharpoons \left[\begin{array}{c} \overset{+}{R-C-C-R'} \\ \mid \quad \mid \\ H_2 \quad H \end{array}\right]$$

The migration of the charge is accompanied by the migration in the opposite sense of a hydrogen atom.

Table 6.4 Heats of Formation of Carbenium Ions [73]

| Ion	Heat of formation (kJ/mol)	Ion	Heat of formation (kJ/mol)
H^+	1537	C | C−C−C$^+$ | C	812
CH_3^+	1097		
$C_2H_3^+$	1185		
$C_2H_5^+$	955		
C=C−C$^+$	930	C−C−C−C$^+$−C	754
C−C−C$^+$	917	C−C−C$^+$−C−C	762
C−C$^+$−C	833	C−C−C$^+$−C | C	682
C−C−C−C$^+$	883		
C−C−C$^+$−C	812		
C | C−C−C$^+$	846	C−C=C−C$^+$	854
C | C−C$^+$−C	737	(cyclopentyl)	854
C$^+$−C−C−C−C−C−C−C	800	(cyclohexyl)	796
C−C$^+$−C−C−C−C−C−C	708	(benzene ring)	1202
C−C−C$^+$−C−C−C−C−C	699	(benzene ring)−CH$_3$	925
C−C−C−C$^+$−C−C−C−C	695		

For reasons of free energy, this reaction takes place in the direction towards formation of a secondary ion from a primary ion and/or the transfer of the electrical charge towards the middle of the molecule. The data of Table 6.5 for the propyl, *n*-butyl and octyl ions supply concrete energy data for justifying this direction of transformation.

Similar to the charge transfer reaction is that for the double bond transfer, which also involves a migration of a hydrogen atom [18, 75]. This reaction is explained by the formation of an intermediary compound absorbed on the catalyst [76]:

$$R_1-\underset{H}{C}=\underset{H}{C}-\underset{H_2}{C}-R_2 \;\rightleftharpoons\; \left[R_1-\overset{+}{\underset{H}{C}}=\underset{H}{C}=\underset{H}{C}-R_2 \right] H^- \;\rightleftharpoons\; R_1-\underset{H_2}{C}-\underset{H}{C}=\underset{H}{C}-R_2$$
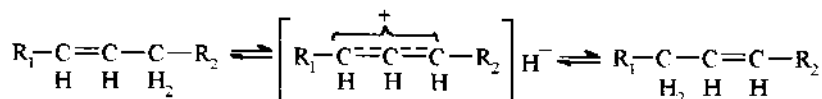
This hypothesis is indirectly confirmed by the finding [77, 78] that in some cases, a migration takes place of the electrical charge between the carbons 1 and 3:

$$(CH_3)_2-CH_2-CH_2-\overset{+}{C}H-CH_3 \rightleftharpoons (CH_3)_2-\overset{+}{C}-CH_2-CH_2-CH_3$$
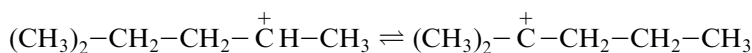
6.3.2.2 Skeletal Isomerization

Skeletal isomerization leads to the conversion of a secondary ion to a tertiary ion or, for hydrocarbons with at least 6 carbon atoms, to the migration of the methyl side-group along the chain.

Table 6.5 Isomerization and Cyclization Heats of Carbenium Ions

| Reaction	Thermal Effect (kJ/mol)
Isomerization	
$\overset{+}{C}-C-C \rightarrow C-\overset{+}{C}-C$	84
$\overset{+}{C}-C-C-C \rightarrow C-\overset{+}{C}-C-C$	71
$C-\overset{+}{C}-C-C \rightarrow C-C^{+}-C$ (with C branch)	75
$C-C-\overset{+}{C}-C-C \rightarrow C-C-C-\overset{+}{C}-C$	−8
$C-C-\overset{+}{C}-C-C \rightarrow C-C-C^{+}-C$ (with C branch)	80
$C-C-\overset{+}{C}-C \rightarrow C-C-\overset{+}{C}$ (with C branches)	−130
$\overset{+}{C}-C-C-C-C-C-C-C \rightarrow C-\overset{+}{C}-C-C-C-C-C-C$	92
$C-\overset{+}{C}-C-C-C-C-C-C \rightarrow C-C-\overset{+}{C}-C-C-C-C-C$	9
$C-C-\overset{+}{C}-C-C-C-C-C \rightarrow C-C-C-\overset{+}{C}-C-C-C-C$	4
Cyclization	
$C=C-C-C-C-C \rightarrow$ ⬡⁺	172

This isomerization type is of practical interest. It is justified by the favorable free energy effect for such a restructuring of the molecule (see Table 6.5).

A reaction mechanism that has found acceptance [18, 73] involves the intermediary formation [79] of cyclopropyl ions. The isomerization of the butyl ion may take place in this case according to the mechanism:

$$C-\overset{+}{C}-C-C \rightleftharpoons \underset{C-\!-\!-C-C}{\overset{\overset{+}{C}}{\triangle}} \rightleftharpoons C-\overset{C}{\underset{+}{C}}-C$$
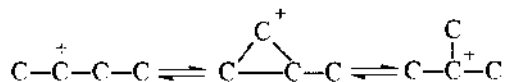
In fact, although any of the three carbon–carbon bonds of the cycle could break, only one of them leads to the formation of the isobutyl ion.

For the amyl ion the mechanism is:

$$C-\overset{+}{C}-C-C-C \rightleftharpoons C-\overset{+}{C}\underset{C-\!-\!-C-C}{\overset{C}{\triangle}} \rightleftharpoons C-\overset{C}{\underset{+}{C}}-C-C$$
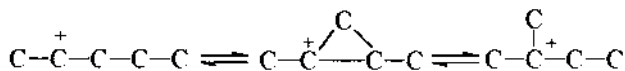
In this case two of the three possible ways of breaking the cycle lead to an iso-structure. This is a partial explanation for the easier isomerization of *n*-pentane compared to *n*-butane.

Since, as mentioned earlier, the heats of adsorption influence only to a small extent the energy balance of the isomerization the thermal effect for the isomerization of the carbenium ions may be calculated correctly on the basis of their heats of formation given in Table 6.5.

6.3.2.3 Hydride Ion Transfer

This transfer is illustrated by the reaction:

$$R_1-H + [R_2^+] \rightleftharpoons [R_1^+] + R_2H$$
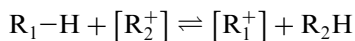
in which, an ion initially adsorbed on the active site interacts with a molecule in the gas or liquid phase or with one that is only physically adsorbed, thereby extracting from it a hydride and escaping in the gas/liquid phase. The active site retains an ion from the molecule that lost the hydride.

This reaction is very important, because it is responsible for the character of chain reaction of the process.

The similar transfer of an alkyl group, which may be expressed by the reaction:

$$R_1-CH_3 + [R_2^+] \rightleftharpoons [R_1^+] + R_2-CH_3$$
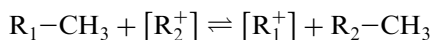
was also observed [80] although the mechanism seems less sure; its existence should not bring any changes in the general mechanism of decomposition.

6.3.2.4 The Breaking of the Carbon–Carbon Bonds

As in thermal decomposition and for similar reasons, carbenium ions undergo breaking of the $C-C$ bonds in β position to the carbon atom that carries the electric charge.

The differences between the decomposition mechanism on acid catalysts, and thermal decomposition are the consequence of the differences between the free energy values of the carbenium ions and those of the radicals.

Thus, the much higher heats of formation of the methyl and ethyl ions than of the higher ions, a difference which is much smaller when radicals are involved (Table 2.3), leads to much lower rates for the β-scissions and to a lower production of methyl and ethyl ions. There exists a much higher ratio $(C_3 + C_4)/(C_1 + C_2)$ in the gases of catalytic cracking than that from the thermal cracking.

As an illustration, the decomposition of the sec-octyl ion is considered:
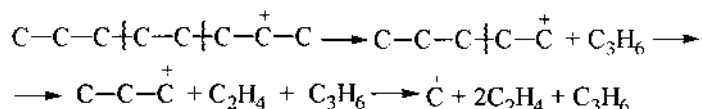

Since the heat of formation of the methyl ion is by 180 kJ/mole larger than for the propyl ion (Table 6.4), the last β-scission will not take place or will take place with a very low rate. In exchange, the propyl ion will suffer a charge isomerization, leading to the liberation of 84 kJ/mole (the same table).

The second difference from the behavior of the radicals is the consequence of very high differences between the heats of formation of the primary, secondary, and tertiary ions. These differences, taking into account the heats of adsorption, are estimated at: 42 kJ/mole between the tertiary ion and the secondary ion and at 105 kJ/mole between the secondary and the primary ion [18].

For radicals, such differences are minimal. As example, for the butyl radical there is no difference between the free energy tertiary and secondary radicals. The difference between the primary and secondary radicals is of only 5.4 kJ/mole (Table 2.5).
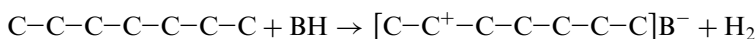
As consequence, the β-scissions that lead to the formation of primary ions will take place with low rates, much lower than those for the charge or skeleton isomerizations. In the case of molecules with a larger number of carbon atoms, repeated isomerizations may take place, so that the the scission to take place will generate a secondary ion. The above considerations may be exemplified by the following scheme for the isomerization and decomposition of the heptyl ion:
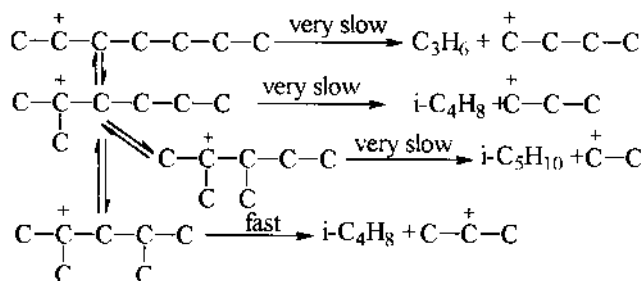

The important practical consequence of the repeated isomerization of alkanes followed by their decomposition is the pronounced iso-alkanic character of the gasolines, which confers to them a high octane number and the prevalence of the iso structure in the C4 cut.

In conclusion, the decomposition of the adsorbed ions on the active sites of the catalyst and their interaction with nonadsorbed molecules leads to a chain of successive reactions, according to the following scheme, written for *n*-heptane.

Chain initiation on a Brönsted center:

$$C-C-C-C-C-C-C + BH \rightarrow [C-C^+-C-C-C-C-C]B^- + H_2$$

or on a Lewis site:

$$C-C-C-C-C-C-C + L \rightarrow [C-C^+-C-C-C-C-C]LH^-$$
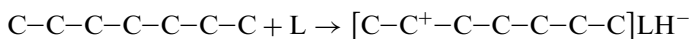
Naturally, all other possible ion structures, especially the secondary ones will be formed.

Chain propagation by isomerization and β-scissions.

The 2-heptyl ion thus formed will undergo isomerization and decomposition reactions represented by the scheme given above for. The 3- and 4-heptyl ions formed by the initiation reaction will undergo similar reactions, but leading to the formation of other final species.

By generalization one may write:

$$[R_i^+] \rightarrow \sum M + [R_j^+] \qquad (a)$$

where $[R_i^+]$ represents the various species of heptyl ions adsorbed on the catalyst; $\sum M$ = sum of the hydrocarbons produced by the decomposition, and $[R_j^+]$ = the ions of low molecular mass that are left adsorbed on the catalyst.

By the transfer of the hydride ion, heptyl ions will be reconstituted:

$$\left[R_j^+ \right] + R_1H \rightarrow R_jH + \left[R_i^+ \right] \tag{b}$$

where: R_1H is the molecule of *n*-heptane.

Reactions (a) and (b) will be repeated, giving a chain character to the decomposition process.

Chain interruption in the case of catalytic cracking takes place following progressive blocking of the active sites by the strong adsorption of ions of high molecular mass, generally produced by polymerization, cyclization, dehydrogenation, and condensation reactions. These ions are not capable of accepting the transfer of the hydride ion (reaction b), owing to very strong forces of attraction to the active site. As a consequence, they are not desorbed from the surface of the catalyst.

A more detailed analysis of the reaction mechanism taking place in the catalytic cracking of the alkanes was performed recently by S. Tiong Sie [81]. His analysis takes into account concomitantly the isomerization reactions by means of nonclassic carbenium ions of cyclo-propyl structure as well as by the cracking of the molecule. The formation of the cyclo-propyl ion is considered to precede the β-scission undergone by the molecule. In Figure 6.16 the classic mechanism and that proposed by S. Tiong Sie are compared.

According to this scheme, the classic mechanism leads to the formation of an alkene and an alkane molecule. The formation of iso-alkanes is explained by independent isomerization reactions that take place in parallel with those of decomposition. The mechanism proposed by S. Tiong Sie leads to the direct formation of iso-alkanes together with that of alkenes.

The comparison with the experimental data of *n*-alkanes cracking on acid catalysts supplies arguments in the support of the suggested mechanism [81]. However, one could argue that the two mechanisms do not exclude each other, and that the β-scission of the secondary ion could take place in parallel with the formation of the cyclo-propyl nonclassic ion, specific to the isomerization reactions. In this situation, the conversion in two directions will depend on their relative reaction rates.

Interesting attempts were made to predict the product distribution obtained in the catalytic cracking of a petroleum fraction [82]. The investigated cut was characterized in terms of the proportions of the various types of carbon atoms, by using mass spectroscopy and nuclear resonance techniques. The fraction was replaced by a number of pseudocomponents, which were assumed to undergo the catalytic reactions, leading to the distribution of products that would have resulted from the actual process. Although, as the authors recognize, the obtained results do not justify the use of this method for predicting the results from commercial operation, the adopted method allows comparative studies and presents an area for future study.

6.3.3 Catalytic Cracking of Various Compounds

The mechanisms of the catalytic cracking reactions presented above allow the examination of the conversions of various classes of hydrocarbon.

Alkanes. The reactivity of *n*-alkanes increases and the activation energy decreases with chain length [83]. As a result, the conversion increases with the length of the chain. This is illustrated by the cracking in identical conditions of hydrocarbons on catalysts of Si-Al-Zr [84]:
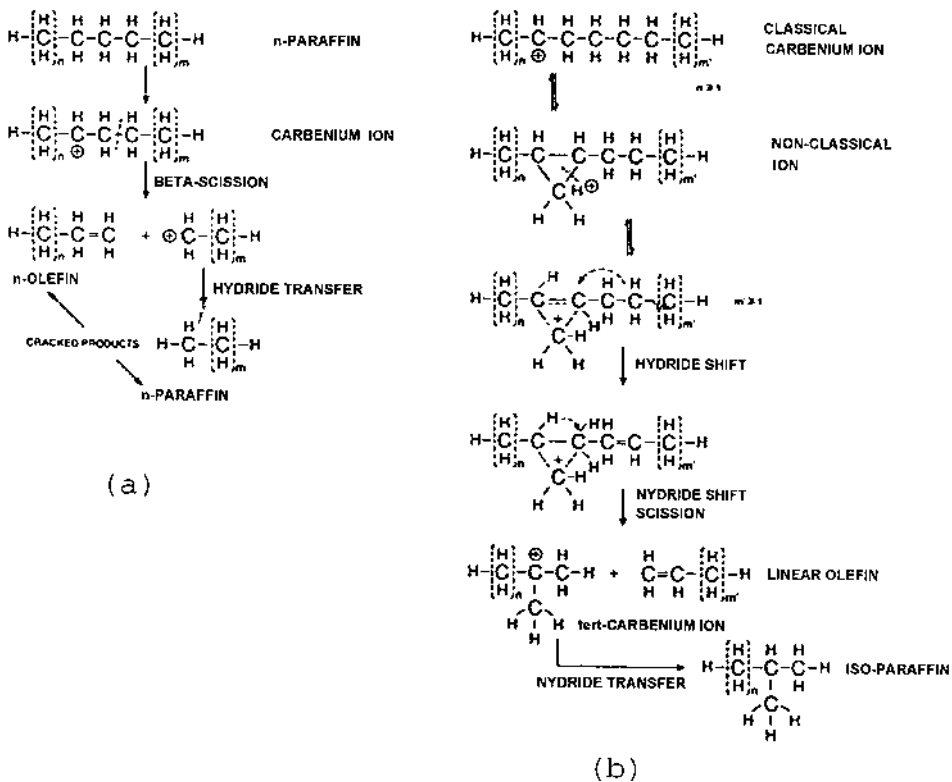
Figure 6.16 Mechanisms of *n*-alkanes catalytic cracking: classical (a) and proposed by S. Tiong Sie (b).

Hydrocarbon	Conversion, wt %
n-C$_5$H$_{12}$	1
n-C$_7$H$_{16}$	3
n-C$_{12}$H$_{26}$	18
n-C$_{16}$H$_{34}$	42

The reactivity increases also with the degree of branching. This is easily explained by the fact that tertiary ions are formed more easily than secondary ions. An exception is made by the hydrocarbons, which have side branches bound to a quaternary carbon atom. Thus, the conversions obtained for various hexanes at 550°C in identical conditions were [85]:

Hydrocarbon	Conversion, wt %
n-C$_6$H$_{14}$	13.8
2-methyl-pentane	24.9
3-methyl-pentane	25.4
2,3-dimethyl-butane	31.7
2,2-dimethyl-butane	9.9

The higher rate of skeletal isomerization than that of decomposition and the fact that the carbenium ions are formed preferably at the tertiary carbon atoms, leads to the *iso*-alkane character of the reaction products. This is true both for the C_4 fraction and naphtha fractions to which the *iso*-alkane character confers a high octane number.

Concerning the gases' composition, the higher heats of formation for the methyl and ethyl ions has as a result the prevalence of C_3 and C_4 hydrocarbons in the gases.

More data concerning the catalytic cracking of individual hydrocarbons and the distribution of the reaction products are contained in several studies [86] and are reviewed in the monograph of B.W. Wojciechowski and A. Corma [18].

Alkenes. The alkenes form carbenium ions easier than alkanes by adsorption on a Brönsted site with the addition of a proton. The practical result is they show a higher rate of cracking than alkanes, the process following the same general rules.

The alkenes adsorb on the surface of the catalyst, as carbenium ions may interact with alkenes in the vapor phase or with those physically adsorbed on the surface of the catalyst, generating alkenes with a high molecular mass. Their participation by cyclization, aromatization and interactions with cyclic hydrocarbons from the vapor phase at the formation of coke on the surface of the catalyst is unanimously accepted.

Cyclo-alkanes. By catalytic cracking, cyclanes produce a high proportion of *iso*-alkanes in addition to important amounts of aromatic hydrocarbons [86–88]. Such a distribution was determined earlier by V. Haensel [89] in the catalytic cracking of alkyl-cyclohexanes, dialkyl-cyclohexanes, dicyclohexyl-decaline, cyclohexane and methyl-cyclopentane. Other studies [90] have shown that higher proportions of hydrogen are produced in the catalytic cracking of cycloalkanes than of alkanes with the same number of carbon atoms.

These results show that the dehydrogenation of cycloalkanes to aromatic hydrocarbons is an important reaction, almost as important as that of ring breaking. In as much as such a dehydrogenation on acid catalysts passes through the intermediary phases of the formation of cyclohexenes and cyclohexadienes, their participation in the formation of coke by interaction with the alkenes (condensations, polymerizations, and dehydrogenations) may be important.

Besides the reactions that affect the ring, the alkyl-cyclanes undergo reactions of breaking the side chains, with the preferred formation of isoalkanes. Due to the high energy of formation of the corresponding ions, no methyl groups and very few ethyl groups are split from the rings.

Aromatic hydrocarbons. The alkyl-aromatic hydrocarbons undergo breaking of the side chains in the same manner as the cyclanes.

The aromatic rings being very stable, no ring breaking occurs, but they may participate in condensation reactions with the formation of coke.

The methyl-aromatics may undergo isomerization reactions by the migration of the methyl groups and by disproportionation.

Detailed studies were performed on the catalytic cracking of cumene and are reviewed in the monograph of B.W. Wojciehowski and A. Corma [18].

Sulfur and nitrogen compounds. There are no published data concerning the decomposition mechanism of these compounds on catalytic cracking catalysts. The nitrogen compounds having a basic character are fixed (probably irreversibly) on the acid centers of the catalyst, in this way preventing their participation in cracking. The result is a deactivation of the catalyst, the degree of which depends on the content and the nature of nitrogen compounds present in the feedstock. Figure 6.17 shows the nitrogen compounds that are present in the crude oil with qualitative indication of their basicity [91].
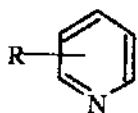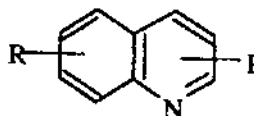
NEUTRAL COMPOUNDS
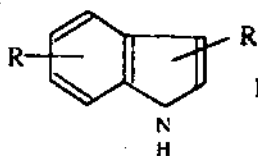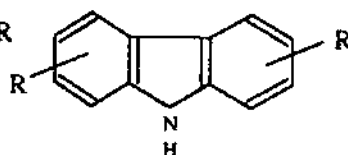
Indoles   Carbazoles
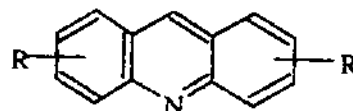
BASIC COMPOUNDS
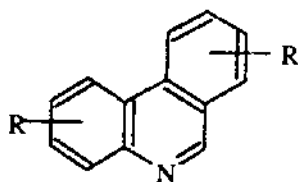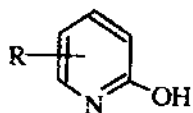
Pyridines   Quinolines   acridines
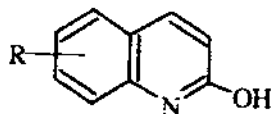
Pnenanthrenes

WEAK BASIC COMPOUNDS

Hydroxypyridines   Hydroxyquinolines

Figure 6.17 Basicity of nitrogen compounds found in crude oil. (From Ref. 91.)

In a recent study [92], a systematic study of the poisoning effect by 34 aromatic hydrocarbons and nitrogen compounds was undertaken and quantitative correlations were obtained. The research is based on a previous work [93], that determined experimentally the poisoning effect of these substances.

The authors define the poisoning effect by the equation:

$$y = 1 - \frac{\xi}{100 - \xi} \cdot \frac{100 - \xi'}{\xi'}$$

where y is the poisoning effect, which takes values between zero and one, ξ equals the percentage conversion in products with boiling temperature below 220°C, which is obtained in the absence of the contaminant, and ξ' is the conversion in presence of the contaminant.

Synthetic feeds were prepared with various contaminants. The amount of contaminant was adjusted to give overall 0.5 wt % nitrogen in the feed for contaminants containing one nitrogen atom, and 1.0 wt % in the feed for contaminants containing two nitrogen atoms. Aromatic hydrocarbons were added in the same proportions as the nitrogen compounds of similar structure in order to see the difference between the poisoning effect of the aromatic structure and that of the nitrogen atom.

A second series of experiments were performed by adding 0.3 wt % of contaminant substance.

The poisoning effect of the substances examined is recorded in Table 6.6 [92]. The comparison of the values obtained for the poisoning effect of similar structures, containing a nitrogen atom or not, such as: of quinoline ($y = 0.541$) with that of naphthalene ($y = 0.222$) and of acridine ($y = 0.621$) with that of anthracene ($y = 0.154$) proves the very strong influence of basicity on the poisoning effect. This effect is explainable by the neutralization of the acid centers of the catalyst by basic contaminants.

In the second study [93], in order to develop a quantitative correlation between the poisoning effect and the structure of the contaminant, 21 parameters were selected and their intervention in such a correlation was tested.

The processing of the whole experimental material and of the 24 parameters calculated for the examined substances lead to the correlation of the contaminant effect (y) with the proton affinity (PA) and the molecular mass (MW) of the contaminant by the equation:

$$y = 0.075 + 0.735(MW)^2(PA)^2 - 0.4067(MW)^3$$

where the proton affinity (PA) is defined for the base (B) by the equation:

$$PA(B) = \Delta H_f(H^+) + \Delta H_f(B) - \Delta H_f(HB^+)$$

where ΔH_f are the heats of formation and (HB^+) is the acid corresponding to base B.

The values (PA) and (MW) are listed also in Table 6.6.

The authors [92] plotted the results (see Figure 6.18), correlating the values of y with PA and MW.

Table 6.6 Poisoning Effect of Some Nitrogen
Compounds and Aromatic Hydrocarbons

Compound	y	MW	PA
Aniline	0.206	93.13	211.1
Pirole	0.160	67.09	215.6
Pirolidine	0.279	71.12	216.9
Pirazine	0.210	80.09	204.1
Pyridine	0.247	79.10	215.1
Piperidine	0.302	85.15	219.9
Naphthaline	0.222	128.18	194.6
Indole	0.299	117.15	211.3
Chinoxaline	0.458	130.15	215.2
Chinoline	0.541	129.16	221.0
1,2,3,4-tetrahydrochinoline	0.552	133.20	215.8
5,6,7,8-tetrahydrochinoline	0.592	133.20	221.6
Antracene	0.154	178.24	196.3
Carbazole	0.238	167.21	210.8
1,2,3,4-tetrahydrocarbazole	0.288	171.24	209.9
Fenazine	0.484	180.21	220.2
Acridine	0.621	179.22	228.9
2-methylpiridine	0.347	93.13	219.0
2-ethylpiridine	0.363	107.16	219.9
2-methyl-5-vynilpiridine	0.368	119.17	220.5
2-vinylpiridine	0.381	105.14	220.1
2,4-dimethylpiridine	0.401	107.16	221.8
5-ethyl-2-methylpiridine	0.449	121.15	221.0
2,3-cyclopentapiridine	0.474	119.17	220.1
2*p*-tolylpiridine	0.491	169.23	223.3
2,6-*di-tert*-butylpiridine	0.565	191.32	228.6
3-methyl-2-phenilpiridine	0.592	169.23	223.5
1-ethylpiperidine	0.418	113.20	223.8
2-ethylpiperidine	0.446	113.20	220.7

Source: Ref. 92.

6.3.4 Mechanism of Coke Formation

The formation of coke belongs inherently to the reactions that take place during catalytic cracking. It results directly from maintaining the overall H/C ratio between the feed and the reaction products. The coke amount can vary in certain limits, depending mainly on the feed, used catalyst, and on the operating conditions. But coke formation can not be avoided completely.

The term coke comprises the total of the products that remain adsorbed irreversibly on the catalyst; in other words, those products not eliminated during the stripping that occurs when the catalyst is transferred from the reactor to the regenerator. Therefore, it contains a whole range of species of different chemical structure characterized by a relative low H/C ratio. Obviously, the species present depend to a large degree on the nature of the feedstock, the content of contaminants Ni, V, and
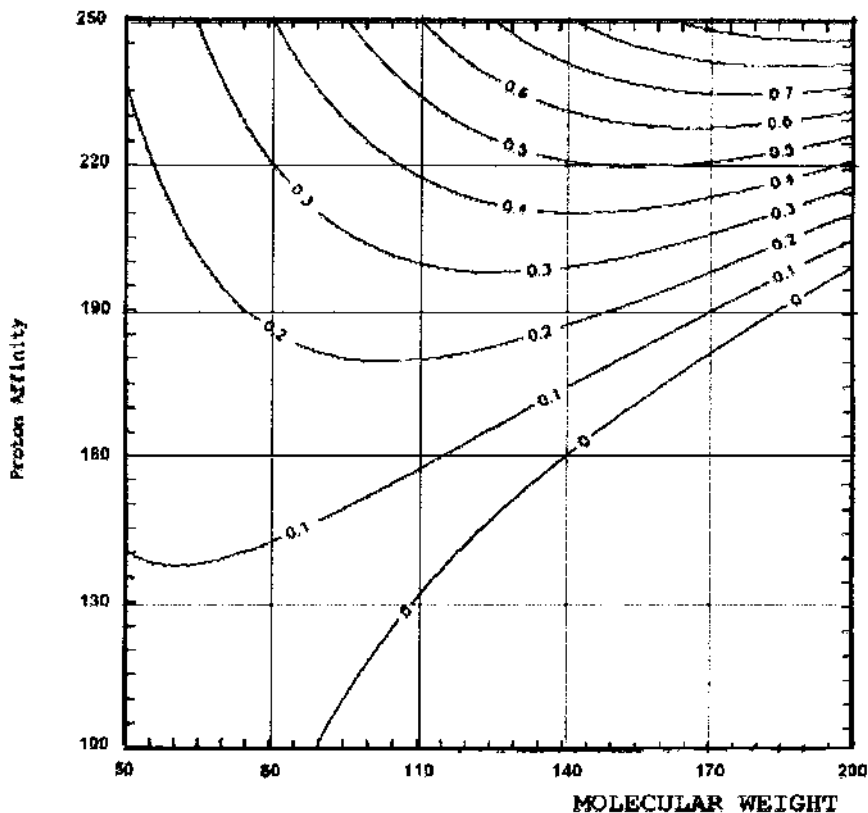
Figure 6.18 Correlation of the poisoning effect with the proton affinity (PA) and molecular mass (MW). (From Ref. 92.)

Fe that catalyze the dehydrogenation reactions, on the nature of the catalyst, and on operating conditions.

The atomic ratio H/C in coke varies in quite broad limits, between 1.0 and 0.3, and decreases during the process [94,95].
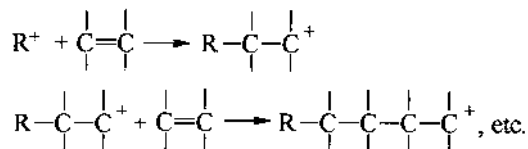
These ratios are obviously indicating the presence in the coke of polycyclic aromatic structures, the only ones which correspond to such ratios.

A large number of my own experimental studies [97] indicate that coke containing such aromatic structures is formed also during the catalytic cracking of gas oils that completely lack polycyclic aromatic hydrocarbons [96], as well as of white oil and of various individual hydrocarbons [93–100]. These studies prove that alkenes participate very actively in the formation of coke. Thus, propylene produces 2.65-times and 1-pentene 8.58-times more coke than cracking in the same conditions of *n*-hexadecane [98].

At present, there is no reaction scheme that can be formulated in a definitive manner. Nevertheless, it can be stated that the formation of coke is a consequence of oligomerization reactions of the alkenes, followed by cyclization, aromatization, alkylation, and condensation. Because these reactions are produced in the adsorbed layer on the catalyst, the thermodynamic analysis of the possible transformations

must take into account concentrations in the adsorbed layer that are similar to those in the liquid state (see Section 6.1).
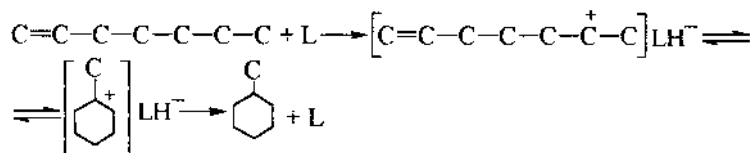
Oligomerization. Oligomerization commonly takes place as a result of the interaction of the adsorbed ions with unsaturated molecules with the alkenes produced by the decomposition reactions:

$$R^+ + \overset{|}{\underset{|}{C}}=\overset{|}{\underset{|}{C}} \longrightarrow R-\overset{|}{\underset{|}{C}}-\overset{|}{\underset{|}{C}}{}^+$$

$$R-\overset{|}{\underset{|}{C}}-\overset{|}{\underset{|}{C}}{}^+ + \overset{|}{\underset{|}{C}}=\overset{|}{\underset{|}{C}} \longrightarrow R-\overset{|}{\underset{|}{C}}-\overset{|}{\underset{|}{C}}-\overset{|}{\underset{|}{C}}-\overset{|}{\underset{|}{C}}{}^+, \text{etc.}$$
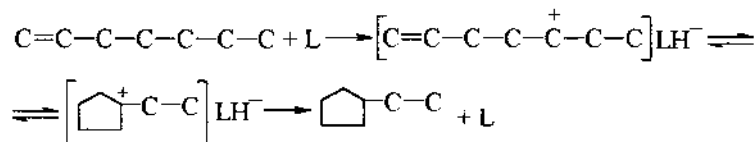
Oligomerization produces ions of increasing molecular mass, which by desorption sets free the corresponding alkenes. The thermodynamic possibility for the occurrence of such reactions in the adsorbed layer is seen in the equilibrium graph of Figure 6.2a. From the same graph it follows that such reactions cannot take place in the conditions of catalytic cracking in gaseous phase.

Cyclization and formation of polycyclic hydrocarbons. The thermodynamic calculations presented in Section 6.1.4 prove that the cyclization of alkenes to cycles of 5 or 6 carbon atoms may take place with high conversions in the conditions of catalytic cracking, irrespective of the phase in which the reaction take place (vapor or liquid). Cyclization is the direction generally favored by thermodynamics and not the splitting of the cycle. The probability of forming cycles of 5 and 6 carbon atoms is actually the same.
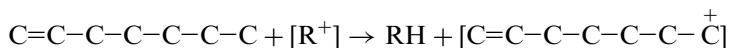
The mechanism of this reaction may be represented in the following way:

$$C{=}C{-}C{-}C{-}C{-}C{-}C + L \longrightarrow \left[C{=}C{-}C{-}C{-}C{-}\overset{+}{C}{-}C\right]LH^- \rightleftharpoons$$

$$\rightleftharpoons \left[\overset{C}{\underset{+}{\bigcirc}}\right]LH^- \longrightarrow \overset{C}{\bigcirc} + L$$

Similarly, cycles of 5 carbon atoms may be formed:

$$C{=}C{-}C{-}C{-}C{-}C{-}C + L \longrightarrow \left[C{=}C{-}C{-}C{-}\overset{+}{C}{-}C{-}C\right]LH^- \rightleftharpoons$$

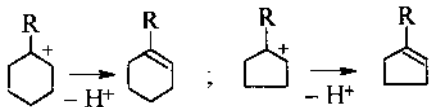$$\rightleftharpoons \left[\overset{+}{\bigcirc}{-}C{-}C\right]LH^- \longrightarrow \bigcirc{-}C{-}C + L$$

The cyclopentyl and cyclohexyl ions may be formed not only by the interaction with a Lewis site, but also by the transfer of a hydride ion:

$$C{=}C{-}C{-}C{-}C{-}C{-}C + [R^+] \rightarrow RH + [C{=}C{-}C{-}C{-}C{-}C{-}\overset{+}{C}]$$

After charge isomerization, the adsorbed alkene may be cyclized to form a cyclohexyl or cyclopentyl ion.

The formed cyclic ions may desorb, producing the corresponding cycloalkenes [73,75]:

Cycloalkenes with rings of five or six atoms may easily undergo reciprocal isomerization. Those with six atoms in the cycle may be disproportioned with the formation of cycloalkanes and of aromatic hydrocarbons [73,75], or could be dehydrogenated directly and form aromatic hydrocarbons [73].

Both the cycloalkenes with five and those with six carbon atoms in the cycle may interact with an alkenyl ion adsorbed on the catalyst with the formation of a bicyclic hydrocarbon:
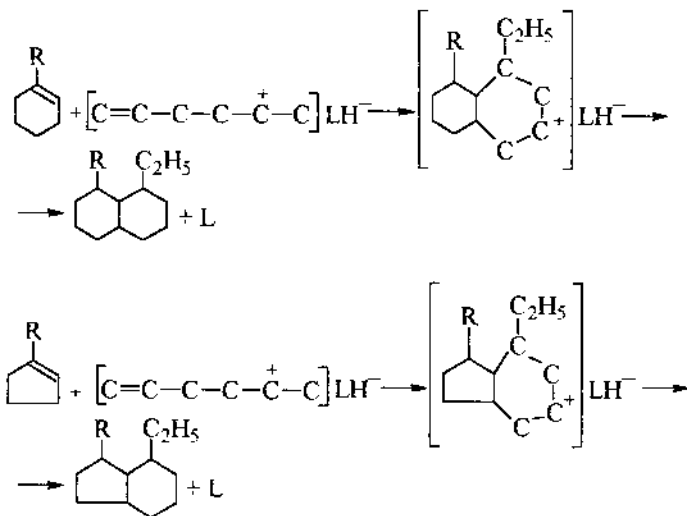
Such reactions may continue and lead to the formation of polycyclic condensed hydrocarbons. Aromatic or hydroaromatic hydrocarbons may also participate in such reactions.

Aromatization. According to the data presented in Section 6.1.6, the dehydrogenation of the 6 carbon atom rings in aromatic hydrocarbons may take place with high conversions in conditions of catalytic cracking. Combined with the previously given reactions, it could lead at the end to the formation of aromatic polycondensated hydrocarbons.

This aromatization process is favored by the catalytic effect of the Ni, V, and Fe deposits formed on the surface of the catalyst derived from the respective organometallic compounds contained in the feed. This phenomenon explains the increase of the conversion to coke when the catalyst is poisoned by metals.

If one accepts such a succession of reactions it obviously follows that the formed coke will contain not only polycyclic aromatic hydrocarbons, which are mostly insoluble in solvents, but also intermediary compounds participating in the successive reactions. Further studies on the various compounds that are soluble in organic solvents [101] will certainly contribute to the more complete elucidation of the paths for coke formation.

The detailed studies concerning the mechanism of coke formation must take into account the possibility of the formation in parallel, even on very active catalysts, of coke along thermal pathways as concluded by some recent studies [102].

6.4 KINETICS OF CATALYTIC CRACKING

The complete analysis of processes involving heterogeneous catalysis requires the examination of the mass transfer phenomena that precede the chemical steps. In processes involving solid catalysts these are:

> The diffusion of the reactants from the bulk fluid to the outer surface of the catalyst particles, as well as diffusion in the opposite sense of the reaction products—external diffusion
> The diffusion through the pores toward the active sites of the catalyst—internal diffusion

If the rates of the diffusion steps are lower or of the same order as the rate of the chemical reaction, the diffusion steps will influence the overall kinetics of the process but in different ways.

The external diffusion occurs before the reaction. For this reason, in the case when it is the slowest of the process steps it will determine the overall kinetics and will impose to it its rate equations. It is said that the process takes place "under external diffusion control."

The internal diffusion through the pores of the catalyst occurs in parallel with the chemical reactions. Its influence on the transformation rate of the feed molecules depends on the manner in which they travel through the pores before they are adsorbed on the active sites. Thus, internal diffusion decreases the reaction rate and influences the overall kinetics, without imposing a specific type of kinetic equation.

The heat transfer is similar to the diffusion phenomena: the external transfer takes place to and from the bulk fluid to the outer surface of the catalyst particles. The internal heat transfer is through the mass of the catalyst particle. Their influence on the overall process increases as the heat of reaction becomes more important.

Catalytic cracking presents some additional particularities. The reactions take place in the conditions of progressive deposition of coke on the active surface of the catalyst, a process so intense that in the formulation of kinetic expressions it is necessary to take into account the gradual decrease of the catalyst activity.

The regeneration by the repeated burning of the coke deposited on the catalyst is a process with the same importance as the reaction itself. The kinetics of coke combustion will be examined with the same degree of attention. Here, a specific trait is the gradual decrease of the rate of coke burning as the combustion penetrates inside the pores. Besides, the unburnt, residual coke left in the catalyst pores decreases catalyst activity.

Since the diffusion phenomena are similar for the reaction and for the regeneration, they will be examined before examining the reaction kinetics for cracking and for coke burning.

6.4.1 External Diffusion

The tangential fluid velocity at the surface of a particle is equal to zero and increases progressively with the distance, to reach at a distance δ the constant velocity in the free space between the particles. For the median section of a spherical particle this velocities profile is represented in the Figure 6.19.

For simplification, in the mathematical treatment of the external diffusion this velocity profile is often assimilated with a film of stationary fluid. From the hydrodynamic point of view, the thickness of such a film is considered to be equal to the *displacement thickness* (δ*) defined as the equality between the fluid flowrate that actually flows around the particle and that which would flow at the velocity of the free space if a hypothetical stationary film of thickness δ* would be present (see Figure 6.19).

The influence of the external diffusion depends obviously on the thickness of this film formed around the catalyst particle.

In the case of processes in a static or moving bed, the theoretical determination of film thickness meets major difficulties, making it necessary to resort to empirical or semi-empirical equations, or to use experimental methods.

The experimental determination of the possible influence of the external diffusion on the overall reaction rate is performed by using fixed bed reactors that allow the variation in sufficiently broad limits of the H/D (high/diameter) ratio for the catalyst layer, keeping constant the feed volume flowrate. In these conditions, the modification of H/D leads to the modification of the fluid linear rate and implicitly
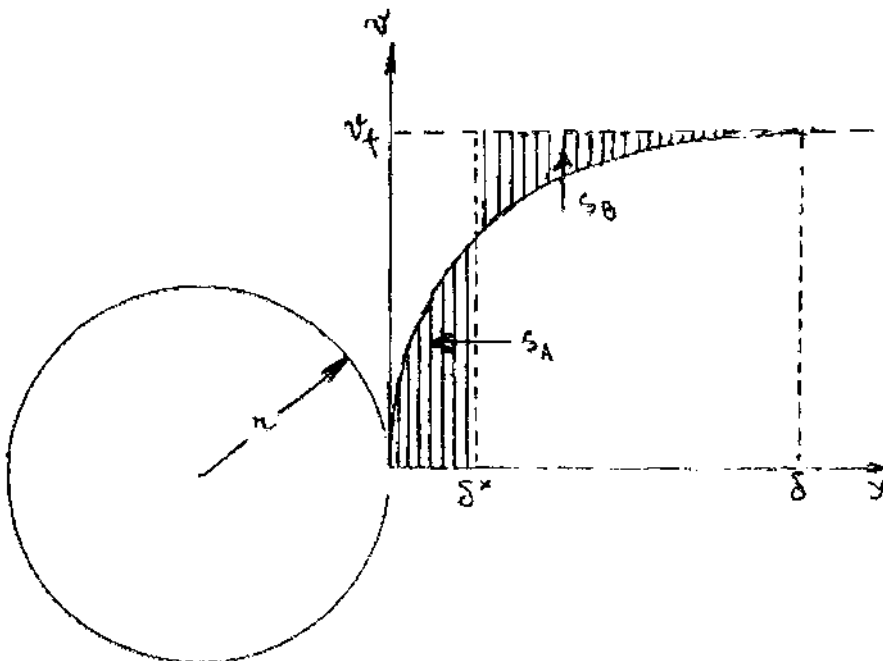

Figure 6.19 Velocity profile in the fluid outside the median section of a spherical particle. Graphical definition of the "displacement thickness" δ*: surfaces $S_A = S_B$.

of the Reynolds number and of the thickness of the boundary layer. In conditions in which the external diffusion influences the overall process rate, higher rates of the fluid and therefore higher ratios H/D will lead to higher conversions (see Figure 6.20).

It must be mentioned that external diffusion modifies not only the conversion, but also the reaction order and the activation energy. If the external diffusion constitutes the rate determining step of the process, the reaction is of first order and the activation energy will take values that are typical for the physical processes of the order of several thousands calories/mol.

In the case of catalytic cracking, the real value of the activation energy for the catalytic process may be masked by the much larger activation energies of the thermal cracking process that occurs in parallel at the temperatures of catalytic cracking. Therefore, the determination of the activation energy is not to be used in this case as a criterion for establishing that the reaction proceeds under the control of external diffusion.

The facts presented above lead to very important conclusions of a general character concerning the manner of performing experiments in order to correctly model an industrial process. Since as a rule, such experiments use the same feed and the same catalyst (with the same particle size, in order to be situated in identical conditions concerning the diffusion through pores) as the commercial process, it results that in order to have identical conditions concerning the influence of the external diffusion, the linear velocity of the reactant in the pilot reactor must be identical or close to that practiced in the industrial plant. This means that the height of the catalyst layer in the pilot plant should be the same as in the industrial plant,
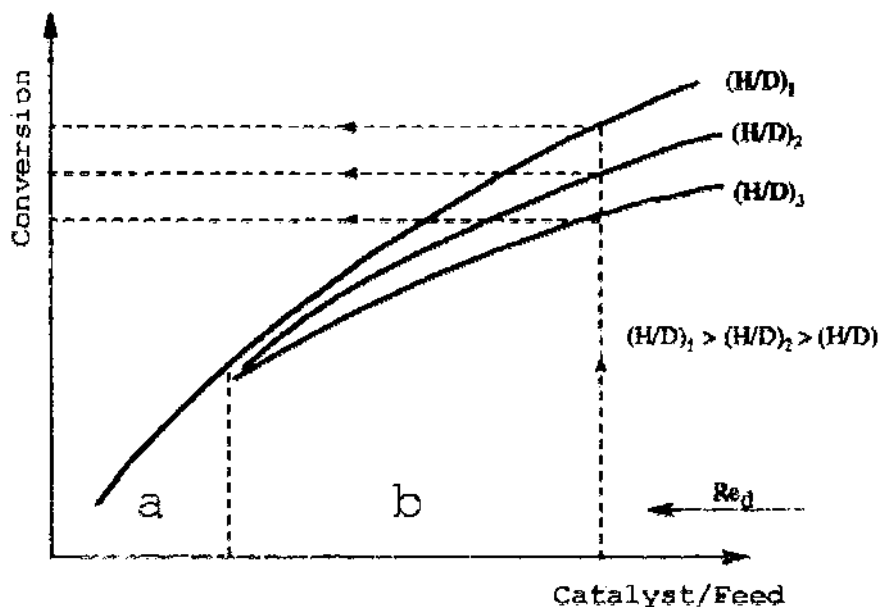

Figure 6.20 Experimental determination of effect of external diffusion. a – no influence; b – increasing influence.

and the cross section of the catalyst bed must be reduced in proportion to the decrease of the feedrate. Other, less expensive methods for measuring kinetic parameters (use of differential reactors and others), will also yield information concerning the effect of external diffusion on the kinetics process [256].

Also, one must avoid the error to consider that in a heterogeneous catalytic process it is sufficient to keep constant the ratio of the feedrate per unit weight of catalyst in order to obtain results that are reproducible at another scale.

In catalytic cracking, the most practiced is the fluidized bed processes, where the catalyst shaped as independent spherical particles is kept suspended in an ascending current of fluid. Accordingly, the problems of the external diffusion will be examined for the case of such particles.

The thickness of the boundary layer is dependent on the Reynolds number expressed by the relation:

$$\mathrm{Re} = \frac{v \cdot d}{v} \tag{6.1}$$

For a spherical particle, the characteristic size that intervenes in Eq. (6.1) is the diameter of the particle.

At very low values of the Reynolds numbers, the Stokes domain, the boundary layer, formed around the spherical particle, has a practical uniform thickness. With increasing Reynolds numbers, the boundary layer is increasingly deformed until it detaches behind the particle when the Reynolds number reaches a value of about 30. The zone occupied by the detached boundary layer occupies a growing fraction of the external surface of the particle. The angle between the incidence point and the border of the detachment zone reaches a maximum value of $Q_D = 109.6°$, at $\mathrm{Re} \geq 300$. At that point, the boundary layer has detached from 1/3 of the surface of the sphere. On the side of the particle from which the boundary layer has detached, vortices are produced that favor the direct access of the fluid to the external surface of the particle.

The change in the shape of the boundary layer with increasing Reynolds number is represented in Figure 6.21.

It is obvious that in the case of a porous catalyst, the areas of detached boundary layer will allow the direct access of the reactants to the external surface of the catalyst, facilitating their penetration into the pores within the catalyst particles. The barrier effect of the external diffusion in situations when the barrier is present will decrease, beginning with $\mathrm{Re} = 30$ and will become practically zero when the Reynolds number approaches 300.

In view of the importance of knowing the variation with the Reynolds number of the detachment angle Q_D and of the surface fraction thus liberated—F_S—, they were plotted in the graph of Figure 6.22a on the basis of published experimental data [103–105].

Concerning boundary layer thickness, the published studies do not offer a general correlation that is valid for all the hydraulic domains. Most of the studies [244–251] refer to attempts to extend the Stokes equations by taking into consideration the inertia forces. The experimental verifications, by Maxworthy [252] proved that the obtained equations are exact only for $\mathrm{Re} \leq 1$.

The study of Jenson [253] concerning the intermediary domain and those of Frössling [254] and Schokemeier [103] concerning the domain of the laminar bound-
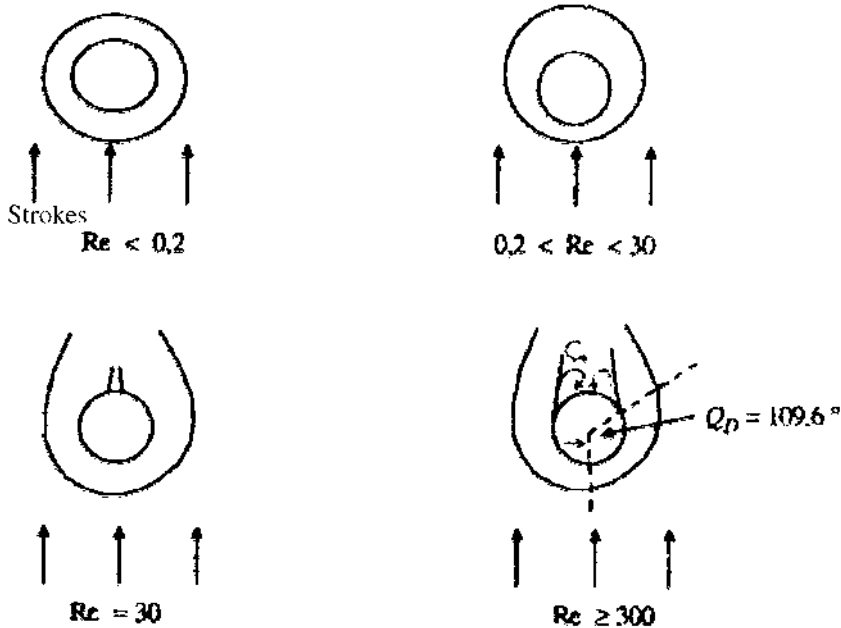
Figure 6.21 Evolution of the boundary layer around a spherical particle in an ascendant flow.

ary layer do not provide analytical expressions for the variation of the fluid velocity, v, as a function of the distance from the wall, y (see Figure 6.19).

The equations deduced by Raseev [106] are based on the hypothesis that, in the middle section of the sphere perpendicular to fluid flow, the tangential tension decreases linearly with the distance, becoming equal to zero at a distance δ. Raseev estimated that this hypothesis is plausible, such a linear variation being valid for the laminar flow through tubes, for the gravitational flow along a plate and in many other cases.

This dependence was expressed by the differential equation:

$$-d\tau = \tau_{0_{90^\circ}} \frac{dy}{\delta}$$

where τ is the tangential tension, τ_0 is the tangential tension at the surface of the sphere in the middle section ($\theta = 90^0$).

The tangential tension can be expressed also as function of the dynamic viscosity by the relation:

$$d\tau = \mu d\left(\frac{dv}{dy}\right)$$

Equating the two expressions, it follows:

$$-\mu d\left(\frac{dv}{dy}\right) = \tau_{0_{90^\circ}} \frac{dy}{\delta} \tag{6.2}$$
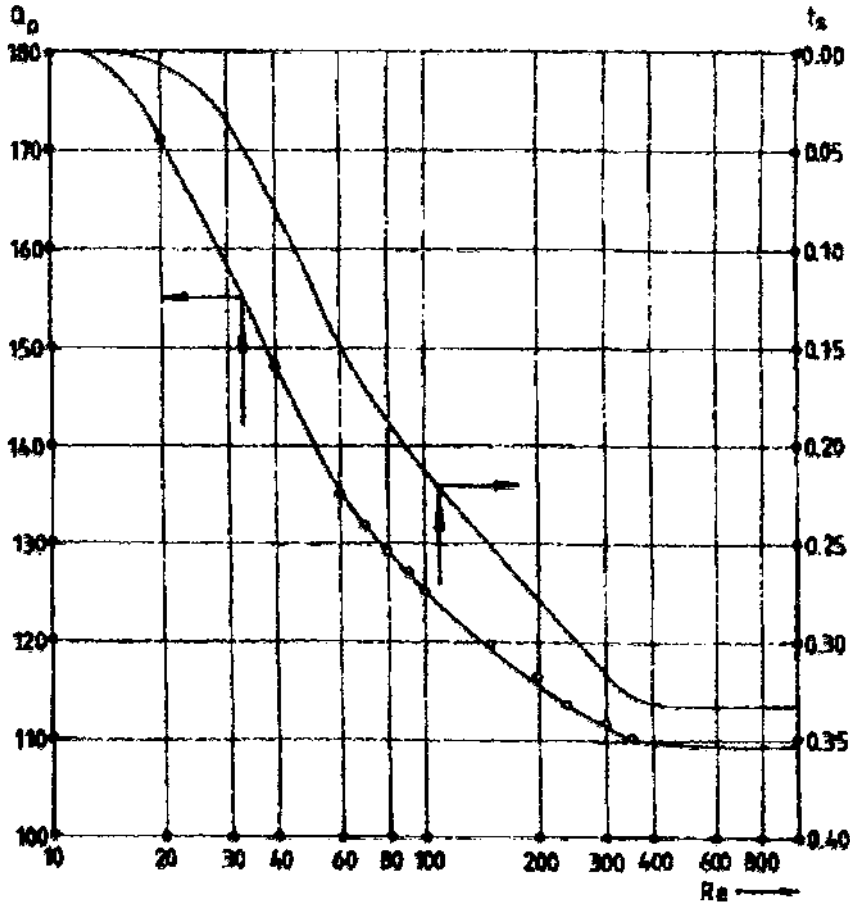
Figure 6.22a Correlation of detachment angle Q_D and of fraction of free surface F_S with Reynolds number.

Integrating this expression and using the boundary conditions $y = 0$ $v = 0$ and for $y = \delta$, $v = v_p$, where v_p is the terminal free-falling velocity, we get:

$$v = -\frac{\tau_{0_{90°}}}{\mu\delta}\frac{y^2}{2} + \frac{v_p}{\delta}y + \frac{\tau_{0_{90°}}}{2\mu}y \tag{6.3}$$

Concerning the second boundary condition, it must be remarked that for a free sphere suspended in an ascending fluid current, the velocity of the fluid beyond the boundary layer, therefore at a distance of at least δ relative to the sphere, will be always equal to the terminal free fall velocity.

By differentiating Eq. (6.3) in terms of y, it is obtained:

$$\frac{dv}{dy} = -\frac{\tau_{0_{90°}}}{\mu\delta}y + \frac{v_p}{\delta} + \frac{\tau_{0_{90°}}}{2\mu}$$

Since, for $y = \delta$, $\dfrac{dv}{dy} = 0$, it follows:

$$\frac{v_p}{\delta} = \frac{\tau_{0_{90°}}}{2\mu}$$

or:

$$\frac{\delta}{r} = \frac{2}{\dfrac{r \cdot \tau_{0_{90°}}}{v_p \mu}} \tag{6.4}$$

Substituting in Eq. (6.3) and performing simplifications gives:

$$\frac{v}{v_p} = -\frac{1}{4}\left(\frac{r \cdot \tau_{0_{90°}}}{v_p \mu}\right)^2 \frac{y^2}{r^2} + \left(\frac{r \cdot \tau_{0_{90°}}}{v_p \mu}\right)\frac{y}{r} \tag{6.5}$$

Introducing the dimensionless parameter:

$$\Re = \frac{r\tau_{0_{90°}}}{v_p \mu} \tag{6.6}$$

Eqs. (6.4) and (6.5) become:

$$\frac{\delta}{r} = \frac{2}{\Re} \tag{6.7}$$

$$\frac{v}{v_p} = -\frac{1}{4}\Re^2 \frac{y^2}{r^2} + \Re\frac{y}{r} \tag{6.8}$$

The dimensionless parameter $\Re$ is the *vorticity* identical to that calculated by Kawagurti [246] and of Jenson [253] and depends on the Reynolds number.

For the domain $0 < \mathrm{Re} < 40$ the calculation of the parameter $\Re$ as a function of the Reynolds number was made on the basis of Stokes equations and of those suggested by different authors [244,246,248,250,253]. For the domain $\mathrm{Re} > 350$ the calculation was made on the basis of the laminar boundary layer [103,254,255]. The obtained values were ploted in Figure 6.22b. For for the domain $40 < \mathrm{Re} < 350$ the curve was drawn by interpolation [106].

For a certain angle θ, considering that the tangential tension decreases linearly with the distance from the sphere wall, analogously to the decrease in the middle section of the sphere, Eq. (6.2) has the form:

$$\mu d\left(\frac{dv}{dy}\right) = \tau_{0\theta}\frac{dy}{\delta} \tag{6.9}$$

Integrating this equation with the boundary condition:

$$v_\theta = 0 \text{ for } y = 0$$
$$v_\theta = v_p \sin\theta \text{ for } y = \delta_\theta$$

it is obtained analogously to Eq. (6.3):

$$v_\theta = -\frac{\tau_{0\theta}}{\mu\delta_\theta}\frac{y^2}{2} + \frac{v_p \sin\theta}{\delta_\theta}y + \frac{\tau_{0\theta}}{2\mu}y \tag{6.10}$$
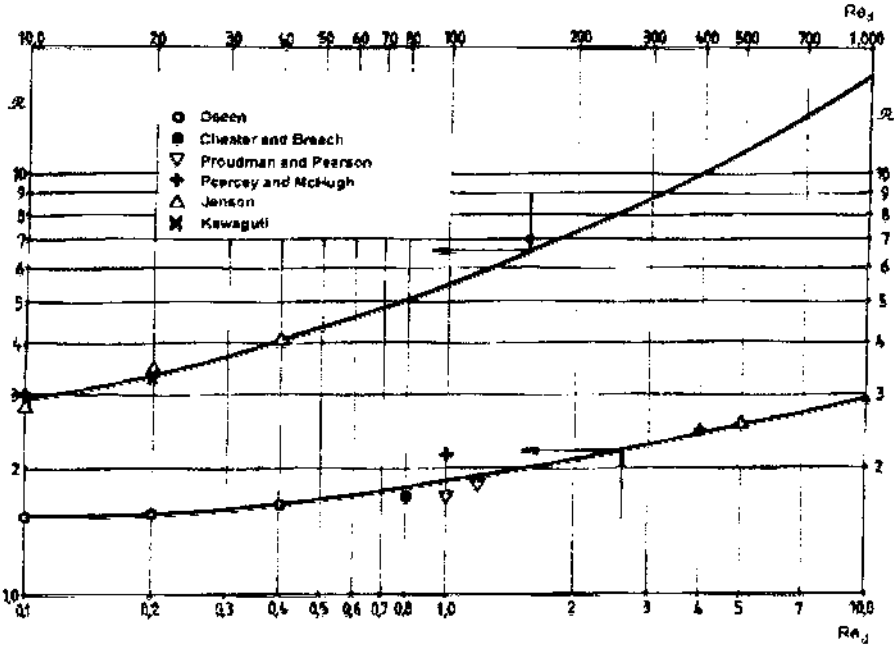
Differentiating with respect to y gives:

Figure 6.22b Correlation of A with Reynolds number.

$$\frac{dv_\theta}{dy} = -\frac{\tau_{00}}{\mu\delta_\theta}y + \frac{v_p \sin\theta}{\delta_\theta} + \frac{\tau_{00}}{2\mu}$$

Since for $y = \delta_\theta$, $\dfrac{dv_\theta}{dy} = 0$, one obtains finally equations similar to those corresponding to the middle section:

$$\frac{\delta_\theta}{r} = \frac{2}{\left(\dfrac{r\tau_{00}}{v_p\mu \sin\theta}\right)} \tag{6.11}$$

and

$$\frac{v_\theta}{v_p \sin\theta} = -\frac{1}{4}\left(\frac{r\cdot\tau_{00}}{v_p\mu \sin\theta}\right)^2\frac{y^2}{r^2} + \left(\frac{r\cdot\tau_{00}}{v_p\mu \sin\theta}\right)\frac{y}{r} \tag{6.12}$$

The dimensionless criterion $\Re$ may be written here as:

$$\Re_\theta = \frac{r\cdot\tau_{00}}{\mu\cdot v_p \sin\theta} \tag{6.13}$$

which simplifies somewhat the writing of Eqs. (6.11) and (6.12) to the shape of Eqs. (6.7) and (6.8).

These equations are of course valid only up to the detaching point θ_D.

Once the velocity profile around the spherical particles is known, the problem of displacing thickness, which, as it was shown, intervenes in the calculation of the external diffusion phenomena, may be addressed.

In this calculation one must take into account that for a spherical particle the equating of the surfaces represented in Figure 6.19, which define the displacing

thickness δ^x, must be done by taking into account the curvature of the sphere. Thus, for the middle section of the sphere, the ring-shaped surfaces must be set equal, corresponding to the distances δ^x and δ from the surface of sphere, using the relation:

$$v_p S^x = 2\pi \int_0^\delta (v_p - v)(r + y)dy \tag{6.14}$$

where S^x, the displacement section, can be correlated with the displacement thickness, δ^x, by using the equation:

$$S^x = \pi(2r\delta^x + \delta^{x2}) \tag{6.15}$$

For a certain angle θ these equations become:

$$v_p S_\theta^x \sin\theta = 2\pi \int_0^{\delta_\theta} (v_p \sin\theta - v_\theta)(r + y)\sin\theta dy \tag{6.16}$$

$$S_\theta^x = \pi \sin\theta(2r\delta_\theta^x + \delta_\theta^{x2}) \tag{6.17}$$

The distance that should be used in the diffusion calculations is the mean displacement thickness, δ^x. Since its calculation by using the Eq. (6.11) is difficulty in the neighborhood of the detaching point $\tau_{00} \to 0$ and therefore $\delta_\theta^x \to \infty$, in the following the indirect calculation of the $\overline{\Re}_\theta$ was used, a much more exact calculation.

For the Stokes domain the velocity profile does not vary with the angle θ:

$$\overline{\Re}_\theta = \Re$$

For the intermediary domain using the values ζ_{00} (vorticity) for different values of the angle θ and Reynolds, given by Jenson [253],

for: $Re_d = 10$ $\overline{\Re}_\theta = 1.006\Re$
for: $Re_d = 20$ $\overline{\Re}_\theta = 1.013\Re$
for: $Re_d = 40$ $\overline{\Re}_\theta = 1.061\Re$
For the boundary layer domain, $Re_d > 350$ the correlation:

$$\overline{\Re}_\theta = 1.536\Re$$

is obtained [106] allowing the graphical interpolation for the interval $40 < Re_d < 350$.

In order to express δ^x as a function of $\overline{\Re}_\theta$ one replaces v_θ given by Eq. (6.12) in (6.16). Carrying out the integration of δ_θ using the expressions (6.11) and (6.13), it follows:

$$S^x = \pi \sin\theta\left(\frac{4}{3}r^2\overline{\Re}_\theta^{-1} + \frac{2}{3}r^2\overline{\Re}_\theta^{-2}\right)$$

By replacing S^x with the expression (6.17), simplifying, and isolating δ_θ^x we get:

$$\frac{\delta_\theta^x}{r} = -1 + \sqrt{1 + \frac{4}{3}\frac{1}{\overline{\Re}_\theta} + \frac{2}{3}\frac{1}{\overline{\Re}_\theta^2}} \tag{6.18}$$

a relation valid for all the values of θ, inclusively for that of the middle section for which $\overline{\Re}_\theta$ must be replaced by $\Re$.

Since, as shown above, for the domain $Re \geq 40$, $\overline{\Re}_\theta \approx \Re$, it follows that for this domain Eq. (6.18) may be written as:

$$\frac{\overline{\delta}_\theta^x}{r} = \frac{\delta_{90^o}^x}{r} = -1 + \sqrt{1 + \frac{4}{3}\frac{1}{\Re} + \frac{2}{3}\frac{1}{\Re^2}} \tag{6.19}$$

the average displacement thickness around the sphere $\overline{\delta}_\theta^x$ is therefore actually equal to the displacement thickness in the middle section.

For the domain Re > 350 the correlation between $\overline{\Re}_\theta$ and $\Re$ is:

$$\overline{\Re}_\theta = 1.536\Re \approx 1.5\Re$$

An approximative calculation for this domain can be made, by accepting for the values $\overline{\delta}_\theta^x$ and $\overline{\Re}_\theta$ an equation that is similar to (6.18). Such a calculation is of interest for the study of external diffusion. Since the boundary layer is detached over 1/3 of the external surface of the spherical catalyst particle, the reactants have access to the active sites without having to cross the boundary layer.

For the domain 40 < Re < 350, $\overline{\delta}_\theta^x$ can be determined by interpolation.

On this basis, the dependence between $\dfrac{\overline{\delta}^x}{r}$ and Re, which is necessary for the calculation of external diffusion, was plotted in Figure 6.23. This figure gives the mean boundary layer around a spherical particle as a function of the Reynolds number given by equation (6.1).

As shown above, to analyze the influence of external diffusion on reaction and regeneration in catalytic cracking, it is necessary to know the Reynolds domain in which the process takes place, or, according to Eq. (6.1), the diameter of the catalyst particles, the velocity, and the kinematic viscosity of the fluid.
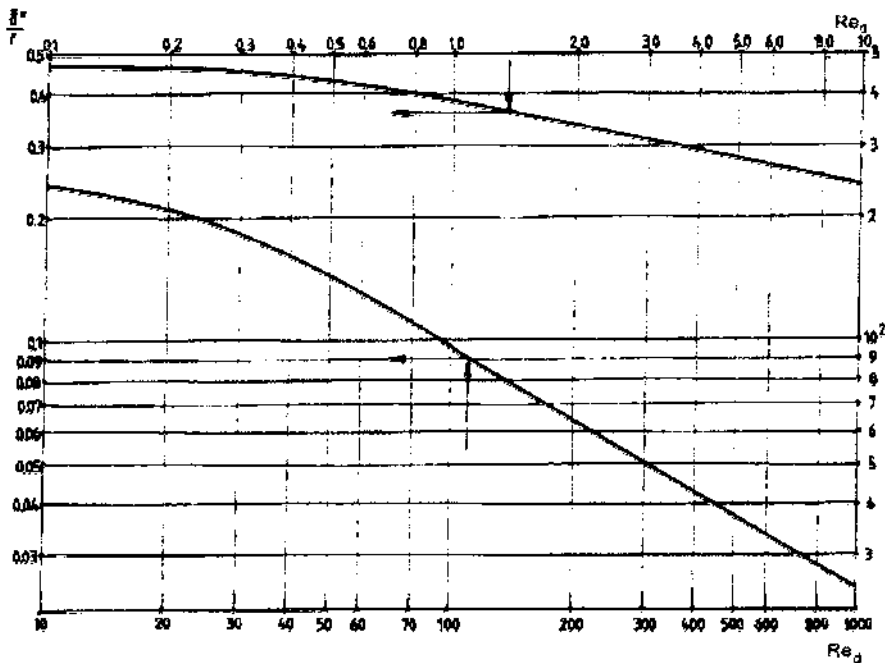

Figure 6.23 Mean boundary layer thickness (δ^*/r) ratio, function of Reynolds number. (From Ref. 106.)

Current fluid catalytic cracking processes use exclusively synthetic micro-spherical catalysts having the characteristics [107]:

diameter $d_p = 55 \times 10^{-6} - 70 \times 10^{-6}$ m

bulk density $\rho_a = 1{,}120 - 1{,}700$ kg/m^3

Since the Reynolds number depends on the properties of the fluid one has to examine the influence of external diffusion separately on the reaction process and on catalyst regeneration.

6.4.1.1 Effect of External Diffusion on Cracking

Besides the size of the catalyst particles, the influence of external diffusion depends on the relative velocity of the fluid particle and on the viscosity of the feed and of the products.

In the early versions of catalytic cracking systems that operated in dense phase, the velocity of the fluid above the catalyst bed was of the order 0.9–1.1 m/s. Since inside of the bed a portion of the flow cross section is occupied by the catalyst, the ascending movement of which is relatively low, the relative velocity between fluid and catalyst particles (the slip velocity) is larger and is estimated at 1.4 m/s.

In modern units such as the riser type, the linear fluid velocity ranges between 3.0 and 4.0 m/s, which is practically equal to the slip velocity.

Assuming as feedstock a heavy gas oils of molecular mass of 300–400, the fluid viscosity for vapors at 500°C and 1.6 bar may be obtained from Figure 6.24.

$$\rho = M\frac{p}{RT} = 7.6 \div 10.1 \text{ kg/m}^3$$

$$\mu_v = 0.0068 \div 0.005 \text{ cP} = 0.68 \cdot 10^{-5} \div 0.5 \cdot 10^{-5} \text{ kg/m} \cdot \text{s}$$

For the products: $M \approx 90$, $p = 1.4$ bar.

$$\rho = 1.98 \text{ kg/m}^3$$

$$\mu = 0.015 \text{ cP} = 1.5 \cdot 10^{-5} \text{ kg/m} \cdot \text{s}$$

Taking into account these data, one may calculate for a reactor operating in dense phase at the reactor inlet:

For distillates with $M = 300$:

$$\text{Re} = \frac{1.6 \cdot 60 \cdot 10^{-6} \cdot 7.6}{0.68 \cdot 10^{-5}} = 94$$

For heavy distillates with $M = 400$:

$$\text{Re} = \frac{1.6 \cdot 60 \cdot 10^{-6} \cdot 10.1}{0.5 \cdot 10^{-5}} = 170$$

For the outlet conditions it follows:

$$\text{Re} = \frac{1.4 \cdot 60 \cdot 10^{-6} \cdot 1.98}{1.5 \cdot 10^{-5}} = 11.2$$
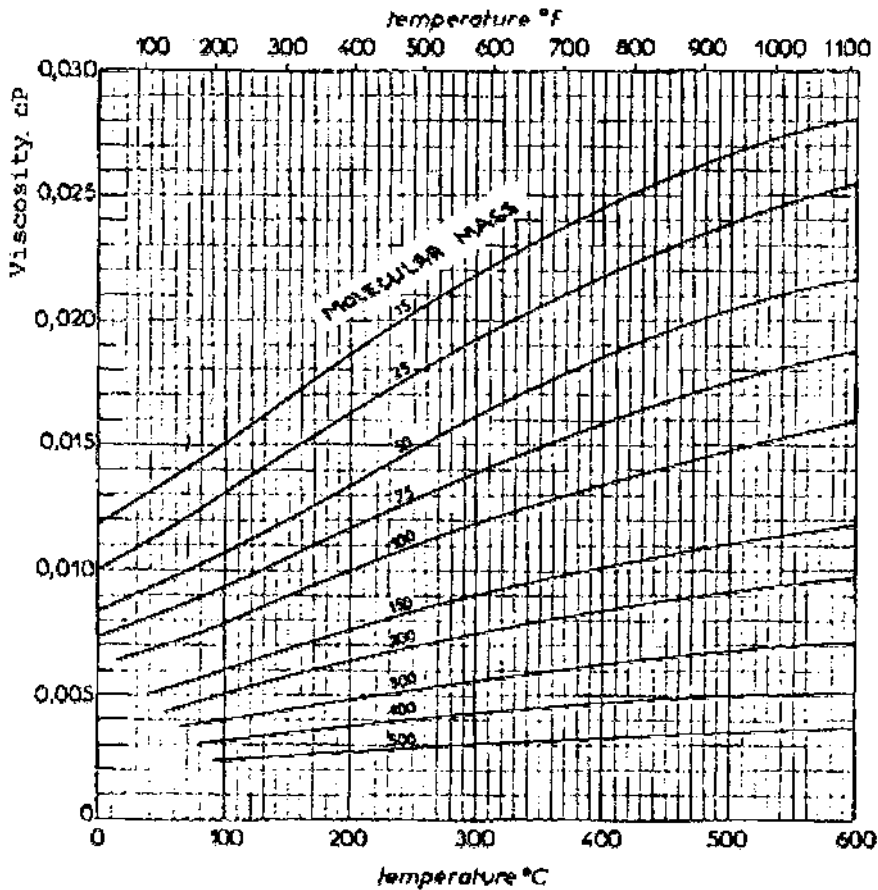
Figure 6.24 Viscosity of hydrocarbons in vapor phase at 1 bar. (From Ref. 108.)

As a result of intense internal mixing, the conditions in a reactor with a dense fluidized bed are close to perfect mixing, i.e., the conditions inside the bed correspond to those at the outlet: that means Re = 11.2. The boundary layer therefore will not be detached in the back of the particles (Figure 6.21) and its mean thickness will be, according to the graph of Figure 6.23: $\delta^* = 0.236 \times r = 0.236 \times 30 = 7.1 \mu$m The external diffusion will thus influence the overall rate of the process.

The total thickness of the boundary layer, is given by Eq. (6.11) and the graph (Figure 6.22b).

For Re = 11.2, Figure 6.22b gives $\Re = 3$ and the relation (6.11):

$$\delta = \frac{2r}{\Re} = \frac{60}{3} = 20 \ \mu\text{m}$$

In order to see which method should be used for calculating external diffusion, it is necessary to check whether the boundary layers of neighboring particles are or are not interpenetrating. Only in the second case the theoretical calculation deduced for free spherical particles may be used.

According to Figure 8.14, the fraction of free volume inside the dense phase fluidized bed of catalytic cracking reactors varies between the limits:

$$1 - \eta_a = 0.160 \div 0.390$$

Because the fluidized bed is equivalent to a mean statistical position in the cubic network of the solid particles, the cubes have sides equal to 2a. One may write:

$$1 - \eta_a = \frac{\frac{4}{3}\pi r^3}{(2a)^3}$$

from which:

$$a = \frac{r}{2}\sqrt[3]{\frac{\frac{4}{3}\pi}{1 - \eta_a}} \tag{6.20}$$

Replacing $(1 - \eta_a)$ and r, it follows:

$$a = 44.5 \ \mu m \text{ and } a - r = 14.5 \ \mu m$$

Since $a - r < \delta$, the boundary layers are overlapping and the only calculation methods that may be used are those based on nondimensional criteria or those directly based on experimental data.

For the riser systems, the pressures at the inlet and outlet of the riser will be of the order of 2.2 respectively 1.6 bar and the Reynolds numbers will be:

For the distillates with $M = 300$:

$$Re = \frac{3.0 \cdot 60 \cdot 10^{-6} \cdot 10.4}{0.68 \cdot 10^{-5}} = 275$$

For the distillates with $M = 400$:

$$Re = \frac{3.0 \cdot 60 \cdot 10^{-6} \cdot 13.8}{0.5 \cdot 10^{-5}} = 490$$

For the outlet condition one obtains:

$$Re = \frac{4.0 \cdot 60 \cdot 10^{-6} \cdot 2.27}{1.5 \cdot 10^{-5}} = 36.3$$

It follows that in the conditions of the riser reactor, external diffusion will not influence the overall reaction rate since the boundary layer will be detached behind the catalyst particles.

6.4.1.2 Effect of External Diffusion on Catalyst Regeneration

The regeneration of the catalyst by the combustion of coke is performed in dense phase in a fluidized bed reactor. In modern units the regeneration is performed in a riser similar to that used for the cracking.

The linear velocities of the fluid are practically the same in the analogous equipment, while in the regeneration the pressure is somewhat lower than in the reactor.

The density and the viscosity of the air and of the flue gases are similar and have the following values*:

For the systems in dense phase, $t = 650°C$ and $p = 1.2$ bar:

density of air $= 0.457$ kg/m^3

$\mu = 0.01716 \times 2.309 = 0.0396$ cP $= 3.96 \cdot 10^{-5}$ kg/m·s

For the mean conditions in the riser: $t = 650°C$; $p = 2$ bar:

density $= 0.761$ kg/m^3

$\mu = 3.96 \times 10^{-5}$ kg/m·s

Based on these data and on the mean linear velocities of the fluid for the two systems, it follows:

For regenerators in dense phase:

$$Re = \frac{1.4 \cdot 60 \cdot 10^{-6} \cdot 0.457}{3.96 \cdot 10^{-5}} = 0.97$$

For regenerators of the riser type:

$$Re = \frac{4.0 \cdot 60 \cdot 10^{-6} \cdot 0.761}{3.96 \cdot 10^{-5}} = 4.61$$

As in the case of the reactors, according to the graph of Figure 6.23 and Eq. (6.11), it follows for:

$Re = 0.97 \qquad \delta^* = 11.6\ \mu \qquad \delta = 32.4\ \mu$

$Re = 4.61 \qquad \delta^* = 8.46\ \mu \qquad \delta = 24.0\ \mu$

For the regeneration in dense phase the fraction of free volume of the fluidized bed varies according to the graph of Figure 7.14, between the limits: $1 - \eta_a = 0.20 - 0.25$.

According to Eq. 6.20, the distance between the microspheres of the catalyst within the bed is:

$$a - r = 11.3 \div 8.4\ \mu$$

The comparison of these values with $\overline{\delta}^*$ and δ proves that there is a significant overlap or interpenetration of the boundary layers that surround the catalyst particles. This situation precludes the use of the theoretical calculation method that was developed for independent microspheres. The only calculation methods that can be used are those based on nondimensional numbers developed by the processing of specific experimental data.

In regenerators of the riser type, the fraction of free volume in the ascending flow varies between the limits:

---

* The viscosities were calculated using Sutherland's law:

$$\mu = \mu_o \frac{273 + C}{T + C}\left(\frac{T}{273}\right)^{1.5}$$

in which for air: $\mu_o = 0.01716$ cP and $C = 111.0$ for temperatures between 289 and 1098 K [109].

$$1 - \eta_a = 0.035 \text{--} 0.080$$

and according to Eq. (6.20) it follows:

$$a - r = 43.9 \text{--} 26.1 \ \mu$$

In all cases $a - r > \delta$; therefore, for regenerators of the riser type the external diffusion rate may be calculated on basis of the theoretical classical methods of reactant diffusion through the boundary layer that surrounds the catalyst microspheres.

The equation that expresses the diffusion of a reactant A towards the external surface of the catalyst particle and that takes into account the diffusion in the opposite direction of the reaction products has the general form [110]:

$$\frac{dp_A}{dy} \frac{p}{RT} = \frac{\phi_{A_y}}{D_A}(p + \beta p_A) \tag{6.21}$$

where:

p_A = the partial pressure of the reactant A in ata
y = the distance from the surface in cm
p = the pressure in the system in ata
R = the gas constant in cm³·ata/mol·degree
ϕ_{A_y} = the reactant flow A at the distance y from the surface in moles/s·cm²
D_A = the diffusion coefficient of the reactant A in cm²/s
β = the number of moles of gases resulting from the reaction per mole of reactant A.

As an example, for the burning of a coke containing 10% H_2 and producing flue gases in which the ratio $CO_2/CO = 1.5$ (data typical for fluid catalytic cracking), $\beta = 0.3$. Since for air, $p_A = 0.21p$, the term βp_A in Eq. (6.3) can be neglected. It follows:

$$-\frac{dp_A}{dy} \cdot \frac{1}{RT} = \frac{\phi_{A_y}}{D_A} \tag{6.22}$$

Since for a microspherical catalyst, the displacement thickness $\overline{\delta}\,*$ is significant compared to the radius of the particles, ϕ_A can be expressed by the equation:

$$\phi_{A_y}(r + y)^2 = \phi_{A_0} r^2$$

Replacing in Eq. (6.21), after the separation of the variables, it follows:

$$\phi_{A_0} r^2 \frac{dy}{(r+y)^2} = -\frac{D_A}{RT} dp_A$$

By the integration of this equation between the limits:

For $y = 0$ $p_A = p_{A_S}$
For $y = \overline{\delta}*$ $p_A = p_{A_f}$

where the subscript S refers to the surface of the catalyst microsphere and f to the flow, the end result is:

$$\phi_{A_0} = \frac{-D_A}{RT\overline{\delta}^*} \cdot \frac{r + \overline{\delta}^*}{r}\left(p_{A_f} - p_{A_S}\right)$$

In order to express the diffusion rate r_{D_A} in moles/s·g cat as is customary in kinetic calculations, the right side of Eq. (6.22) must be multiplied by S—the external surface of all the microspheres contained in a gram of catalyst. It results:

$$r_{D_A} = \frac{-D_A \cdot S}{RT\overline{\delta}^*} \cdot \frac{r + \overline{\delta}^*}{r}\left(p_{A_f} - p_{A_S}\right) \qquad (6.23)$$

wherein:

$$S = \frac{4\pi r^2}{\frac{4}{3}\pi r^3 \cdot \gamma_a} = \frac{3}{r\gamma_a} \qquad (6.24)$$

r being the radius of the microspheres of catalyst.

The use of Eq. (6.23) requires the value of the diffusion coefficient. To this purpose, published values [111], theoretical calculations [112], or empirical methods such as that of Wilke and Lee [113] or of Fuller et al. [114–116] may be used, which are satisfactory for engineering calculations and also can be found in the monograph of Smith [112].

In the following calculations, the diffusion coefficient of oxygen through air was used, which has the value [117] 0.138 cm^2/s.

At 650°C the corrected value of the diffusion coefficient is:

$$D_T = D_0\left(\frac{T_T}{T_0}\right)^{1.5} = 0.138\left(\frac{923}{293}\right)^{1.5} = 0.772 \text{ cm}^2/\text{s}$$

Using Fuller's equation:

$$D_{AB} = \frac{0.00143\,T^{1.75}}{pM_{AB}^{0.5}\left[(\sum v)_A^{1/3} + (\sum v)_B^{1/3}\right]^2} \qquad (6.25)$$

where:

$\quad D_{AB}$ = binary diffusion coefficient in cm^2/s
$\quad M_{AB}$ = $2[1/M_A + 1/M_B]^{-1}$, M_A and M_B = molecular masses of the substances
$\quad p$ = pressure in bar
$\quad \sum v$ = sums of the atomic diffusion volumes.

For the diffusion of oxygen towards the external surface of the microspheres of the catalyst, considering that the diffusion takes place through the prevalent nitrogen layer at the temperature of 650°C and a pressure of 2 bar one obtains:

$$M_{AB} = 2\left[\frac{1}{32} + \frac{1}{28}\right]^{-1} = 29.87$$

$$D_{O_2N_2} = \frac{0.00143 \cdot 923^{1.75}}{2.0 \cdot 29.87^{0.5}\left[16.3^{1/3} + 18.5^{1/3}\right]^2} = 0.7535 \text{ cm}^2/\text{s},$$

a result which is very close to the one obtained before.

For the catalyst having $\overline{d} = 60 \cdot 10^{-4}$ cm and the apparent density $\gamma_a = 1.4$ g/cm^3, according to relation (6.6):

$$S = \frac{3}{r \cdot \gamma_a} = \frac{3}{30 \cdot 10^{-4} \cdot 1.4} = 714 \text{ cm}^2/\text{g}$$

the external diffusion rate for the regeneration in the riser system will be, according to the relation (6.5):

$$r_D = -\frac{0.7535 \cdot 714}{0.0821 \cdot 10^3 \cdot 923 \cdot 8.46 \cdot 10^{-4}} \cdot \frac{60 + 8.46}{60} \left(p_{A_f} - p_{A_S} \right)$$

$$= -9.57 \left(p_{A_f} - p_{A_S} \right) \text{ mols/s} \cdot \text{g cat}$$

The very high value of the mass transfer coefficient proves that in the conditions of the riser, the external diffusion does not exercise any influence on the overall coke burning rate.

A calculation for the regenerator in dense phase is provided in Chapter 8. It must be remarked that for such regenerators the estimate shows that the external diffusion strongly influences the burning of coke [118,119], while, as shown, it is weaker or missing for the riser systems.

In the case of a moving catalyst bed, the influence of external diffusion on reaction and regeneration may be evaluated by means of the methods used for processes with a stationary catalyst [112]. Since the cracking processes with moving a catalyst bed have no current interest, these problems aren't dealt with here.

6.4.2 Pore Diffusion

Internal diffusion through the pores of zeolitic catalyst is treated differently from the classical catalysts.

Classical methods are fully applicable to pore diffusion in classical catalysts. In zeolites, one takes into account specific effects due to the regular structure of the pores that leads to the phenomena called *shape selectivity*.

This selectivity is the consequence of the impossibility of hydrocarbon molecules, which exceed the pore diameter, penetrating the zeolite micropores. The result is that some components of the feed will be cracked selectively with much higher rates than others.

This situation is enhanced in the cracking of residual feedstocks, the very heavy components of which can penetrate only to the active sites of the matrix.

The most adequate method for expressing the effect of the diffusion influence through the pores of the classic catalyst is by means of the effectiveness factor η, which is defined as the ratio of the observed reaction rate to that which would occur in the absence of diffusion effects within the pores of the catalyst:

$$\eta = \frac{r'}{r} \tag{6.26}$$

where:

r' = the experimentally observed reaction rate
r = the rate that would occur in absence of diffusion effects, or corresponding to the use of the whole catalyst internal surface.

Eq. (6.26) allows the experimental determination of the effectiveness factor, using for the determination of the rate r very small catalyst particles for which the internal diffusion cannot decrease the rate of the process.

The effectiveness factor can be calculated using the Thiele modulus, h, using for plan particles the relation:

$$\eta = \frac{1}{h} th \cdot h \tag{6.27}$$

and for spherical particles the equation:

$$\eta = \frac{1}{h} \left(\frac{1}{th \cdot 3h} - \frac{1}{h} \right) \tag{6.28}$$

The graph of Figure 6.25a replaces such calculations and demonstrates among others that there are but small differences the between the value of the effectiveness factors of catalyst particles of different shapes. It is estimated [112] that these differences are smaller than the precision in the evaluation of the diffusion coefficient that intervenes in the calculation of module h.

The general expression of the module h is [120–123]:

$$h = L \frac{r_{AS}}{\sqrt{2}} \left[\int_{C_{Ae}}^{C_{AS}} D_e \cdot r_A dC_A \right]^{1/2} \tag{6.29}$$

where:

r_{AS} and r_A = reaction rates at the external surface, respectively in the pores, both expressed on basis of volume of catalyst particle
C_{AS} = concentration of the reactant at the external surface
C_{Ae} = concentration of the reactant at equilibrium; it is equal to zero for irreversible reactions.

For irreversible reactions of the nth order, Eq. (6.29) becomes:

$$h = L \left(\frac{n+1}{2} \right)^{1/2} \left[\frac{k \rho_S C_{AS}^{n-1}}{D_e} \right]^{1/2} \tag{6.30}$$

and for irreversible reactions of the order I:

$$h = L \left[\frac{k \rho_S}{D_e} \right]^{1/2} \tag{6.31}$$

In Eqs. (6.29)–(6.31), the terms are defined as

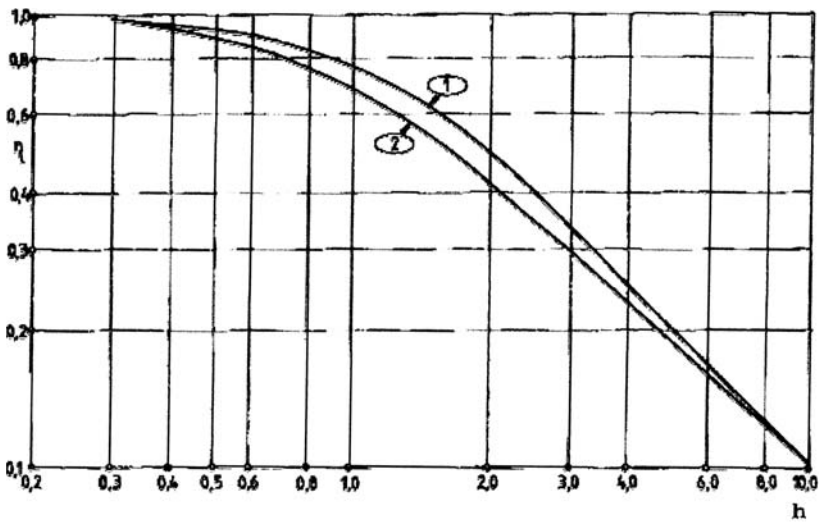k = reaction rate constant
ρ_S = particle density

Figure 6.25a Effectiveness factor η as function of Thiele modulus. 1 – planar particle (Eq. 6.9), 2 – spherical particle (Eq. 6.10).
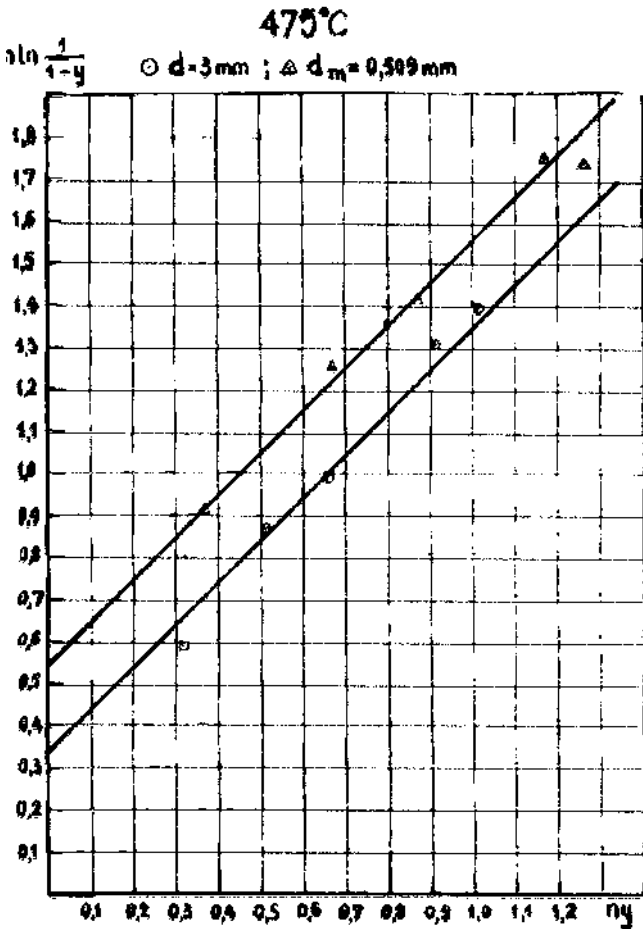

Figure 6.25b Effect of catalyst particle diameter on reaction rate [136]. $\Delta - d = 3.0$ mm, $o - d = 0.6$ mm.

D_e = effective diffusion coefficient

L = characteristic length, given by the ratio of the volume of the particle and its geometric surface [120]. For spheres $L = d/6$.

For zeolites with a 1 μm crystal size [237]:

$$L = \frac{10^{-6}}{6} \, \text{m}^{-1}$$

and for 0.1 μm crystal size (submicron zeolites):

$$L = \frac{0.1 \times 10^{-6}}{6} \, \text{m}^{-1}$$

It follows that the decrease of the size of the zeolite crystals increased the reaction rate. This was confirmed experimentally [237].

The effective diffusion coefficient is expressed by the equation:

$$D_e = \frac{1}{1/D_{AB} + 1/(D_K)_A} \tag{6.32}$$

where D_{AB} is the coefficient for the reactant A diffusing through the substance B, and $(D_K)_A$ is the Knudsen diffusion coefficient of reactant A:

$$(D_K)_A = 9.7 \cdot 10^3 \cdot a \sqrt{\frac{T}{M_A}} \tag{6.33}$$

In this last equation a is the particle radius in cm.

Concerning the influence of internal diffusion on overall kinetics, it is well-known that besides the decrease of the reaction rate, a strong diffusion effect will cause the reaction order to approach the 1st order and the activation energy to decrease, sometimes to only half of the value in absence of the diffusion barrier.

Since the diffusion rate is much less influenced by the temperature than is the reaction rate, there are situations where the effect of diffusion is manifested only after a certain temperature is exceeded.

Studies of catalytic cracking on classic catalysts allowed one to draw interesting conclusions concerning the influence of the internal diffusion. For example, early studies [124] on the influence of internal diffusion at the cracking of isopropylbenzene and of other alkylbenzenes showed that the reaction rate is influenced only when the diameter of the catalyst particles exceeds 0.080 mm. Further studies [125] using a classic catalyst with 10% Al_2O_3 and an average pore diameter of 30 Å, determined the temperatures above which the diffusion influences the overall rate of the process (Table 6.7) for granules of different diameters.

Studies on cracking of crude oil fractions lead to similar conclusions. In one of our studies [1] we investigated catalytic cracking at 450°C of several atmospheric gas oils with a distillation range of 250–360°C and of vacuum gas oils with a distillation range 300–450°C on a classic catalyst containing 12% Al_2O_3. The results showed a doubling of the reaction rate constant when switching from catalyst particles of 3

Table 6.7 Temperature Above Which Internal
Diffusion Influences Reaction Rate

Catalyst particles diameter (mm)	Temperature °C
0.056	690
0.290	380
0.630	345
1.750	307

Source: Ref. 125.

mm to particles having sizes in the range of 0.4–0.6 mm as depicted in Figure 6.25b
[136]. Other authors [126,127] obtained similar results.

These studies show that internal diffusion strongly influences the reaction rate
in moving bed processes that use catalysts as granules of 3–5 mm diameter and do
not influence the process rate in reactors with the catalyst in fluidized bed.

It would be wrong to believe that when using classic catalysts selectivity is not
related to the penetration of some components of the feed into the pores. This effect
on selectivity is related only to the difficulties of pore penetration by some compo-
nents with a very high molecular mass such as the asphaltenes, resins, and organo-
metallic compounds. It is much less specific than with zeolite catalysts.

This effect is illustrated by the data from the Table 6.8, which give the nickel
content of the catalyst powder obtained by the progressive erosion of the external
surface of used catalyst particles [128]. The table shows that the metal (nickel) con-
tent of the surface layer is four times the average concentration of metal in the whole
particle.

In addition to the problems seen in classic catalysts, zeolites have specific ones
related to steric hindrances for the penetration of some feedstock components in the
micropores. The dimensions of the access openings into the pores of various zeolites
are shown (Figure 6.12) compared to the sizes of the hydrocarbons of various
structures, illustrating steric limitations. The data of Figure 6.26 includes the values
of the corresponding diffusion coefficients [129]. The figure shows that important
variations of the diffusion coefficients may result for small variations of the mole-
cular diameters.

Table 6.8 Nickel Content in the Dust Obtained by
External Surface of Erosion of Catalyst Granules

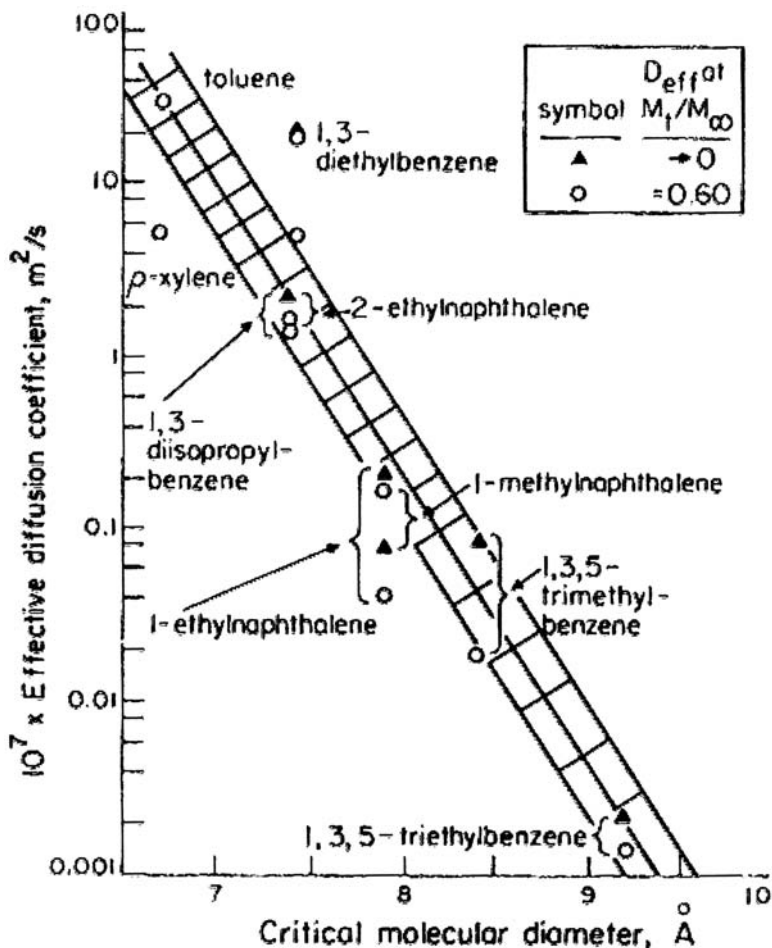| Dust obtained by erosion (wt %)	Ni content in dust
0.5	0.0403
1.5	0.0408
4.5	0.0318
100.0	0.0105

Source: Ref. 128.

Figure 6.26 Diffusion coefficient as function of molecule diameter. ▲– far from equilibrium, ○ – 0.6 of equilibrium. (From Ref. 129.)
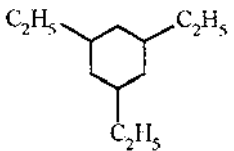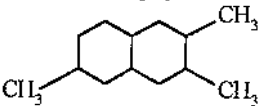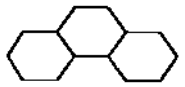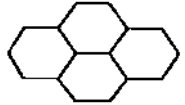
As a result, some components of the feed have access to all active sites of the catalyst, while others have access only to a fraction of them. Therefore, the relative reaction rates will be influenced by the shape of the components that will react, an example of *shape selectivity*.

As an illustration, whereas with classic catalysts the cracking rate of the cycloalkanes increases with the number of rings in the molecule, with zeolite catalysts it decreases because the molecules of larger sizes do not have access to the active sites. The data of Table 6.9 [130] illustrate this difference.

Similarly, with alkanes the rate of reaction depends on the degree of branching, as shown in the data of Table 6.10 [131]. Besides the limitations due to branching, the table illustrates also the much higher reactivity of alkenes compared to alkanes.

It is obvious that the selectivity obtained from various zeolites depends on their specific structure, on the size, and the shape of the pores. On the basis of this

Table 6.9 Relative Reaction Rate of Different Hydrocarbons on Classic Silica-Alumina Catalysts and on Zeolites

Hydrocarbon	Classic Si–Al catalyst	Zeolite REHx catalyst	Reaction rate ratio zeolite catalyst/classic catalyst
	140	2370	17.0
	190	2420	13.0
	205	953	4.7
	210	513	2.4

Source: Ref. 130.

knowledge, the zeolites to be incorporated in the matrix are selected according to the objectives of the process using the catalyst.

6.4.3 Reaction Kinetics

6.4.3.1 Overall Kinetic Equations

Among the first kinetic equations for the catalytic cracking of gas oil were those published in 1945 by A. Voorhies [132].

His equation correlates the average conversion $\bar{x}$ obtained on a stationary bed of catalyst with the volume flowrate w and the contact time τ, and has the form:

$$\bar{x} = \left(\frac{A'_c}{A'_f w}\right)^{1/N_f} \tau^{(N_c-1)/N_f} \tag{6.34}$$

where A'_c, A'_f, N_c, and N_f are the parameters that depend on the feedstock and on the catalyst, the subscripts indicating if they refer to the catalyst (c) or to the feed (f).

On basis of experimental measurements, Voorhies also established an empirical equation for coke formation:

$$C_c = A'_c \tau^{N_c} \tag{6.35}$$

where C_c is the coke amount as weight percent, on the catalyst.

The experiments allowed the calculation of the parameters A'_c and N_c, and then, by means of Eq. (6.14), of the parameters A'_f and N_f, lead to a second empirical equation:

Table 6.10 Reaction Rate Constants and Efficiency Factors for Some Alkanes and Alkenes at 538°C and 1 Bar

Hydrocarbon		Efficiency factor (η)	Reaction step rate, (s^{-1})
n-hexane	C−C−C−C−C−C	1.000	29
3 methyl-pentane	C−C−C−C−C−C with C below	1.000	19
2,2-dimethyl-butane	C−C−C−C with C above and C below	0.300	12
n-nonane	C−C−C−C−C−C−C−C−C	1.000	93
2,2-dimethyl-heptane	C−C−C−C−C−C−C with C above and C below	0.130	63
Hexene-1	C=C−C−C−C−C	0.860	7530
3-methyl-pentene-2	C−C=C−C−C−C	0.500	7420
3,3-dimethylbutene-1	C=C−C−C with C above and C below	0.028	4950

HZSM-5 catalyst with pores length 1.35 µm.
Source: Ref. 131.

$$v = A'_f \bar{x}^{N_f} \tag{6.36}$$

where v is the weight percent of coke in relation to the amount of feed.

From among these equations, the one relating coke formation to residence time (6.35) is still being recommended [11].

In 1946, by considering catalytic cracking as a first order process, A.V. Frost [133] suggested the use of the kinetic equation deduced by T.V. Antipina [134] for first order heterogeneous catalytic reactions in plug flow. This equation assumes that all participating substances follow the Langmuir adsorption law, and that the reaction step is rate controlling.

Catalytic cracking is written as:

$$A \rightarrow v_1 A_1 + v_2 A_2 + \cdots + v_n A_n \tag{a}$$

and the reaction rate r_A is expressed by:

$$r_A = k_S \theta_A \tag{6.37}$$

where k_S is the rate constant of the surface reaction and θ_A is the surface fraction occupied by the reactant A.

By using b_i for the adsorption coefficients and p_i for the partial pressure, and by accepting the Langmuir adsorption law, Eq. (6.17) becomes:

$$r_A = \frac{k_S b_A p_A}{1 + b_A p_A + b_{A_1} p_{A_1} + b_{A_2} p_{A_2} + \cdots + b_{A_n} p_{A_n}} \qquad (6.38)$$

Using x for the conversion and δ for the increase of the number of moles resulted from the stoichiometry of the reaction:

$$\delta = \sum v_i - 1$$

one obtains for the partial pressures the expressions:

$$p_A = p \frac{1 - x}{1 + \delta x}$$

$$p_{A_i} = p \frac{v_i x}{1 + \delta x}$$

Substituting in (6.38) and performing the simplifications, it follows:

$$r_A = \frac{k_S b_A p (1 - x)}{1 + b_A p + (\delta - b_A p + p \sum b_i v_i) x}$$

Using w for the volume feed rate, for an integral plug flow reactor it follows:

$$\frac{1}{w} = \int_0^x \frac{dx}{r_A}$$

Substituting r_A and integrating, one obtains eventually:

$$\alpha = w \left[\ln \frac{1}{1 - x} - \beta x \right] \qquad (6.39)$$

where α and β are given by the equations:

$$\alpha = \frac{k_S b_A p}{1 + \delta + p \sum b_i v_i} \qquad \beta = \frac{\delta - b_A p + p \sum b_i v_i}{1 + \delta + p \sum b_i v_i} \qquad (6.40)$$

Taking into account that the adsorption of coke is very strong, G.M. Pancencov estimated [135] that the adsorption of the other components may be neglected from the denominator of Eq. (6.38) and this equation becomes:

$$r_A = \frac{k_S b_A p_A}{1 + b_c p_c} \qquad (6.41)$$

which, after making the substitutions and integrating, leads to the final equation:

$$k = w \left(\ln \frac{1}{1 - x} - x \right) \qquad (6.42)$$

where the reaction rate constant k is given by the expression:

$$k = \frac{k_S b_A}{b_c v_c}$$

For the case $\beta = 1$, Eq. (6.42) is identical with (6.39).

A large number of studies have confirmed this equation. In our experimental work [97,136,137] feedstocks were prepared by solvent refining and had aromatic carbon content determined by the method n-d-M comprised between 0 and 60% and distillation range between 200–450°C. In all cases, the deviation of the constant β from unity was below the limits of the experimental errors.

The simplification brought by G.M. Pancencov [135] can thus be considered correct and Eq. (6.42) is recommended.

An equation identical to that of Frost was suggested in 1958 by Voge [84] and is used by Decroocq et al. [4].

6.4.3.2   Correlation of Kinetic Constants with Feed Composition

As early as 1966, Raseev showed that compounds with aromatic structures that strongly adsorbed on the catalyst surface decrease the activity of the catalyst and the overall rate of the catalytic cracking reaction [136].

Four fractions with distillation ranges of: 200–250°C, 250–300°C, 300–350°C, and 350–450°C, were prepared using a Romanian crude oil. From each fraction, aromatic concentrates were prepared by means of solvent extraction. The content of aromatic carbon atoms (C_A) in the raffinate and extract were 50–57% C_A and 0.0–2.1% C_A respectively. By mixing them in different proportions, five feeds were obtained with various contents of aromatic carbons. The cyclo-analysis was performed by the n-d-M method [178] while, for the fractions with high C_A content, the Hazelwood method was used [179].

Each feed was cracked in a fixed bed micropilot unit, using a classical Si–Al catalyst [136,137,153].

The kinetic Eq. (6.39) was fitted to the results and the values of the constants α and β were obtained.

For all the feeds and cracking temperatures (450°C, 475°C, and 500°C) the value of the constant β was β = 1.

The rate constant α was be correlated with the content of aromatic carbons C_A determined by cyclo-analysis, and the general equation was obtained:

$$\alpha = a(1 - 1.38C_A) \tag{6.43}$$

where C_A is expressed in weight fractions and α is a constant dependent on the distillation range of the feed and on the cracking temperature (see Table 6.11).

Table 6.11   Constant *a* Values, Eq. (6.43)

Feed distillation limits (°C)	Temperature (°C)		
	450	485	500
200–250	0.0909	–	0.2464
250–300	0.1775	–	0.3990
300–350	0.1985	–	–
350–400	0.3850	0.5122	–

Source: Ref. 1.

The feed characteristics were correlated with the percentage of coke v by using the equation:

$$v = dw^{-b} \tag{6.44}$$

By processing the experimental data the value of $b = 0.6$ for the atmospheric distillates and $b = 0.7$ for the vacuum distillates were obtained.

The constant d was correlated with the percentage of aromatic carbons C_A in the atmospheric distillate, as determined by cyclo-analysis, obtaining the equations [136,153]:

Fraction	200–250°C	$d = (1.635 + 2.93 \times C_A)10^2$
	250–300°C	$d = (3.182 + 2.83 \times C_A)10^2$
	350–400°C	$d = (4.074 + 3.68 \times C_A)10^2$

For the vacuum distillate, a correlation could be obtained with the content of hydrogen of the feed H_2 expressed by fractions by weight using the relations [97,137]:
For cracking at 450°C:

$$d = 0.1546 - 0.798 \ H_2$$

and for cracking at 485°C:

$$d = 0.1741 - 0.843 \ H_2$$

Similar studies using a white paraffin oil with additions of different proportions of α-methylnaphthalene [97] resulted in same type of correlations with the percentage of aromatic carbon atoms, C_A.

6.4.3.3 Catalyst Decay

The difficulties encountered in the analysis of kinetics of catalytic cracking derive mainly form the rapid decrease of catalyst activity during the reaction or catalyst decay, which affects the interpretation of the experimental results.

Two hypotheses were advanced concerning the cause of this decay:

1. The coke deposits forming on the catalyst
2. The duration of the catalyst use or the time on stream.

Various authors [18,138] take into account several variants concerning each of the two hypotheses of deactivation and formulate the corresponding kinetic expressions.

The decrease in catalyst activity as result of coke deposits is considered [137–141] to be a process of the first order, that may be expressed by the equation:

$$\phi_c = e^{-\alpha_c C_c} \tag{6.45}$$

where ϕ_c is the fraction of the catalyst activity remaining after a weight fraction C_c of coke was deposited on the catalyst, and α_c is the deactivation constant.

If the irreversible adsorption of coke is admitted as a cause of catalyst deactivation, one may write, similar to Eq. (6.41):

$$\phi' = \frac{1}{1 + \beta C_c} \tag{6.46}$$

As in (6.45), if deactivation is correlated to the duration of use of the catalyst τ_t, it will be expressed by the equation:

$$\phi_t = e^{-\alpha_t \tau_t} \tag{6.47}$$

Most of the studies [142–144] consider that in this case too, deactivation is a first order process. Nevertheless, some studies produced correlations considering the process to be of order zero [145], second order [146,147] or fractional [132,148]. In the latter case, the differential equation will have the form:

$$\frac{d\phi}{d\tau_t} = \alpha_m \phi^m \tag{6.48}$$

where the exponent m varies between 0 and 1.

The problem of deactivation was also approached by using expressions of the form (6.48) [18,149]. but they lead to additional mathematic difficulties and are not used much.

There are various opinions concerning the degree to which the deactivation of the catalyst affects the rate of the various reactions taken into consideration. In some studies, [11,150,151] it is assumed that since the reactions are catalyzed by the same active sites, the factor ϕ affects them identically and has thus the same value for all the reactions. In other studies [138], one considers it necessary to use various values of ϕ modifying the value of the constant α, depending on the reaction taken into consideration.

6.4.3.4 Three Components Modeling

The practical need to know not only the overall conversion, but also the coke amount and separately the yields of gasoline, $C_3 + C_4$ etc., imposed the use of increasingly complex kinetic models. The different behavior of the alkenes, cycloalkanes, and of the aromatic hydrocarbons imposed that some models also take into account the proportions in which these different classes of hydrocarbons are contained in the feedstock, which of course complicates the model.

Among these, the most simple is the model with three components, represented by the scheme:
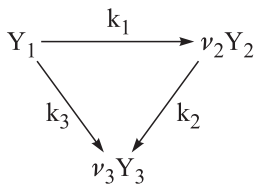
where Y_1 is the gas oil, Y_2 is the gasoline, Y_3 is the gases and the coke.

The first and the better known kinetic treatment based on this scheme was given by Weekman and Nace [152] and it is expressed by the following system of differential equations:

$$\frac{dy_1}{d(1/n)} = -k_0 y_1^2 \phi_t \tag{6.49}$$

$$\frac{dy_2}{d(1/n)} = \left(k_1 \nu_2 y_1^2 - k_2 y_2\right)\phi_t \tag{6.50}$$

$$\frac{d\phi_t}{d(1/n)} = -\alpha\phi_t \tag{6.51}$$

where:

y_1 and y_2 are the weight fractions of gas oil, and gasoline respectively

n is the mass reaction rate expressed as (mass of feed)/(mass of catalyst) · (hour), $k_0 = k_1 + k_3$, v_2 and v_3 stoichiometric coefficients

ϕ_t is the degree of deactivation of the catalyst expressed by Eq. (6.48), with m = 1

The results were fitted by using a 2nd order kinetics for the decomposition reaction of the gas oil and 1st order for the decomposition of gasoline (6.49).

The integration of Eqs. (6.39)–(6.51) for plug flow conditions through a fixed bed of catalyst leads to the following system of equations:

$$y_1 = \frac{1}{1 + \dfrac{k_0\phi_t}{n}} \tag{6.52}$$

written also as:

$$x = 1 - y_1 = \frac{\dfrac{k_0\phi_t}{n}}{1 + \dfrac{k_0\phi_t}{n}} \tag{6.53}$$

$$y_2 = r_1 r_2 e^{-r_2/y_1} \left[\frac{1}{r_2} e^{r_2} - \frac{y_1}{r_2} e^{r_2/y_1} - \mathrm{Ein}(r_2) + \mathrm{Ein}\left(\frac{r_2}{y_1}\right) \right] \tag{6.54}$$

where

$$r_1 = \frac{k_1 v_1}{k_0} \qquad r_2 = \frac{k_2}{k_0} \qquad \mathrm{Ein}(x) = \int_{-\infty}^{x} \frac{e^x}{x} dx$$

Eqs. (6.52) and (6.54) give the instantaneous conversions that decrease with increasing deactivation of the catalyst. In processes with a stationary catalyst bed, such as those used in laboratory studies, one measures the final conversions of a complete cracking cycle. These conversions correspond thus to average conversions, which can be determined by the integration of Eqs. (6.52–6.54).

For the average gasoline conversion $\bar{y}_2$, the equation will be:

$$\bar{y}_2 = \int_{0}^{1} y_2 d\left(\frac{\tau_t}{\tau_s}\right) \tag{6.55}$$

where τ_t is the time on stream of the catalyst, and τ_s is the total duration of the cycle.

The average conversion $\bar{y}_2$ of Eq. (6.54) can be calculated by using numerical methods.

The average total conversion $\bar{x}$ is given by:

$$\bar{x} = \frac{1}{\alpha_t} \ln \left[\frac{1 + \dfrac{k_0}{n}}{1 + \dfrac{k_0}{n} e^{-\alpha_t \tau_s}} \right] \quad (6.56)$$

The system of equations (6.48–6.56) remains the same if ϕ_c—deactivation depending on the coke deposited on the catalyst (Eq. 6.45)—is used in place of ϕ_t.

Eqs. (6.52) and (6.54) allow the calculation of the total conversion and of the conversion to gasoline. The conversion to gases C_1–C_4 and coke is obtained by difference.

In order to obtain the conversion to coke by itself, it is necessary to use equations of the type (6.35) or (6.36). For systems in which the catalyst circulates between the reactor and the regenerator, the residence time of the catalyst in the reactor τ is easy to determine and the use of a type (6.35) equation is recommended. It is usually written in a simplified form, where C is the weight percent coke on the catalyst:

$$C = A\tau^N \quad (6.57)$$

Note [11] that the value of the constant A depends on the catalyst, the feed, and the operating conditions, whereas the constant N varies very little with these factors and usually has a value of about 0.5.

The three components model, using first or second order kinetics for the cracking reactions of gas oil was utilized in many studies [151,155].

Thus, J.M. Kolesnicov, I.N. Frolova, and H.A. Lapshina [180] studied the cracking of a petroleum gas oil fraction with a density of 0.869 on a natural silimanite catalyst activated with sulfuric acid. The data were correlated by using kinetic equations of the 1st order of the form (6.39) and a three components model. The following values were obtained for the rate constants:

at 450°C	$k_1 + k_3 = 0.095$ g/g·h	$k_2 = 0.260$ g/g·h
at 480°C	$k_1 + k_3 = 0.131$ g/g·h	$k_2 = 0.326$ g/g·h
at 510°C	$k_1 + k_3 = 0.208$ g/g·h	$k_2 = 0.480$ g/g·h

D.W. Kraemer and H.J. Lasa [181] used a similar model but where the formation of coke was not included. They used 2nd order kinetics for the gas oil decomposition reaction. The results obtained in this study do not seem plausible. By processing the data, the value $k_2 = 0$ was obtained for the decomposition of gasoline to gases. Also, a strong influence of temperature was seen on the constant k_3 while its effect on the constant k_1 was almost insignificant.

N.N. Samoilova, V.N. Erkin, and P.J. Serikov [151] use the same three components kinetic model but took into account the chemical composition of the feed. They also took into account the time rate deactivation of the catalyst, using to this purpose Eq. (6.47). The study proved that the constant α_t in Eq. (6.47) does not depend on the nature of the feed.

The experimental data was processed using a 1st order kinetic equation for the decomposition of the vacuum distillates and also 1st order kinetics for the decomposition of gasoline.

The decomposition of the vacuum distillate (sum of the constants $k_1 + k_3$) was correlated with the ratio of the content of aromatic hydrocarbons to that of alkanic hydrocarbons in the feed—A/P by means of the exponential relation:

$$k_1 + k_3 = a_0(A/P)^{-b} \tag{6.58}$$

The values of the constants a and b for different temperatures are given in Table 6.12.

The apparent activation energies for the decomposition of vacuum distillates is situated between 24.7 and 28 kJ/mole.

M. Larocca, S. Ng, and H. de Lasa [159] make a distinction between the alkanic, cyclo-alkanic, and aromatic hydrocarbons contained in the feed in the framework of the kinetic model of Figure 6.29.

The work uses the exponential equation to express the deactivation of the catalyst as a function of the amount of deposited coke.

The gas oil feed was injected in the He stream that fluidizes the microspherical catalyst in the reactor. The rate constants were determined for three commercial catalysts, separately for alkanes, cycloalkanes, and aromatic hydrocarbons at various temperatures. On this basis, the behavior of these classes of hydrocarbons were compared.

The composition of the feed was also taken into account in other studies that dealt with the kinetics of catalytic cracking [18,156,237].

6.4.3.5 Three Components Modeling Applied to Moving Bed and Fluidized Bed Systems

The kinetic reactions deduced by Weekman and Nace were successfully applied to the design of systems involving moving beds, fluidized beds in dense phase [11], and in riser systems [154] presented in this section.

The accepting of a kinetic equation of 2nd order for the cracking of gas oil (E.6.49–6.51) was (Krishnaswamy and Kittrell [150]) compared with an identical model wherein the cracking reaction was of the 1st order, but another equation for the deactivation of the catalyst was considered. The system of differential equations used in their work was:

$$\frac{dy_1}{d(1/n)} = -k_0 y_1 \phi \tag{6.59}$$

Table 6.12 Eq. (6.58)
Constants

Temperature (°C)	a_0	b
420	1.16	0.36
440	1.24	0.39
460	1.29	0.44
480	1.33	0.48
510	1.39	0.50
530	1.46	0.50

$$\frac{dy_2}{d(1/n)} = (k_1 \upsilon_1 y_1 - k_2 y_2)\phi \qquad (6.60)$$

$$\frac{d\phi}{d(1/n)} = -\beta y_1 \phi \qquad (6.61)$$

Different from Eq. (6.51) used by Weekman and Nice, Eq. (6.61) for the catalyst deactivation contains y_1, which is a weight fraction of feed.

Both systems of equations were integrated for systems of the riser type and compared with the experimental data [154]. For the usually used conversions, practically identical results were obtained. It is therefore possible to use in calculations two equation systems:

In the system described by Eqs. (6.49–6.51) the cracking of gas oil is a reaction of the 2nd order and the deactivation of the catalyst is independent of the feed concentration.

In the equation system (6.59–6.61), all the reactions are of the 1st order while the deactivation of the catalyst depends on the feed concentration.

In connection with this agreement it is to be remarked that Eq. (6.59) is in fact an equation of the 2nd order, since ϕ depends on y. This explains the similarity between the expressions for the integral equations obtained with the two models.

It must be emphasized that both equation systems are formulated for quasi-homogeneous reaction systems, which confers them a semi-empirical character. From this point of view, an interesting paper [156] reports that kinetic processing uses Langmuir adsorption isotherms and makes a comparison of the results with those obtained when using 2nd order, quasihomogeneous kinetics, expressed by the equations (6.49–6.51).

Another study [156] used a pulsed reactor, which made the assumption that the deactivation phenomena for the catalyst were negligible.

By accepting as in the previously cited works [135] that the adsorption of one of the reaction products is very strong, it leads to the expression:

$$-[\ln(1-x)] - x = k\frac{RT}{p_0}\left(\frac{b}{b_p}\right)\frac{G}{F} \qquad (6.62)$$

where:

p_0 is the partial pressure of the feed, b and b_p are the adsorption constants for the feed and for the products

G is the amount of the catalyst,

F is the feedrate in gas phase

It is easy to understand that by including the adsorption constants in the rate constant and by using the volume feedrate, an expression identical with (6.42) is obtained.

Eq. (6.62) gives good agreement with the experimental data, including those that served to verify Eqs. (6.52–6.54). This agreement is illustrated in Figure 6.27, which shows an almost linear correlation between the corresponding expressions for the two types of equations for conversions ranging between $x = 0.3$ and $x = 0.8$. This finding led to the conclusion [156] that homogeneous 2nd order kinetics is only
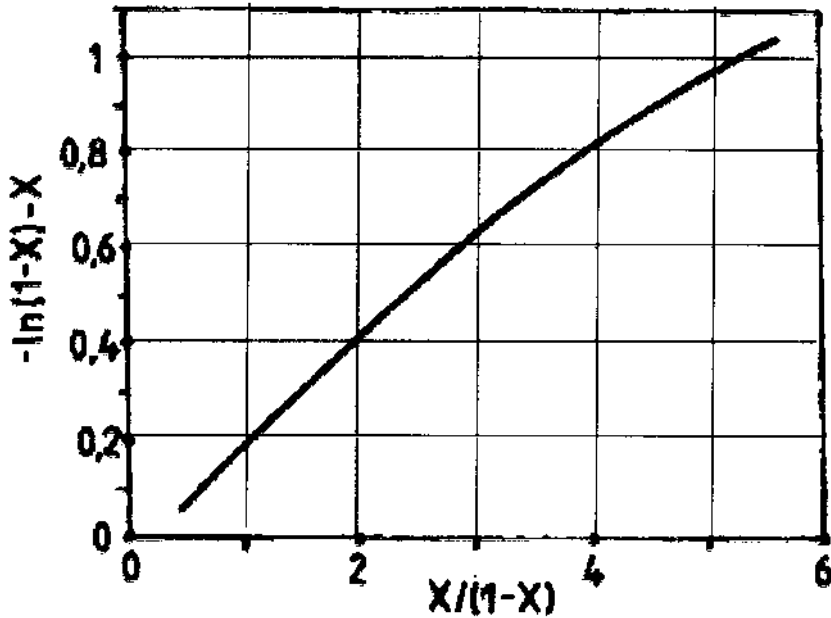
Figure 6.27 Conversion for second order reaction rate in homogenous system, versus for first order rate, in heterogeneous system, with strong adsorption of one of the reaction products. (From Ref. 156.)

a mathematical approximation of heterogeneous 1st kinetics, hindered by the coke which is formed in the process.

The mathematical form of Eq. (6.62) makes it difficult to treat models made of a number of simultaneous reactions. Therefore, in such cases the system of Eqs. (6.52–6.54) is used.

Eqs. (6.49–6.51) were used to derive the integral form not only for systems involving a stationary catalyst, but also for: (a) cracking in a fluidized bed in dense phase and (b) in reactors of the riser type, which were treated as systems with a cocurrent moving bed.

Dense phase fluidized bed reactors[*].   The most simple treatment is that of B. Goss, D.M. Nace, and S.E. Voltz [157], which applies the same effectiveness factor K_f to all the rate constants. Thus, Eqs. (6.53) and (6.56) become:

$$x = \frac{K_f \dfrac{k_0 \phi_t}{n}}{1 + K_f \dfrac{k_0 \phi_t}{n}} \tag{6.63}$$

$$\bar{x} = \frac{1}{\alpha_t} \ln \left[\frac{1 + K_f \dfrac{k_0}{n}}{1 + K_f \dfrac{k_0}{n} \phi_t} \right] \tag{6.64}$$

---

[*] The treatments that follow imply the existence of good fluidization.

Eq. (6.54) remains unchanged since it contains ratios of the rate constant and not absolute values.

The more exact equations deduced by Weekman and Nace [152] are also recommended in review articles [11]. The authors consider that the catalyst in the fluidized bed is perfectly mixed and that the ascending flow of reactants has a constant velocity across the entire cross section of the reactor, as it passes through the bed.

In this situation, in the equations system (6.49–6.50), ϕ_1 is constant, Eq. (6.51) disappears, and ϕ can be expressed by Eq. (6.46).

The Eq. (6.49) becomes:

$$\frac{dy_1}{d(1/n)} = -\frac{k_0}{1 + \beta C_c} y_1^2 \tag{6.65}$$

Integrating between the limits $y = 1$ for $n = \infty$ and y for n, it results:

$$y_1 = \frac{1 + \beta C_c}{1 + \beta C_c + k_0/n} \tag{6.66}$$

and

$$\varepsilon = \frac{k_0/n}{1 + \beta C_c + k_0/n} \tag{6.67}$$

where ε is the total conversion: $\varepsilon = 1 - y_1$.

Weekman and Nace [152] introduce an extended variable for the reaction time of the form:

$$\frac{x}{(1 + \alpha_t \tau_t)w}$$

where:

x is the height, expressed as fraction of the height of the fluidized bed

$\alpha_t \tau_t$ is the exponent of Eq. (6.47) that expresses the deactivation of the catalyst function on the time on stream

w is the volumetric rate.

Introducing this variable, the Eq. (6.49) becomes:

$$\frac{dy_1}{dx} = \frac{k_0}{(1 + \alpha_t \tau_t)w} y_1^2 \tag{6.68}$$

which, after integration gives:

$$y_1 = \frac{1 + \alpha\tau}{1 + \alpha\tau + k_0/w} \tag{6.69}$$

and

$$\varepsilon = \frac{k_0/w}{1 + \alpha\tau + k_0/w} \tag{6.70}$$

These two equations differ from (6.66) and (6.67) only by the manner of expressing the deactivation of the catalyst, i.e., depending on the time on stream τ

and not on the amount of deposited coke C_c, and by expressing the feedrate in terms of volume instead of mass flowrate.

Concerning the conversion to gasoline y_2, since the integrated Eq. (6.54) involves only the ratios of the rate constants and assuming that all the constants are affected by the same deactivation factor ϕ, it results that this equation remains valid also for cracking in a fluidized bed.

The equation that expresses the maximum conversion to gasoline y_{2max} is obtained by equating to zero the differential equation (6.50), from which it results:

$$y_{2\,max} = \frac{k_1 v_2}{k_2}(1 - \varepsilon_{y\,max})^2 \tag{6.71}$$

If y_{2max} is expressed as a weight fraction, the stoichiometric coefficient v_2 must be omitted.

In order to express the volume rate corresponding to the maximum of gasoline, one writes w of Eq. (6.70) in explicit form. In the obtained equation ε is substituted by $\varepsilon_{y\,max}$ written from Eq. (6.71) in explicit form. Eventually, one obtains:

$$w_{y_{2\,max}} = \frac{k_0}{(1 + \alpha\tau)\left[\sqrt{\dfrac{k_1 v_1}{k_2 y_{2\,max}}} - 1\right]} \tag{6.72}$$

Similarly, using the expression (6.67) in the place of (6.70) it results:

$$n_{y_{2\,max}} = \frac{k_0}{(1 - \beta C_c)\left[\sqrt{\dfrac{k_1 v_1}{k_2 y_{2\,max}}} - 1\right]} \tag{6.73}$$

Riser and cocurrent moving bed reactors. These reactors are characterized by the cocurrent moving of the catalyst and the reactant, which leads to kinetic equations of the same form.

Generally, the simplifying assumption is accepted that the residence time of the catalyst in the reactor is identical to that of the vapors that circulate through the system [154]. In these conditions the residence time of the catalyst τ_1 contained in the exponent of Eq. (6.47) may be expressed by:

$$\tau_1 = \frac{1}{w} = \frac{\overline{\rho}}{n} \tag{6.74}$$

with the condition that w should be expressed in the same time units as used in Eq. (6.47); $\overline{\rho}$ represents the mean density of the vapor stream flowing through the reactor.

Substituting in (6.47) and then in (6.49), one obtains:

$$\frac{dy_1}{d(1/n)} = -k_0 y_1^2 e^{-\alpha\overline{\rho}/n} \tag{6.75}$$

By integrating this equation within the limits $y = 1$ for $n = \infty$ and y for n, it follows:

$$\frac{1}{y_1} - 1 = \frac{k_0}{\alpha\overline{\rho}}\left(1 - e^{-\alpha\overline{\rho}/n}\right) \tag{6.76}$$

which is identical with the equation obtained by Paraskos [154], and confirmed by his experimental determinations. Weekman and Nace [18] using a different path obtained at the end an equivalent equation.

Concerning the equations that express the conversion to gasoline (6.54) and the maximum of gasoline (6.71), they remain the same because in these equations only the ratios of the rate constants intervene, which are considered to be affected in identical manner by the catalyst deactivation phenomenon.

In order to obtain the feedrate corresponding to the maximum of gasoline, in Eq. (6.76) one substitutes $y_1 = 1 - \varepsilon$ and $\overline{p} = \tau_1 n$. One obtains:

$$1 - \varepsilon = \frac{1}{1 + \dfrac{k_0}{\alpha n \tau_t}(1 - e^{-\alpha \tau_t})}$$

For the conditions of maximum conversion to gasoline, one replaces $(1 - \varepsilon)$ by $(1 - \varepsilon_{y\max})$ from Eq. (6.71). After regrouping it follows:

$$n_{y_2 \max} = \frac{k_0(1 - e^{-\alpha \tau_t})}{\alpha \tau_t \left[\sqrt{\dfrac{k_1 v_2}{k_2 y_{2\max}}} - 1\right]} \tag{6.77}$$

Since gasoline represents the main product of catalytic cracking, the analysis of the influence of process factors and their selection to the purpose of maximizing gasoline yield is a problem of utmost importance. But, the obtained Eqs. (6.54) and (6.71) combined with (6.73) for the fluidization in dense phase, or with (6.77) for systems with riser reactor, make such an analysis very difficult.

By simplifying the system to one represented by:

$$A \xrightarrow{k_1} B \xrightarrow{k_2} C$$
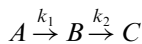
Wojciechowski and Corma [18,158] deduced equations that allowed computer simulation of the variation of the conversion to gasoline, as a fraction of the total conversion. The results were plotted as curves corresponding to various reaction conditions. Despite the fact that the published representations [18] have qualitative character, they allow some conclusions with general character which are given in the Section 6.4.4.

The quantitative dependency of the conversion to gasoline versus the conversion of the gas oil was calculated by the above equations [152], and the results are compared to experimental data in Figure 6.28.

6.4.3.6 Systems With Four and More Components

A model with three components (lumps) was developed by Larocca et al. [159] in a study that focused especially on the modeling of catalyst deactivation. The study used a pulsed reactor. For the processing of the data the model with three components, described previously, and a model with five components reproduced in Figure 6.29 were applied. This latter model considers that in the cracking process, the alkanes (paraffins, P), cyclo-alkanes (naphthenes, N), and aromatic hydrocarbons (A) in the feed behave differently from each other.
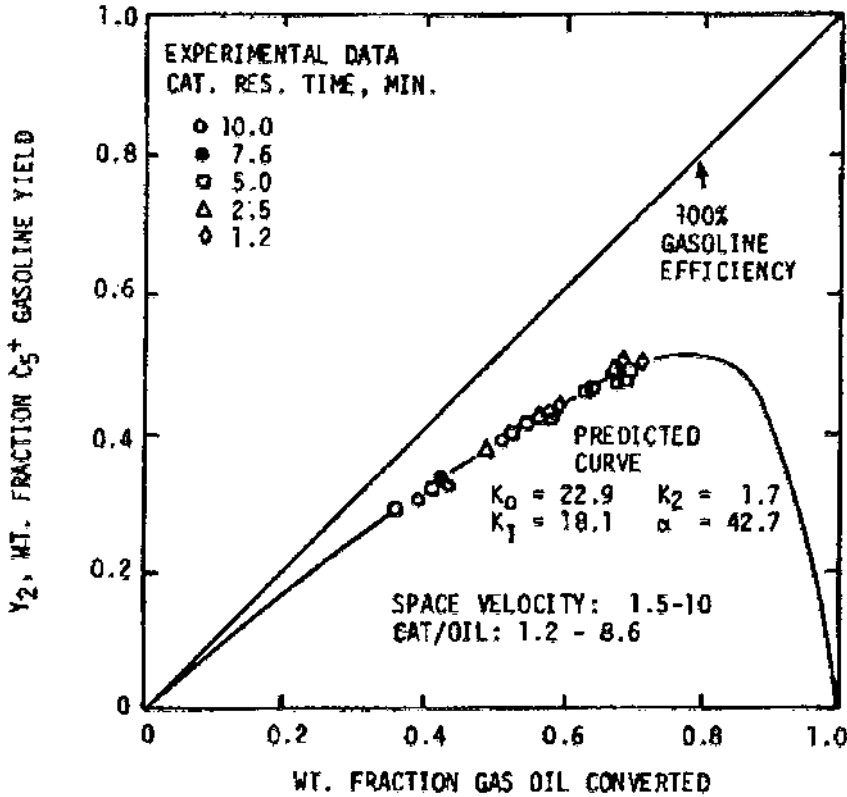
Figure 6.28 Comparison of the kinetic model with experimental data for a moving bed system. (From Ref. 152.)

The model is described by a system of differential equations corresponding to the pulsed flow reactor, considering that all the reactions are of 1st order, and that the deactivation of the catalyst is expressed by the equation:

$$k = k_0 \tau_t^{-m} \tag{6.78}$$

where:

k_0 and k are the rate constants at the beginning of the run and after a time on stream τ_t

m has the value 0.1–0.2.

The most important development of the three components model is a model with four components (Figure 6.30) [160] that separates the conversion to gases from the conversion to coke.

Expressing the concentrations Y in weight fractions, accepting 2nd order kinetics for the three cracking reactions of gas oil and 1st order kinetics for the other reactions, the authors formulate the following system of differential equations:

$$\frac{dY_1}{d\tau} = -(k_{12} + k_{13} + k_{14})\phi Y_1^2 \tag{6.79}$$
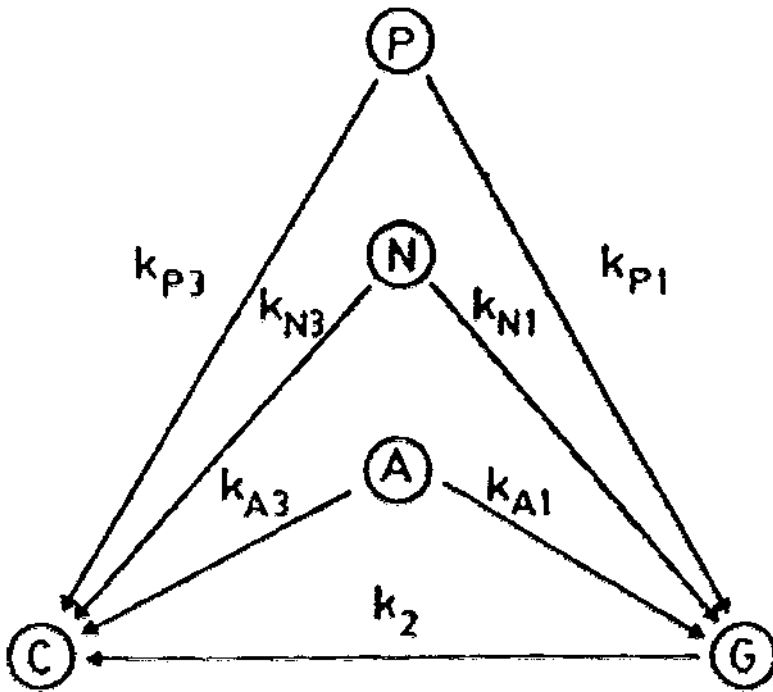
Figure 6.29 Five components (lumps) model. P – alkanes (paraffins), N – cyclanes (naphthenes), A – aromatics in the feed. G – gasoline, C – gases (C_1–C_4) and coke. (From Ref. 159.)
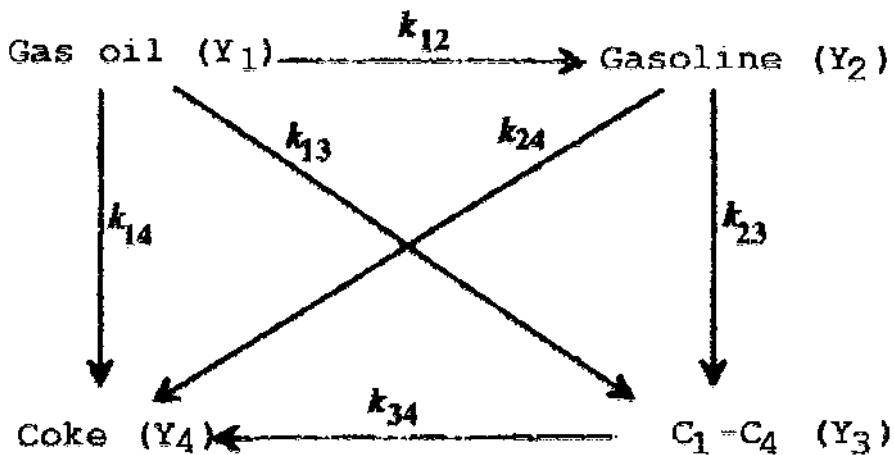

Figure 6.30 Four components (lumps) model. (From Ref. 160.)

$$\frac{dY_2}{d\tau} = k_{12}\phi Y_1^2 - (k_{23} + k_{24})\phi Y_2 \tag{6.80}$$

$$\frac{dY_3}{d\tau} = k_{13}\phi Y_1^2 + k_{23}\phi Y_2 - k_{34}\phi Y_3 \tag{6.81}$$

$$\frac{dY_4}{d\tau} = k_{14}\phi Y_1^2 + k_{24}\phi Y_2 + k_{34}\phi Y_3 \tag{6.82}$$

where ϕ is the catalyst deactivation function and the subscripts to the rate constants k are those indicated in Figure 6.29.

The system was solved in the same manner as the model with three components, obtaining the same type of integrated equations for gas oil and gasoline.

For the conversion to coke, the equation has the form:

$$
\begin{aligned}
Y_4 = {} & 1 - a(1 - r_1)(1 - \varepsilon) - \frac{r_1(r_{34} - br_2)}{(r_{34} - r_2)}\exp\left(r_2 - \frac{r_2}{1 - \varepsilon}\right) \\
& - \frac{r_1 r_2(r_{34} - br_2)}{(r_{34} - r_2)}\exp\left(-\frac{r_2}{1 - \varepsilon}\right)\left[\text{Ein}\left(\frac{r_2}{1 - \varepsilon}\right) - \text{Ein}(r_2)\right] \\
& - \left[(1 - a)(1 - r_1) - \frac{r_1 r_2(1 - b)}{(r_{34} - r_2)}\right]\exp\left(r_{34} - \frac{r_{34}}{1 - \varepsilon}\right) \\
& - \left[(1 - a)(1 - r_1)r_{34} - \frac{r_1 r_2 r_{34}(1 - b)}{(r_{34} - r_2)}\right]\exp\left(-\frac{r_{34}}{1 - \varepsilon}\right)\left[\text{Ein}\left(\frac{r_{34}}{1 - \varepsilon}\right)\right. \\
& \left. - \text{Ein}(r_{34})\right]
\end{aligned}
\tag{6.83}
$$

where:

$$\varepsilon = 1 - Y_1, \quad a = k_{14}/(k_{13} + k_{14}), \quad b = k_{24}(k_{23} + k_{24}),$$
$$r_1 = k_{12}/(k_{12} + k_{13} + k_{14}), \quad r_2 = (k_{23} + k_{24})/(k_{12} + k_{13} + k_{14}),$$
$$r_{34} = k_{34}/(k_{12} + k_{13} + k_{14}), \quad \text{Ein}(x) = \int_{-\infty}^{x}\frac{e^x}{x}dx$$

The constants r_1 and r_2, which contain the expressions for the rate constants, result from the processing of the model with three components. The constants a, b, and r_{34}, which appear only in the model with four components, were obtained by processing data obtained in a Kellogg riser pilot plant.

The agreement between the conversion to coke calculated by Eq. (6.83) with that measured in the pilot plant or in a industrial plant is presented graphically in the original paper [160]. The maximum deviations are of the order $\pm$ 15–20%.

Another article [161] used the model with four component lumps but ignored, which seems logical, the direct formation of coke from gases.

Models with a much higher number of components were also suggested, either in order to detail the composition of the gases or to take into account the differences in the behavior of the feed components.

To the first category belongs the model proposed by John and Wojciechowski [162], reproduced in Figure 6.31 and that suggested by Corma et al. [163]. To the
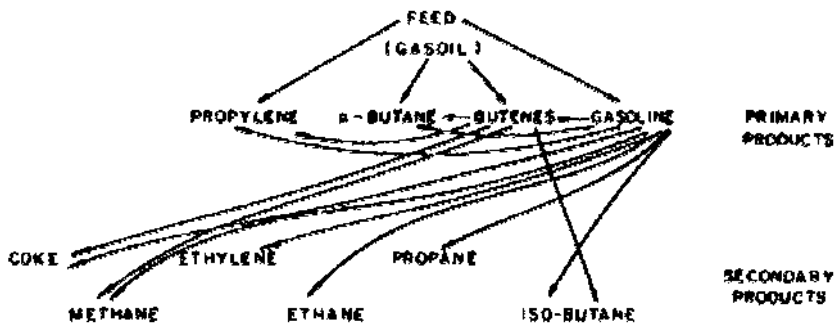
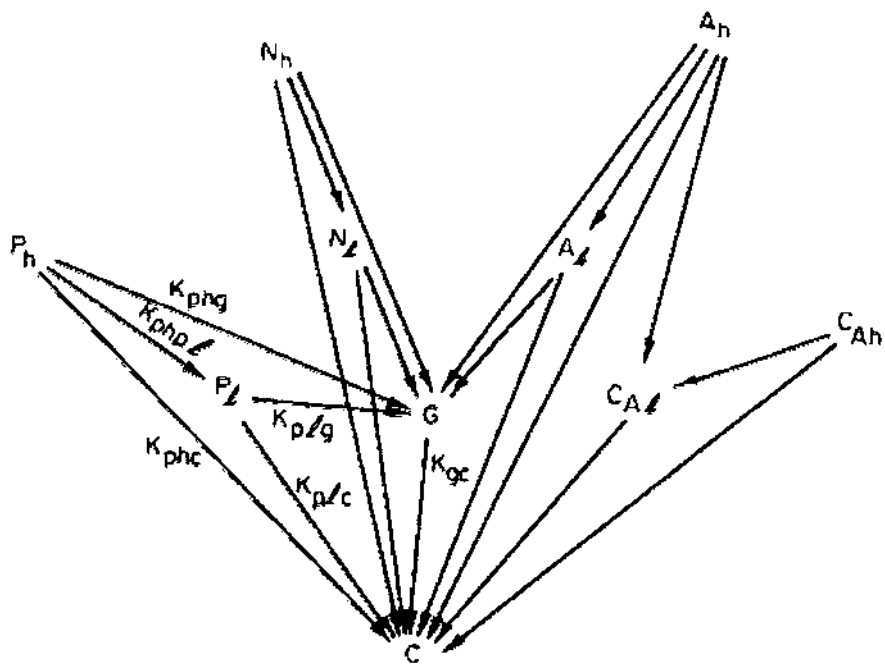**Figure 6.31** Model proposed by John and Wojciechowski. (From Ref. 162.)

Figure 6.32 Ten-lump kinetic model scheme. P_1 = wt % paraffinic molecules, 222–342°C; N_1 = wt % naphthenic molecules 222–342°C; C_{A1} = wt % carbon atoms among aromatic rings, 222–342°C; A_1 = wt % aromatic substituent groups (222–342°C); P_h = wt % paraffinic molecules, >342°C; N_h = wt % naphthenic molecules, >342°C; C_{Ah} = wt % carbon atoms among aromatic rings, >342°C; A_h = wt % aromatic substituent groups (>342°C); G = G lump (C_5-222°C); C = C lump (C_1–C_4 + coke); C_{A1} + P_1 + N_1 + A_1 = LFO (222–342°C); C_{Ah} + P_h + N_h + A_h = HFO (>342°C).

second category belongs the model with 10 components suggested by Jacob et al. [164,165], depicted in Figure 6.32.

This latter model (Figure 6.32) takes into account in a detailed manner the chemical composition of the feed, as well as its structure in terms of distillation fractions, which allows its use for feeds containing components of a variety of natures. However, it has the disadvantage that it calculates only the overall yield of gases C_1–C_4 + coke resulted from the process. In order to compensate for this disadvantage, Olivera and Biscaia Jr. [166] completed the Jacob's model by separately modeling the formation of coke and the formation of primary and secondary gases.

The kinetic model of Jacob was further compared with the three above models. Finally four models resulted, as follows:

Model 1. From Figure 6.31, without completions, where the deactivation of the catalyst is described by a hyperbolic equation similar to Eq. (6.24):

$$\phi(t_c) = \frac{1}{1 + \beta t_c^{\gamma}} \tag{6.84}$$

where t_c is the duration of catalyst use, and β and γ are constants.

The other three models are based on the model of Figure 6.31 completed with the separate accounting for gas and coke formation, and which differ from each other by the catalyst deactivation equation considered.

Model 2. Uses the deactivation equation (6.84) and has the same value for the constants β and γ for gas oil and gasoline.

Model 3. Uses different values of the deactivation rate ϕ for gasoline and for gas oil, both being expressed by exponential equations of the form (6.47).

Model 4. Uses also different values for ϕ for gasoline and gas oil, but the deactivation is expressed, depending on the coke amount deposited on the catalyst, by exponential expressions of the form (6.45).

The experimental data for gasoline cracking obtained in an isothermal reactor with a fixed bed of catalyst were processed by means of each of the four models obtaining the following conclusions:

> The reaction rates for gasoline cracking to secondary gases and to coke have rates equal to zero.
> The catalyst activity decreases faster during the cracking of primary gas than for gasoline cracking.
> Model 4, in which the deactivation of the catalyst depends on the deposited coke, gives the best agreement with the experimental data.

Thus, model 4, is recommended for modeling the catalytic cracking of gas oil.

A recent study [239] compared the 3-, 4-, and 5-lumps kinetic models with experimental data obtained at 480°C, 500°C, and 520°C in a micro-activity reactor (ASTM D 3907–92). The best results were obtained by using the 5-lumps kinetic model (Figure 6.33).

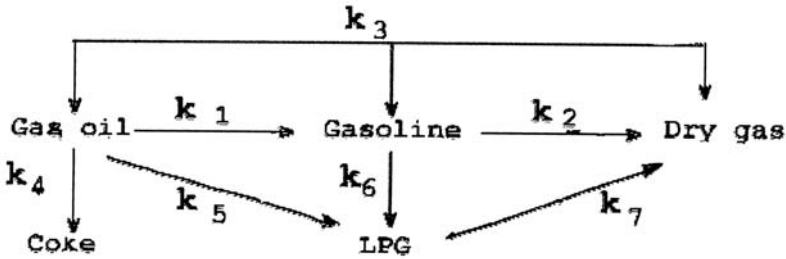For catalyst deactivation, the exponential expression (6.45) was used, with $\alpha = 0.0875$.

Figure 6.33 5 lumps kinetic model. (From Ref. 239.)

The obtained kinetic constants and activation energies (10^3 kcal/mol) were:

$k_1 = 0.1942$ $\quad$ $E_1 = 13.7$
$k_2 = 0.0032$ $\quad$ $E_2 = 10.8$
$k_3 = 0.0001$ $\quad$ $E_3 = 11.8$
$k_4 = 0.0140$ $\quad$ $E_4 = 7.6$
$k_5 = 0.0357$ $\quad$ $E_5 = 12.5$
$k_6 = 0.0061$ $\quad$ $E_6 = 17.5$
$k_7 = 0.0020$ $\quad$ $E_7 = 9.5$

In another study [161], a kinetic model with four components, similar to that of Figure 6.30 but without the reaction for coke formation from gases ($k_{34} = 0$), served for the determination of the kinetic constants of the 2nd order reaction for gas oil cracking and of 1st order gasoline cracking. The deactivation of the catalyst was considered the same for all the reactions and was expressed by an exponential equation where the variable was the time the catalyst was on stream (6.47).

The constants were derived by processing published data concerning the performance of a catalyst with high activity in a riser type reactor. The conversion was defined in terms of the weight percent of gasoline, gases, and coke.

The kinetic parameters deduced for a single feed and a catalyst are collected in Table 6.13.

A seven-lump model used by Al. Khattaf and de Lasa [237] gives the kinetic equation for the formation of alkanes, alkenes, naphthenes, aromatics, coke, and methane.

A new treatment of the kinetics of gas oil catalytic cracking [167], takes into account in detail the reaction mechanism involving carbenium ions. This approach is close to the ''mechanistic modeling'' used in the pyrolysis of the gas oil, discussed in Section 5.14.

Before the model was actually formulated, several necessary simplifications were brought to the reaction mechanism. For example, the rate of extraction of a hydride ion by a Lewis site was considered to be independent of the nature of the alkane hydrocarbon from which the extraction took place. Only the extractions from secondary or tertiary carbon atoms were considered.

The equations for the rates of formation of the carbenium ions were written on the basis of the classic interaction reactions of the alkanes with the active Lewis sites

Table 6.13 Kinetic Constants for 4-lump Model

Kinetic constants	Temperature (°C)			A (h^{-1})	E (kJ/mol)
	482.2	548.8	615.5		
α^a	1.944	10.140	31.102	$3.017 \cdot 10^8$	117.7050
k_{12}	15.644	39.364	79.408	$9.778 \cdot 10^5$	68.2495
k_{13}	3.323	9.749	28.020	$4.549 \cdot 10^6$	89.2164
k_{14}	1.297	3.302	6.102	$3.765 \cdot 10^4$	64.750
$k_1 = k_{12} + k_{13} + k_{14}$	20.264	52.415	113.440	$1.937 \cdot 10^6$	72.2526
k_{23}	0.711	1.370	2.470	$3.255 \cdot 10^3$	52.7184
k_{24}	0.411	0.753	1.384	$7.957 \cdot 10^3$	63.4580
$k_2 = k_{23} + k_{24}$	1.122	2.123	3.854	$4.308 \cdot 10^3$	51.6726

^{a} α, constant from the equation $\phi = e^{-\alpha \tau}$.
Source: Ref. 161.

and of the alkenes with the Brönsted centers. From here, the equations for the rates of formation by way of β scissions of the alkanes and alkenes were deduced.

By application of the steady states theorem to the carbonium ions produced on the two types of sites, the rate equations for the catalytic cracking of the considered hydrocarbons were derived.

This method of calculation was applied for the determination of the rate constants of the elementary reactions considered in the catalytic cracking of alkanes. This approach can be extended to the catalytic cracking of cyclo-alkenes and alkyl-aromatic hydrocarbons.

The determined reaction rates are initial rates that do not take into account the catalyst deactivation as a consequence of coke deposits.

It seems that this study opens new promising ways for the treatment of the kinetics of catalytic cracking of petroleum fractions.

The effect of adding residues derived from different crude oils in proportions of up to 20% to the vacuum distillates feed was studied. The study however, does not supply the necessary elements for the generalization of the conclusions and for their application to the catalytic cracking of other feeds.

6.5 EFFECT OF PROCESS CONDITIONS

The process conditions influencing the catalytic cracking may be grouped as follows:

Temperature
Pressure
Feed composition
Feed recycling
Catalyst behavior
Catalyst/feed ratio

The influence of the volume feedrate results from Section 6.4 (on the kinetics of catalytic cracking).

6.5.1 Temperature

In catalytic cracking as in other processes, the influence of temperature on the reaction rate is expressed by the Arrhenius equation:

$$k = A e^{-E/RT} \tag{6.85}$$

It must be remarked that in heterogeneous catalytic process, the activation energy experimentally measured (in conditions where the diffusion phenomena do not influence the reaction rate) is an apparent energy E^X that includes the heats of adsorption of the reactants and of desorption of the products. The connection between the apparent activation energy and the activation energy of the reaction itself E is given by the relation:

$$E^X = E - \lambda_A + \lambda_B \tag{6.86}$$

where λ_A and λ_B are the heats of adsorption of the reactants, respectively of the products.

The second remark refers to the very large differences between the activation energies calculated by various researchers on basis of experimental data that vary between the limits 20–125 kJ/mole. In a previous work [1] examples were given and the causes of these differences were analyzed.

There are two main reasons that lead to such large differences:

The form of the kinetic equation used for calculating the rate constants at two temperatures

The influence of the diffusion phenomena on the conditions in which the determinations were carried out

The first cause of errors can be avoided by using the Arrhenius equation written as:

$$\ln \frac{k_{T_1}}{k_{T_2}} = \frac{E}{R} \left(\frac{1}{T_2} - \frac{1}{T_1} \right) \tag{6.87}$$

and replacing the ratio of the rate constants by the ratio of the reaction times required for obtaining the same degree of conversion at the two temperatures.

Indeed, since any kinetic equation may be written as:

$$k = w \cdot f(x),$$

it results that for two temperatures and for a specified conversion x constant, one may write:

$$\frac{k_{T_1}}{k_{T_2}} = \left(\frac{w_{T_1}}{w_{T_2}} \right)_{x=\text{const}} \tag{6.88}$$

which allows replacing in Eq. (6.67) the ratio of the rate constants with the ratio of the volume rates at constant conversion. There is no need to know the expression for the reaction rate equation.

Thus the activation energies for the formation of coke deposits on the catalyst can be calculated even if certain kinetic equations are missing.

Concerning the influence of diffusion phenomena, the only solution is to use experimental techniques that eliminate such influences. This approach is used in

numerous studies [154,156,157,158]. Before accepting the obtained values for the activation energies, it is necessary to perform an analysis of the experimental technique and of the calculation methods.

The analysis of the published data allows one to conclude that the average values of the activation energies vary with the characteristics of the catalyst and of the feed.

For the lower alkanes, the activation energies [83] show a decrease of the activation energy with the molecular mass.

n-C_6H_{14}	153 kJ/mol
n-C_7H_{16}	123 kJ/mol
n-C_8H_{18}	104 kJ/mol

For atmospheric and vacuum petroleum fractions, the majority of the published studies [4] suggest values ranging between 40 and 60 kJ/mole. Our own studies of the catalytic cracking of a vacuum distillate using a microspherical, classic, equilibrium catalyst extracted from an industrial plant lead to values of about 60–70 kJ/mole [97]. It was also verified that the addition of α-methyl-naphthalene did not sensibly modify the value of the activation energy.

The variation of the apparent activation energy with the molecular mass shows a higher value of the activation energies corresponding to the decomposition of the gasoline to gases as compared to the formation of gasoline from the feed [1,127].

Since the formation and the decomposition of gasoline constitute two successive reactions, it results that, similarly to the thermal cracking, the increase of the temperature in catalytic cracking leads to the decrease of the maximum of gasoline yield. This conclusion was deduced theoretically [1] and was experimentally confirmed, among others, by determinations performed in a riser type pilot plant, depicted in Figure 6.34 [169].

The variation of the conversion to gasoline as a function of the overall conversion as shown in Figure 6.35, demonstrates that this conversion goes through a maximum that decreases as the riser outlet temperature increases.

With increasing temperature, the proportion of cycloalkanes dehydrogenation and thermal cracking reactions will also increase, since they have larger activation energies than those of catalytic cracking. The result is the increase of the unsaturated and aromatic character of the gasoline and as a consequence the increase of the research and motor octane numbers.

These conclusions are confirmed also by the experimental data obtained in the pilot plant (see Figure 6.33) [169]. Thus, Figures 6.36 and 6.37 show the variation with the temperature of the yield (as a percentage) of isobutene and isopentenes, Figure 6.38 shows the production of benzene and Figures 6.39 and 6.40 give the Research and Motor octane numbers for gasoline.

The data in these graphs were obtained for two feeds and two equilibrium catalysts, the main characteristics of which are reproduced in Tables 6.14 and 6.15.

There is no data concerning the activation energy for the formation of coke. This is due to the absence of kinetic reliable equations describing the formation of coke in the conditions of the process.
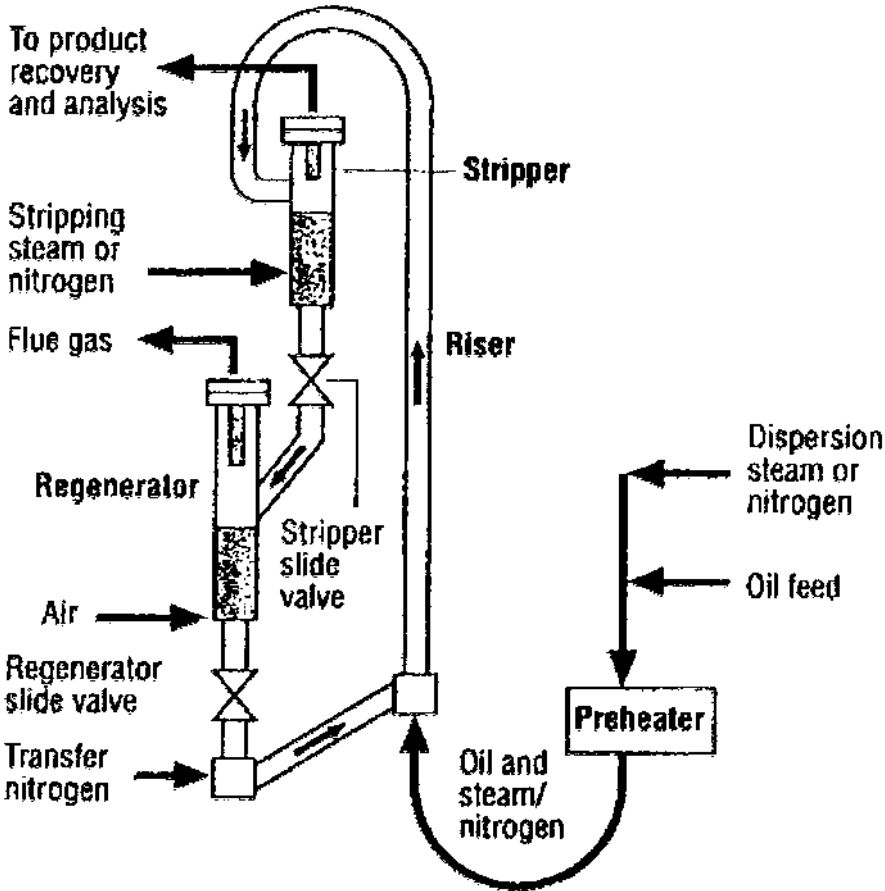
Figure 6.34 Pilot plant with riser reactor. (From Ref. 169.)

Eq. (6.87) combined with (6.88), which eliminates the need to know the form of the kinetic equations, leads to the value $E = 25$ kJ/mole [97], which appears to decrease as the aromatic character of the feed becomes stronger.

The lower value of the activation energy compared to that of the overall conversion of the feed explains the decrease of the percentage of coke at higher reaction temperature, in conditions of constant total conversion (see Table 6.16) [170].

Although the data in the table refers to a classic catalyst, it shows the same trend for the performance of a zeolite catalyst, discussed earlier. The increase in temperature produces the increase of the octane number, the unsaturated character of the gases, and the aromatic character of the gasoline, as illustrated by the density increase.

The variations of gasoline characteristics with the reaction temperature are depicted in detail in Figure 6.41 [171].

With increasing temperature the activation energy may decrease. This is the effect of the diffusion phenomena, which however are less influenced by temperature than the reaction kinetics (see Figure 6.42).
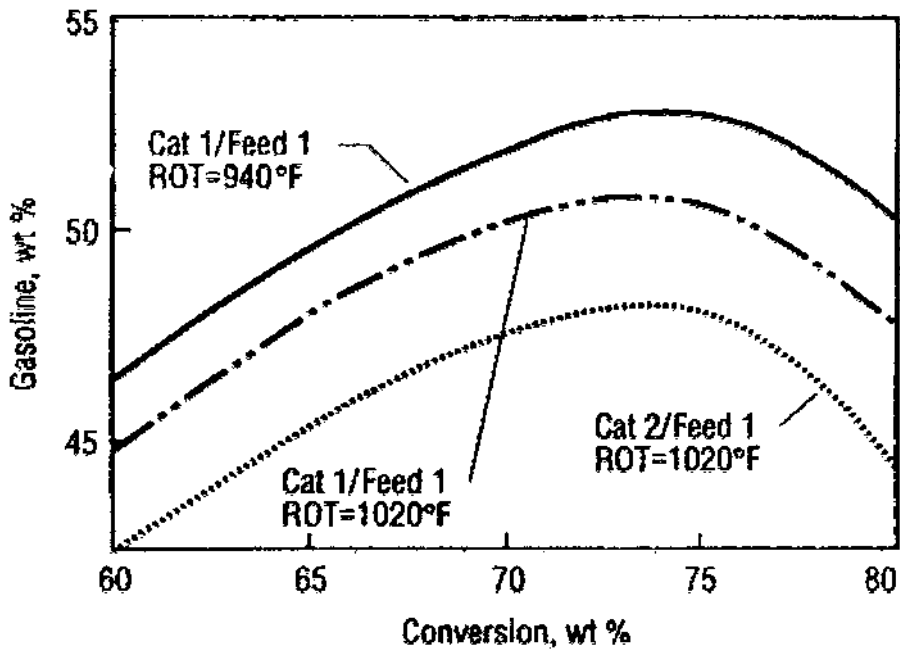
Figure 6.35 Conversion to gasoline function of the overall conversion at two temperatures and two catalysts. ROT riser outlet temperature. (From Ref. 169.)
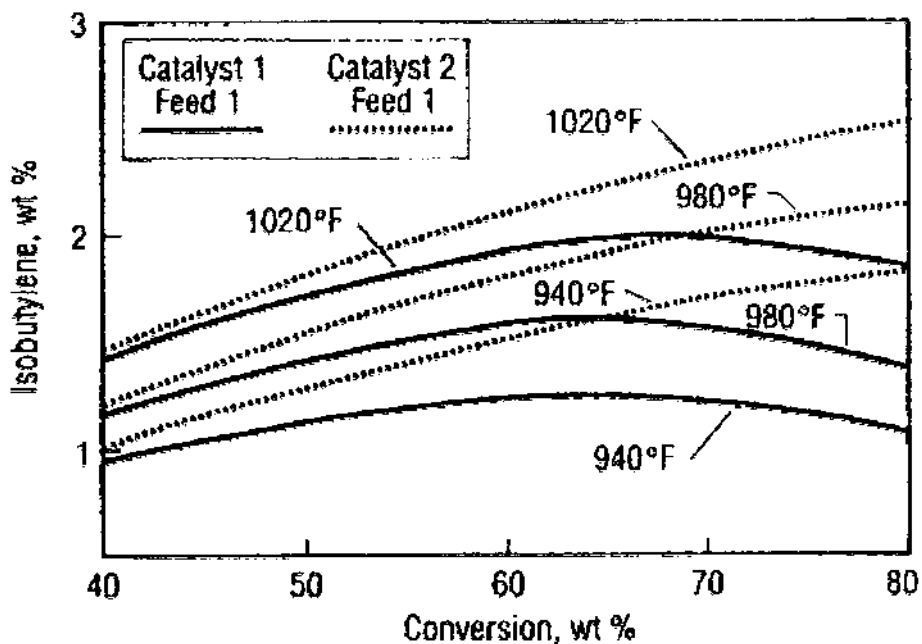

Figure 6.36 Conversion to isobutene for two catalysts, at various riser outlet temperatures. (From Ref. 169.)
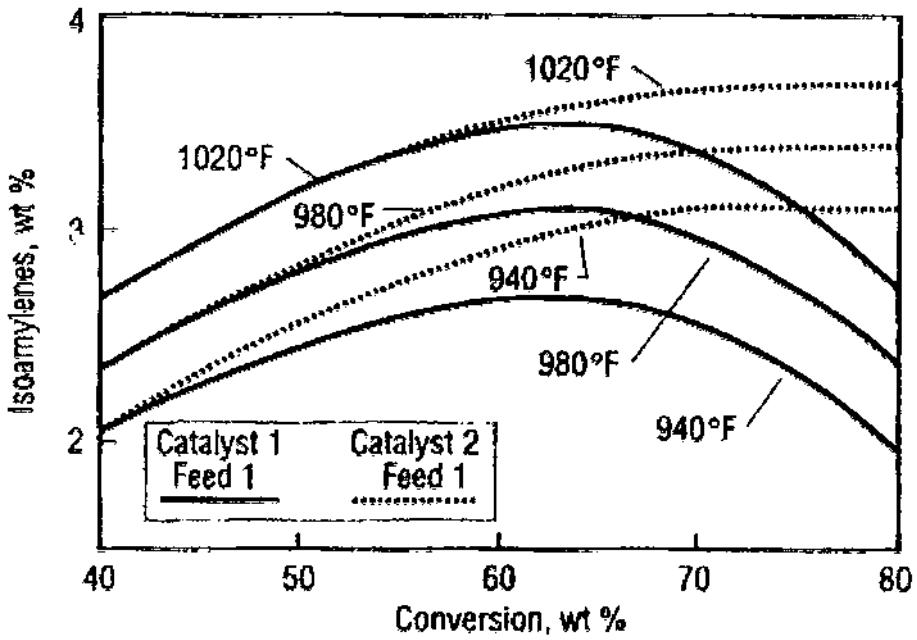
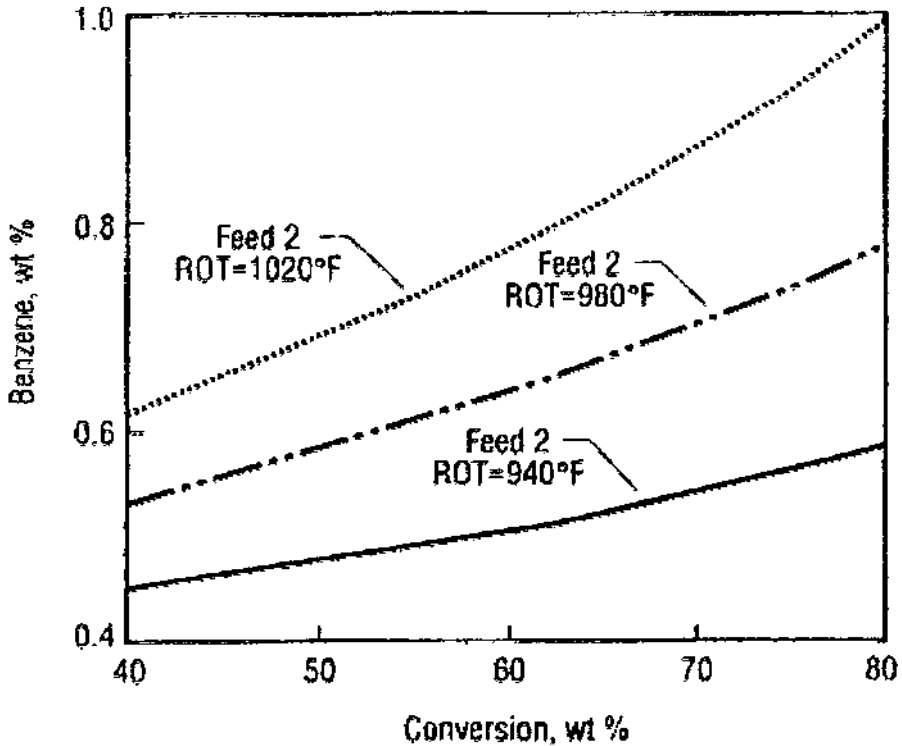**Figure 6.37** Conversion to isopentene for two catalysts and various ROT values. (From Ref. 169.)

Figure 6.38 Conversion to benzene function of overall conversion for two outlet riser temperatures ROT. (From Ref. 169.)
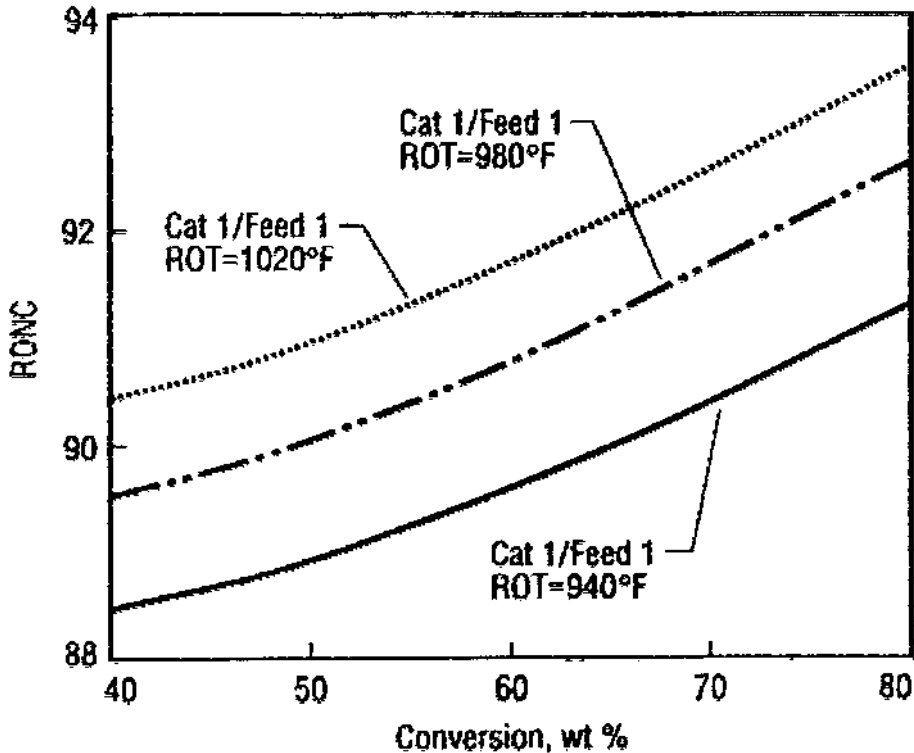
Figure 6.39 Research octane number as function of conversion for various riser outlet temperatures. (From Ref. 169.)

Taking into account the narrow range of temperatures, ranging from 470–545°C where the catalytic cracking is performed, it is difficult to verify if any change in the activation energy occurs within this tight interval. The low values of the previously cited activation energy [1] allow the assumption that the external diffusion influences in some cases the reaction rate. Thus, R.Z. Magaril [73] considers that for spherical catalysts with a diameter of 3–5 mm used in the moving bed processes, the transition to control by external diffusion takes place at temperatures of 480–510°C, while for microspherical catalysts used in the fluidized bed processes, takes place at 540–560°C. Since these estimates refer to classic synthetic catalysts with 12–25% Al_2O_3, one can assume that for zeolite catalysts, which are more active, the transition to control by the external diffusion will occur at still lower temperatures.

It must be remarked that the temperature for the transition from reaction control to diffusion control is different for the decomposition reaction of the feed to gasoline and that of gasoline to gas. The difference is a result of the apparent activation energy that is higher for the decomposition of gasoline than for its formation, and of a higher diffusion coefficient for the molecules of gasoline than for the molecules of feed. Accordingly, the diffusional barrier will intervene at higher temperatures for the gasoline formed in the process than for the feed submitted to catalytic cracking. The influence of the external diffusion can be a decrease of the maximum of gasoline yield.
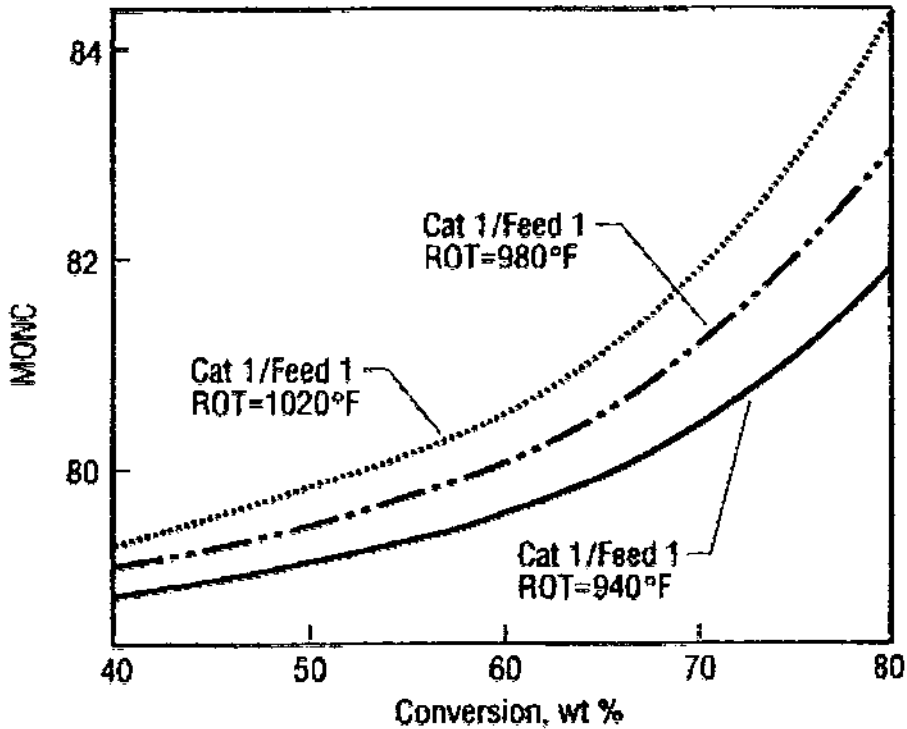
Figure 6.40 Variation of motor octane number function of conversion for various riser outlet temperatures. (From Ref. 169.)

The influence of the internal diffusion is similar to that of the external diffusion, with the difference that it is strongly influenced by the structure and size distribution, and by the size of the feed molecules. Besides, even the very strong influence of the internal diffusion cannot reduce the value of the apparent activation energy by more than half of the activation energy of the actual reaction.

The high differences among the structures of the catalysts and the variety of feeds used in catalytic cracking makes it difficult to formulate generally valid conclusions concerning the influence of the internal diffusion on the overall rate. It can however be stated that such influences are minimal when microspherical catalysts are used and may become important for granular catalysts used in the moving bed processes.

6.5.2 Pressure

In catalytic cracking the pressure varies within very narrow limits determined by the type of unit and by the catalyst circulation system. It doesn't constitute a process parameter to act on in the selection of the operating conditions of the unit.

However, it is very important to understand the effect of pressure upon catalytic cracking reactions. This effect explains the differences in the performances of various types of units and allows to make improvements to the design of units of a given type.

Table 6.14 Feed Used in Experiments. Fig. 6.35–6.40 and 6.46, 6.47

Characteristics	Feed 1	Feed 2
Density, 15°C	0.9188	0.9554
Distillation (°C)		
5%	278	286
50%	455	423
90%	565	504
S total, wt %	0.55	0.29
N total, wt %	0.18	0.36
N basic, wt %	0.056	0.12
C, wt %	86.72	87.72
H, wt %	12.27	11.61
Conradson coke, wt %	0.89	0.15
V, ppm	0.6	0.02
Ni, ppm	0.4	0.04
Fe, ppm	7.0	0.03
Na, ppm	1.8	0.50
Refraction index at 67°C	1.4950	1.5069
Aniline point (°C)	80.0	60.0
Molecular mass	371	322

Data refers to Figures 6.35–40, 6.46, 6.47.

Table 6.15 Equilibrium Catalysts used in Experiments

Characteristics	Catalyst 1	Catalyst 2
Specific surface m^2/g		
zeolite	41.7	109.3
matrix	109.1	46.4
Rare earths content		
cerium	0.72	0.04
lanthan	1.07	0.17
neodim	0.51	0.05
parazeodim	0.16	0.03
Metals content (ppm)		
iron	3,410	10,800
nickel	647	2,220
vanadium	447	2,045
natrium	2,387	6,100
bismuth	–	10
stibium	–	< 10
Microactivity MAT	74	66

Data refers to Figures 6.35–40, 6.46, 6.47.

Table 6.16 Temperature Influence on the Catalytic Cracking of a Gas Oil

Characteristics	Mean reactor temperature °C		
	454	482	510
Volumetric rate, h^{-1}	0.8	1.3	2.0
Conversion, wt %	55.1	55.1	55.1
Yields, wt %			
$\quad H_2$	0.04	0.05	0.06
$\quad CH_4$	0.71	0.85	1.29
$\quad C_2H_4$	0.40	0.55	0.75
$\quad C_2H_6$	0.60	0.75	1.05
$\quad C_3H_6$	2.40	3.35	4.40
$\quad C_3H_8$	2.10	2.15	2.15
$\quad i\text{-}C_4H_{10}$	5.10	4.20	3.35
$\quad n\text{-}C_4H_8$	2.90	4.00	5.60
$\quad n\text{-}C_4H_{10}$	1.40	1.30	1.25
$\quad$ Gasoline debutanised	34.6	33.5	32.2
$\quad$ Light gas oil	15.8	13.8	12.4
$\quad$ Heavy gas oil	29.1	31.1	32.5
$\quad$ Coke	4.85	4.20	3.70
Gasoline characteristics			
$\quad$ vapor pressure (torr)	374	379	384
$\quad$ Density	0.7511	0.7579	0.7649
$\quad$ Octane number F_1 with vapor			
$\quad$ Tension 517 torr	91.2	94.0	95.0
$\quad$ Tension 517 torr, with 0.8 ml/l TEP	97.6	98.6	99.0

$d = 0.882$.
Source: Ref. 170.

In the thermodynamic analysis of cracking processes (Section 6.1) it was shown that the pressure favors the polymerization reactions that take place in the layer adsorbed on the catalyst surface and lead to the formation of coke.

These theoretical conclusions are fully confirmed by the experimental data [172] on the influence of the pressure on the reactor performance of a catalytic cracking pilot plant presented in Table 6.17.

The data show the obvious increase of the coke percentage formed as the pressure in the reactor increases. Pressure has no significant effect on the yield and the quality of other obtained products, excepting the decrease of the unsaturated character of the products illustrated in the table by the relative yield of butylenes.

Since in the industrial units the pressures in the reactor and in the regenerator are interdependent, an increase of the pressure in the reactor leads to an increase of the pressure in the regenerator and thus to a higher burning rate of the coke. It results in a decrease of the residual coke and an increase of the mean activity of the catalyst. For this reason the increase of the pressure in industrial systems must be analyzed by taking into account the modifications of performance that will be produced in both vessels.
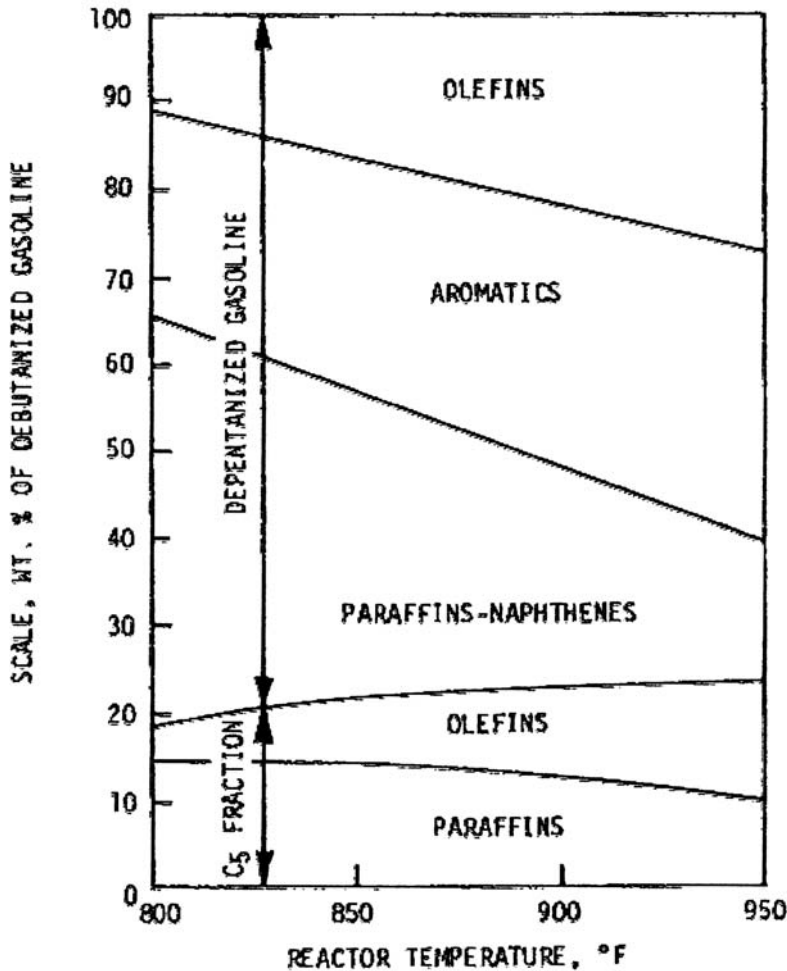
Figure 6.41 Effect of temperature on the debutanized gasoline and composition of C_5 fraction. (From Ref. 171.)

6.5.3 Feed Composition

The basis of the feed for catalytic cracking is the wide cut fraction obtained from the vacuum distillation of crude oil, and occasionally with the addition of some atmospheric gas oil.

As a rule, the product from the bottom of the fractionating column of the catalytic cracking unit is added to the feed with the purpose of recovering the entrained catalyst. This product has generally a distillation initial boiling point of about 420–450°C.

The feed can include also gas oils from visbreaking and coking and also the extracts from solvent refining of lube oils and the deasphalted oils, which sometimes may have been hydrotreated.
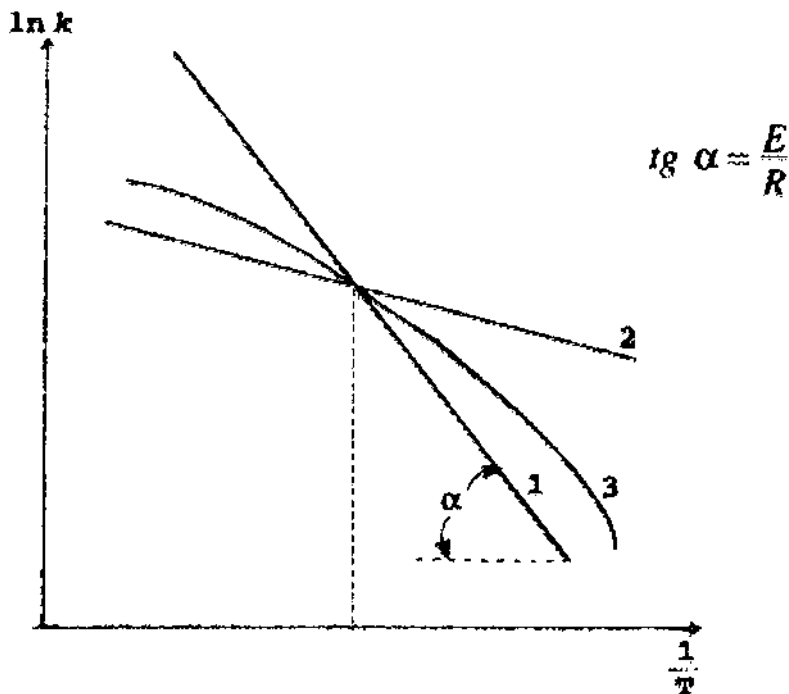
Figure 6.42 Effect of temperature on the external diffusion and reaction rates: 1 – reaction; 2 – external diffusion, 3 – resulting rate.

The improvements brought to the catalytic cracking make it possible to include in the feed variable proportions of residual fractions in general residue from the atmospheric distillation on the condition of not exceeding some limits for the Conradson carbon and the content of metals. Atmospheric residues also may be directly submitted to catalytic cracking.

The recycling of gas oils, especially of the heavy ones, strongly influences the results of the process due to their aromatic character. Since recycling constitutes an independent process parameter, it is examined separately in the next section.

Table 6.17 Pressure Influence on the Yields in a Catalytic Cracking Pilot Unit at Equivalent Technological Conditions [172]

	Hydrocarbons partial pressure (bar)		
	0.69	1.72	2.76
Global conversion (vol %)	69.30	70.40	75.70
Gasoline (vol %)	53.10	52.60	51.20
Coke (wt %)	7.40	9.60	12.40
Butylenes relative yield	1.00	0.86	0.72

Source: Ref. 172.

Currently, for estimating the performance of catalytic cracking, the characterization factor of the feed is used, as suggested by Watson and Nelson [173]. Expressed in metric units [174] it is given by the expression:

$$K = \frac{1.216\sqrt[3]{T}}{d} \tag{6.89}$$

where:

T = molar mean boiling temperature in degrees K
d = the density at $15.56°C$.

The data of Table 6.18 show the correlation between the characterization factor and the yields to gasoline and to coke for fractions obtained from the crude oil distillation and for the recycled gas oils [175].

Since the units are generally obliged to work in conditions that should lead to a constant conversion to coke, the data of Table 6.19 supply correlations between the characterization factor, the conversion, and the yield to gasoline at a constant conversion of 5.3% to coke [175].

The influence of the distillation limits of the feed on the yield in products is illustrated in Figure 6.43 [176]. From this figure, the increase of the mean boiling temperature of the feed increased the conversion and the yields for all the products. However, the yield in gasoline increased with the alkane character of the feed and it may vary in the opposite direction if the feed is strongly aromatic (Figure 6.44) [177].

The data of tables 6.17 and from the Figures 6.43 and 6.44 correspond to a conventional catalyst and to the fluidization in dense phase.

The conversion of different classes of hydrocarbons depending on the severity of the process is given in the graphs from Figure 6.45a–c [177]. These results were obtained in a pilot plant using a conventional catalyst, reaction temperature of $482°C$, and a feed with 50% vol distillate at $371°C$.

In these graphs the severity was expressed by the ratio:

$S/100n$

Table 6.18 Correlation Between Characterization Factor UOP and Gasoline Yields at Constant 60% Conversion

	Fresh feed		Recycle	
K_{UOP}	vol % gasoline	wt % coke	vol % gasoline	wt % coke
11.0	–	–	(35.0)	–
11.2	(49.5)	(12.5)	37.0	(11.5)
11.4	47.0	9.1	39.0	9.0
11.6	45.0	7.1	40.0	7.2
11.8	43.0	5.3	41.09	6.0
12.0	41.5	4.0	(41.5)	(5.3)
12.2	(40.0)	(3.0)	–	–

Estimated values in parenthesis.
Source: Ref. 175.

Table 6.19 Correlation Between the UOP
Characterization Factor and Gasoline Yield at
Constant (5.1%) Conversion in Coke

	Fresh feed		Recycle	
K_{UOP}	Conversion %	vol % gasoline	Conversion %	vol % gasoline
11.0	–	–	30.0	20.0
11.2	50.0	39.0	39.0	26.5
11.4	52.0	40.0	45.0	31.5
11.6	56.0	41.5	51.0	35.5
11.8	60.0	43.5	57.0	39.0
12.0	(70.0)	(52.0)	60.0	41.0
12.2	–	(66.0)	–	–

Estimated values in parenthesis.
Source: Ref. 175.
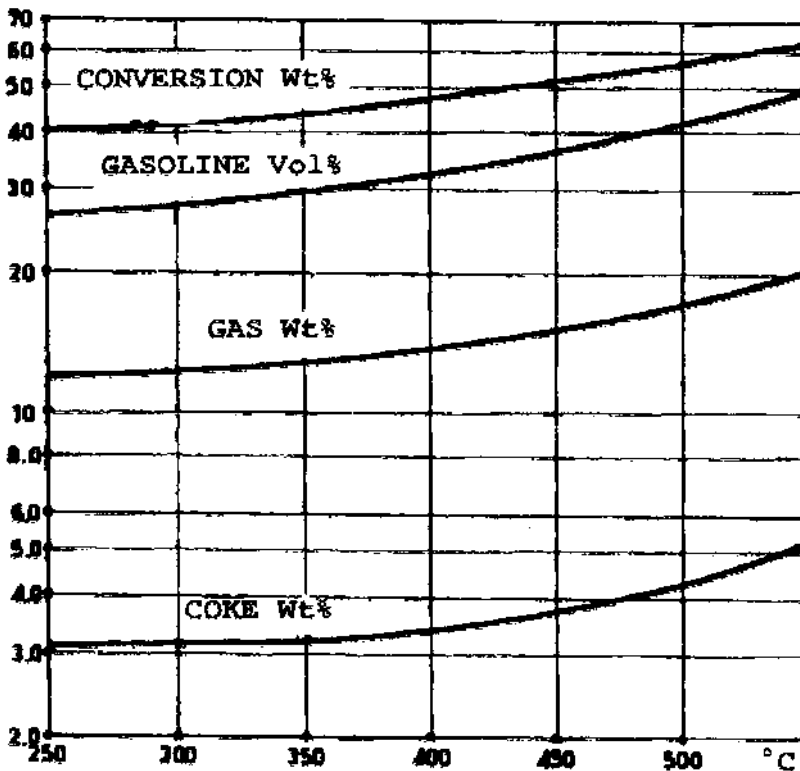
Figure 6.43 Effect of the average boiling point temperature of the feed on the conversion
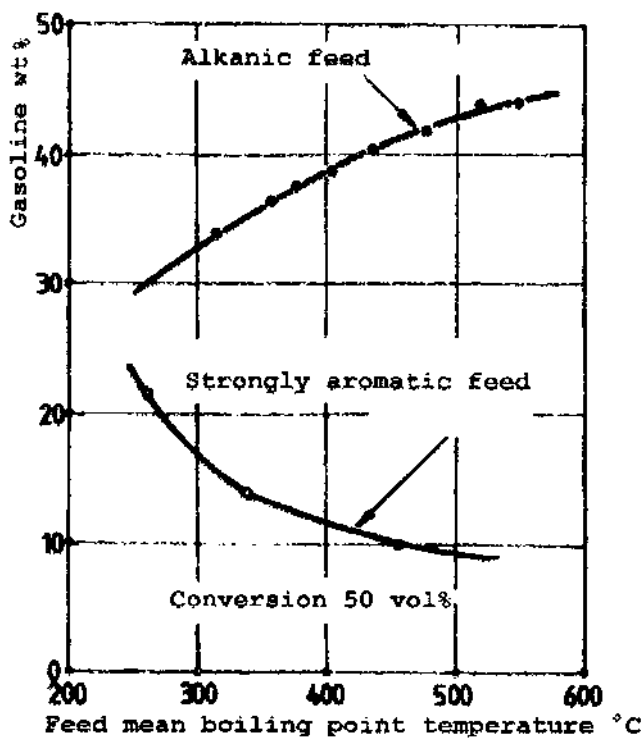and products yields. Cracking at 482°C. (From Ref. 176.)

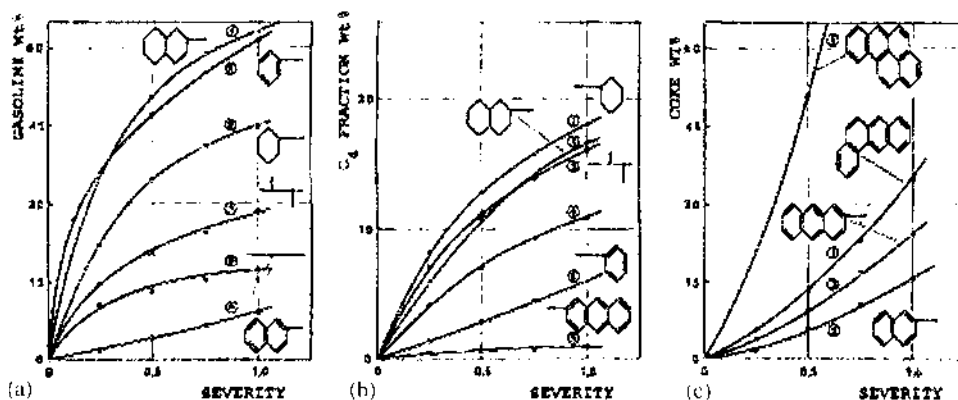**Figure 6.44** Influence of the feed volumetric mean boiling point temperature on gasoline yields. (From Ref. 177.)

Figure 6.45 Conversion of different classes of hydrocarbons depending on process security. Weight percent of products: (a) gasoline; (b) C4 fraction; (c) coke.

where:

S = catalyst surface in m^2/g

n = feeding rate expressed by the kg liquid feed on the kg of catalyst per hour.

For riser systems, the zeolite equilibrium catalysts have the characteristics reproduced in Table 6.15 and two representative feeds from Table 6.14. The results of cracking are reproduced in Figures 6.35–6.40 and 6.46–6.47 [169].

6.5.3.1   Effect of Sulfur and Nitrogen Compounds

The sulfur compounds don't seem to exercise a direct action on the catalytic cracking process. Indirectly indications exist [1] that they should favor the deposit of the heavy metals and especially of iron under a dispersed form on the catalyst surface, emphasizing in this way its noxious effect.

The influence of sulfur and nitrogen on the reaction kinetics of catalytic cracking was recently analyzed [238], considering also the feed n-d-M composition and the kinetic equations proposed. It was found that sulfur content has a strong influence on kinetic constants while the effect of nitrogen is less important.

The distribution of the sulfur among the products is shown in Table 6.20 [183], from which it results that almost half ends up in the gases as hydrogen sulfide and a small part in the gasoline and gas oil. The portion that ends up in the residue and coke vary in large limits, possibly depending on the nature of the sulfur compounds in the feed.

For a unit of the riser type and a zeolite catalyst, the sulfur distribution among the products is given in the graphs of Figure 6.48. The cracking runs were carried out
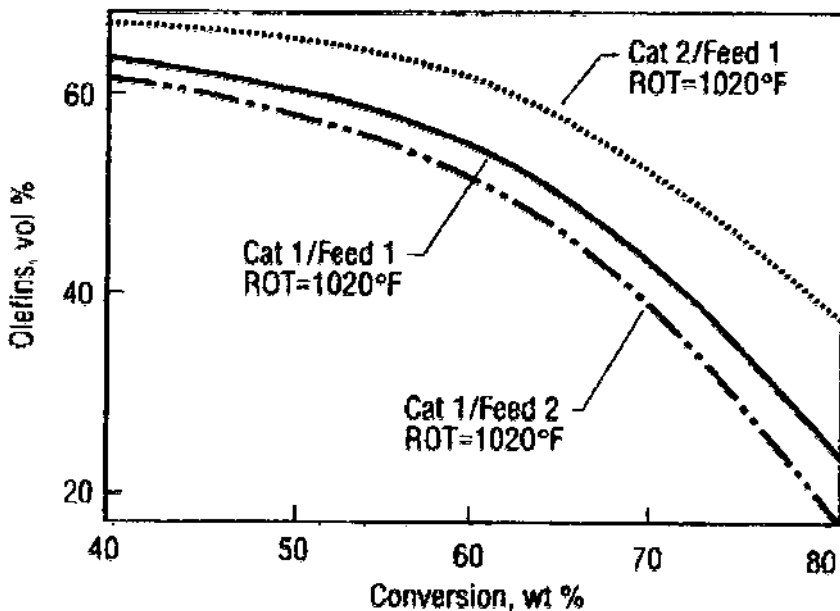

Figure 6.46   Alkenes content of gasoline for two feeds and catalysts. Riser outlet temperature: 549°C. (From Ref. 169.)
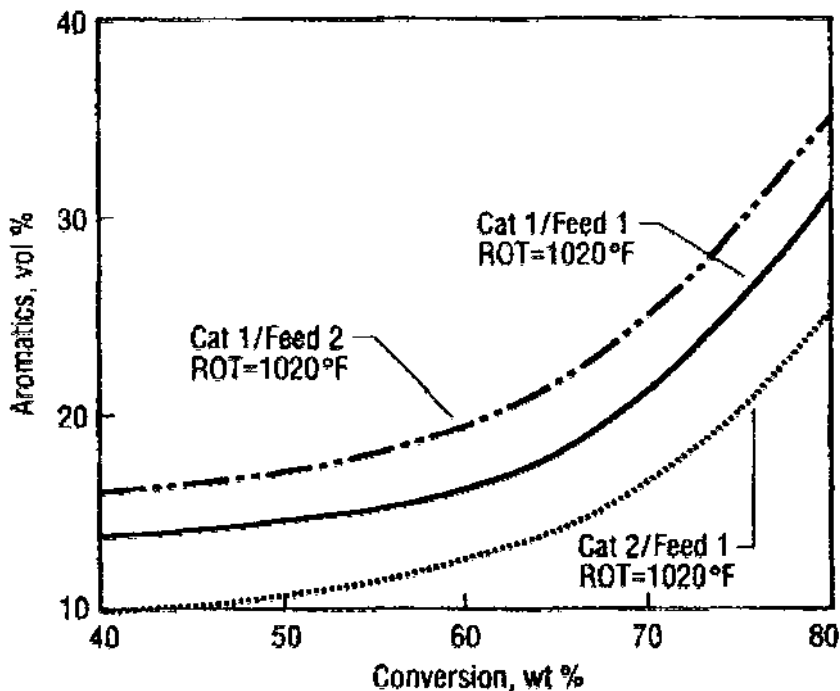
Figure 6.47 Aromatics content of gasoline for two feeds and catalysts. Riser outlet temperature: 549°C. (From Ref. 169.)

at temperatures of 555°C and 516°C, at conversions ranging from 76.3–84.1%. The feed was a Kuwait gas oil the sulfur content of which was decreased by hydrofining or deasphalting.

Despite the fact that the gasoline produced in catalytic cracking contains only 3–5% of the sulfur contained in the feed, this is almost exclusively as mercaptans requiring purification of the gasoline.

The influence of nitrogen compounds was discussed in Chapter 6.3.3.

Table 6.20 Sulfur Distribution in Catalytic Cracking Products

| Feed		Sulfur distribution, wt %				
Origin	S wt %	Gases + H$_2$S	Gasoline	Gas oil	Fuel	Coke
Straight-run residue, Cabinda	0.21	53.6	6.8	10.9	9.4	19.3
Gas oil, South Louisiana	0.46	46.5	4.4	15.0	27.5	6.6
Gas oil, California	1.15	60.2	9.5	20.7	6.8	2.8
Gas oil, West Texas	1.75	42.9	3.5	28.0	20.5	5.1
Gas oil, Kuwait	2.66	46.5	3.8	21.1	17.3	11.3
Desasphalted straight run residue + Kuwait gas oil	3.14	50.0	6.9	17.3	15.3	10.5

Source: Ref. 183.
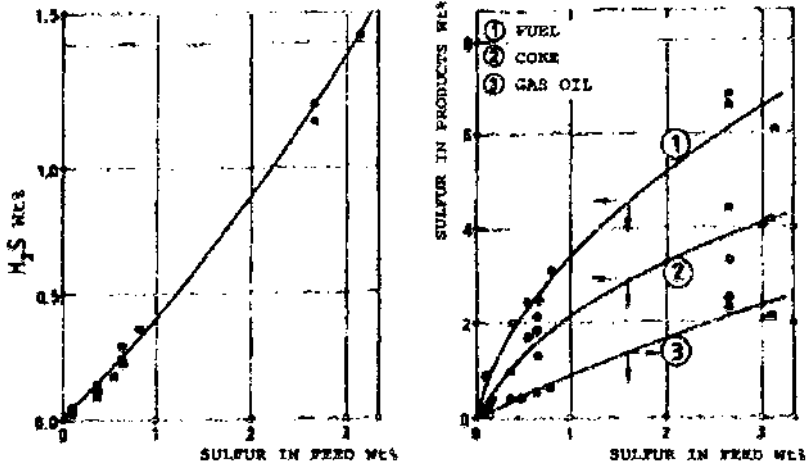
Figure 6.48 Effect of sulfur content in the feed on the sulfur content in the products. (From Ref. 176.)

6.5.3.2 Effect of Sodium and Heavy Metals

The residues fed to catalytic cracking may contain sodium from the NaOH introduced in the crude for fighting acidic corrosion in the atmospheric distillation tower.

Sodium is also introduced in the steam generating boilers and is also used in the treatments applied to the recycled gas oil [243].

The sodium will neutralize a portion of the active sites of the catalyst and thereby it will reduce its stability. In larger amounts, sodium can lead to the sinterization of the catalyst and the partial closing of the access to the pores. Vanadium has a similar effect on pore closing.

The volatile compounds of the heavy metals: Ni, V, Cu, and Fe are decomposed in contact with the catalyst and the metal is deposited on its surface as such or as sulfide.

The deposited nickel has a ''parasite'' catalytic activity, promoting dehydrogenation, aromatization, and coke formation. This parallel catalytic activity is very damaging because a portion of the hydrocarbons that are present will undergo reactions different from those that are typical for catalytic cracking. Thus, the alkyl-cycloalkanes, instead of forming iso-alkanes on the acid sites of the catalyst, will be dehydrogenated on the metallic sites, leading finally to formation of coke [207].

Finally, the metals poisoning leads to a decrease of the conversion. At a constant conversion, the result is a higher yield of light gases, including hydrogen, a decrease of the gasoline production, and an increase in coke [184, 185] (Table 6.21).

The poisoning effect is not the same for all four metals. (Fe seems to be less poisoning) and it depends to some extent also on the composition of the feed on the operating conditions and on the type of catalyst. Thus, the presence of sulfur in the feed emphasizes the noxious effect of iron (see also Section 6.5.3.2).

The poisoning effect of the metals deposited on the surface of the catalyst decreases in time possibly due to the progressive loss of their dehydrogenation

Table 6.21 Metals Poisoning Effect at Constant 70% Conversion

N, V, Fe on catalyst (ppm)	180	1130	3500
kg feed/kg catalyst per hour	16.5	10.2	5.8
Issues			
C_3 (wt %)	5.8	6.6	7.1
C_4 (wt %)	14.0	14.0	13.0
Gasoline (wt %)	61.0	59.0	54.0
Coke (wt %)	2.4	3.1	7.3

Arco pilot plant fluidized bed cracking; feed mid-Continent 262–570°C fraction; zeolite catalyst; Temperature 499°C, catalyst/feed circulation ratio = 8, 0.05% coke; on regenerated catalyst.
Source: Ref. 177.

catalytic effect and in numerous cases it becomes zero, after the unit is fed for 1–2 weeks with uncontaminated feed.

In the distillates, the amount of the heavy metals generally does not exceed 1 ppm if the distillation end point is not higher than 600°C. They are contained in higher amounts in the oils produced in the deasphalting of the residues, from contaminations with residues of the fractions produced by vacuum distillation, and from leaks in the heat exchangers. The contamination due to the metals resulted from the erosion of the equipment is negligible.

The most efficient solution for preventing the contamination with metals is the hydrofining of the feed, a problem explored in Section 10.1.4.

6.5.4 Feed Recycling

The recycling coefficient K is defined by the relation:

$$K = \frac{A}{A_0} = \frac{A_0 + F}{A_0} = \frac{B}{Z} \qquad (6.90)$$

where:

A_0 is the fresh feed
F is the recycled feed
B is the yield in gasoline
Z is the conversion to gasoline at the outlet from the reactor.[*]

A small portion of the recycle, 3–5% of the feed, is made of "decant oil," i.e., the bottom fraction of the fractionating column containing the catalyst dust entrained from the reactor. The small amount of this "compulsory recycle" does not have a significant effect on the yield of the process.

A recent article [186] refers to results obtained in the laboratory and verified at the industrial scale that an addition of 1.5–18% of this product leads to an increase

---

[*] In some publications [4] the notion of recycle flow is used, which represents the ratio between the recycled amount and the fresh feed: F/A_0.

of about 2.2% in the conversion to gasoline and an increase of about 2.4 units for the motor octane number. This favorable effect is difficult to explain since it disappears when a larger amount of product is added. The recycled product has a density of 0.9959 and contains 52.5% polycyclic aromatic hydrocarbons.

The main portion of the recycle is made of the fraction that distills within the range 340–455°C.

In the case of the classic catalysts, the recycling displaces the maximum gasoline yield towards higher conversions with the net result of higher yields. Results obtained in this manner are illustrated in Figure 6.49 [187].

For zeolite catalysts of high activity, the maximum gasoline yield is situated at overall conversions that are higher than those for classic catalysts. In this condition, recycling becomes less interesting and is either completely eliminated or reduced to not more than 15% of the fresh feed.

6.5.5 Catalyst Behavior

Specific issues of the behavior of the catalyst during the operation of industrial units are discussed below.

6.5.5.1 Comparative Performances

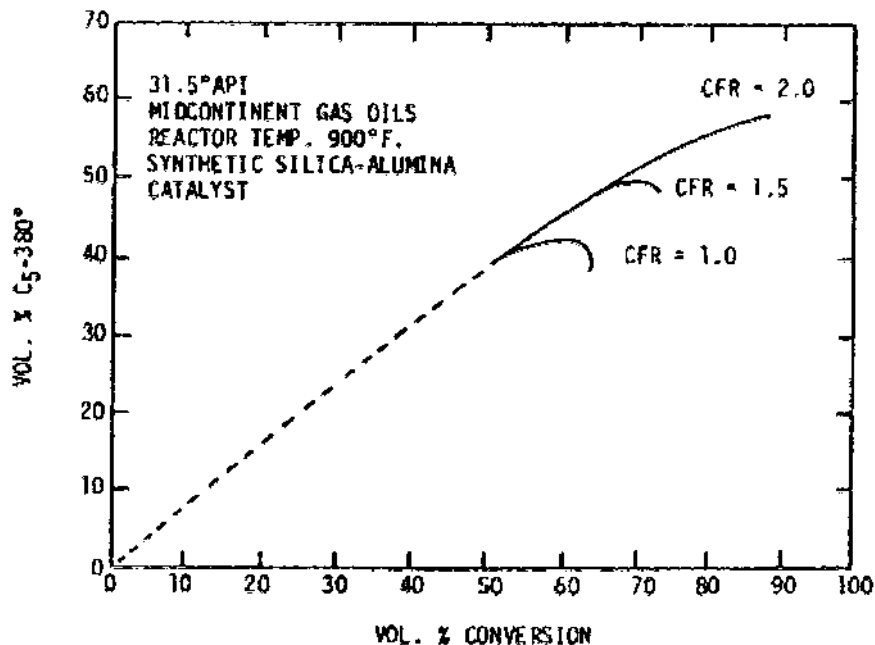The performance of amorphous catalysts are compared to that of zeolite catalysts, in Figures 6.50 and 6.51 [188].

Figure 6.49   Effect of recycle on gasoline yield. Mid-continent gas oil $d = 0.868$, cracking on synthetic Si-Al catalyst at 482°C. (From Ref. 187.)
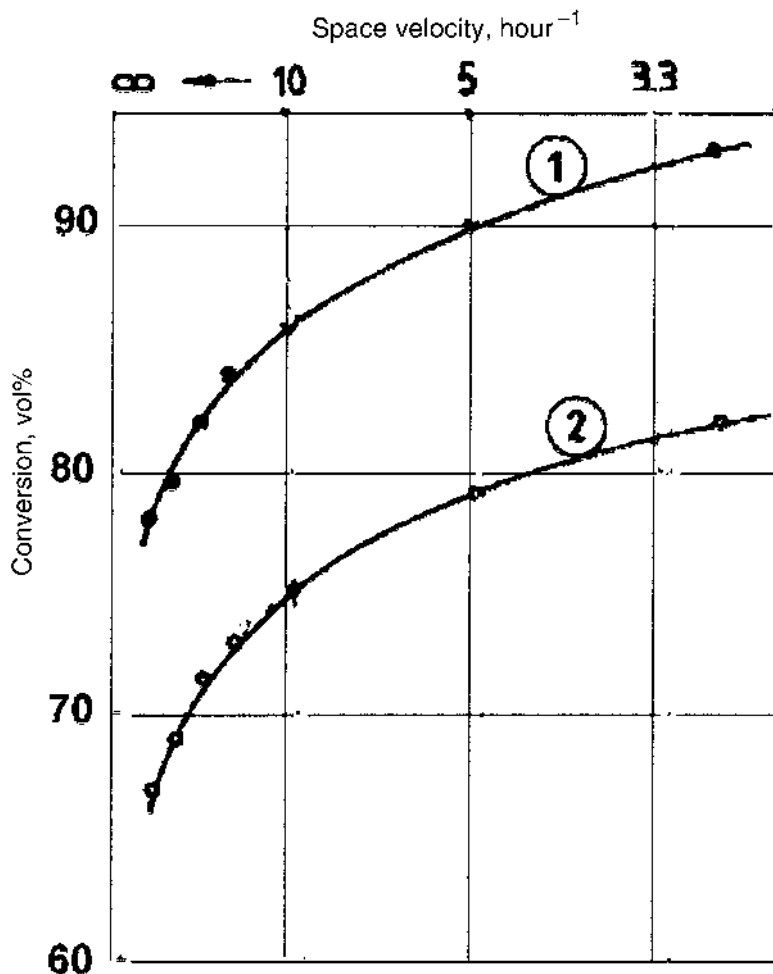
Figure 6.50 Conversion versus space velocity, for two catalysts. 1 – amorphous catalyst, 2 – zeolite catalyst. (From Ref. 188.)

These plotted results were obtained in a pilot plant with a fluidized bed reactor using: (a) an amorphous catalyst with 28.1% Al_2O_3, specific surface of 119 m^2/g, pore volume 0.35 cm^3/g and (b) the zeolite catalyst Davison XZ-25, having 28.2% Al_2O_3, specific surface 105 m^2/g, pore volume 0.28 cm^2/g. The feed was a gas oil $d = 0.857$, $K = 12.9$, S wt% $= 0.19$, distillation range 375–611°C. The unit was operated without recycle, at the temperature of 510°C using a ratio catalyst/feed $= 7$.

The effect of the zeolite content on the product yield and on the octane number at a constant conversion of 70% is shown in Figure 6.52 [189]. In these experiments, a gas oil from West Texas and a REY catalyst were used. The catalyst was pretreated by heating during 12 hours at 827°C in air, with ±20% steam. The test conditions were: $t = 493$°C and catalyst/feed ratio $= 5$.
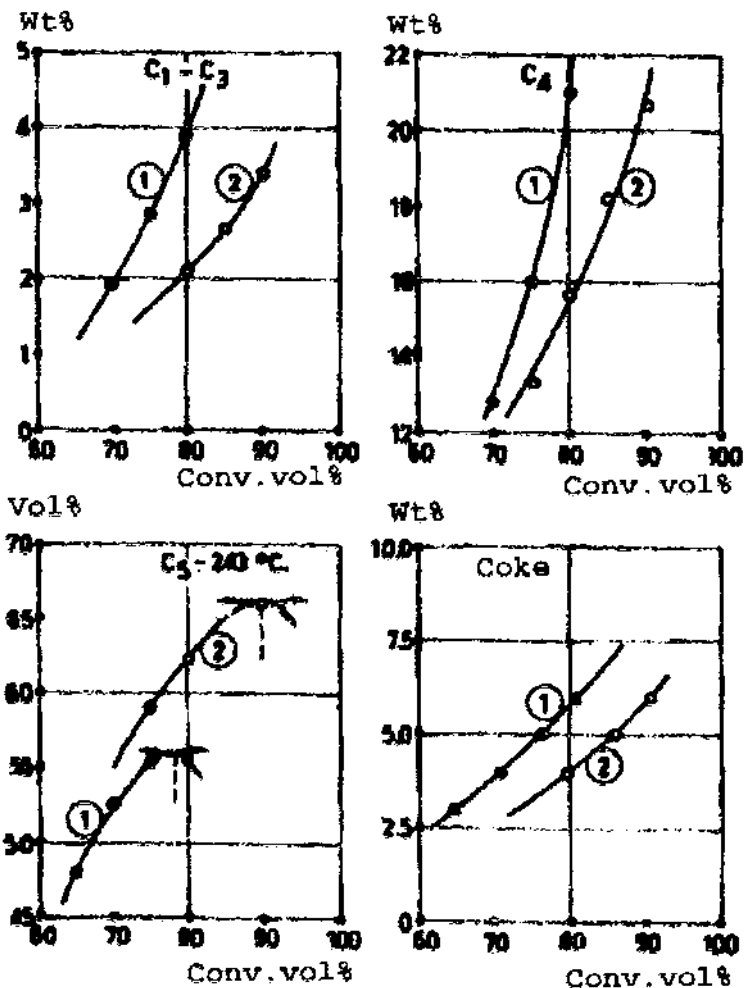
Figure 6.51 Products yields function of conversion for: 1 – amorphous catalyst, 2 – zeolite catalyst. (From Ref. 188.)

More detailed information concerning the performances of the catalysts produced with different types of zeolites and matrices are given in J. Scherzer's monograph [6] and in other publications [64,190,191,240]. Among others, these improvements resulted in a substantial increase of the resistance to poisoning by vanadium [64]. Another study [34] presents the improvements brought to the zeolite catalysts by work performed in the French Institute of Petroleum.

The continuing improvements of the catalysts led to process improvements and to a decrease of the percentage of coke produced, with a concomitant increase of conversion. Figure 6.53 presents this evolution [6].

The nature and the structure of the catalyst also influences the research and motor octane number of the gasoline [192,193]. The variations are between 2–3 octane units.
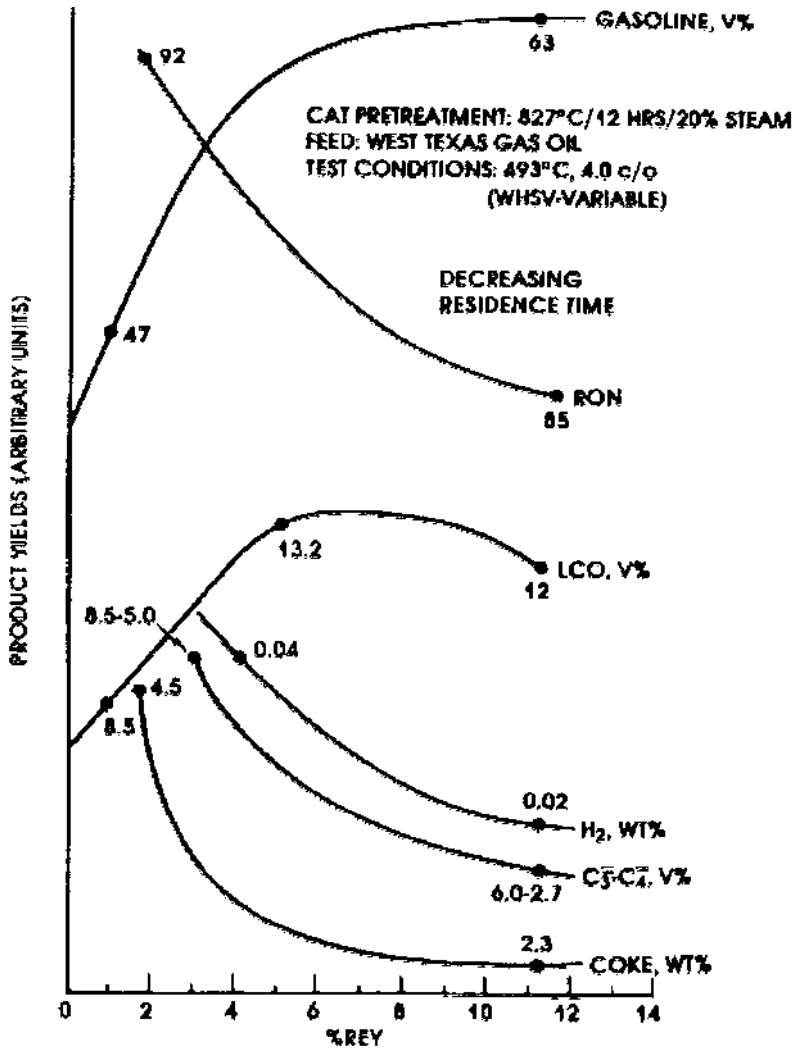
Figure 6.52 Effect of zeolite content on yields. (From Ref. 189.)

6.5.5.2 Residual Coke on Regenerated Catalyst

The percentage of residual coke remaining on the catalyst after regeneration influences sensibly the conversion. This influence is illustrated by the graph of Figure 6.54 [194]. The graph plots the results obtained in a pilot plant using Davison catalyst in a fluidized bed, fed with a West Texas gas oil having $d = 0.893$, distillation range 354–502°C, characterization factor 12.1, and sulfur content 0.30%. The catalyst, AGZ-50 of Davison, was pretreated during 12 hours with steam diluted by 20% air at 826°C. Following this treatment, the catalyst had a specific surface of 120 m^2/g and a pore volume of 0.32 cm^3/g.

The influence of the residual coke on the product yields at different values of the conversion is given in Figure 6.55 [195]. The graph shows that the negative influence of the residual coke increases with increasing conversion.
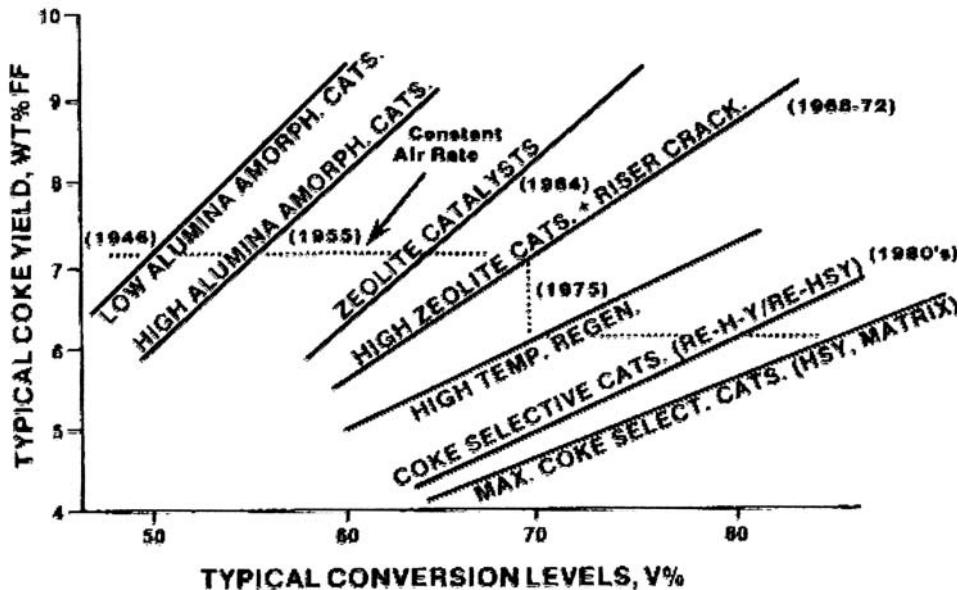
Figure 6.53 Evolution of the decrease in coke yield with conversion in catalytic cracking. (From Ref. 6.)

The larger amount of coke obtained when using a catalyst with a higher level of residual coke appears to be due to its catalytic action, which drives the reactions to higher degrees of decompositions to produce coke and gases [195,196].

6.5.5.3 Catalyst Aging

In operation, catalytic cracking catalysts are submitted to an aging phenomenon, which is due mainly to:

> Hydrothermal aging: repeated contact with steam at high temperatures, which takes place at each regeneration cycle
> Deposition of heavy metals, especially Ni and V, on the surface of the catalyst.

To these main effects, one can add the action of sodium, which may be present accidentally in the feed or in the water drops entrained by the steam.

Hydrothermal aging. A term that defines the combined action of steam and of high temperatures. It is of textural nature for the matrix and of structural nature for the zeolite [197]. It is manifested strongest during the initial contact cycles of the new catalyst and its intensity is highest at higher temperature levels.

The effect on the matrix is manifested by the decrease of the specific surface and of the catalytic activity of its active sites. At the same time the porosity may be affected, which decreases the accessibility of the reactants to the zeolite crystals situated within the matrix.

The effect on the zeolite is manifested especially by the replacement of the tetrahedral aluminum atoms located on the walls of the zeolite cells with silicon atoms, probably originating in the amorphous structures. The result is an increase
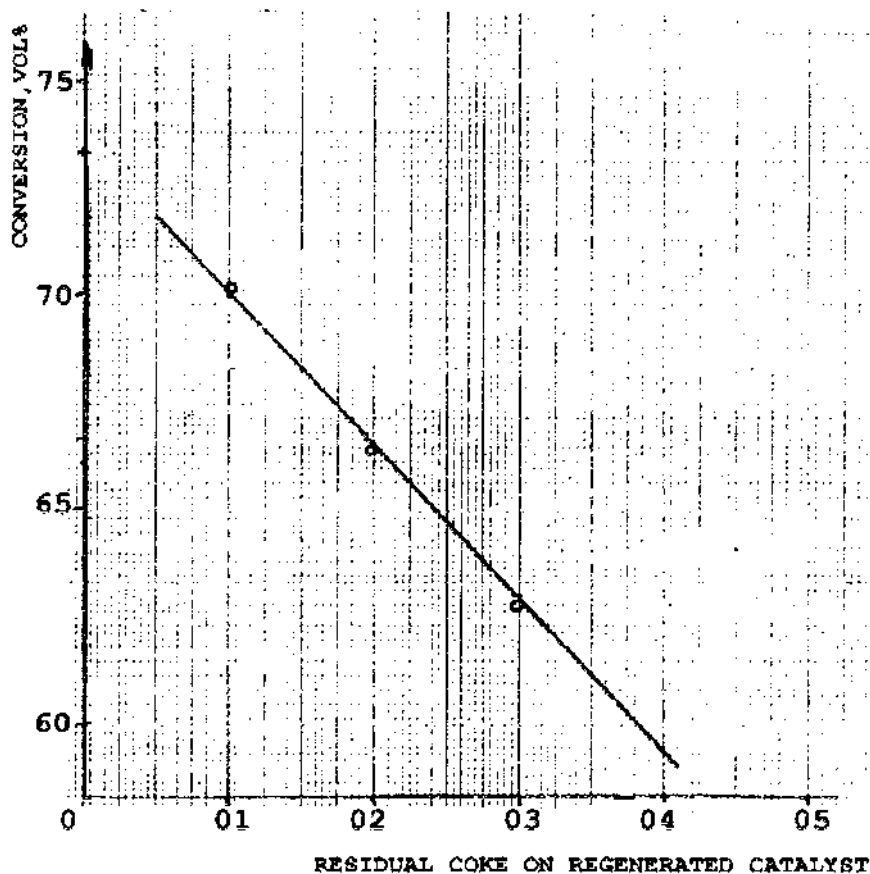
Figure 6.54 Effect of residual coke on conversion. (From Ref. 194.)

of the Si/Al ratio within the structures that are accessible to the reactants and as consequence, a decrease of the catalytic activity.

These modifications lead to the formation of structures that are more stable from the hydrothermal point of view. At temperatures above 850°C the zeolite is completely destroyed.

The zeolite and the matrix have different aging rates. For this reason, by expressing the aging of the catalyst by an Arrhenius equation, one obtains the following overall equation:

$$k = A_m e^{-E_M/RT} + A_z e^{-E_Z/RT} \tag{6.91}$$

where:

$k =$ the constant of the deactivation rate, expressed generally in units of days^{-1}

E_M and $E_Z =$ the deactivation energies for the matrix and for the zeolite respectively

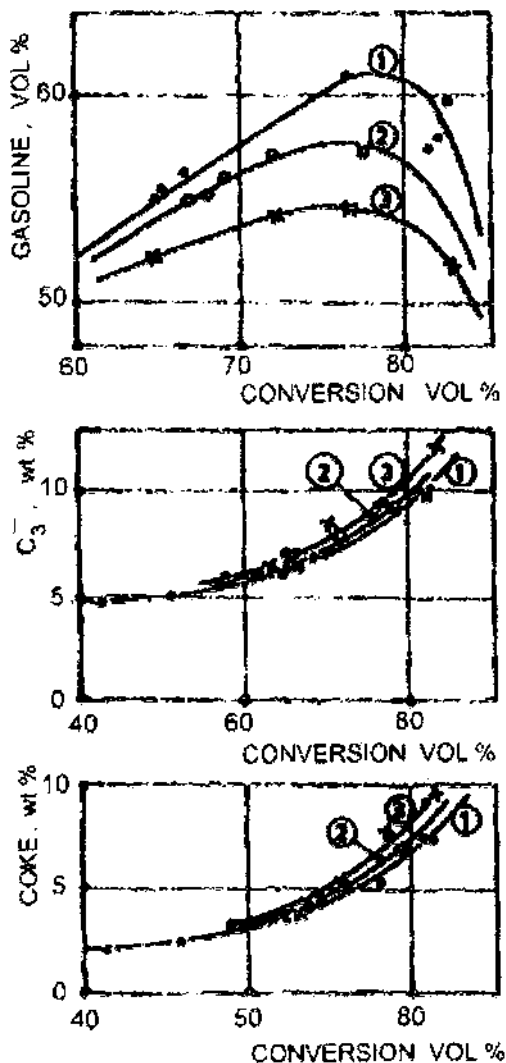A_m and $A_z =$ the respective pre-exponential factors.

Figure 6.55 Effect of residual coke on product yields. 1 – 0.1 wt % coke, 2 – 0.2 wt % coke, 3 – 0.4 wt % coke. (From Ref. 195.)

According to the studies of Chester and Stover [198], $E_Z > E_M$, and therefore, the deactivation of the matrix is rate determining at moderate temperatures, while at higher temperatures, the deactivation of the zeolite becomes rate determining. The two rates are equal at about 780°C. The variation of the deactivation rate constant with the temperature is shown in Figure 6.56.

The presence of the rare earths hinders the extraction of the aluminum atoms from the walls of the zeolite cells, thus increasing the hydrothermal stability of the catalyst [199,201]. An opposite effect, the decrease of the stability, is produced by Na_2O. These influences are depicted in Figure 6.57. Catalyst REY contains zeolite Y
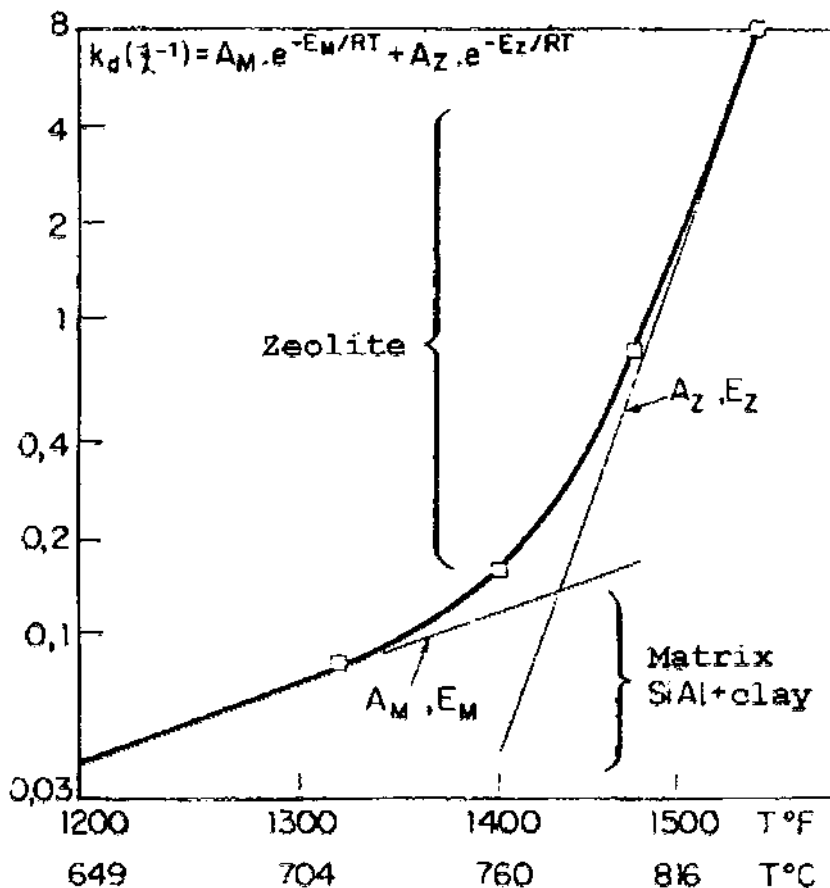
Figure 6.56 Rate constant for thermal deactivation. Catalyst was steam treated for 12 hours before test. (From Ref. 198.)

and rare earths, whereas HY does not. A better hydrothermal stability have the ultrastable catalysts promoted with rare earths, USY [197,201].

Aging due to metals. Vanadium and nickel are the metals with the strongest poisoning action.

The effect of nickel is straightforward; it consists of the formation on the surface of the catalyst of metallic sites that are active in dehydrogenation reactions. As a result, the poisoning with nickel leads to an increase of the hydrogen content in the gases and of the coke deposited on the surface of the catalyst. The consequence is a decrease of catalyst activity. The data of Table 6.22 illustrate these effects of the poisoning by nickel and, in parallel, the quite different effects of catalyst degradation by the action of vanadium [202].

Other metals, such as the iron, have, especially in the presence of sulfur, effects similar to those of nickel. These effects are much weaker, and they are generally neglected in the evaluation of the aging phenomenon.
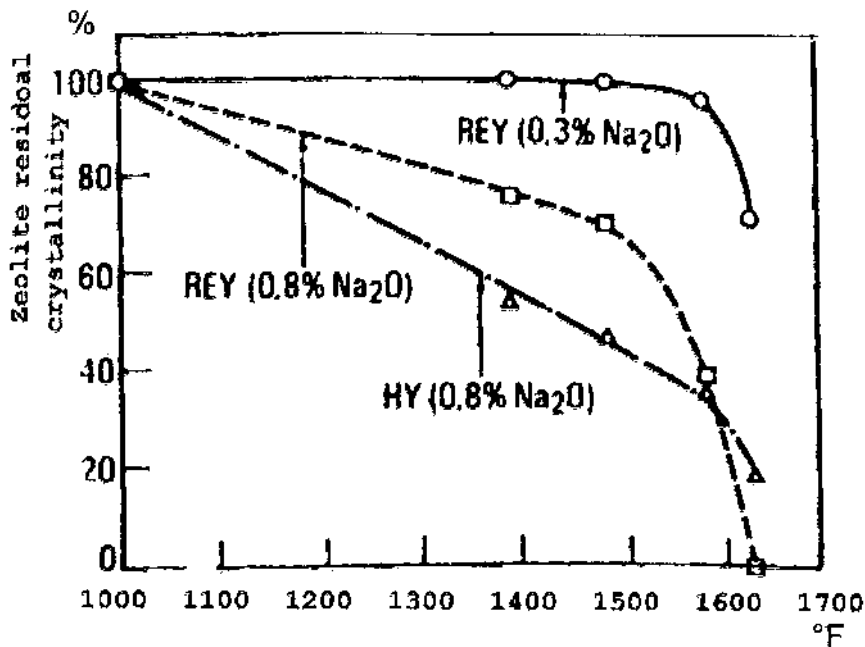
Figure 6.57 Hydrothermal stability of several catalyst (REY stands for Rare Earths Y zeolite). (From Ref. 202.)

While the aging due to nickel does not modify the crystalline structure of the zeolite and does not decrease the conversion, the aging caused by vanadium very strongly influences the crystal structure and strongly decreases the conversion (see Table 6.22).

This effect is due to the fact that the vanadium, which is deposited on the catalyst after its contact with the feed, migrates during regeneration to the zeolite crystals. In order that this migration takes place, the temperature must exceed 550–560°C, the medium must be weakly oxidizing, in order to maintain the vanadium as oxide, and steam must be present.

Table 6.22 Catalyst Aging – Ni and V Action

Contaminants	0 %	0.33% Ni	0.67% V	0.33% Ni + 0.67% V
% crystallinity dry air at 677°C		Reference basis		
% crystallinity after 8 hours stripping at 723°C and 2 bar with 100% H_2O	84	84	38	38
conversion, % vol[a]	80	82	61	61
H_2 (wt %)	0.014	0.274	0.109	0.244
coke (wt %)	3.3	5.8	1.9	2.5

[a] Test at 482°C, $n = 16$ h^{-1}, catalyst/feed ratio $= 3$.
Source: Ref. 202.

The destruction of the zeolite, after the vanadium has reached by migration the zeolite crystals is explained by the most authors [197,203–206] in terms of the formation of an eutectic with a low melting temperature between V_2O_5 and the zeolite. This explanation is in agreement with the known effects of the interactions between V_2O_5 and silica. The presence of sodium emphasizes the effect of the vanadium.

The V_2O_5 interacts also with the oxides of the rare earths that are present in the zeolites Y and REY, especially with the lanthanum. The ultrastable zeolites Y, without rare earths of the USY type seem to be less affected.

Electron microscographs showed the modifications of the catalyst surface structure following the action of vanadium [206].

Aging caused by the action of vanadium and nickel on some industrial catalysts were the object of experimental studies to determine the effect of aging on kinetic constants. The experimental results were fitted to both the model with 3 components (lumps) and that with 5 components of Figure 6.29. The kinetic constants obtained for the catalysts impregnated with Ni and V were compared with those corresponding to the fresh catalyst [207].

Another study analyzes aging caused by the action of nickel and of vanadium in parallel with the protective action of antimony. The kinetic treatment uses the model with 4 components in which the gases and the coke form separate components. Also, the effects of aging on the values of the kinetic constants are obtained in this study [208].

Both cited studies are of high interest for the detailed examination of the aging phenomenon.

It is to be remarked that caution should be exercised when extrapolating the results obtained in the laboratory (where the poisoning of the catalyst occurs usually with Ni and V naphthenates), to the conditions of industrial plants, where poisoning is due to organometallic compounds, such the porphyrins. In fact differences between the effects of the two types of poisonings have been pointed out [209].

6.5.5.4 Equilibrium Activity

The analysis of the means used for decreasing the aging effects must take into account that in industrial plants, the activity of the catalyst is maintained at the desired level by the addition of fresh catalyst, a level called "equilibrium activity."

The rate of catalyst addition varies generally in the range 0.4–0.57 kg/m^3 feed for the catalytic cracking of gas oils and of vacuum distillates and in the range 1.0–1.2 kg/m^3 feed for residue cracking.

The correlation between the metal content of the feed, the amount of catalyst added, and the content of metals of the equilibrium catalyst is given as a graph in Figure 6.58a [210].

From this graph it follows that the decision concerning the added amount of fresh catalyst towards a given feed depends on the metal content of the feed and on the tolerance towards the metals of the equilibrium catalyst.

The rate of hydrothermal aging, can be decreased by: reducing the sodium content of the zeolite, the incorporation of rare earths in the structure, and the use of high stability catalysts, of the type USY.

When fighting catalyst aging as a consequence of metal deposits, a method other than the use of additives, which was mentioned in Section 6.2.4.3, is recommended. The method is to decrease the zeolite content and to use high stability
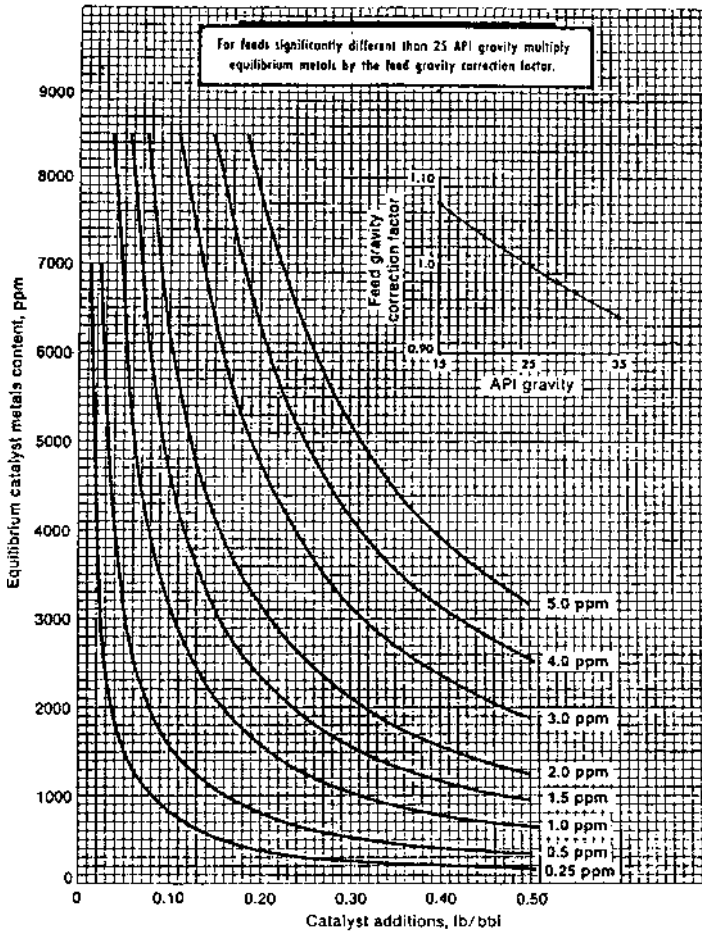
Figure 6.58a Metals content of equilibrium catalyst function of the fresh catalyst to feed ratio and the metals content in the feed. The plot is for sp. gr. = 0.904. For other sp. gravity, multiply result by correction factor. (From Ref. 210.)

catalysts. The latter resist at temperatures even above 760°C in the regenerator and tolerate, without the destruction of the crystalline network, a vanadium content of 6000 ppm and of nickel of 2000 ppm, figure 6.58b and 6.58c [211].

A favorable effect also follows from the increase of pore diameter, together with the decrease of the specific surface of the matrix.

The larger pores make easier the diffusion of the heavy components of the feed and limit the amount of liquid that remains in the catalyst after stripping, therefore reducing the thermal load of the regenerator. These favorable process effects are accompanied by the less important dispersion of the nickel and by a reduction of lower production of gases and of coke.

6.5.5.5 Test Methods

Testing methods for catalytic cracking catalysts refer to their physical-mechanical characteristics and to those directly related to selectivity and activity.
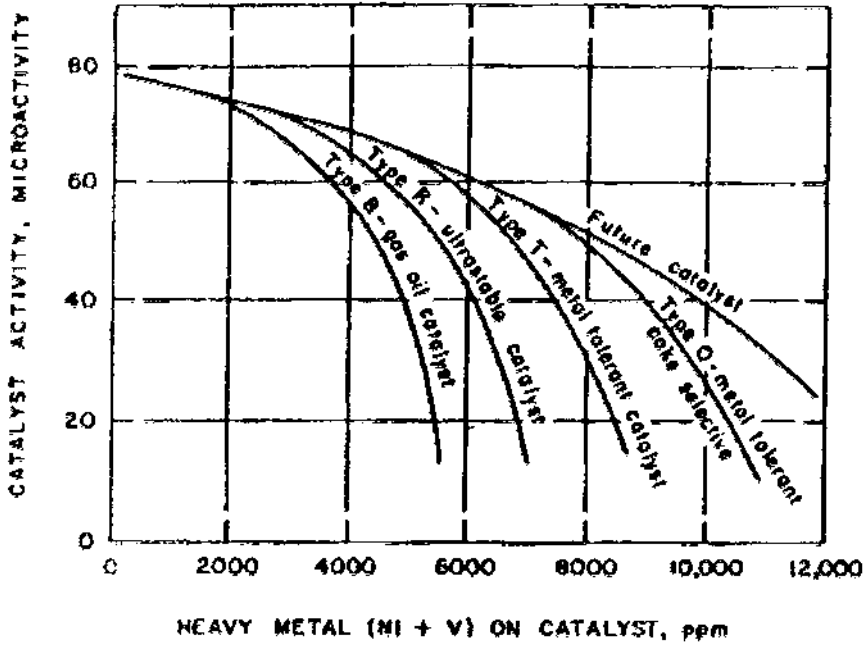
Figure 6.58b Catalyst activity loss due to heavy metals. (From Ref. 211.)
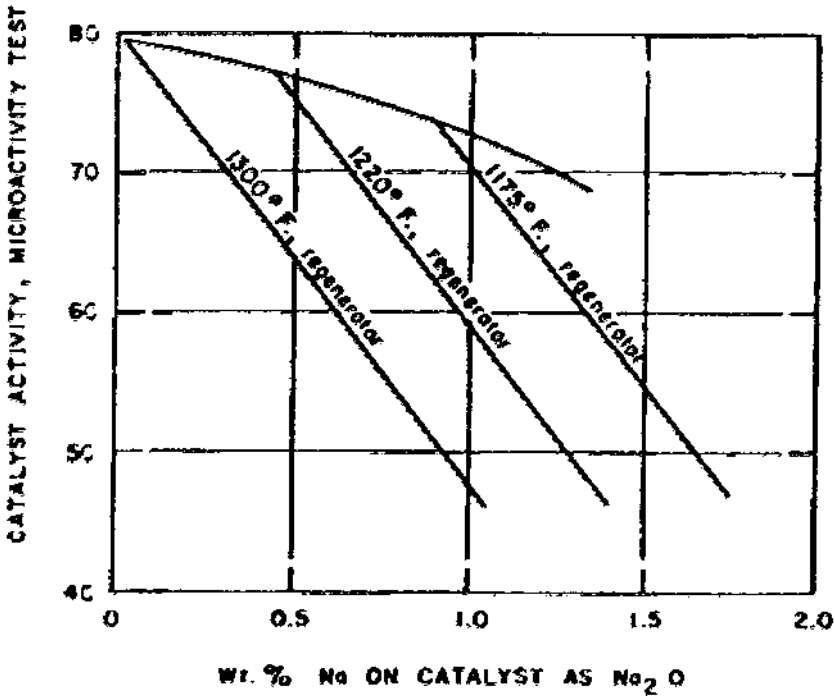

Figure 6.58c Catalyst activity loss due to sodium contamination. (From Ref. 211.)

The physical-mechanical, characteristics, much of them common to other catalysts, have some aspects that are specific to the catalyzed reactions, but especially to the process in fluidized bed with continuous transport of the catalyst between the reactor and the regenerator. In the following, only the specific standardized methods of testing will be examined.

The attrition resistance. This determines to a large extent the amount of fresh catalyst that must be added (makeup). It is related to the catalyst dust that leaves the system and influences fluidization by modifying the dimensional distribution of the catalyst contained in the reaction system.

Generally, the resistance to attrition decreases with increasing zeolite content, limiting it to a maximum of about 35%. A decrease of the zeolite crystal size and their good dispersion within the matrix improves the resistance at attrition. It could be improved also by the use of specific binders and other similar measures [6].

Quantitatively, the resistance to attrition is determined by the method ASTM D-4058. There are also other frequently used methods recommended by catalyst manufacturers. The perfecting of these methods is ongoing [212].

Pores size distribution. This has a great importance for adequate performance of the catalyst and must be correlated with the nature of the feed [6].

The determination of the pore size distribution, is based on the usual methods for measuring adsorbtion isotherms: The adsorption of nitrogen is used for pores with diameters of 20–600 Å (ASTM D-4222 and D-4641) and porosimetry by mercury penetration for pores of 600–20,000 Å (ASTM D-4284).

The specific surface area is generally determined by the BET method, which measures the adsorption isotherm of nitrogen (ASTM D-3663).

Particle size distribution. Playing an important role in fluidized bed processes that use exclusively microspherical catalysts with sizes comprised between 60–80 μm, the particles with diameters below 40 μm and especially below 20 μm are not retained by most cyclone systems. Those above 140 μm can cause fluidization difficulties.

For size characterization the screening through standard sieves are used as well as correlations between the dispersion of laser beams and the size of the particles (ASTM D-4464) or an electronic counter (ASTM D-4438).

Fluidization characteristics. It was stated [213] and became generally accepted that only a direct characterization of the fluidization qualities of the catalyst is reliable for catalyst evaluation, since data supplied by particle size analysis are considered insufficient.

The information published [213] concerning the type of equipment used operation and calculation methodology, and the obtained results supply some interesting elements. But so far, no information is available on a standardized test that should be accepted and introduced in practice.

Thermal and hydrothermal stability. Catalyst stability is also the object of specific tests, consisting of thermal and hydrothermal treatment at different severities. The treatment is followed by the determination of specific physical characteristics (crystal structure by X-ray techniques, specific surface area and pore size distribution) that are compared with the respective properties before the treatment.

For fresh catalysts, the deactivation of the catalyst with steam is described in ASTM D-4463.

Activity and selectivity indexes. Since 1940, when the first testing method of the activity of catalytic cracking catalysts appeared, standard all other testing methods advanced together with the evolution of catalytic cracking technology [1,11].

Fluidized bed processes require specific methods. Popular current applications use low amounts of catalyst: Micro-Activity Test (MAT) and Micro Catalytic Cracking (MCC) in the U.S. In Russia and the new Caucasus republics favor the OCT 38.01161–78 method.

The methods differ by the amount of catalyst used for testing: 5 g in the MAT and OCT methods and between 4–20 g in the MCC method. The methods differ also by the duration, amount, and nature of the feed, and by the reaction temperature: 482°C in the MAT method, 510°C in the MCC method, and ranging between 494–518°C in the OCT method.

Results of studies comparing the MAT and OCT methods [214] favored using the MAT method, which is the standardized method ASTM 3907–92. This method refers to the testing of the equilibrium catalysts or of the fresh ones treated by steam stripping in the laboratory before performing the test. This procedure correlates the results of the test with identical measurements on fresh catalyst and, what is more important, correlates with the results obtained in the industrial units.

The analysis of these problems [215] lead to a series of recommendations for improving stripping conditions of the fresh catalysts, the increase of the temperature for the MAT test from 482 to 515°C, the increase of the feedrate, etc., aimed at bringing the test conditions closer to those encountered in commercial operation. The MAT method and its possible improvement is analyzed in other publications [216,217].

Since the activity index defines the total conversion, which is not sufficient for estimating the performance of the catalyst, one also makes use of the term "selectivity" which defines the proportion of a specified product (usually gasoline and the fraction C_4) obtained at a given conversion. Usually, to define the selectivity, the yields to all products are given (including gases and coke) allowing a complete evaluation of the performance of the catalyst. The term "selectivity index" which is used occasionally, represents the ratio of gasoline or gasoline + the C_4 fraction, to the total conversion.

Interesting information on the correlation of the MAT test data with the results obtained at semipilot and pilot scale, are given in the monograph of McKetta [11].

6.5.6 Effect of Catalyst/Feed Ratio

In catalytic cracking with moving or fluidized bed, the catalyst circulates continuously between the reactor and the regenerator. The intensity of this circulation, is expressed by the ratio between the weights catalyst G_{cat} and feed G_{feed} that circulate through the reactor in unit time:

$$a = \frac{G_{cat}}{G_{feed}} \qquad (6.92)$$

The increase of the contacting ratio decreases the amount of coke on the catalyst measured at the outlet of the reactor. By decreasing the content of coke on the catalyst, the activity of the catalyst (and therefore the conversion) increases if the other operating parameters remain unchanged. The data of Table 6.23, obtained in a Davison pilot plant in fluidized bed for three catalysts and a feed with distillation range of 260–427°C illustrate this effect. In all the measurements, the mean reactor temperature was 482°C, the feed rate $r = 2h^{-1}$.

In Figure 6.59 the influence of the feedrate on the conversion is represented for different values of the contacting ratio. The data were obtained in the pilot plant in fluidized bed (Amoco), at the mean reaction temperature of 495°C and at a pressure of 1.38 bar. The used feed had: $d = 0.883$, distillation end point $= 393°C$ and the following composition (wt %): 27.1 alkanes, 43.9 cyclo-alkanes, 29.0 aromatics, and 0.59 sulfur. The residual coke on the catalyst in all cases was $= 0.10\%$.

At constant conversion, increasing the contacting ratio leads to a decrease of the yields of hydrogen and of the C_1–C_4 gases, leaves unchanged the yield in gasoline, and leads to an increase of coke.

This last result is explained by the amounts of liquid products remaining in the pores of the catalyst and are sent to the regenerator. These transported amounts increase with increasing contacting ratio. No generally valid correlation can be given since the amounts of liquid remaining in the pores depend on pore size distribution and stripping conditions. A large number of experimental data obtained in pilot plants and in the industrial units allowed the formulation of the following empirical correlation [4]:

$$\frac{x}{1-x} = C \cdot n^{-0.35} \cdot a^{0.65} \cdot e^{-7000/T} \tag{6.93}$$

where:

  x is the conversion
  $C =$ a constant depending on the nature of the feed and of the catalyst
  $n =$ specific feedrate (kg feed on kg catalyst/hour within the reactor)
  $a =$ catalyst/feed ratio.

The catalyst/feed ratio should not exceed values that correspond to the minimum residence time of the catalyst in regenerator, necessary to ensure the level of desired residual coke.

Table 6.23 Catalyst Feed Ratio Influence on the Conversion

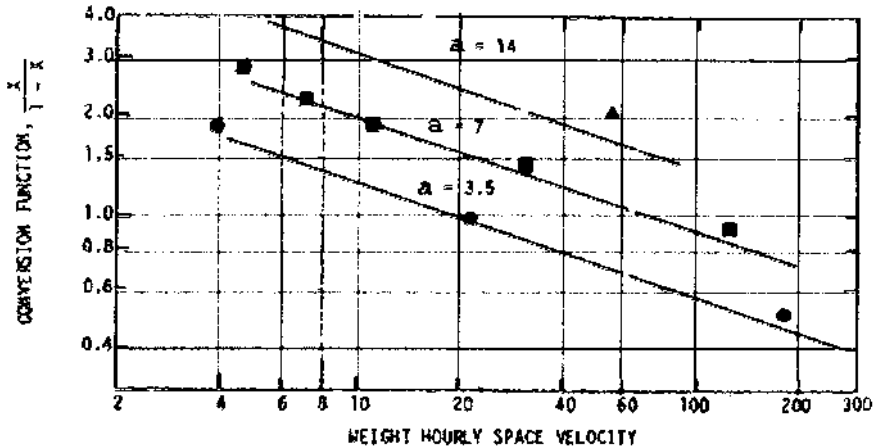| Catalyst	$a = 3$	$a = 6$
XZ-40	84.8%	90.2%
DZ-7	83.1%	86.8%
XZ-25	72.4%	84.6%

Source: Ref. 218.

Figure 6.59 Effect of feedrate and catalyst/feed ratio on conversion. (From Ref. 219.)

6.6 CATALYST REGENERATION

Regeneration of catalysts is performed in the regenerator by continuously burning the coke deposited on the catalyst.

6.6.1 Coke Composition

In fluid catalytic cracking the content of hydrogen in the coke is in the range of 5–10% and can be obtained by using the graph of Figure 6.60 [220]. Analytical expressions are given in the same article [220].

In the moving bed units, the content of hydrogen in the coke ranges between 2.5–8%.

The amount of hydrogen in the coke may be determined directly by elemental analysis. But the analysis must differentiate between the water resulted from the combustion of hydrogen contained in coke and water content of the catalyst or water adsorbed by the catalyst.

Such a method was proposed and tested with good results [221]. It is based on the determination of the weight loss of the catalyst during elemental analysis.

Noting with h and c the amounts of hydrogen and carbon in the coke, $a =$ the water contained in the catalyst, $\Delta G =$ the weight loss of the catalyst submitted to elemental analysis, and H_2O and $CO_2 =$ the measured amounts of water and carbon dioxide, one may write:

$$H_2O = a + \frac{18.016}{2.016} \cdot h$$

$$CO_2 = \frac{44}{12} \cdot c$$

$$\Delta G = a + h + c$$
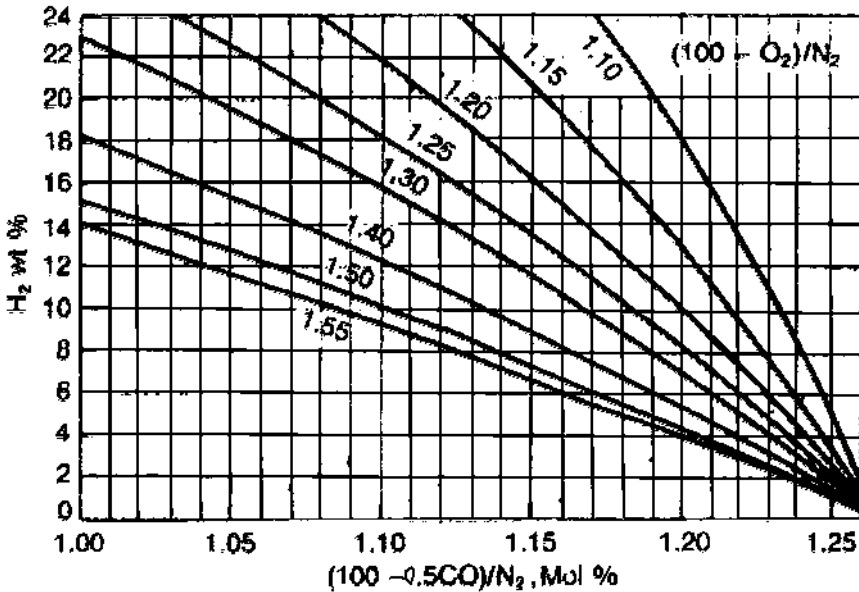
yielding the final equations:

Figure 6.60 Correlation of hydrogen content of coke with the composition of flue gases. [220]. O_2, CO, and N_2 must be expressed as mole %.

$$c = 0.273CO_2$$
$$h = 0.126(H_2O + 0.273CO_2 - \Delta G) \tag{6.94}$$

6.6.2 Flue Gas Composition

It is of great interest to compare the composition of the flue gases corresponding to thermodynamic equilibrium with the one actually measured.

In Figure 6.61 [212] the curves for thermodynamic equilibrium at 660°C are plotted as a function of the contribution of oxygen calculated for the burning of a coke having the following composition (weight %):

Carbon   85.90
Hydrogen   10.00
Sulfur   1.15
Nitrogen   2.99

The scale on the abscissa of the graph, relative oxygen input (ROI), is defined as the amount of oxygen supplied to the regenerator, divided by the amount of oxygen theoretically required to burn all the coke hydrogen to H_2O, half of the coke carbon to CO, and the other half to CO_2.

For ROI = 0.8 all the hydrocarbons are burnt;
For ROI = 1.2 the CO is completely burnt and excess O_2 begins to appear in the flue gases.

For the thermodynamic calculation, the reactions of the nitrogen contained in the coke were simulated by the reaction between NH_3 and NO from which N_2 and
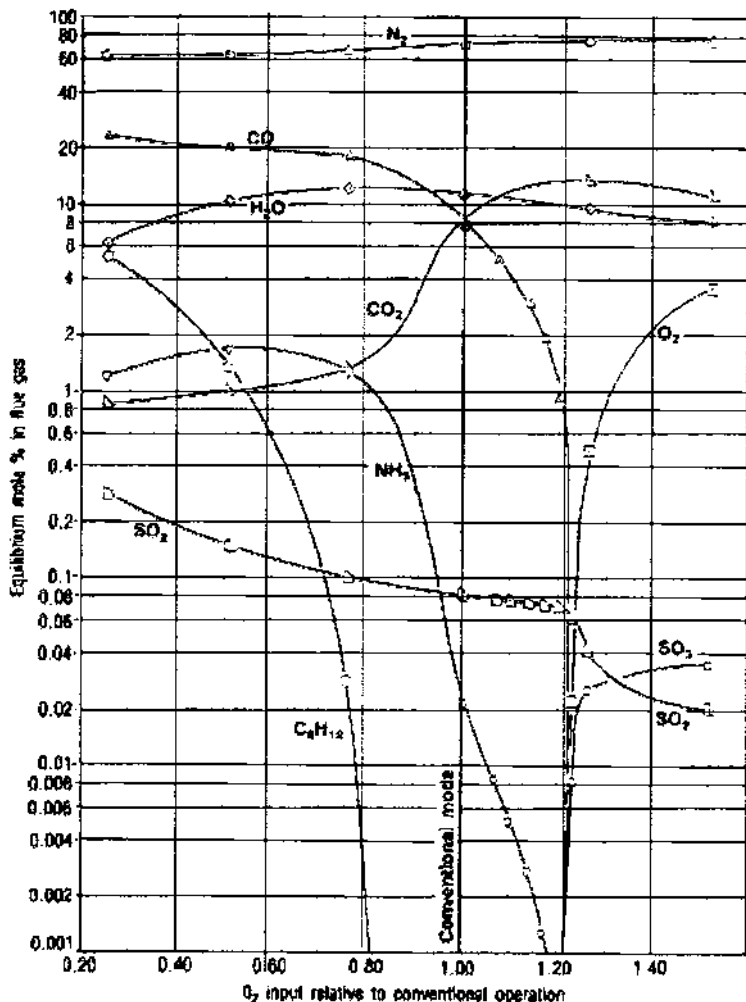
Figure 6.61 Equilibrium composition of flue gases at 660°C as a function of oxygen input. (From Ref. 222.)

H_2O are formed. The comparison of this equilibrium calculation with typical conditions for coke burning corresponding to ROI = 1.04 is given in Table 6.24. The table shows important differences between the calculated equilibrium composition and that measured experimentally. The differences are due to the differences between the burning rates but possibly also to the hindrance exerted by the catalyst on some of the reactions, such as the combustion of CO to CO_2. Such an effect could explain the combustion of CO→ CO_2 above the catalyst bed, which was observed occasionally.

Concerning the behavior of the sulfur contained in the feed, a graphic correlation was established between the SO_2 content in the gases and the sulfur content of the feed (see Figure 6.62 [183]).

Table 6.24 Comparison of Equilibrium and Representative Coke Burning Flue Gas Composition ROI = 1.04

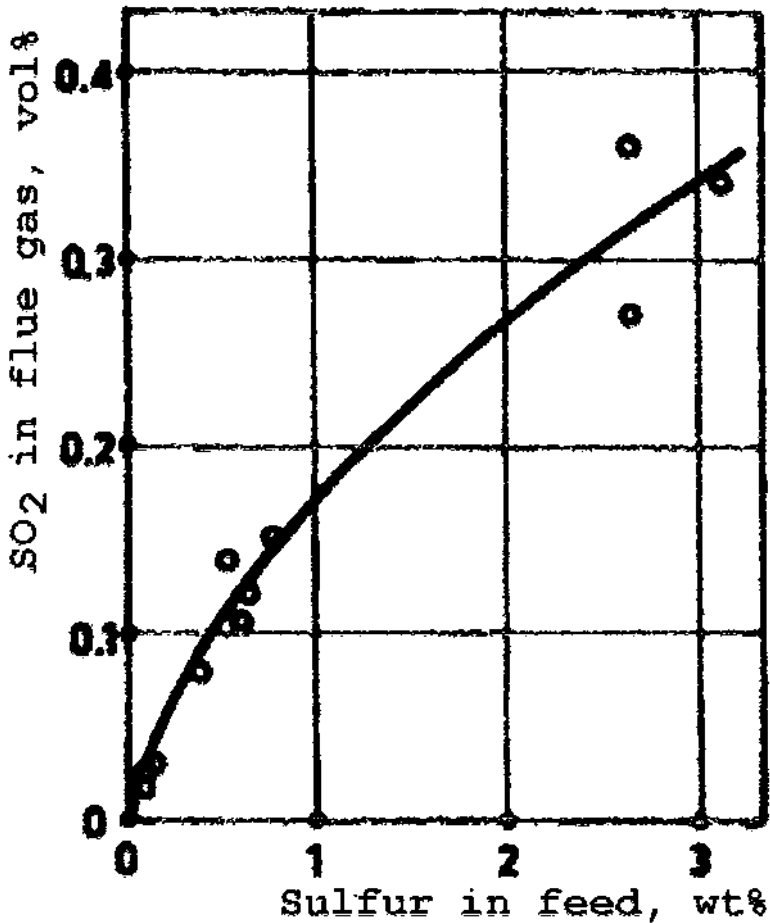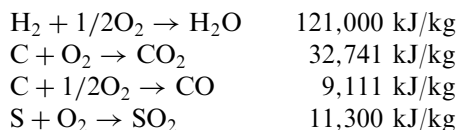| Component	Equilibrium composition	Real composition
O_2, % mol	0.0	0.10
CO, % mol	8.8	10.46
CO_2, % mol	7.5	8.65
H_2O, % mol	11.7	~ 10.0
NH_3, ppm	308	1285
SO_2, ppm	824	561
SO_3, ppm	0	5
NO, ppm	0	33

Figure 6.62 Correlation between the concentration of sulfur in the feed and of SO_2 in flue gases. (From Ref. 183.)

In practical conditions used for burning coke in fluid catalytic cracking units, the CO_2/CO ratio in the flue gases is about 1.5. It increases if the catalyst is poisoned by heavy metals. The more recently promoted zeolite catalysts perform the complete combustion of CO to CO_2 (see Section 6.2.4.3).

6.6.3 Thermal Effect in Regeneration

The thermal effect of regeneration is dependent on the hydrogen content of the coke and on the CO_2/CO ratio in the flue gases. It can be calculated on the basis of the thermal effects of the following reactions:

$$H_2 + 1/2O_2 \rightarrow H_2O \qquad 121,000 \text{ kJ/kg}$$
$$C + O_2 \rightarrow CO_2 \qquad 32,741 \text{ kJ/kg}$$
$$C + 1/2O_2 \rightarrow CO \qquad 9,111 \text{ kJ/kg}$$
$$S + O_2 \rightarrow SO_2 \qquad 11,300 \text{ kJ/kg}$$

In order to avoid these calculations, interpolations can be made based on the data of Table 6.25.

6.6.4 Kinetics of Regeneration

6.6.4.1 Effect of the Diffusion Barriers

For processes in a moving bed, which use as catalysts granules with 3–6 mm diameters, the studies of Adelson and Zaitzeva [223] prove that the diffusion limitation is manifested at temperatures above 550–600°C. This influence is accounted for in equations for the overall burning rate developed by the same authors and discussed in the next section.

From the facts presented in Section 6.4.1.2, it followed that external diffusion strongly influences the regeneration of the catalyst in a fluidized bed operating in dense phase. This fact was also confirmed by other studies [118,119]. According to the represented calculations, in riser systems, the influence of external diffusion is negligible.

The influence of internal diffusion depends to a great extent on the structure and size distribution of the pores so that no valid generalizations can be given. It is possible that internal diffusion influences the overall rate for catalysts shaped as granules with diameters of 3–6 mm, especially when coke situated in the central

Table 6.25 Thermal Effect of Coke Burning, kJ/kg Burned Coke

CO_2/CO ratio in flue gas	Hydrogen content in coke wt %		
	4.0	8.0	12.0
0	14,590	19,010	23,400
1	24,075	28,070	32,090
2	27,215	31,085	34,960
4	29,745	33,535	37,300
10	31,820	35,505	39,210

part of the granule is combusted. In fluidized bed processes, that use microspherical catalysts with diameters of 40–70 μm, the influence of internal diffusion is less probable. This consideration is most probably valid for zeolite catalysts with channel macropores. For these processes, internal diffusion would play a part only when conditions are used for drastically reducing the residual coke.

6.6.4.2 Kinetics of Coke Burning

For regeneration of catalyst particles used in catalytic cracking processes with moving bed, Adelson and Zaitzeva suggested the equation:

$$\tau = \frac{c\gamma_v\delta}{\beta C_o V} + \frac{c\gamma_a R^2 \left[3 - 2\delta - 3(1 - \delta)^{2/3}\right]}{6\beta C_o n\bar{r}f\sqrt{T}} - \frac{\ln(1 - \delta)}{\beta C_o k} \tag{6.95}$$

where:

- τ = total burning time in s
- c = weight fraction of coke on the catalyst
- δ = weight fraction of burnt coke to total coke
- β = amount of burnt coke in g/cm^3 of oxygen at the specified ratio CO_2/CO in the flue gases
- C_o = fractions in volume oxygen in the regeneration air
- V = cm^3 air/cm^3 catalyst
- R = mean radius of the catalyst granules in cm
- $\bar{r}$ = mean radius of the pores in cm
- f = volume of the pores referred to the volume of the granule
- T = regeneration temperature in Kelvin degrees
- k = apparent rate constant for the burning of coke in cm^3/g·s
- n = constant depending on the percentage of coke on the catalyst, having the value of 162 for 2% coke

The apparent constant of the reaction rate k is given by the equation:

$$k = 7.33 \cdot 10^{10} e^{-146,850/RT} \tag{6.96}$$

Eq. (6.95) was verified by using a catalyst containing 2% coke from an industrial plant and by applying various regeneration conditions. A number of these results are collected in Table 6.26, where are written separately the three terms of Eq. (6.95) corresponding to the durations of the external diffusion, the internal diffusion, and of the reaction. The total is compared with the experimentally measured duration, the result being quite satisfactory.

The table shows that at temperatures below 500°C, the slowest process is the reaction. At higher temperatures, the diffusion phenomena increasingly influence the overall rate and become rate controlling at temperatures above 600°C. The external diffusion becomes rate determining at lower rates of the regeneration air, due to the increased thickness of the boundary layer at the lower Reynolds numbers.

Since Eq. (6.95) was verified only on one synthetic catalyst and only for an initial coke content of 2%, caution must be applied in its use.

For regeneration in fluidized bed the following equation was suggested by Johnson and Maryland [224]:

$$v = k_1 P_o (1 + k_2 P_s) C^n \tag{6.97}$$

Table 6.26 Regeneration Duration Calculated with Eq. (6.95) Compared with Experimental Data

Regeneration		τ calculated with Eq. (6.95)				τ
Temp. (°C)	Vol. air/vol catalyst·hour	Diffus. ext. τ (min)	Diffus. int. τ (min)	React. τ (min)	τ total (min)	experimental (min)
453	1500	4.2	5.7	98.1	109.0	109.0
471	1500	4.2	5.7	55.1	65.0	65.0
504	1500	4.1	5.5	18.4	28.0	28.0
556	200	31.5	5.4	4.8	41.7	39.5
600	200	31.2	5.2	1.6	38.0	36.2
615	1500	4.0	5.0	1.1	10.1	9.0
660	1500	4.0	4.8	0.4	9.2	8.2

Granules radius 1.65 mm. Initial coke on catalyst 2%. Burned coke/initial coke = 0.7.

where:

$$v = \text{burning rate of coke in kg coke per 1,000 kg of catalyst per hour}$$
$$P_o \text{ and } P_s = \text{partial pressures of oxygen and steam in kg/cm}^2$$
$$C = \text{average coke content on the catalyst within the regenerator}$$
$$n = \text{constant with value close to unity}$$
$$k_1 \text{ and } k_2 = \text{kinetic constants shown in the graph of the Figure 6.63 [1], based on the data of [224].}$$

From the values of the rate constants, the apparent activation energies are of the order of 171,600 J/mol.

Eq. (6.97) was deduced and verified for the burning of coke deposited on natural bentonite catalysts with an initial coke content of 0.13–0.60%, the regeneration being performed at temperatures of 510–565°C [224–225]. The equation has an empirical character and should not be used without additional plant verifications and on catalysts used in current operation.

A study by Tone, Niura, and Otaka [226] reports the results of experimental tests carried out in a differential reactor, which eliminates the influence of the diffusion steps, at temperatures of 500–560°C.

A synthetic catalyst was used, containing 25% Al_2O_3, having a porosity of 0.76, and a specific surface of 496 m^2/g.

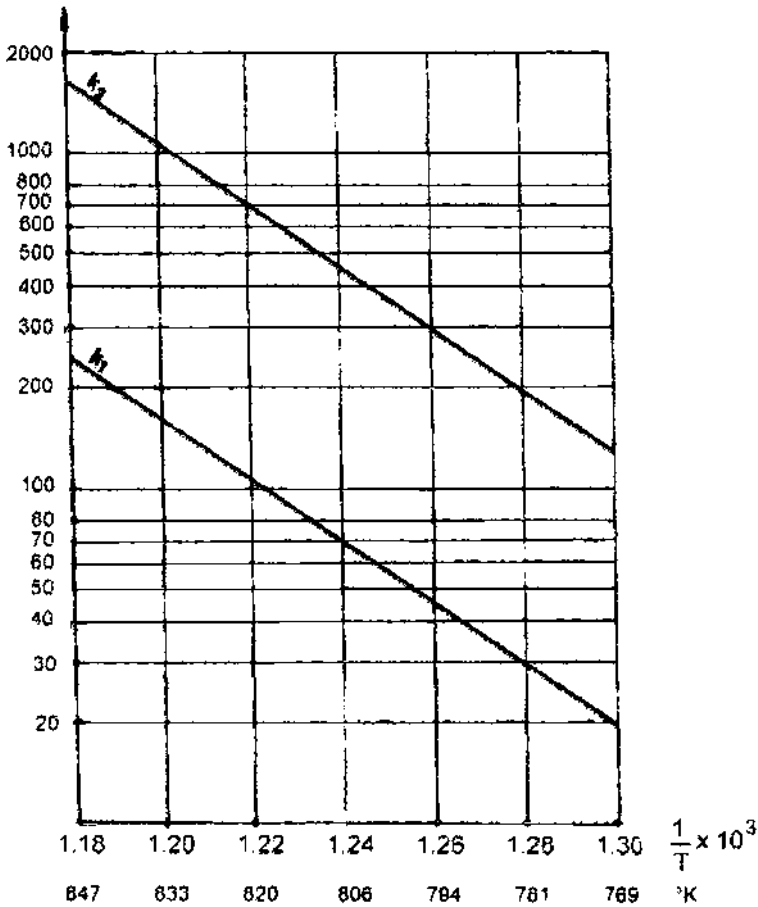The reactions were represented by the scheme:
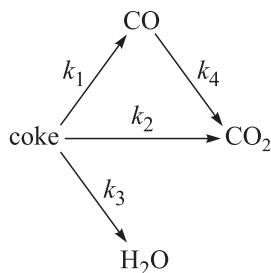
Figure 6.63 Temperature dependence of the constants k_1 and k_2 in Eq. (6.97).

and the following four rate equations were obtained:

$$
\begin{aligned}
r_1 &= k_1 n_C p_{O_2} \\
r_2 &= k_2 n_C p_{O_2} \\
r_3 &= k_3 n_H p_{O_2} \\
r_4 &= k_4 p_{CO}
\end{aligned}
\tag{6.98}
$$

where:

  n_C and n_H represent the content of carbon and hydrogen in the coke, expressed
    in moles carbon or hydrogen per g of catalyst
  p_i = partial pressures in atm

The formation of the final products is expressed by the equations:

for CO formation
$$F \cdot \frac{\Delta y_1}{\Delta w} = r_1 - r_4$$

for CO_2 formation
$$F \cdot \frac{\Delta y_2}{\Delta w} = r_2 + r_4 \qquad (6.99)$$

for H_2O formation
$$F \cdot \frac{\Delta y_3}{\Delta w} = r_3$$

where:

    Subscripts 1, 2, and 3 correspond to CO, CO_2 and water; Δy_i = difference expressed in molar fractions between the inlet and outlet of the reactor

    Δw = weight of the catalyst in g

    F = feedrate in moles/minute.

It results that the reaction rates r_i are expressed in moles of carbon or hydrogen converted per g of catalyst per minute.

The linearization of the experimental data, including those of other researchers, led to the following equations of the reaction rate constants:

$$k_1 = 9.923 \cdot 10^9 \cdot \exp\left(-\frac{153,000}{RT}\right) \qquad \text{l/ min} \cdot \text{bar}$$

$$k_2 = 2.578 \cdot 10^6 \cdot \exp\left(-\frac{107,350}{RT}\right) \qquad \text{l/ min} \cdot \text{bar}$$

$$k_3 = 6.557 \cdot 10^4 \cdot \exp\left(-\frac{76,240}{RT}\right) \qquad \text{l/ min} \cdot \text{bar} \qquad (6.100)$$

$$k_1 = 4.003 \cdot 10^9 \cdot \exp\left(-\frac{57,650}{RT}\right) \qquad \text{mol/g} \cdot \text{cat} \cdot \text{min} \cdot \text{bar}$$

It is to be remarked that the burning of hydrogen contained in the coke takes place at a higher rate than that of carbon (Figure 6.64), which leads to a lower value for the hydrogen in the residual coke than in the initial one.

In a recent study, a system of differential equations was proposed for modeling coke burning and the composition of the flue gases [241]. This equations system is based on a large number of experiments realized on OCTADINE 1169 BR Engelhard catalyst with MAT activity of 71 wt %.

In another paper [242] one and two steps riser regeneration systems were studied to find the best way of introducing and distributing air, with the idea to improve the regenerator system. The result of such optimization was a carbon content of less than 0.1 wt % in the regenerated catalyst and operation at riser temperature lower than 730°C.

6.6.5 Effect of the Regeneration Conditions

6.6.5.1 Temperature

The lowest temperature level for regeneration is limited by the rate of coke burning. The highest level was limited in the past by the ability of the catalyst to resist high temperatures. Following refinements made to the catalysts, the temperature is now limited by metallurgical considerations, namely by the resistance at high temperatures of the metals of the regenerator and of the transport lines for the flue gases.
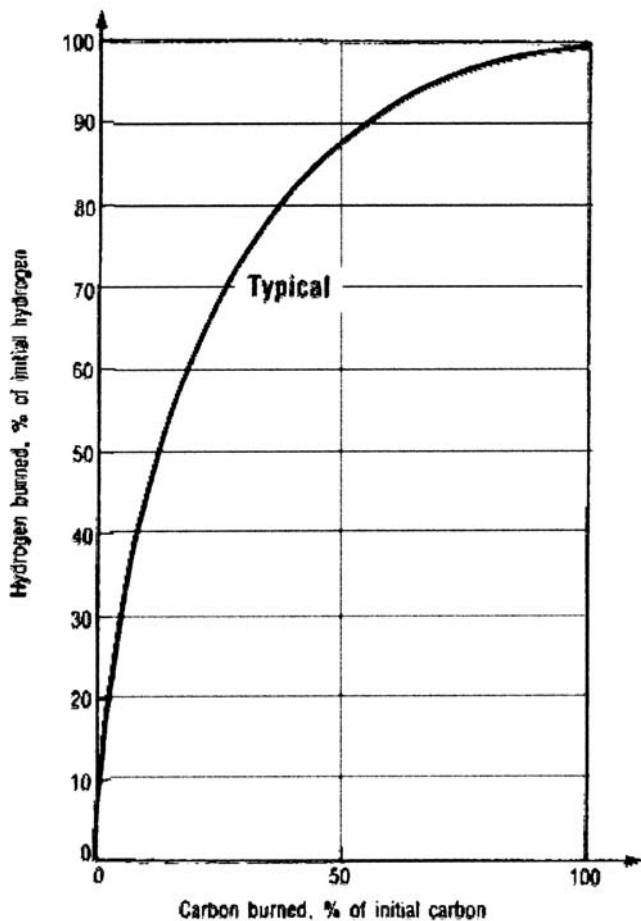
Figure 6.64 Relative combustion velocity of coke carbon and hydrogen at 700°C. (From Ref. 227.)

Increasing the temperature while maintaining constant the other working parameters increases the burning rate of coke and accordingly decreases the residual coke. Since the decrease of residual coke leads to the increase of the average activity of the catalyst, the regenerator is operated at the maximum possible temperature while taking into account the limitations mentioned above.

6.6.5.2 Pressure

As it results from Eqs. (6.97) and (6.98) the rates for burning carbon in CO and CO_2, as well as for burning hydrogen, are directly proportional to the partial pressure of oxygen.

The initial partial pressure may be increased by increasing the total pressure in the regenerator or by the addition of oxygen in the air fed to regeneration.

The pressure in the regenerator depends on the type of unit and does not constitute a controllable process parameter in the operation of the plant. The addi-

tion of oxygen in the air fed to the regenerator is an efficient measure suggested as early as 1980 [228] and was applied beginning with 1986 in the Gibraltar refinery [229]. The extension of this measure is limited by economic reasons.

The average oxygen partial pressure in the regenerator depends also on the air excess, a parameter on which the operator may act to the extent allowed by the performance of the turbo-blower and by the requirement of not exceeding reasonable linear velocities for the air and flue gases in the regenerator.

Finally, the increase of pressure and excess air, while keeping constant the other parameters, leads to the decrease of residual coke, which is illustrated in Figure 6.65 [230].

6.6.5.3 Catalyst Characteristics

The structure and the size distribution of the catalyst pores have a strong influence on the regeneration rate. This observation is in agreement with the fact that at the high regeneration temperatures used at present, even if the internal diffusion is not controlling the rate, it influences it to a large extent.

At otherwise constant parameters, the catalyst structure strongly influences the residual coke. The existence of the channeling macropores makes easier the access of
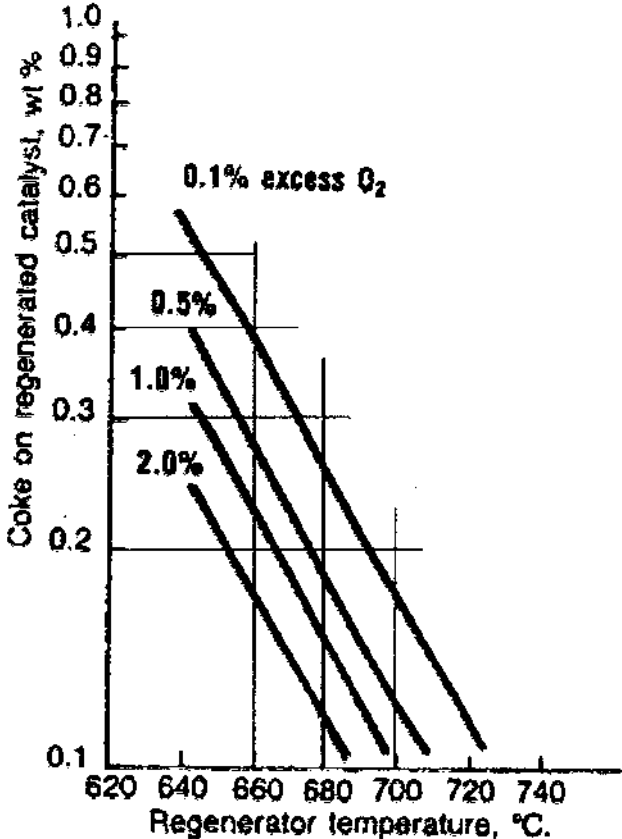

Figure 6.65 Residual coke as a function of temperature and excess air. (From Ref. 230.)

the oxygen to the coke particles located in the center of the granule and decreases the residual coke. For this reason the presence of the macropores is a desired feature of catalyst structure.

The characterization of the catalysts from the point of view of regenerability requires special methods [1].

Ni and V content is an important factor for the performance of the equilibrium catalyst present in the reaction system. In addition to the unfavorable influence on the cracking reactions discussed earlier, these metals can modify the thermal balance of the regenerator by the catalytic action of the combustion of CO to CO_2, due especially to nickel. In older units, the CO/CO_2 ratio was maintained at a certain level in order not to thermally overload the regenerator. The effect of the mentioned metals was to cause especially combustion in the diluted phase, above the catalyst bed. It seems that the alumosilica had an inhibiting effect and prevented $CO \rightarrow CO_2$ combustion inside the bed.

In modern units the situation is completely different. They are designed for a maximum heat production in the regenerator, in order to eliminate the supplementary equipment for the combustion of the CO contained in the flue gases. In this situation it is desired to achieve as completely as possible a combustion of the CO in the regenerator. Additives to promote burning contribute to this goal.

In this case the burning also takes place above the catalyst bed. This leads to a difference between the temperature of the dilute and the dense phases within the regenerator. This difference is illustrated in Figure 6.66 [230].

The control of the regeneration regime by increasing the level of the catalyst bed was tested at a refinery in Peru [231]. The disadvantage of the method is the necessity to increase the catalysts inventory, which has a negative impact on the economics of the operation.
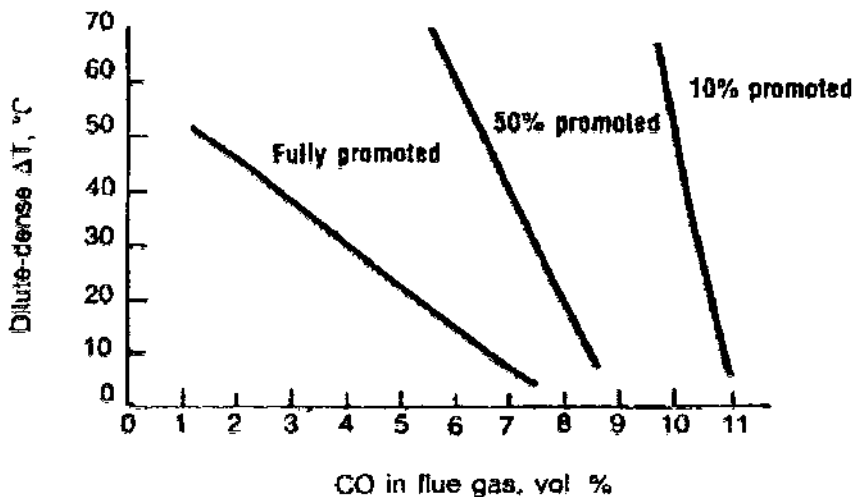

Figure 6.66 Effect of promoters on the CO content in flue gases. (From Ref. 230.)

REFERENCES

1. S Raseev. Procese distructive de prelucrare a titeiului, Editura Tehnica, Bucuresti, 1964.
2. S Raseev Stud Cercet Chim 5: 261,2S5, 1957.
3. DR Stull, EF Westrum Jr., GC Sinke. The Chemical Thermodynamics of Organic Compounds, Malabar, Florida: Robert E. Krieger Publ. Co., 1987.
4. D Decroocq, R Bulle, S Chatila, JP Franck, Y Jacquir, Le craquage catalytique des coupes lourdes, Technip, Paris, France 1978.
5. DG Tajbl, UOP Fluid Catalytic Cracking Process, Handbook of Petroleum Refining Processes, RA Meyers, ed., New York: McGraw-Hill, 1986.
6. J Scherzer, Octane-Enhancing Zeolitic FCC Catalysts, New York-Basel: Marcel Dekker, Inc., 1990.
7. ND Zelinski, Neftianoie i slanzevoie hoziaistvo, 2, No 9–12: 3, 1921.
8. SR Sergheenko Ocerk razvitia himii i pererabotki nefti, Akad URSS, Moscow, 1955.
9. AN Sachaven, Conversion of Petroleum, New York: Reinhold Publ. Co. 1948.
10. L Ubbelhode, N. Voronin, Petroleum, 7: 9, 1911.
11. Petroleum Processing Handbook; John J McKetta, ed. New York-Basel-Hong-Kong: Marcel Dekker, Inc., 1992.
12. JE Naber, M Akbar. "Shell's residue fluid catalytic cracking process", In: Hydrocarbon Technology International-1989/90, P Harrison, ed. Sterling Publ. Intern. London, 1990.
13. W Franz, P Gunther, CE Hofstandt, Fifth World Petroleum Congress, Section III,123, New York, 1959.
14. EJ Gohr. Development of the fluid catalytic cracking process (in Russian), Fourth World Petroleum Congress, Rome 1955. Gostoptehizdat Moskow, Vol. 4, 1956 p. 139.
15. P Courty, C Marcilly. Preparation of Catalysts III, 485, Elsevier, Amsterdam, 1983.
16. LLB Ryland, MW Tamele, JN Wilson. Catalysis, Editor. PH Emmett, ed. vol. VII, p. 1, New York: Reinhold, 1960.
17. HP Boehm, H Knozinger. Catalysis-Science and Technology, vol. 4, JR Anderson, M Boudart, Springer, ed. Berlin, 1983.
18. BW Wojciechowski, A Corma. Catalytic Cracking, New York: Marcel Dekker, Inc., 1986.
19. L Thomas Ch., Ind Eng Chem 41: 2564, 1949.
20. VI Vernadski. Ocerki gheochimii, Gorneftizdat 1934 p. 108.
21. K Hashimoto, T Masuda, H Sasaki. Ind Eng Chem 27: 1792, 1988.
22. BC Gates. Catalytic Chemistry, New York: John Wiley & Sons Inc., 1991.
23. EG Derouane. Intercalation Chemistry, MS Wittmgham, AJ Jacobson, eds. New York: Academic Press, 1982, p. 10.
24. PK Maher, CV McDaniel. U.S. Patent 3,402,996, 1968. DW Breck. U.S. Patent 3,130,007, 1964; JC Pitman, LJ Raid, U.S. Patent 3,473,589, 1969.
25. DW Breck. Zeolite Molecular Sieves, New York: John Wiley & Sons, Inc., 1974.
26. DW Breck. EM Fanigen, RM Milton. Abstr. 137th Meeting Am. Chem. Soc., Apr. 1960.
27. H Robson. Chem. Techn. 8: 176, 1978.
28. LD Rollman. Adv. Chem. Ser. (Inorg. Compd. Unusual Prop.-2) 173 387, 1979.
29. EM Flanigen. Pure Appl Chem 52: 2191, 1980.
30. LB Sand. Pure Appl Chem 52: 2105, 1980.
31. M Mengel. Chem. Tech. (Heidelberg) 10: 1135, 1981.
32. RM Barrer, Zeolites 1: 130, 1981.
33. LD Rollmann. NATO ASI, Ser, E., 1984, 80 (Zeolites Sci. Technol.), Portugal: 109, 1983.

34. C Marcilly. Raport nr. 14, Catalytic cracking-evolution of FCC catalysts. Published in OAPEC-IFP Workshop 5–7 July 1994, French Petroleum Institute, Rueil-Malmeson, France.
35. S Benton. Oil and Gas Journal 93: 98, 1 May 1995.
36. A Humphries, JR Wilcox. Oil and Gas Journal 87: 45, 6 Feb. 1989.
37. K Rajagopalan, ET Habib Jr. Hydrocarbon processing 61: 43, Sept. 1992.
38. AT Lengade. Hydrocarbon Conversion Catalysts, Can. Pat. 967, 136, 1975.
39. WA Welsh, MA Seese, AW Peters. Catalyst Manufacture, U.S. Patent 4,458,023 (1984).
40. RJ Nozemack, JA Rudesil, DA Denton, RD Feldwick. Catalyst Manufacture, U.S. Pat. 4,542,118, 1985.
41. J Scherzer, DP McArthur. Ind. Eng. Chem. Res. 27: 1571, 1988.
42. L Upson, S Jams. Meeting NPRA, Mars 1982.
43. WA Blanton, RL Flanders. U.S. Patent 4,115.249 (1978) and 4,071,436 (1978).
44. LL Upson, H Van der Zwan. Oil and Gas J 85: 23 Nov., 64, 1987.
45. L Rheaume, RE Ritter, JJ Blazek, JA Montgomery. Oil and Gas J 74(20): 103, 1976.
46. AW Chester, AB Schwartz, VA Stover, JP McWilliams. Prepr Div Pet Chem, Am Chem Soc. 24: 624, 1979.
47. FD Harzell, WA Chester. Hydrocarbon Processing 59 (7): 137, 1979.
48. VR Zinoviev, MJ Levinbuc, UK Sapieva. Himia i tehnologhia topliv i masel. (2): 9, 1993.
49. VR Zinoviev, MJ Levinbuc, VE Varsaver. Himia i tehnologhia topliv i masel. (4): 6, 1993.
50. AS Krishna, CR Hsieh, AR English, TA Pecoraro, CW Kuehler. Hydrocarbon Processing 70 (11): 59, 1991.
51. RJ Bertolacini, GM Lehmann, EG Wollaston. U.S. Patent 3,835,031, 1974; S Jin, JA Jaecker, U.S. Patent 4,472,267, 1984; JW Bryne, Nat. Petr. Ref. Assoc., AM-84-55, 1984.
52. U Alkemade, S Cartlidge, JM Thomson. Oil and Gas J. 88: 52, 1 Oct 1990.
53. LA Jandieva, SM Gairbekova. Himia i tehnologhia topliv I masel, (4): 5, 1993.
54. MW Anderson, ML Occelli, SL Suib. Journal of Catalysis, 122 (2): 374, 1990.
55. U.S. Patent 4, 791, 083.
56. EV McDaniel, PK Mahler. U.S. Patent 3,292,192, 1966; 3,449,070, 1968.
57. GW Skeels, DW Breck. Proc. 6th Interllat. Zeolites Conf. Reno, Nevada, 1983.
58. DW Breck, H Blass, GW Skeels. U.S. Patent 4,503,023, 1985.
59. LL Upson, RJ Lawson, WE Cormier, FJ Baars. Oil and Gas J. 88: 64, 1 Oct. 1990.
60. NY Chen, WE Garwood. J Catal 47: 249, 1977.
61. NY Chen, LR Gorring, HR Irland, TR Stein. Oil and Gas J 75 (23): 165, 1977.
62. AA Avidan, Oil and Gas J: 90, 59, May 18 1992.
63. P O'Connor, F van Houtert. Ketjen CataL Symposium, Scheveninsen Holland, 1986.
64. P O'Connor, LA Gerritsen, JR Pearce, PH Desai, A Humphries, S Janik. Catalyst Development in Resid FCC, AKZO Catalyst Symposium, Mai 1991, Scheveningen, Holland.
65. JE Penick. U.S. Patent 4,064,639, 1977.
66. AB Schwartz. U.S. Patent 4,072,600, 1978.
67. AW Chester. U.S. Patent 4,107,032, 1978.
68. EM Arnett, JW Larsen. J Am Chem Soc 91: 1438, 1969.
69. W Haag, MR Dessau, Proc. 8th Intern. Congr. Catal., Berlin 1984, vol 2, p. 305.
70. AG Evans, M Polanyi, J Chem Soc 69: 252, 1947.
71. HO Pritchard, Chem Rev 52: 529, 1953.
72. BS Greensfelder. The Chemistry of Petroleum Hydrocarbons, vol. II, BT Brooks, ed. New York: Reinhold Publ. Co., 1955, p. 137.

73. RZ Magaril, Teoreticeskie osnovy himiceskih protesov pererabotki nefti, Himia, Moscow, 1976, p. 165.
74. JL Franklin, Thermodynamic Aspects, Carbonium, Ions, GA Olah, PR von Schleyer eds. New York: Interscience, 1968, vol. I, p. 85.
75. JE Germain, Catalytic Conversion of Hydrocarbons, London-New York: Academic Press, 1969.
76. J Turkevich, RK Smith, J Chem Phys 16: 466, 1948.
77. OA Reutov, TN Shatkina, Dokl Akad Nauk SSSR 133: 606, 1960.
78. PS Skell, RJ Maxwell, J Am Chem Soc 84: 3963, 1962.
79. DM Brouwer, JM Oelderik, Recl. Trav. Chem. Holland 87: 721, 1968.
80. H Hogeveen, AF Bickel, Reel Trav Chim Holland 88: 371, 1969.
81. TS Sie, Ind Eng Chem 31: 1881, 1992; 32: 397, 1993.
82. DK Liguras, DT Alien, Ind Eng Chem 28: 665, 1989; 28: 674, 1989.
83. GM Pancenkov, AS Kazanskaya, Zh. Fiz. Chim. 32: 1779, 1958.
84. HH Voge, Catalysis, PH Emmett, ed. vol. VI, 1958, p. 407, 466.
85. GM Good, HH Voge, BS Greensfelder. Ind Eng Chem 39: 1032, 1947.
86. E Angelescu, P Gurau, G Pogonaru, G Musca, Pop Gr, Pop Ec, Rev Roum de Chimie 35: 229, 1990.
87. A Corma, A Lopez Angudo, React Kinet Catal Lett 16: 253, 1981.
88. VV Kharlamov, TS Starostina, KhM Minachev, Izv. Acad.-Nauk USSR 10: 2291, 1982.
89. V Haensel, Adv Catal 3: 179, 1951.
90. BS Greensfelder, HH Voge, GM Good. Ind Eng Chem 41: 2573, 1949.
91. J Scherzer, DP McArthur, Oil and Gas J 84 76: 27 Oct. 1986.
92. TC Ho, AR Katritzky, SY Cato, Ind Eng Chem 31: 1589, 1992.
93. CM Fu, AM Schaffer, Ind Eng Chem 24: 68, 1985.
94. AC Oblad, T Milliken, GA Mills, The Chemistry of Petroleum Hydrocarbons, vol. II, BT Brooks, ed. New York: Reinhold Publ. Co., New York, 1955.
95. BV Klimenok, EA Andreev, VA Bordeeva, Izv. Akad. Nauk SSSR 5: 526, 1956.
96. TM John, RA Pachovsky, BW Wojciechowski. Adv Chem Ser 133: 422, 1974.
97. KR Al Latif, Ph.D. Thesis directed by S Raseev, Inst. Petrol Gaze, Ploiesti, 1975.
98. JW Hightower, PH Emmet, J Am Chem Soc 87: 939, 1965.
99. DA Best, BW Wojciechowski, J Catal 47: 11, 1977.
100. CC Lin, SW Park, W Hatcher, Ind Eng Chem Process Des Dev 22: 609, 1983.
101. M Guisnet, P Magnoux, Appl Catal 54: 1, 1989.
102. CT Ho, Ind Eng Chem Res 31: 2281, 1992.
103. FW Scholkemeier, Arch d Math 1: 270, 1949.
104. VG Jenson, Proc Roy Soc London A249: 346, 1959.
105. S Taneda, Repts Res Inst Appl Mech 4: 99, 1956.
106. S Raseev, Ph.D. Thesis, Bucarest, 1972.
107. B Jazayeri, Hydrocarbon Processing 7Q (5): 93, 1991.
108. P Wuithier, Le Petrole, Rafinage et Geme Chimique, I Tome, Technip., Paris, 1972.
109. Rascioty osnovnyh protsesov i aparatov neftenererabotki, Editor EN Sudacov, Himia, Moscova, 1979.
110. OA Hougen, KM Watson, Chemical Process Principles, vol. Ill, In Kinetics and Catalysis, New York: John Wiley & Sons, Inc., 1947.
111. RC Reid, JM Prausnitz, BE Poling, The Properties of Gases and Liquids, 4th ed. Chap. 11, New York: McGraw-Hill Book Co., 1987.
112. JM Smith, Chemical Engineering Kinetics, 3rd ed. New York: McGraw-Hill Book Co., 1981.
113. CR Wilke, CY Lee, Ind Eng Chem 47: 1253, 1955.
114. EN Fuller, JC Giddings, J Gas Chromatogr, 3: 222, 1965.

115. EN Fuller, K Ensley, JC Giddings, J Phys Chem 75: 3679, 1969.
116. EN Fuller, PD Schettler, JC Gilddings, J Ind Eng Chem 58 (5): 18, 1966.
117. Enciclopedia de Chimie, vol. 5, p. 132, Editura Stiintifica si Enciclopedica, Bucuresti, 1988.
118. J Pansing, J Am Inst Chem Eng 2: 71, 1956.
119. A Babicov, B Solar, L Glazov, J Liberzon, R Basov, T Melik-Ahnazarov, A Elsin, V Zarubin, Himia tehnologhia topliv i masel 9, No. 1, 1993.
120. R Aris, Chem Eng Sci, 6: 262, 1957.
121. R Aris, Ind Eng Chem Fund 4: 227, 1965.
122. EE Petersen, Chemical Reaction Analysis, Englewood Cliffs: Prentice-Hall, New Jersey, 1965.
123. GF Froment, KB Bischoff, Chemical Reactor Analysis and Design, New York: John Wiley & Sons, Inc., 1979.
124. TE Comgan, Chem Eng Propr 49: 603, 1953.
125. CD Prater, RM Lago, Advances in Catalysis and Related Subjects, WG Frankenburg, ed. vol. 8, 1956.
126. MFL Johnson, Ind Eng Chem 49: 283, 1957.
127. GM Pancencov, JM Jarov, Trudy Moskv Inst Neftianoy I Gazovoi Prom 37: 3, 1962.
128. EV Bergstrom, VO Bowles, LP Evans, JW Payne, Fourth World Petroleum Congress, sect. III, Rome, 1955.
129. RM Moore, JR Katzer, AlChEJ 18: 816, 1972.
130. DM Nace, Ind Eng Chem Prod Res Dev 9: 203, 1970.
131. WO Haag, RM Lago, PB Weisz. Faraday Disc Chem Soc 72: 317, 1981.
132. A Voorhis Jr., Ind Eng Chem 37: 318, 1945.
133. AV Frost, Vestnik Mosc Gos Univ., nr. 3, p. 11 and 4,117, 1946.
134. TV Antipina, Dokl Akad Nauk SSSR 53: 47, 1946.
135. GM Pancenkov, VP Lebedev, Himicescaia Kinetika i Kataliz, ed. Univ. Mosc., 1961.
136. V Tescan, S Raseev, Bul. Instr. Petr. si Gaze 14: 93, 1966.
137. S Raseev, HA Hassan, Bul Inst Petr si Gaze 15: 73, 1967.
138. LL Oliveira, EC Biscaia Jr., Ind Eng Chem 28: 264, 1989.
139. GF Froment, KB Bischoff, Chem Eng Sci 16: 189, 1961.
140. RP DePauw, GF Froment, Stud Surf Sci Catal 6: 1, 1980.
141. JW Beeckman, GF Froment, Ind Eng Chem Fundam 18: 245, 1979.
142. EFG Herington, EK Rideal. Proc Roy Soc (London), A184, 434, 1945.
143. VW Weekman Jr, Ind Eng Chem Process Des Dev 7: 90 (1968).
144. A Corma, A Lopez Agudo, J Nebot, F Tomas, J Catal 77: 159, 1982.
145. EB Maxted, Adv Catal 3: 129, 1951.
146. HV Maat, L Moscou, Proc 3th Int. Congr. Catal, Amsterdam, 2, 1277, 1964.
147. AL Pozzi, HF Rase, Ind Eng Chem 50: 1075, 1958.
148. FH Blanding, Ind Eng chem 45: 1186, 1953.
149. J Gustafson, Ind Eng Chem Process Des Dev 11: 4, 1972.
150. S Krishmaswamy, JR Kittrell, Ind Eng Chem Process Des Dev 17: 200, 1978.
151. NN Samoilova, VN Erkin, PJ Serikov, Himia i Tehnologhia Topliv i Masel, No 10: 11, 1990.
152. VW Weekman, DM Nace, AlChE J 16: 397, 1970.
153. V Tescan, S Raseev, Bul Inst Petrol Gaze 15: 81, 1967.
154. JA Paraskos, YT Shah, JD McKinney, NL Carr, Ind Eng Chem Process Des Dev 15: 165, 1976.
155. RA Pachowsky, BW Wojciechowski, Canad J Chem Eng 49: 365, 1971.
156. JF Coopmans, P Mars, RL de Groot, Ind Eng Chem Res 31: 2093, 1992.
157. B Gross, DM Nace, SE Voltz, Ind Eng Chem Process Des Develop 13: 199, 1974.
158. AN Ko, BW Wojciechowski, Progr React Kinet, 12:201 1984.

159.   M Larocca, S Ng, H de Lasa, Ind Eng Chem Res 29: 171, 1990.
160.   LC Yen, RE Wrench, AS Ong, Oil Gas J, Jan. 11, 67 (1988).
161.   L Liang-Sun, C Yu-Men, H Tsung-Nieu, Canad J Chem Eng, 67: 615, 1989.
162.   TM John, BW Wojciechowski, J Catal, 37: 240, 1975.
163.   A Corma, J Juan, J Martos, JM Soriano, 8th International Congress on Catalysis, Berlin, vol. II, (1984), p. 293.
164.   SM Jacob, B Gross, SE Voltz, AIChE J., 22(4): 701, 1976.
165.   PB Weisz, "Kinetics and Catalysis in Petroleum Processing", 10th World Petroleum Congress vol. 4, 1980, p. 325.
166.   LL Oliveira, EC Biscaia, Jr., Ind Eng Chem Res 28: 264, 1989.
167.   W Feng, E Vynckier, GF Froment, Ind Eng Chem Res 32: 2997, 1993.
168.   JW Dean, DB Dadyburjor, Ind Eng Chem Res 28: 271, 1989.
169.   M Schlossman, WA Parker, LC Yen, Chemtech 41: Febr. 1994.
170.   PH Emmett, Catalysis, New York: Reinhold Publ Co, 1956.
171.   CR Olsen, MJ Sterba, Chem Eng Progr 45: 692, 1949.
172.   CL Hemler, UOP Process Div, Sc Petr Council Yugoslav Academy, 13 June 1975.
173.   KM Watson, EF Nelson, Ind Eng Chem 25: 880, 1933.
174.   S Raseev, Proprietatile fizice si fizico-chimice ale hidrocarburilor, titeiului si fractiunilor de tite, Published in "Manualul chimistului, Vol. 2, ed. AGIR, Bucuresti, 1948.
175.   WL Nelson, Oil and Gas J 60: 11 June 1962.
176.   HE Reif, RF Kress, JS Smith, Petr Refiner 40: 237, 1961.
177.   PJ White, Oil and Gas J 66: 112, 20 May 1968.
178.   K Van Nes, HA van Westen, Aspects of Constitution of Mineral Oils, New York: Elsevier, 1951.
179.   N Hazelwood, Analitical Chem 163, June, 1954.
180.   LM Kolesnicov, IN Frolova, HA Lapsina, Nauka Kiev 6:111, 1981.
181.   DW Kraemer, HJ Lasa, Ind Eng Chem 27: 2002, 1988.
182.   LE Kruglova, SN Hodjiev, SL Andreev, VV Tcheremin, Himia tehnologhia topliv masel, No. 10, 1991, p. 11.
183.   GP Huling, JD McKinney, TC Readal, Oil and Gas J 73: 13, 19 May 1975.
184.   RN Cimbalo, RL Foster, SJ Wachtel, Oil and Gas J 70: 112, 15 May 1972.
185.   VJ Pentcev, AJ Bontcev, Himia i tehn. topliv masel 26 (3): 10, 1991.
186.   MS Useinova, AM Guseinov, VM Kapustin, VA Jaurov, Himia i tehnologhia topliv masel, 28, No 11: 13, 1993.
187.   JB Pholenz, Oil and Gas J 61: 124, 1 Avr. 1963.
188.   JJ Blazek, Oil and Gas J 71: 66, 8 Nov 1973.
189.   JB Magee, JJ Blazek, Zeolite Chemistry and Catalysis, Editor JA Rabo, ed. American Chem Soc, Washington, 1976.
190.   AK Rhodes, Oil and Gas J 92: 41, 10 Oct 1994.
191.   CC Wear, RW Matt, Oil and Gas J 86: 71, 25 July 1988.
192.   PH Desai, RP Haseltine, Oil and Gas J 87: 68, 23 Oct 1989.
193.   WS Letzsch, JS Magee, LL Upson, P Valeri, Oil and Gas 7: 57, 86, Oct 31, 1988.
194.   RE Ritter, WR Grace, Oil and Gas 7: 41, 73, 8 Sept 1975.
195.   SJ Watchel, LA Bailie, RL Foster, HE Jacobs, Oil and Gas J 70: 104, Apr 10, 1972.
196.   JL Giandjonts, PJ Serikov, VN Erkin, TH Melik-Ahnazarov, Himia Tehn Topl Masel (9): 9, 1992.
197.   C Marciuy, Revue de l'Institut Francois du Petrole 42: 481, 1992.
198.   AW Chester, WA Stever, IEC PRD 16 (4): 285, 1977.
199.   LA Pine, RJ Maher, WA Wachter, Ketjen Catalysts Symp, Amsterdam, 1984, p. 19.
200.   J Magnusson, R Pudas, Katalistic's 6th Annual FCC Symp, Munchen, Germany, 22–23 May 1985.
201.   JB McLean, EL Morehead, Hydrocarbon Processing 70 (2): 41, 1991.

202. RE Ritter, L Rhéamne, WA Welsh, JS Magee, Oil and Gas J 79: 103, July 1981.
203. RJ Campana, AS Krishna, SJ Yanik, Oil and Gas J 81: 128, Oct 31, 1983.
204. L Upson, S Jaras, J Dalin, Oil and Gas J, 80: 135, Sept 20 1982.
205. CJ Groenenboom, FW Van Houtert, J Van Maare, H Elzeman, Ketjen Catalysis Symp, Amsterdam, (1984), p. 55.
206. ML Occelli, SAC Gould, Chemtech 24:24–27, May 1994.
207. M Larocca, H Farag, S Ng, H de Lasa, Ind Eng Chem Res 29: 2181, 1990.
208. H Farag, S Ng, H de Lasa, Ind Eng Chem Res 32: 1071, 1993.
209. BM Jitomirski, EM Soskin, VA Stankevitch, EA Klimtseva, Himia i tehnol topliv masel, (7): 11, (1989).
210. PG Thiel, Oil and Gas J 78: 132, 18 Aug, 1980.
211. DF Tolen, Oil and Gas J 79: 90, 30 March 1981); 83: 91, 1984.
212. D Geldart, AL Radke, Powder Technology 47: 157–165, 1986.
213. GW Brown, Oil and Gas J, 88: 46, 15 Jan, 1990.
214. L Maksimiuk, EJ Tselidi, Neftepererabotka i Neftehimia 1: 14, 1991.
215. RJ Campegna, JP Wick, MF Brady, DL Fort, In: Refining and Petrochemical Technology Yearbook, PennWell Books, Tulsa, Oklahoma, 1987 p. 70.
216. GDL Carter, G McElhiney, Hydrocarbon Processing 68: 63, 1989.
217. DA Keyworth, WY Turner, TA Reid, Oil and Gas J 86: 65, 14 March 1988.
218. JA Montgomery, WS Letzsh, Oil and Gas J 69: 60, 22 Nov 1971.
219. C Wollaston, WJ Haflin, WD Ford, CJ D'Souza, Hydrocarbon Processing 54 (9): 93, 1975; Oil & Gas J 73: 87, 22 Sept 1975.
220. R Sadeghbeigi, Hydrocarbon Processing 70: 39, Feb. 1991.
221. S Raseev, I Georgescu, Petrol si Gaze 22. (2): 108, 1971.
222. DP McArthur, HD Simpson, K Baron, Development in Catalytic Cracking, published by Oil and Gas J, 1983.
223. SV Adelson, AJ Zaiteva, Himia i tehnol. Topiv i masel 7(1): 25, 1962.
224. MFL Johnson, HC Maryland, Ind Eng Chem 47: 127, 1955.
225. WF Pansing, J Am Inst Chem Eng 2: 71, 1956.
226. S Tone, S Miura, T Otake, Bulletin of Japan Petroleum Institute 14(1): 76, May 1972.
227. JL Mauleon, SB Sigaud, Oil and Gas J 85: 52, 23 Febr 1987.
228. DP Bhasin, MS Liebenson, G Chapman, J Hydrocarbon Processing 62, Sept 1983.
229. JP de Haro, AJ Gonzales, N Schroder, O Stemberg, Oil and Gas J 90: 40, 11 May 1992.
230. LL Upson, H van der Zwan, Oil and Gas J 85: 65, 23 Nov 1987.
231. RE Wong, Hydrocarbon Processing 72: 59, Nov 1993.
232. A Pekediz, D Kraemer, A Blaseth, H De Lasa, Ind Eng Chem Res 36: 4516–4522, 1997.
233. JI Mauleon, JC Curcelle, Oil and Gas J 64–70, 21 Oct 1985.
234. X Zhao, TG Robene, Ind Eng Chem 38: 3847–3854, 1999.
235. X Zhao, TH Harding, Ind Eng Chem 38: 3854–3859, 1999.
236. L Nalbandian, IA Vasalos, Ind Eng Chem 38: 916–927, 1999.
237. S Al-Khataff, H De Lasa, Ind Eng Chem Res 38: 1350–1356, 1999.
238. J Ancheyta-Juarez, F Lopez-Isunza, E Angular-Rodriguez, Ind Eng Chem Res 37: 4637–4640, 1998.
239. J Ancheyta-Juarez, F Lopez-Isznza, E Angular-Rodriguez, JC Moreno-Mayorga, Ind Eng Res, 36: 5170–5174, 1997.
240. K-H Lee, B-H He, Ind Eng Chem 37 (5): 1761–1768, 1998.
241. JM Arandes, I Abajo, I Fernandez, D Lopez, J Bilbao, Ind Eng Chem (9) 3255–3260, 1999.
242. D Bai, J-X Zhu, Y Jin, Z Yu, Ind Eng Chem 36, (11) 4543–4548, 1997.
243. JR Harris, Hydrocarbon Processing 75: 63, 1996.

244. CW Osen, Arch Math Astr Phys 6: 29, 1910; 7: 1, 1911.
245. S Goldstein, Proc Roy Soc London A123: 225, 1929.
246. M Kawaguti, Repts Inst Sci Techn Un Tokyo 2: 4, 1948.
247. S Timotika, T Aoi, Quart Journ Mech and Appl Math 3 (Pt. 2): 140, 1950.
248. T Pearcey, B McHugh, Phil Mag 46(7): 783, 1955.
249. J Proudman, JRA Pearson, J Fluid Mech 2: 237, 1957.
250. W Chester, DR Breach, J Fluid Mech 37: 751, 1969.
251. M Van Dyke, J Fluid Mech 44: 365, 1970.
252. T Maxworthy, J Fluid Mech 23: 360, 1965.
253. VG Jenson, AIChE Meeting, Chicago, III, Dec. 1957.
254. N Frossling, Lunds Universitèts Arsskrift, NF Avd 2, 35: 4, 1940.
255. T Oroveanu, Mecanica fluidelor viscoase, Ed. Tehnica, Bucharest, 1967.
256. JM Smith, Chemical Engineering Kinetics, International Student Edition, Singapore: McGraw-Hill, 6th Printing 1987, p. 535–537.